Exploring morphological phylogenetics of fossil hominins

by

Mana Dembo

M.A., University of British Columbia, 2007
H.B.Sc., University of Toronto, 2005

Thesis Submitted in Partial Fulfillment of the
Requirements for the Degree of
Doctor of Philosophy

in the
Department of Archaeology
Faculty of Environment

SIMON FRASER UNIVERSITY

Summer 2016

Approval

Name: **Mana Dembo**

Degree: **Doctor of Philosophy**

Title: ***Exploring morphological phylogenetics of fossil hominins***

Examining Committee: **Chair:** David Burley
Professor

Mark Collard
Senior Supervisor
Professor

Arne Mooers
Supervisor
Professor

Pablo Nepomnaschy
Internal Examiner
Associate Professor
Faculty of Health Science

Mike Lee
External Examiner
Professor
Department of Biological Science
Flinders University

Date Defended/Approved: May 26, 2016

Abstract

A reliable phylogeny is critical for the study of hominin evolution, yet there remains considerable debate about the relationships among hominin species. Phylogenetic analyses conducted to date differ in various analytical aspects such as the fossil samples and characters used to infer their relationships. Given the importance of a phylogeny in the study of hominin evolution, four studies were designed to address some key issues in the phylogenetic analysis in palaeoanthropology. The first study investigated the effects of using small samples in standard phylogenetic analyses. The second study used tip-dated Bayesian analysis to test various phylogenetic hypotheses pertaining to three recent debates. The third study used the same method to evaluate the phylogenetic and temporal placement of a newly discovered species, *Homo naledi,* in the hominin phylogeny. The fourth study explored the impact of cranial modularity on the choice of characters used to reconstruct the phylogeny of the hominins.

Results suggest that small sample sizes can be problematic in phylogenetic analyses of extant hominoids. However, the choice of character coding methods may mitigate the effects of small samples. Bayesian phylogenetic analyses were conducted to evaluate various hypotheses from three recent debates and some hypotheses can be strongly refuted based on current evidence. The results of the analyses suggest that there is strong evidence that *Homo naledi* belongs to the clade of *Homo* and *Australopithecus sediba*, but its place within this clade is currently ambiguous. The results of this study place the fossil at approximately 1 Ma. Different cranial regions contain conflicting phylogenetic signals, but none of the regions particularly stand out as having more homoplastic characters. The hominin phylogeny is necessary to study hominin evolution, and as such, it is important to improve the methods used to reconstruct the evolutionary relationships of hominins. The use of Bayesian phylogenetic methods is promising for palaeoanthropology as it can narrow the scope of debate surrounding phylogenetic hypotheses. It allows us to highlight where ambiguities in the data and the model exist and demonstrate the limit of the interpretation of the current fossil evidence.

Keywords: Palaeoanthropology; hominin evolution; morphological phylogenetics; Bayesian analysis; parsimony analysis

Acknowledgements

There are many people whose continuous support guided me throughout the PhD degree. First and foremost, I would like to thank my committee members: Mark Collard, whose unfailing support and guidance allowed me to learn so much, and Arne Mooers, whose contagious enthusiasm and vision redirected these studies when necessary. There are various collaborators whose help and input were greatly appreciated: Nick Matzke, Davorka Radovčić, Heather Garvin, Myra Laird, Lauren Schroeder, Jill Scott, Becky Ackermann, and Darryl de Ruiter. I would also like to thank the members of Human Evolutionary Studies Program (past and present) for the stimulating discussions and presentations that provided me with a rich training to develop as a scientist.

Surviving grad school would not have been possible without the much needed friendships and interventions. I have met many great people who helped me along the way. A special thank you to Marina Elliott and Luseadra McKerracher, who will always have a spoon-shaped place in my heart. Friends who provided laughs and pointless banter regularly on Thursdays, I thank you.

Lastly, I am immensely grateful to my family for their love and support while I spent many years learning about the fossils that I love. In particular, I would like to thank Jack for humouring me and letting me be the big geek that I am. Thank you for waiting.

Table of Contents

List of Tables

List of Figures

Chapter 1.

Introduction

1.1. Aims and objectives

A reliable phylogeny is critical for the study of hominin evolution. Without such a phylogeny, we cannot develop scenarios that account for the evolution of the fossil hominins (Tattersall and Eldredge, 1977). For instance, a phylogeny provides a context for exploring various hypotheses of adaptive changes in hominin evolution. Researchers can use a phylogeny to distinguish between morphological similarities due to shared common ancestry versus morphological similarities due to similar adaptations to a particular function or environment. Thus, a phylogeny is central to understanding the processes that operated in the course of hominin evolution.

However, there remains considerable debate about the relationships among fossil hominin species. Some hominin relationships have been generally supported in the phylogenetic analyses conducted to date (e.g. Skelton et al., 1986; Chamberlain and Wood, 1987; Wood and Chamberlain, 1987; Stringer, 1987; Skelton and McHenry, 1992; Wood, 1991, 1992; Lieberman et al., 1996; Strait et al., 1997; Strait and Grine, 2004; Argue et al., 2009; Irish et al., 2013). Yet, there are some inconsistent relationships reported in these studies, such as the placement of *Australopithecus africanus* (e.g., Strait and Grine, 2004 versus Irish et al., 2013). The reasons for such ongoing phylogenetic debates must be elucidated. My thesis is that many uncertainties concerning hominin phylogenetic relationships may be the result of the analytical issues that are outlined in detail in a later section.

This dissertation addressed some key issues in the phylogenetic analysis in palaeoanthropology. The studies were designed to explore one of three topics, namely the effects of using small sample sizes in phylogenetic analyses, the use of a new method—tip-dated Bayesian analysis—to test various phylogenetic hypotheses, and the choice of characters

used to reconstruct the phylogeny of the fossil hominins. The aim of this project was to improve the methods used by palaeoanthropologists to study phylogenetic relationships of hominin species by evaluating some outstanding issues related to the phylogenetic analyses of fossil hominin species.

The remainder of this chapter provides a background on the morphological phylogenetics of hominin species and the outstanding issues stemming from these studies. It concludes with an outline of four studies that comprise the dissertation.

1.2. Background

1.2.1. Hominin systematics

Human ancestors diverged from ancestors of chimpanzees and bonobos at least five to nine million years ago based on molecular evidence (Rogers and Gibbs, 2014), and this divergence date may be pushed back as early as 13 million years ago based on recent work (Venn et al., 2014). What happened in our lineage after its divergence from the chimpanzee and bonobo lineage is known primarily from the hominin fossil record. During the last 160 years, palaeoanthropologists have discovered numerous fossils that shed light on how hominins have evolved. A speciose interpretation of the hominin fossil record currently suggests that there could be as many as 29 species in the tribe Hominini (Figure 1.1) spanning the last seven million years (Wood and Boyle, 2016). The pace of discovery has increased rapidly in recent years: since 1995, 12 new species have been announced (Brunet et al., 1995; Bermúdez de Castro et al., 1997; Asfaw et al., 1999; Haile-Selassie, 2001; Senut et al., 2001; Leakey et al., 2001; Brunet et al., 2002; Gabounia et al., 2002; Brown et al., 2004; Berger et al., 2010; Haile-Selassie et al., 2015; Berger et al., 2015). There is now a substantial body of fossil evidence that suggests the existence of over 20 hominin species during the course of hominin evolution.

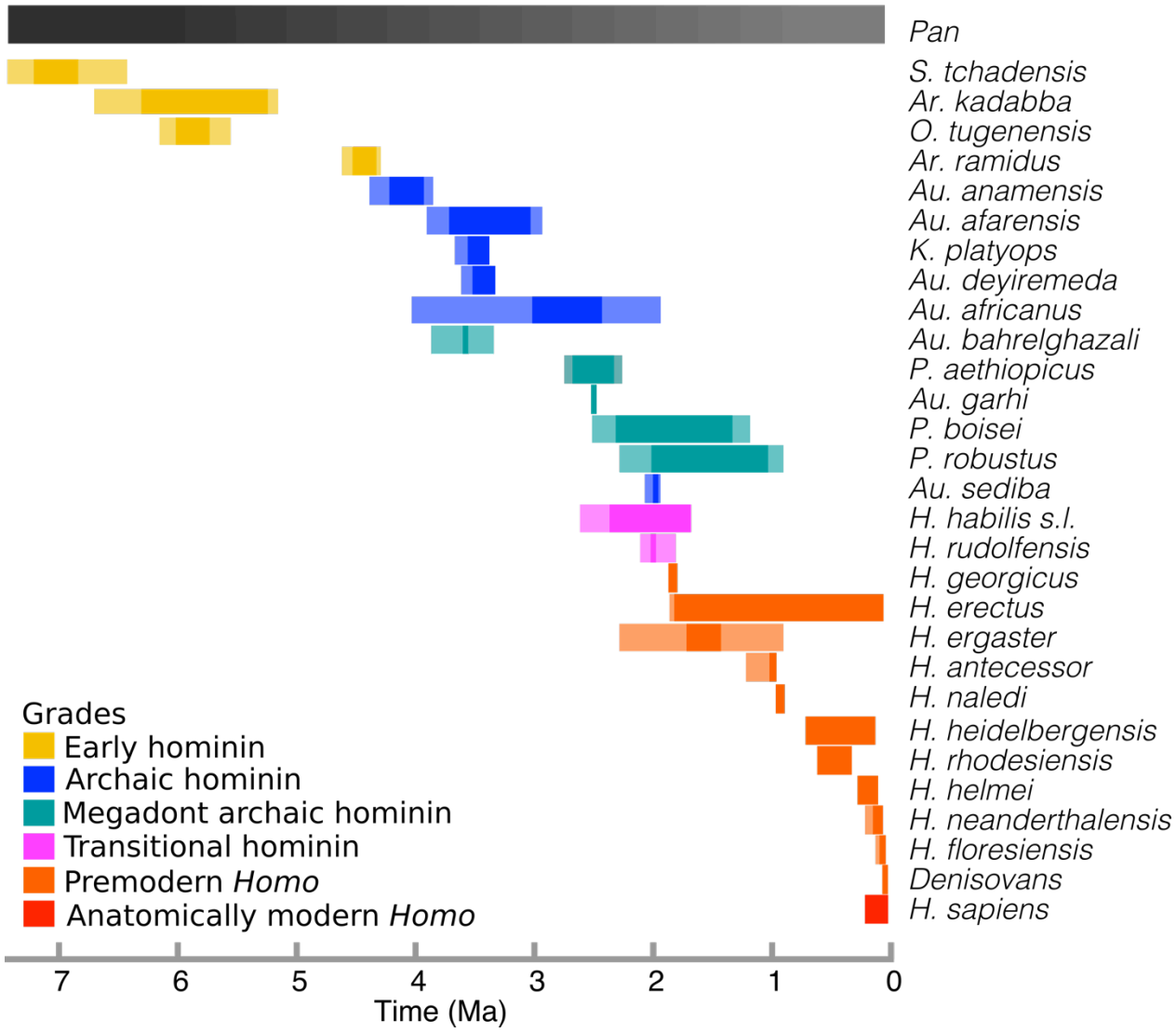

Figure 1.1 Taxonomy of fossil hominins
Data for this figure are taken from Wood and Boyle (2016). The uncertainties in the geological dates associated with the fossil specimens are indicated by the lighter shade in the figure. Hominins are colour coded by their grade adaptations as specified by Wood and Boyle (2016).

The classification of these hominin species and understanding their evolutionary significance requires the knowledge of their phylogenetic relationships. Since most genus concepts that are currently in use in palaeoanthropology hold that genera should be monophyletic (Collard and Wood, 2015), a phylogeny can shed light on the taxonomic status of hominin species. In addition, phylogenetic trees can illuminate the processes involved in hominin evolution such as convergent evolution, diversification, mode and pattern of speciation, and biogeography (e.g., Eldredge and Gould, 1972; Tattersall and Eldredge, 1977; Skelton and

McHenry, 1992; Strait and Wood, 1999). Indeed, phylogenetic trees form the basis of our understanding of hominin evolution of the last seven million years.

1.2.2. Morphological phylogenetics in palaeoanthropology

The first formal analysis of fossil hominin phylogeny was reported by Niles Eldredge and Ian Tattersall in the mid 1970s (Eldredge and Tattersall, 1975). Since then, many studies have attempted to estimate the evolutionary relationships of fossil hominin species (e.g. Stringer 1987; Chamberlain and Wood 1987; Skelton and McHenry, 1992; Wood, 1991, 1992; Lieberman et al., 1996; Strait et al., 1997; Strait and Grine, 2004; Cameron and Groves, 2004; Martinón-Torres et al., 2007; Smith and Grine, 2008; Gonzáles-José et al., 2008; Zeitoun 2009; Argue et al., 2009; Berger et al., 2010; Irish et al., 2013; Mounier et al., 2015; Mounier et al., 2016).

These phylogenetic studies adopt one of three approaches. The first set of studies primarily focuses on resolving the relationships among species of a particular genus. The phylogenetic relationships among species in the genus *Homo* have been targeted in several studies (Gonzáles-José et al., 2008; Zeitoun, 2009; Mounier et al., 2015, 2016). Hominin species outside of the genus of interest are often excluded from these analyses, or if they are included, they are often treated as outgroup taxa, and only one or two specimens per taxon are sampled.

Another set of studies aims to place a newly discovered species on the hominin tree (Argue et al., 2009; Berger et al., 2010; Irish et al., 2013). These studies generally use data from known hominin species that are temporally and morphologically similar to the new species, and they tend to focus on features that distinguish the new species from other hominins. The tree topology is then used to provide a context for the implications of the new find. For instance, based on the results of a phylogenetic analysis, Berger et al. (2010) suggest that *Au. sediba* may be an ancestor of genus *Homo*, or a close relative to the species that gave rise to the genus *Homo*.

The third set of studies uses phylogenetic analyses to explore the alpha taxonomy of various hominin species. For example, the alpha taxonomy of *Homo habilis sensu lato* was evaluated by splitting the fossil specimens that are traditionally assigned to one species into two taxa (Chamberlain and Wood, 1987; Wood, 1992; Lieberman et al., 1996). When the specimens

were divided into two taxa, the most parsimonious tree was shorter than when it was treated as one taxon. These results of the phylogenetic analysis support the suggestion that *Homo habilis sensu lato* included two hominin species, *Homo habilis sensu stricto* and *Homo rudolfensis*.

1.2.3. Problems with morphological phylogenetics in palaeoanthropology

There are problems and limitations in hominin phylogenetic analyses (Trinkaus, 1990; Corruccini, 1994; Lieberman et al., 1996; Asfaw et al., 1999; Collard and Wood, 2000; Curnoe, 2003; Hawks, 2004). One concerns the samples of fossil specimens used in analyses. Due to the effects of preservation and recovery, the samples used in hominin phylogenetics are often small and incomplete. Several researchers have suggested that small sample sizes may be problematic because intra-taxon variability may not be captured and evaluated accurately (Trinkaus, 1990; Hawks, 2004; Smith, 2005). However, the impact of the use of small and incomplete fossil samples on the accuracy of hominin phylogeny is not well understood.

The reliability of morphological data has also been questioned more generally (e.g., Pimentel and Riggins, 1987; Stevens, 1991; Thiele, 1993; Collard and Wood, 2000, 2001; Wiens, 2001, 2004; Scotland et al., 2003; Smith and Turner, 2005). Because osseous morphology is influenced by the interaction of genes, activity, and other non-genetic factors (Lieberman, 1999; Lockwood and Fleagle, 1999), certain morphological data may be more prone to homoplasies, which are similarities not due to common ancestry (Collard and Wood, 2000, 2001; Lycett and Collard, 2005). For example, basicranial characters are predicted to preserve a strong phylogenetic signal because the basicranium is under strict developmental constraints and therefore it less influenced by activity (Olson, 1981; Lieberman et al., 1996; Wood and Lieberman 2001). In contrast, characters of the face have been argued to be relatively poor indicators of phylogeny due to the more flexible developmental process of the face (Lieberman, 1999; Harvati and Weaver 2006a). This has led some to caution against accepting phylogenies of fossil hominins reconstructed using a large proportion of facial characters because of the potential for homoplastic characters (Skelton and McHenry, 1992; McCollum 1999).

Concerns with small sample sizes and homoplasies are coupled with concerns regarding the sampling of both species and characters. Most studies to date have focused on either early hominins (e.g., Kimbel et al., 2004) or later hominins (e.g., Martinón-Torres et al., 2007). The

dataset used by Strait and Grine (2004) is the largest published dataset that includes the oldest putative hominin species *Sahelanthropus tchadensis* and the most recent hominin species, *Homo sapiens*. However, this dataset excludes some well-known species such as *H. neanderthalensis,* and *H. heidelbergensis*. Therefore, all of the phylogenetic studies of fossil hominins to date have not included all widely accepted species of the last seven million years. In addition, different studies use different characters in their phylogenetic analyses. All studies have relied heavily on craniodental characters, but beyond that, there is little overlap in the characters chosen for analysis. The inconsistent and weakly supported phylogenies of fossil hominins may be the result of the use of partial, incomplete data, and this needs to be investigated further.

Lastly, all of the phylogenetic studies of fossil hominins have been conducted using maximum parsimony analysis. While this method is useful for generating trees, it is not well suited to formally evaluating the relative support for competing hypotheses of phylogenetic relationships. Over the past few decades, other methods of phylogenetic inference for extant organisms, particularly Bayesian methods of phylogenetic analysis, have been used increasingly in evolutionary biology (see review in Huelsenbeck et al., 2008). Recently, their use has been extended to fossil morphological data, such that geological (time) data can be incorporated (Lee et al., 2014a). Palaeoanthropologists have not yet explored the use of Bayesian approaches to study fossil hominin phylogenetic relationships. The adoption of such methods allows palaeoanthropologists to both (i) incorporate geological dates associated with hominin fossils into the analysis and (ii) directly compare the strength of support for competing evolutionary hypotheses.

1.3. Description of the PhD research

Four studies are presented here. They are designed to address some of the foregoing issues in the phylogenetics of fossil hominin species outlined above. The first study (reported in Chapter 2) investigates the effects of using small sample sizes in standard maximum parsimony phylogenetic analyses. The sample sizes used in palaeoanthropological phylogenetics tend to be small and it has been assumed that small samples are not problematic in reconstructing reliable hominin phylogenies. However, the findings from recent studies suggest palaeoanthropologists may need to exercise more caution when using small sample sizes in

phylogenetic analyses (Wiens and Servedio, 1998; Hawks, 2004). Using a dataset on extant hominoid craniodental measurements, I systematically reduce the number of specimens included in the taxa to explore the effects of small sample size on the outcome of the phylogenetic analyses.

The second study (Chapter 3) addresses two issues in morphological phylogenetics, namely the use of partial, inconsistent datasets and the reliance on inference methods that build, rather than test, hypotheses of relationship. A global supermatrix of craniodental characters for 20 hominin species was compiled from 13 published studies and I use a tip-dated Bayesian method to test between published hypotheses pertaining to three "hot" palaeoanthropological debates. This study is the first to apply the Bayesian approach to phylogenetics in palaeoanthropology and it demonstrates the considerable promise of this method for dealing with palaeoanthropological data that contain a large proportion of missing data. This study was published in the Proceedings of the Royal Society B in July, 2015.

The third study (Chapter 4) uses the same analytical methods and expands the supermatrix outlined in the previous chapter. This study focuses on the phylogenetic relationships of a newly discovered hominin species, *Homo naledi* (Berger et al., 2015) and addresses the important question of where *Homo naledi* is placed in the hominin tree. I conduct tip-dated Bayesian phylogenetic analyses to reconstruct the phylogeny, to test various phylogenetic hypotheses, and to estimate a date of *H. naledi* based on the rate of morphological evolution. This study was accepted for publication in Journal of Human Evolution in April, 2016 and is currently in press.

The tip-dated Bayesian analysis was once again conducted in the last study (Chapter 5) to explore the impact of cranial modularity on hominin phylogenetics. It has been suggested that certain regions of the hominin skull are more reliable than others as sources of phylogenetic information. Basicranial morphology is predicted to retain a strong phylogenetic signal because it is under strict developmental constraints and therefore it less influenced by activity (Olson, 1981; Lieberman et al., 1996; Wood and Lieberman 2001). In contrast, the face has been predicted to be a less reliable indicator of phylogeny because it is developmentally more flexible and thus responds to both selection and activity during development (Lieberman, 1999; Harvati and Weaver 2006a). The study seeks to evaluate whether the phylogenetic signals from the four functional regions of the skull vary and to test if the trees produced from the functional regions

are significantly different from each other. I evaluate whether cranial modularity greatly influences the phylogenetic signal retained in each region and whether it is problematic to combine the data from these functional regions to reconstruct the phylogeny of fossil hominins.

Chapter 2.

An assessment of the impact of small samples on the reconstruction of hominin phylogeny

2.1. Introduction

Knowledge of the phylogenetic relationships of fossil hominins is necessary for understanding hominin evolution. Without a reliable phylogeny, little confidence can be placed in hypotheses regarding the number and nature of adaptive changes in human evolution (Tattersall and Eldredge, 1977). For instance, a phylogeny provides a context for exploring various hypotheses of adaptive changes. Researchers can use a phylogeny to distinguish between morphological similarities due to shared common ancestry versus morphological similarities due to similar adaptations to a particular function or environment. Moreover, a phylogeny can help associate events in hominin evolution with environmental changes and patterns of faunal evolution. For example, if closely related species are found in different regions, this evidence can be used to hypothesize that a vicariance or dispersal event must have taken place in the course of hominin evolution (Tattersall and Eldredge, 1977; Strait and Wood, 1999). Thus, it is important to evaluate and improve methods for reconstructing the phylogenetic relationships of the fossil hominin species.

The phylogenetic relationships of fossil hominin species have been reconstructed many times over the last 40 years (e.g., Eldredge and Tattersal, 1975; Delson et al., 1977; Skelton et al., 1986; Chamberlain and Wood, 1987; Wood and Chamberlain, 1987; Stringer, 1987; Skelton and McHenry, 1992; Wood, 1991, 1992; Lieberman et al., 1996; Strait et al., 1997; Wood and Collard, 1999; Manzi et al. 2001; Strait and Grine, 2004; Cameron and Groves 2004; Gilbert 2008; Smith and Grine 2008; Argue et al., 2009; Berger et al. 2010; Irish et al., 2013; Mounier et al., 2015; Dembo et al., 2015; Mounier et al., 2016). However, these studies have produced inconsistent and, in many cases, weakly supported phylogenies. This has led to discussion

among palaeoanthropologists about potential reasons why fossil hominin morphological data may not always yield reliable estimates of their phylogenetic relationships (Trinkaus, 1990; Corruccini, 1994; Lieberman et al., 1996; Asfaw et al., 1999; Collard and Wood, 2000; Curnoe, 2003; Hawks, 2004).

One potential impediment to the reconstruction of fossil hominin phylogeny is the number of fossil specimens available to palaeoanthropologists. The samples used in phylogenetic studies of the fossil hominins tend to be small. The number of specimens per species ranges from one to 40, but typically averages 15 individuals per species (Table 2.1). But even this is misleadingly high, because few specimens are complete enough for all characters to be recorded on them. Therefore, the fossil samples used in the phylogenetic analysis can be much smaller depending on the character.

There are two reasons for the continued use of small sample sizes in phylogenetic analyses of hominin species. The nature of the hominin fossil record is such that, either by necessity or by choice, researchers typically rely on small samples of fossil specimens to reconstruct the phylogenetic relationships. Reliance on small samples is unavoidable at times because the availability of fossil material is limited. For instance, the species *Australopithecus garhi* is represented by a single specimen, BOU-VP 12/130 (Strait and Grine 2004; Smith and Grine 2008; Cameron and Groves 2004; Berger et al. 2010). In other cases, researchers choose to sample only the more complete specimens, presumably to reduce the impact of missing data on the results of the analyses (e.g. Kramer et al. 2001; Manzi et al. 2001; Argue et al. 2009).

It is normally assumed that the small size of the samples used in fossil hominin phylogenetic analyses does not adversely affect the accuracy of the phylogenies recovered. However, there is reason to be skeptical about this assumption. Three recent studies support such skepticism. In a simulated phylogenetic study of fossil hominins, Hawks (2004) found that the true tree was less likely to be the most parsimonious tree when samples were small and variable. In geometric morphometric studies of primate crania, Cobb and O'Higgins (2004) discovered that samples of fewer than 40 individuals yielded unreliable estimates of the cranial ontogeny of the common chimpanzee, while Cardini and Elton (2007) found that samples of fewer than 30 individuals produced inaccurate estimates of mean cranial shape in guenons. Although the latter two studies are not phylogenetic in orientation, they raise questions about the accuracy of published fossil hominin phylogenetic analyses because they suggest that more

than 30 to 40 specimens are required to accurately capture the cranial morphology of a primate species, a condition met by very few phylogenetic studies of fossil hominin species.

Table 2.1 Sample sizes used in previously published studies.

NA indicates that the species was included in the analysis, but the sample size was not reported in the original study. The dash (-) indicates species that were excluded from the study.

Species	Chamberlain & Wood (1987)	Skelton & McHenry (1992)	Lieberman et al. (1996)	Strait et al. (1997)	Cameron & Groves (2004)	Strait & Grine (2004)	Argue et al. (2009)
S. tchadensis	-	-	-	-	1	1	-
Ar. ramidus	-	-	-	-	NA	5	-
A. anamensis	-	-	-	-	NA	3	-
A. afarensis	11	15	4	28	26	26	1
A. garhi	-	-	-	-	1	1	-
A. africanus	7	25	5	31	18	32	3
K. platyops	-	-	-	-	3	2	-
P. aethiopicus	-	7	3	8	1	8	-
P. robustus	7	13	6	25	22	26	-
P. boisei	7	16	4	37	17	39	-
H. habilis	10	16	9	18	10	18	2
H. rudolfensis	-	-	5	10	10	10	1
H. ergaster/ erectus	14	-	3	7	9	7	5
H. georgicus	-	-	-	-	-	-	3
H. floresiensis	-	-	-	-	-	-	2
H. rhodesiensis	-	-	-	-	-	-	1
H. sapiens	-	-	-	NA	NA	NA	11

The aim of the present study was to evaluate the extent to which small sample sizes may compromise hominin phylogenetic inference. To do this, we analysed craniodental data from a group of extant hominoids to simulate the data typically used in hominin phylogenetic analyses. We first generated subsample datasets with reduced sample sizes by randomly sampling the master dataset. We then scored the characters using only those samples, and conducted

parsimony analyses using these datasets. The impact of small sample sizes was assessed using two approaches. We compared the results of the parsimony analyses across datasets of different sample sizes to evaluate whether decreasing sample sizes had a significant effect on the results of the parsimony analysis. We hypothesized that the goodness-of-fit statistics, which are often used to evaluate the reconstructed phylogeny, should be lower with reduced sample sizes. We also compared the tree topologies reconstructed using reduced sample sizes and the master dataset of the hominoids. This was conducted to evaluate how well trees reconstructed using smaller samples approximated the tree reconstructed using the master dataset. We reasoned that, if small sample size affects the accuracy of the tree, the topologies of trees obtained from small samples should be more incongruent with the trees reconstructed using the master dataset with the largest number of specimens used for phylogenetic analysis. We chose to not compare the tree topologies to the molecular tree to assess accuracy because the trees reconstructed from the master dataset were incongruent with the molecular tree. Thus, we opted to compare the changes to the tree topologies based on smaller sample sizes by comparing them to the master dataset tree topologies.

The data employed in the study are continuous measurements that capture craniodental shape differences among extant hominoid species. To use such data to reconstruct phylogenetic relationships, it is necessary to discretize them. Numerous methods of converting quantitative data into discrete character states for phylogenetic analysis have been developed (Mickevich and Johnson, 1976; Colless, 1980; Thorpe, 1984; Archie, 1985; Thiele, 1993; Wiens, 2001; Gilbert and Rossie, 2007; Gilbert et al., 2009). However, at the moment, there is no agreement regarding the most appropriate method to use for craniodental data of fossil hominins. Consequently, we employed three coding methods in this study, two of which have been utilized in the past to reconstruct phylogenetic relationships of extant apes and fossil hominins (Collard and Wood 2000, 2001; Strait and Grine 2004; Bjarnason et al., 2010), and the third method, gap-weighting, that was recently demonstrated to outperform other coding methods in a study using quantitative characters of plants (Garcia-Cruz and Sosa, 2006).

2.2. Materials and Methods

The full (or "master") dataset comprised values for 76 measurements recorded on mixed sex samples of four ingroup and two outgroup species. The ingroup species were *Gorilla gorilla*

(n=37), *Homo sapiens* (n=71), *Pan troglodytes* (n=32) and *Pongo pygmaeus* (n=41); the outgroup species were *Colobus guereza* (n=24) and *Papio hamadryas* (n=30). The measurements pertain to the cranium, mandible, and dentition, and are standard variables used to compare the skulls of primate species (Appendix A, Table A1). The data have been employed in several previous studies (Wood, 1975; Wood et al., 1991; Collard and Wood, 2000, 2001, 2007; Collard and Lycett, 2009).

Following several studies (Collard and Wood, 2000, 2001; Nadal-Roberts and Collard, 2005; Bjarnason et al., 2010), the craniodental measurements were adjusted to control for the potentially confounding effects of body size differences by dividing each measurement for a given specimen by the geometric mean of all the measurements for that specimen (Jungers et al., 1995). The geometric mean is calculated as the n^{th} root of the product of n measurements. This method of size correction has been criticized for its failure to account for size-related shape change (Jolly, 2001; Gilbert and Rossie, 2007; Gilbert et al., 2009). However, it was used in the present study because the aim of this study is to investigate the impact of small sample sizes, and the effects of allometry would be present regardless of the sample sizes used to reconstruct phylogenetic relationships. In addition, it is more straightforward to implement than the alternatives.

We began by creating subsamples from the size-corrected master dataset that varied in the number of specimens per species. We created subsamples of 20, 15, ten, five, and three specimens per species. Specimens were randomly selected from the master dataset for each sample size. For each subsampled dataset, the ratio of females to males across all species was held constant at 1:1. The random selection process was repeated ten times for each sample size, leading to a total of 50 datasets. This part of the study was carried out with a script written specifically for the purpose in R (R Development Core Team, 2015).

Next, we coded each of the 50 datasets. As noted earlier, three coding methods were used: divergence coding (Thorpe, 1984), homogeneous subset coding (Simon, 1983), and gap-weighting (Thiele, 1993). These methods convert continuous measurements into discrete character states by ordering the taxa according to the mean of the size-corrected values along an attribute axis. They differ from in how the attribute axis is divided into character states (Simon, 1983; Thorpe, 1984; Thiele, 1993).

Divergence coding tests for statistically significant differences in the taxon means for all pairwise combinations of taxa for each character. A score of +1, 0, or -1 is given based on the statistical comparison of the means between two taxa. If a taxon is significantly larger in the character mean than another taxon, the larger taxon scores +1 and the smaller taxon scores -1. If the character means are not significantly different, both taxa score 0. After a taxon mean has been compared to those of all other taxa, a matrix is filled with scores based on these pairwise tests of significance. Each row of the matrix is then tallied for a given taxon and positivized. The positivized score for each taxon becomes the character state assigned for that character. Thus, the attribute axis is divided if the differences in the means between taxa are statistically significant and the differences between taxa are proportional to the differences in the mean character values of the taxa. In our study, we used the Mann-Whitney U test to evaluate the significance of the differences between species. Parametric tests were not used because the samples often violated the assumptions of normal distribution and homogeneous variances (Sokal and Rohlf, 1995). We generated one set of character state matrices with the p-value at the conventional level of 0.05. Another set of character state matrices was generated with Bonferroni correction to adjust the p-values. We used Bonferroni correction since we effectively conducted multiple unplanned comparisons of means of taxa, and as such, the p-values should be adjusted to account for these comparisons. We also used a different test, Dunn's test, which is a non-parametric pairwise multiple comparisons test that also corrects for multiple comparisons. This resulted in three versions of divergence coding. The statistical analyses involved in divergence coding were implemented in a script written in R.

Homogeneous subset coding also tests for significant difference between all pairwise combinations of taxa. The taxa are assigned to a subset in which all taxa within the subset are not statistically different from each other. When the taxa share membership in the same subset, they are assigned the same character state. The attribute axis, therefore, is divided when the taxa within a subset are not statistically homogeneous. It is possible that a taxon can be assigned to more than one subset. When this occurs, one possible solution is to assign a unique character state to distinguish itself from the other members of either of the subsets (e.g., Strait and Grine, 2004). In the present study, however, we opted to code such species as variable rather than assigning it a unique character state, because polymorphic characters most accurately represent the fact that a taxon belongs to more than one subset. Thus the taxon with variable states was treated as polymorphic in the phylogenetic analyses. As with the previous

coding method, the tests of significance between taxa were conducted using the Mann-Whitney U test. Again, we generated two sets of character state matrices, one with the p-value of 0.05, and another with p-values adjusted using the Bonferroni correction procedure. We also conducted Dunn's test that corrects for multiple comparisons. Homogeneous subset coding was conducted using a script written in R.

Gap-weighting differs from the previous two coding methods in that it does not use a test of significance to divide the attribute axis. In this method, the attribute axis is divided based on a critical value determined *a priori* (Chappill, 1989). In gap-weighting, the means of character values of taxa are rank-ordered and if the differences of the means exceed the critical value, they are assigned different character states. The axis is often divided into the maximum number of character states allowed by the program used for phylogeny reconstruction. For instance, the program Nona (Goloboff, 1999) allows up to ten states for a character, while PAUP* (Swofford, 2003) allows up to 32 states for a character. In our study, we used the program MorphoCode (Schols et al., 2004) to carry out gap-weighting. Gap-weighting was carried out twice. In the first, the craniodental measurements were coded into ten states, which is the minimum number of states used by MorphoCode. In the second, the characters were coded into 26 possible states, which is the maximum number of states accepted by the program.

We carried out a series of phylogenetic analyses using these datasets to investigate the effects of small sample size on the outcome of these analyses. We subjected the 50 randomly sampled datasets to maximum parsimony analysis to reconstruct the phylogenetic relationships of the hominoids, and then compared a range of output variables across different sample sizes. In the parsimony analyses, the character states were treated as ordered, and *C. guerza* and *P. hamadryas* were specified as the outgroup taxa. PAUP's exhaustive tree-search option was used to identify the most parsimonious tree(s). Two of the output variables we recorded were the length of the most parsimonious tree(s) and the number of most parsimonious trees. The best tree is the one in which the number of evolutionary changes is minimized on the tree. If there are multiple trees that are equally parsimonious, this indicates greater ambiguity in the dataset. We also recorded the number of characters that were parsimony-informative and parsimony-uninformative for the most parsimonious tree(s), and the number of polymorphic states in each matrix. In addition, we recorded three goodness-of-fit indicators, the consistency index (CI) with parsimony-uninformative characters included, the CI after exclusion of parsimony-uninformative characters, and the retention index (RI). The CI measures how well the character(s) fits the tree

by comparing total tree length to the minimum possible–CI drops from 1.0 towards 0 as homoplasies increase (Kluge and Farris, 1969). The RI compares the observed amount of homoplasy relative to the maximum amount possible in the dataset (Farris 1989). In contrast to the CI, RI is not affected by the character state frequencies or the number of taxa in the character matrix (Farris 1989). In order to compare these measures across our different subsamples, we used the Jonckheere-Terpstra test, which indicates whether or not sample medians are ordered in a particular direction. The p-values associated with this test indicate that there is a statistically significant trend between sample sizes and these variables. Parsimony analysis was carried out in PAUP* 4.0b10 (Swofford, 2003) and the Jonckheere-Terpstra test was implemented in the R package "coin" (Hothorn et al., 2008).

We also assessed the impact of small sample sizes by comparing the trees reconstructed with various sample sizes to the phylogeny inferred from the master dataset (Appendix A, Figure A1). If the assumption made in hominin phylogenetic studies that we can use small samples to represent hominin species is correct, then we expect that trees reconstructed using small samples should not be incongruent from the trees estimated using the master dataset. Therefore, we assessed the congruence between the most parsimonious trees from 50 randomly sampled datasets and the tree reconstructed from the master dataset using the symmetric-difference metric in PAUP*. The symmetric-difference metric compares the topologies of two trees by evaluating how many partitions two trees share. A score of zero indicates an identical tree topology and the value increases as fewer partitions are shared between the most parsimonious tree and the master dataset tree. When there were multiple most parsimonious trees, we took the average of the symmetric-difference metric across all of the comparisons. The symmetric-difference metrics of different sample sizes were evaluated with Jonckheere-Terpstra tests in R.

2.3. Results

The results of the parsimony analyses with variable sample sizes per species across different coding schemes are presented in Figures 2.1-2.8 and the overall results of the Jonckheere-Terpstra tests are reported in Table 2.2. Below we report patterns for each data-coding scheme separately.

Table 2.2 P-values of the Jonckheere-Terpestra tests evaulating statistically significant trends between sample sizes and the results of the parsimony analysis.

The asterisk indicates significant result at p<0.05.

Coding method	# MP trees	Tree length	CI	CI adjusted	RI	# constant chars	# pars-inf chars	# pars-uninf chars	Tree distance
Standard divergence	0.725	0.000*	0.000*	0.000*	0.885	0.018	0.000*	0.000*	0.300
Divergence Bonferroni	1.000	0.000*	0.000*	0.000*	0.927	0.000*	0.031*	0.171	0.200
Divergence Dunn's	0.001*	0.000*	0.000*	0.000*	1.000	0.000*	0.000*	0.000*	0.000*
Standard subset	0.002*	0.000*	0.029*	0.997	0.000*	0.023*	0.000*	0.000*	0.000*
Subset Bonferroni	0.282	0.000*	0.000*	0.083	0.000*	0.000*	0.000*	0.000*	0.008*
Subset Dunn's	0.000*	0.000*	0.000*	0.000*	0.000*	0.000*	0.000*	0.000*	0.000*
Gap 10 states	0.977	0.595	0.603	0.648	0.156	1.000	0.327	0.337	0.614
Gap 26 states	1.000	0.460	0.466	0.493	0.271	1.000	0.398	0.405	0.506

2.3.1. Standard divergence coding

The results of the standard divergence coding with variable sample sizes are presented in Table 2.3. Reducing sample size decreased the length of the most parsimonious trees (p=0.000), but the number of equally parsimonious trees did not increase as sample size was reduced (p=0.725). There was a decrease in the number of parsimony-informative characters and a corresponding increase in the number of parsimony-uninformative characters with smaller samples (both p=0.000). Trees reconstructed with smaller samples were supported by higher CIs, regardless of whether or not the number of parsimony-uninformative characters was taken into account (CI: p=0.000; CI adjusted: p=0.000). In contrast, RI did not change with changes in sample size (p=0.116).

When the most parsimonious trees were compared to the tree inferred from the master dataset, the symmetric-difference metric did not change significantly with reduced sample size (p=0.300). The topology tests indicated that the trees reconstructed with smaller samples were not significantly different from the full-dataset tree than the trees reconstructed with larger samples.

Table 2.3 The results of the parsimony analysis using standard divergence coding

Sample size	# MP trees	Tree length	CI	CI adjusted	RI	# constant chars	# pars-inf chars	# pars-uninf chars	Tree distance
3	1.1	715.4	0.70872	0.69243	0.4089	1.3	67.8	6.9	2.1
5	1	780.4	0.69424	0.67833	0.40207	1	68.9	6.1	1.9
10	1	891.9	0.67604	0.66194	0.39906	0.4	70	5.6	2.3
15	1.1	939.8	0.67436	0.6672	0.39008	0.2	73	2.8	1.7
20	1.1	971.3	0.67209	0.66623	0.40002	0.6	73	2.4	1.6

2.3.2. Divergence coding with Bonferroni correction

In contrast, the use of Bonferroni correction during divergence coding had a major impact on the results of the parsimony analyses (Table 2.4). With this character coding method, no significant differences in taxon means were detected at the two smallest sample sizes (n=3 and n=5). This resulted in all six species having the same character state for all 76 characters. Because constant characters cannot be used to reconstruct a phylogenetic tree, we could not conduct further analysis with sample sizes of three and five specimens per species with this coding method. Therefore, only the datasets with sample sizes of ten, 15, and 20 specimens per species were used to reconstruct trees.

For these datasets, trees reconstructed with reduced sample sizes were significantly shorter than the trees with larger sample sizes (p=0.000), but there were no differences in the number of equally parsimonious trees across the sample sizes of 10, 15, and 20 individuals per species (p=1.000). The reduction in the number of specimens per sample led to a decrease in the number of parsimony-informative characters (p=0.031) while the number of parsimony-uninformative characters did not increase significantly with smaller sample sizes (p=0.180) (Table 2.3). Higher CIs were associated with trees derived from smaller samples (p=0.000) and this remained the case even after correcting for the number of parsimony-uninformative

characters (p=0.000). Again, the RI was not significantly affected by the reduction in sample size (p=0.081).

The results of the Jonckheere-Terpstra test showed that the symmetric-difference metric did not increase significantly with sample sizes of 10, 15, and 20 specimens per species coded using divergence coding with Bonferroni correction (p=0.200).

Table 2.4 The results of the parsimony analysis using divergence coding with Bonferroni correction

Sample size	# MP trees	Tree length	CI	CI adjusted	RI	# constant chars	# pars-inf chars	# pars-uninf chars	Tree distance
3	NA	NA	NA	NA	NA	76	0	0	NA
5	NA	NA	NA	NA	NA	76	0	0	NA
10	1	700.8	0.70236	0.68198	0.40966	2.8	65.4	7.8	1.4
15	1	792	0.68321	0.66159	0.40237	2.1	66.3	7.6	1.6
20	1.2	860.6	0.67917	0.65816	0.40205	2	66.6	7.4	0.6

2.3.3. Divergence coding with Dunn's test

The tree length of the most parsimonious trees decreased with reduced sample sizes (p=0.000), and the number of equally parsimonious trees increased as sample size was reduced (p=0.001). There was a decrease in the number of parsimony-informative characters and a corresponding increase in the number of parsimony-uninformative characters with smaller samples (both p=0.000). Trees reconstructed with smaller samples were supported by higher CIs, regardless of whether or not the number of parsimony-uninformative characters was taken into account (CI: p=0.000; CI adjusted: p=0.000). In contrast, RI did not change with changes in sample size (p=1.00).

When the most parsimonious trees were compared to the tree inferred from the master dataset, the symmetric-difference metric increased significantly with reduced sample size (p=0.000). The topology tests indicated that the trees reconstructed with smaller samples became more incongruent with the full-dataset tree than the trees reconstructed with larger samples.

Table 2.5 The results of the parsimony analysis using divergence coding with Dunn's test

Sample size	# MP trees	Tree length	CI	CI adjusted	RI	# constant chars	# pars-inf chars	# pars-uninf chars	Tree distance
3	2.4	66	0.988	0.906	0.740	44.8	2.7	28.5	3.943
5	1	267	0.811	0.788	0.426	8.7	53	14.3	4
10	1.2	578.2	0.679	0.666	0.421	1.7	69.3	5	1.8
15	1	695.3	0.668	0.655	0.413	1	69.9	5.1	1.8
20	1	781.7	0.660	0.636	0.407	1	67.8	7.2	2

2.3.4. Standard homogeneous subset coding

Table 2.6 summarizes the results yielded by the datasets that were coded using standard homogeneous subset coding. The trees reconstructed from smaller samples were shorter than trees reconstructed from larger samples (p=0.000). There were also were more equally parsimonious trees with small samples than with large samples (p=0.002). The number of parsimony-informative characters decreased significantly as sample size was reduced (p=0.000), and there was a corresponding increase in the number of parsimony informative characters (p=0.000). The trees had significantly higher CIs with smaller samples (p=0.029), but this was not observed when the parsimony-uninformative characters were removed from the calculation of the CI (p=0.997). The RI decreased significantly as sample size decreased (p=0.000), which resulted from the increase in the number of polymorphic characters with smaller sample sizes (p=0.000).

In the tree topology comparison, the symmetric-difference metric increased significantly with smaller samples (p=0.000). The trees reconstructed from matrices containing more specimens were more similar to the master dataset tree topology.

Table 2.6 The results of the parsimony analysis using standard subset coding

Sample size	# MP trees	Tree length	CI	CI adjusted	RI	# constant chars	# pars-inf chars	# pars-uninf chars	Tree distance
3	2.2	186.9	0.783	0.743	0.395	1.3	53.8	20.9	4.567
5	1.5	203.7	0.773	0.747	0.418	1	59.7	15.3	2.2
10	1.3	242.6	0.760	0.746	0.499	0.4	66.3	9.3	1.3
15	1.1	269.7	0.769	0.760	0.547	0.2	69	6.8	0.5
20	1.2	285.7	0.768	0.761	0.573	0.6	69.9	5.5	0.133

2.3.5. Homogeneous subset coding with Bonferroni correction

Table 2.7 presents the results obtained using the Bonferroni-corrected version of homogeneous subset coding. As in the analyses that utilized Bonferroni-corrected divergence coding, no statistically significant differences between species were found at the two smallest sample sizes. Consequently, the coded character state matrices for sample sizes of three and five specimens per species did not produce trees or associated tree statistics. Thus, only the datasets with sample sizes of ten, 15, and 20 specimens were used for further analyses.

The trees reconstructed with larger samples were significantly shorter than those of smaller samples ($p=0.000$). But the number of equally parsimonious trees did not change significantly with changes in sample sizes ($p=0.282$). The CI increased with smaller sample sizes ($p=0.000$), but this was not significant after correcting for the number of parsimony-uninformative characters ($p=0.083$). In matrices based on smaller samples, there were greater numbers of polymorphic states ($p=0.000$). Consequently, RI decreased significantly with smaller samples ($p=0.000$).

When comparing the tree topologies of the most parsimonious trees to that of the master dataset tree, the symmetric-difference metric did increase significantly as the sample sizes were reduced ($p=0.008$).

Table 2.7 The results of the parsimony analysis using subset coding with Bonferroni correction

Sample size	# MP trees	Tree length	CI	CI adjusted	RI	# constant chars	# pars-inf chars	# pars-uninf chars	Tree distance
3	NA	NA	NA	NA	NA	76	0	0	NA
5	NA	NA	NA	NA	NA	76	0	0	NA
10	1.4	178.1	0.784	0.747	0.405	1.8	54.4	19.8	3
15	1.1	206.9	0.774	0.753	0.470	1.1	61.4	13.5	2
20	1.2	233.4	0.755	0.739	0.472	1	64.2	10.8	2

2.3.6. Subset coding with Dunn's test

Table 2.8 summarizes the results of the parsimony analysis. The tree length of the most parsimonious trees decreased with reduced sample sizes (p=0.000), and the number of equally parsimonious trees increased as sample size was reduced (p=0.000). There was a decrease in the number of parsimony-informative characters and a corresponding increase in the number of parsimony-uninformative characters with smaller samples (both p=0.000). Trees reconstructed with smaller samples were supported by higher CIs, regardless of whether or not the number of parsimony-uninformative characters was taken into account (both p=0.000). RI also increased significantly with changes in sample size (p=0.000).

Table 2.8 The results of the parsimony analysis using subset coding with Dunn's test

Sample size	# MP trees	Tree length	CI	CI adjusted	RI	# constant chars	# pars-inf chars	# pars-uninf chars	Tree distance
3	NA	NA	NA	NA	NA	44.8	0	31.2	NA
5	20.2	76.9	1.000	1.000	0.000	8.7	10	57.3	5.116
10	2.2	123.3	0.859	0.812	0.545	1.7	51.4	22.9	4.58
15	1.5	150.3	0.802	0.773	0.456	1	60.4	14.6	3.2
20	1	171.3	0.777	0.757	0.451	1	64	11	2

When the most parsimonious trees were compared to the tree inferred from the master dataset, the symmetric-difference metric increased significantly with reduced sample size (p=0.000). The topology tests indicated that the trees reconstructed with smaller samples

became more incongruent with the full-dataset tree than the trees reconstructed with larger samples.

2.3.7. Gap-Weighting with 10 states

Table 2.9 summarizes the results obtained with the datasets coded using gap-weighting with ten discrete states. Reduction in sample size had no impact on tree length (p=0.595), number of equally parsimonious trees (p=0.977), number of parsimony-informative characters (p=0.327), or the number of parsimony-uninformative characters (p=0.337). The goodness-of-fit measures also did not change significantly as sample size was reduced (CI: p=0.603, CI adjusted: p=0. 648, RI: p=0.156).

The reduction in the sample sizes also did not have a significant impact on the tree topologies of the most parsimonious trees when compared to the master dataset tree. The symmetric-difference metric did not increase significantly with smaller sample sizes (p=0.614).

Table 2.9 The results of the parsimony analysis using gap coding with 10 states

Sample size	# MP trees	Tree length	CI	CI adjusted	RI	# constant chars	# pars-inf chars	# pars-uninf chars	Tree distance
3	1	969.6	0.706	0.702	0.391	0	75.6	0.4	2.4
5	1	964.8	0.709	0.709	0.391	0	75.4	0.6	2
10	1.1	967.1	0.707	0.705	0.396	0	75.3	0.7	2.5
15	1.1	965	0.709	0.706	0.401	0	75.7	0.3	1.5
20	1.2	966.6	0.708	0.706	0.397	0	75.6	0.4	2.9

2.3.8. Gap-weighting with 26 states

Results were similar when characters were converted into the maximum number character states selected (Table 2.10). Reducing sample size did not significantly affect the output variables associated with the most parsimonious tree. The length of the trees obtained from small samples did not differ significantly from the length of trees obtained from larger samples (p=0.460); the number of equally parsimonious trees remained unchanged across different sample sizes (p=1.0); and there were no differences in the number of parsimony-informative characters across different sample sizes (p= 0.398). In addition, the measures of

goodness-of-fit—the CI and RI—did not change significantly as sample size was reduced (CI1: p=0.466, CI adjusted: p= 0.493, RI: p=0.271).

Reducing sample size also did not significantly affect the topology of the most parsimonious tree(s) in the analyses of the datasets coded using gap-weighting with 26 states per character. The comparison of the most parsimonious trees with the master dataset tree revealed that there were no significant differences between the trees reconstructed from smaller samples and larger samples (p=0.506).

Table 2.10 The results of the parsimony analysis using gap coding with 26 states

Sample size	# MP trees	Tree length	CI	CI adjusted	RI	# constant chars	# pars-inf chars	# pars-uninf chars	Tree distance
3	1	2690.4	0.706	0.706	0.392	0	76	0	2.4
5	1	2675.1	0.710	0.709	0.391	0	75.9	0.1	1.8
10	1	2680.6	0.709	0.709	0.398	0	76	0	2.8
15	1	2683.2	0.708	0.708	0.399	0	76	0	1
20	1	2686.6	0.707	0.707	0.394	0	76	0	2.8

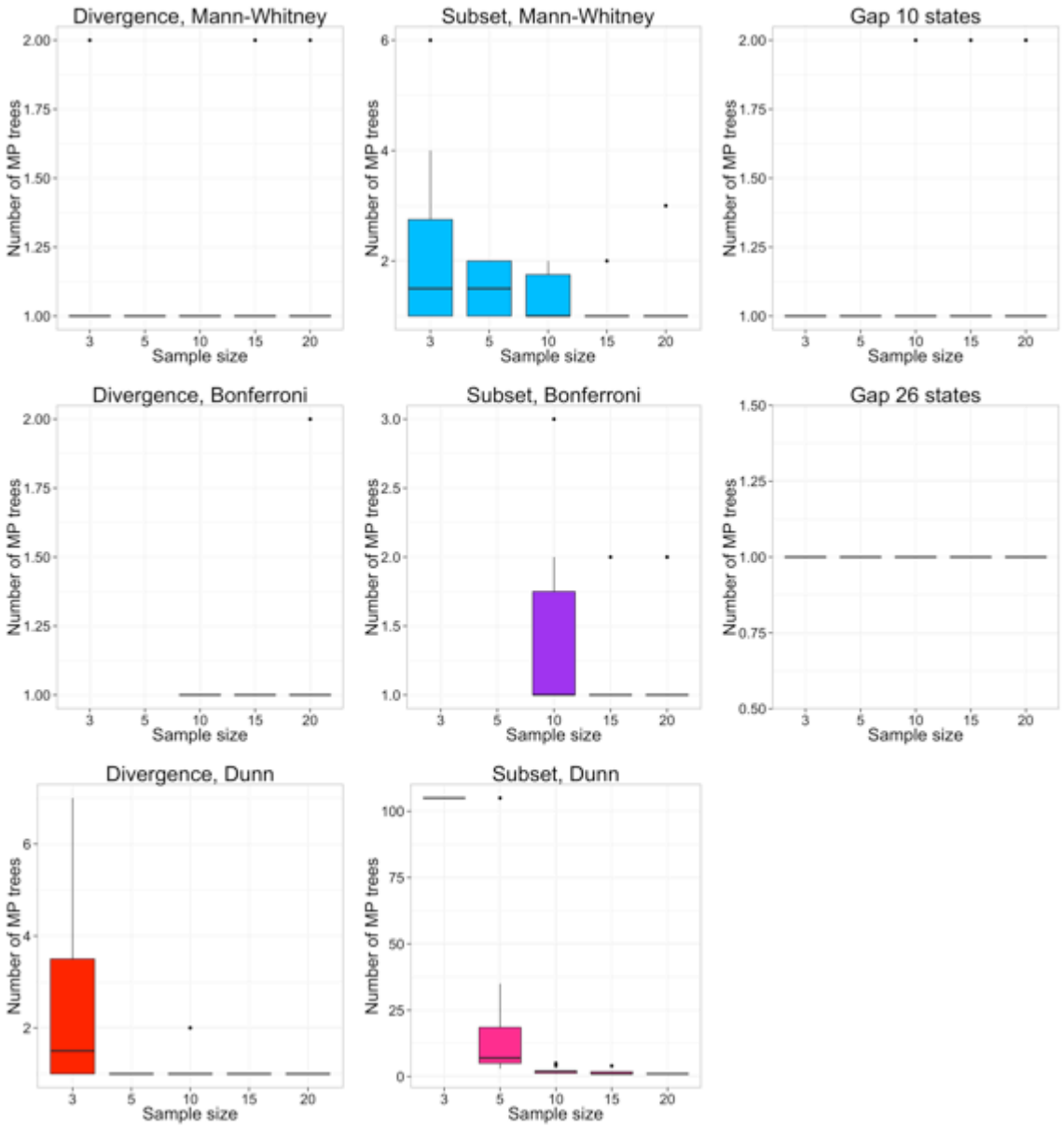

Figure 2.1 Boxplots of sample sizes versus number of most parsimonious trees.
The scale on the y-axis varies across the different analyses.

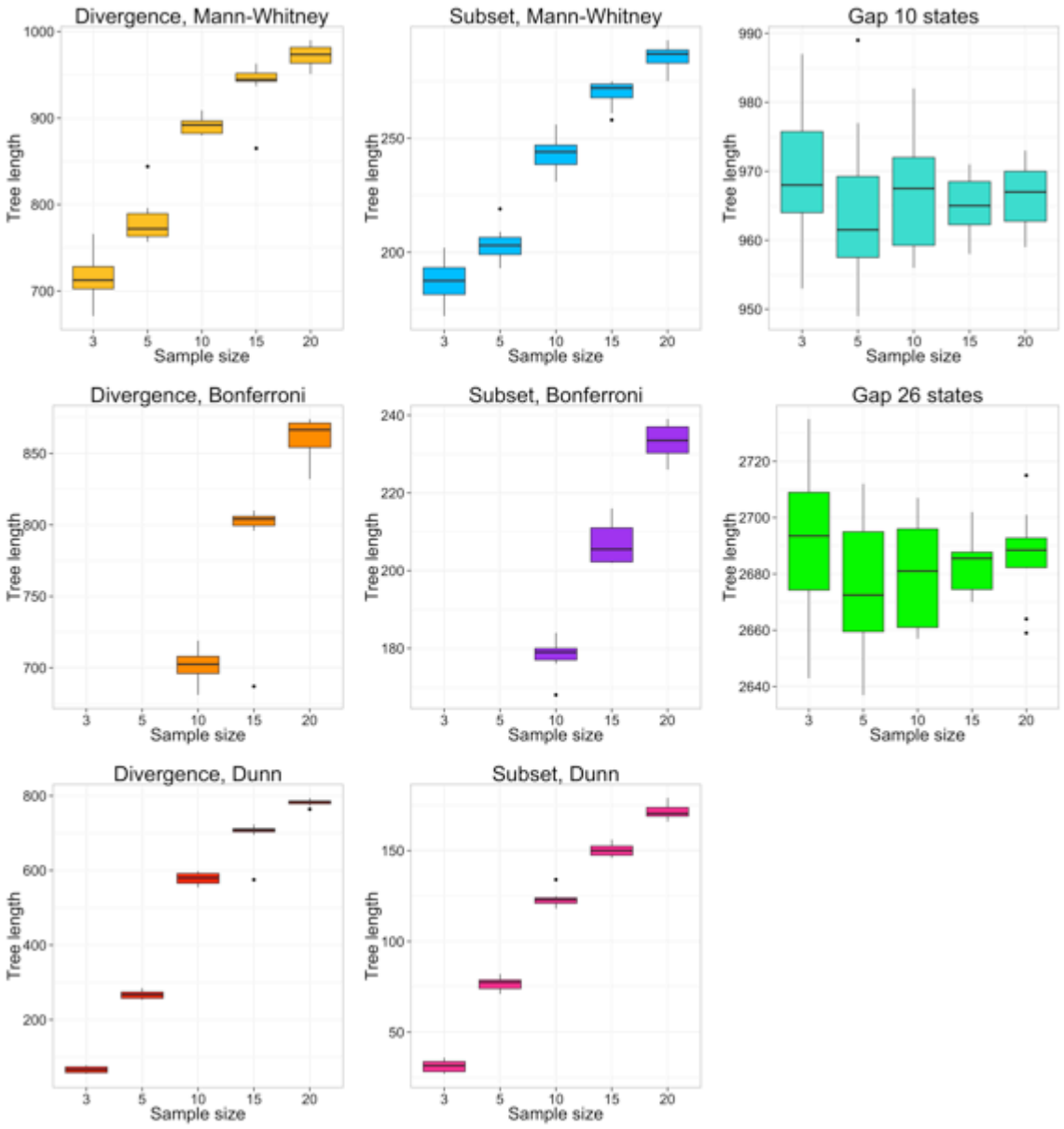

Figure 2.2 Boxplots of sample size versus tree length of the most parsimonious tree
The scale on the y-axis varies across the different analyses.

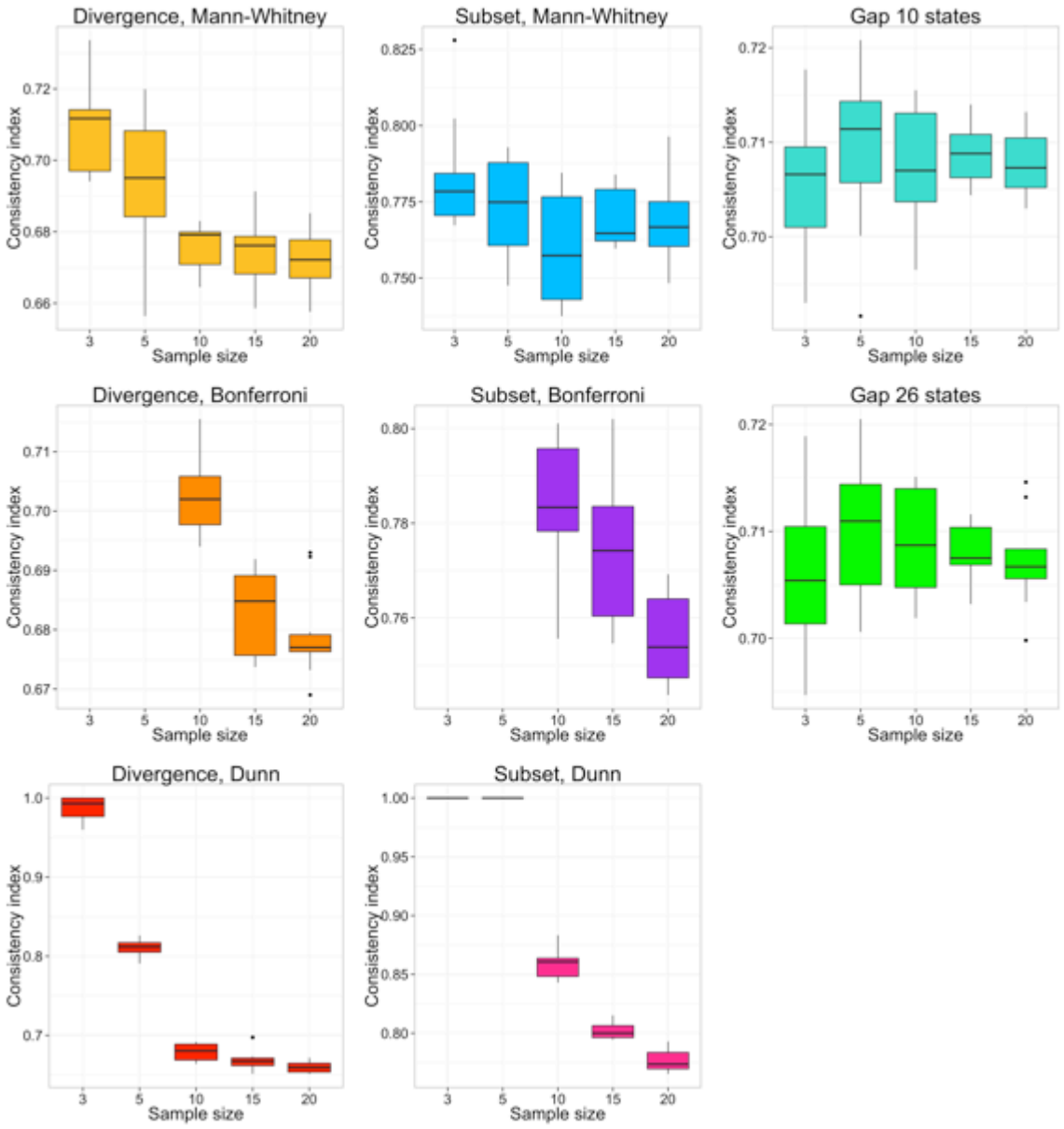

Figure 2.3 Boxplots of sample size versus consistency index.
The scale on the y-axis varies across the different analyses.

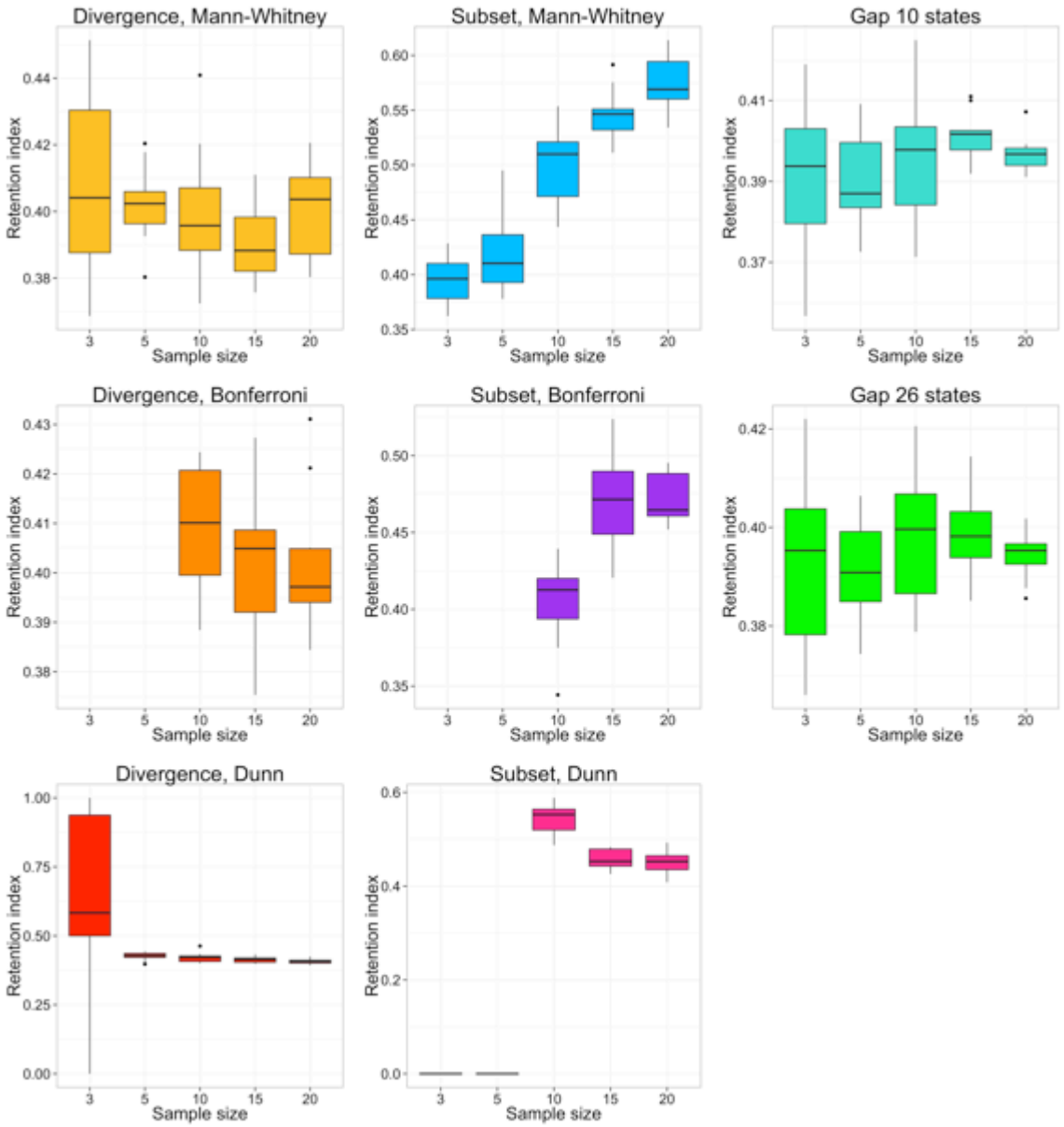

Figure 2.4 Boxplots of sample size versus retention index.
The scale on the y-axis varies across the different analyses.

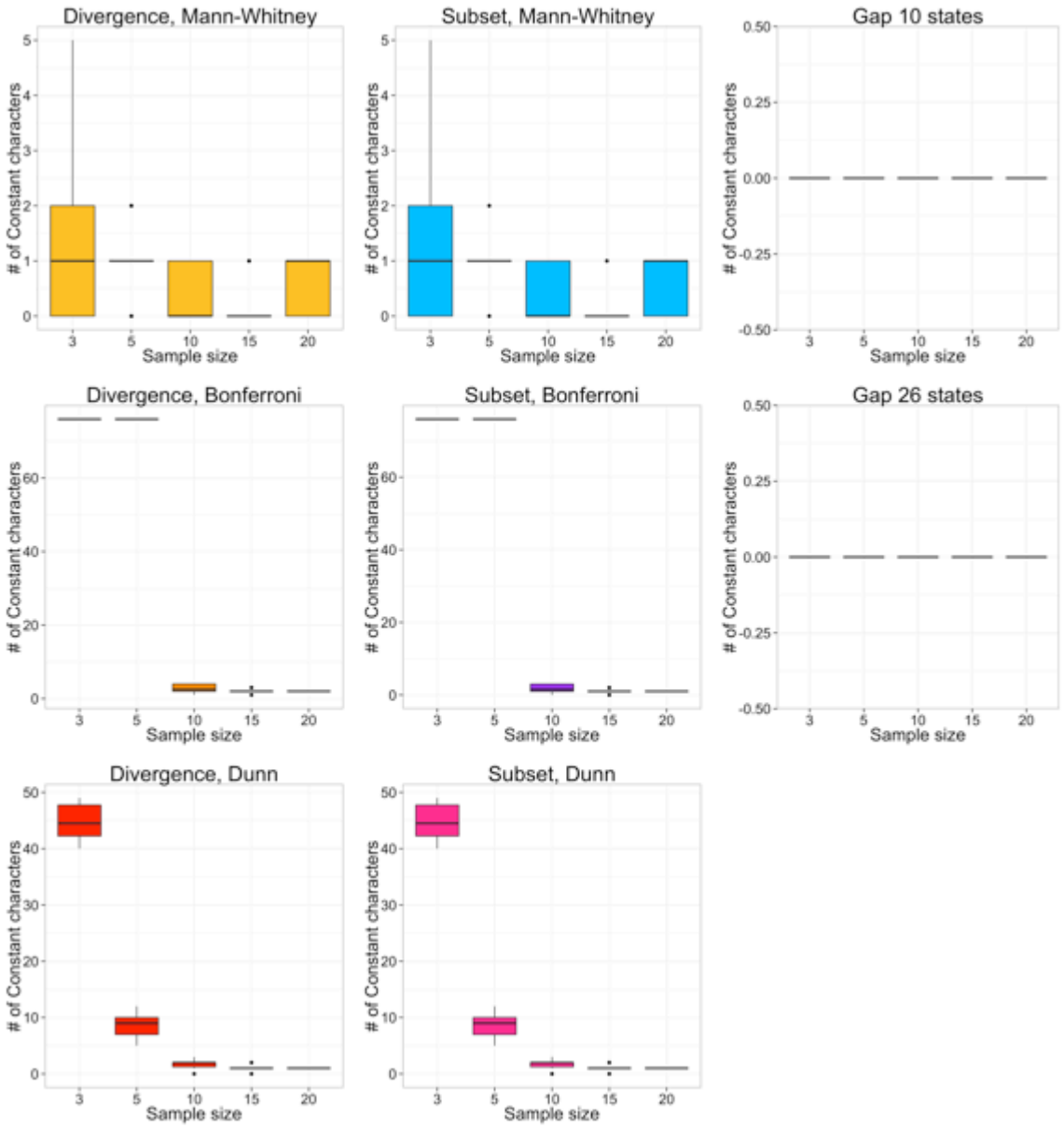

Figure 2.5 Boxplots of sample size versus the number of constant characters.
The scale on the y-axis varies across the different analyses.

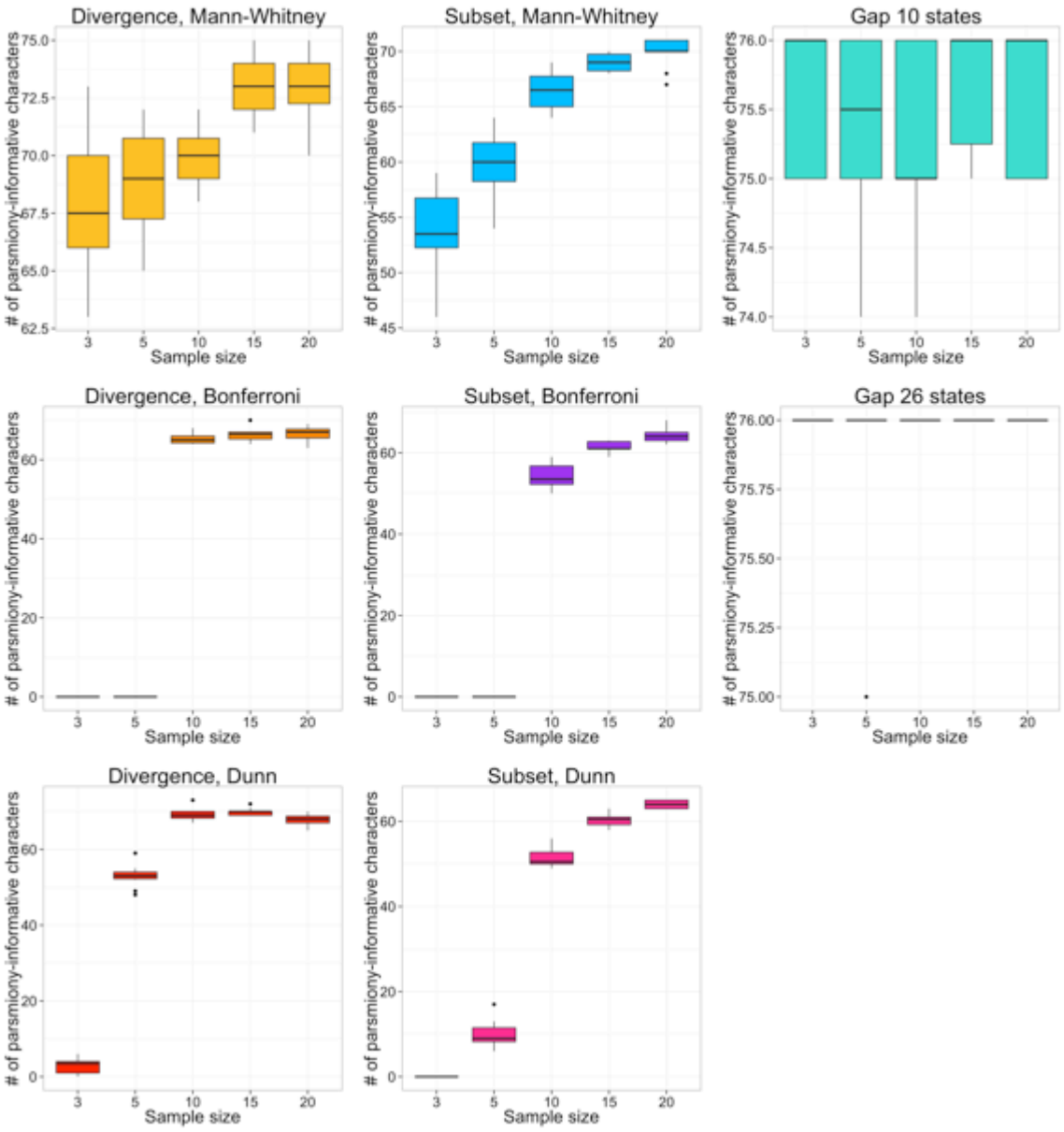

Figure 2.6 Boxplots of sample size versus the number of parsimony-informative characters.

The scale on the y-axis varies across the different analyses.

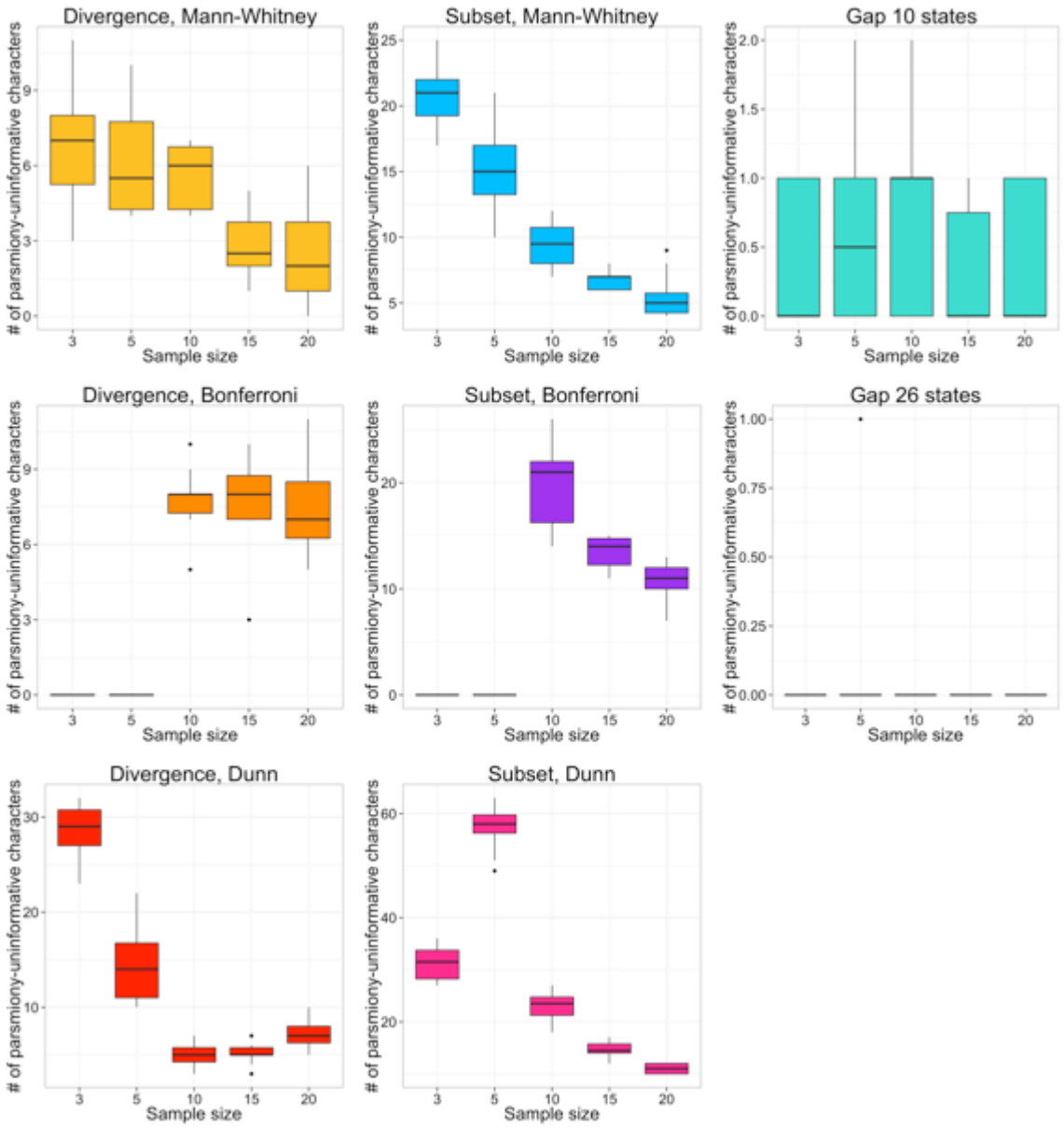

Figure 2.7 Boxplots of sample size versus the number of parsimony-uninformative characters.

The scale on the y-axis varies across the different analyses.

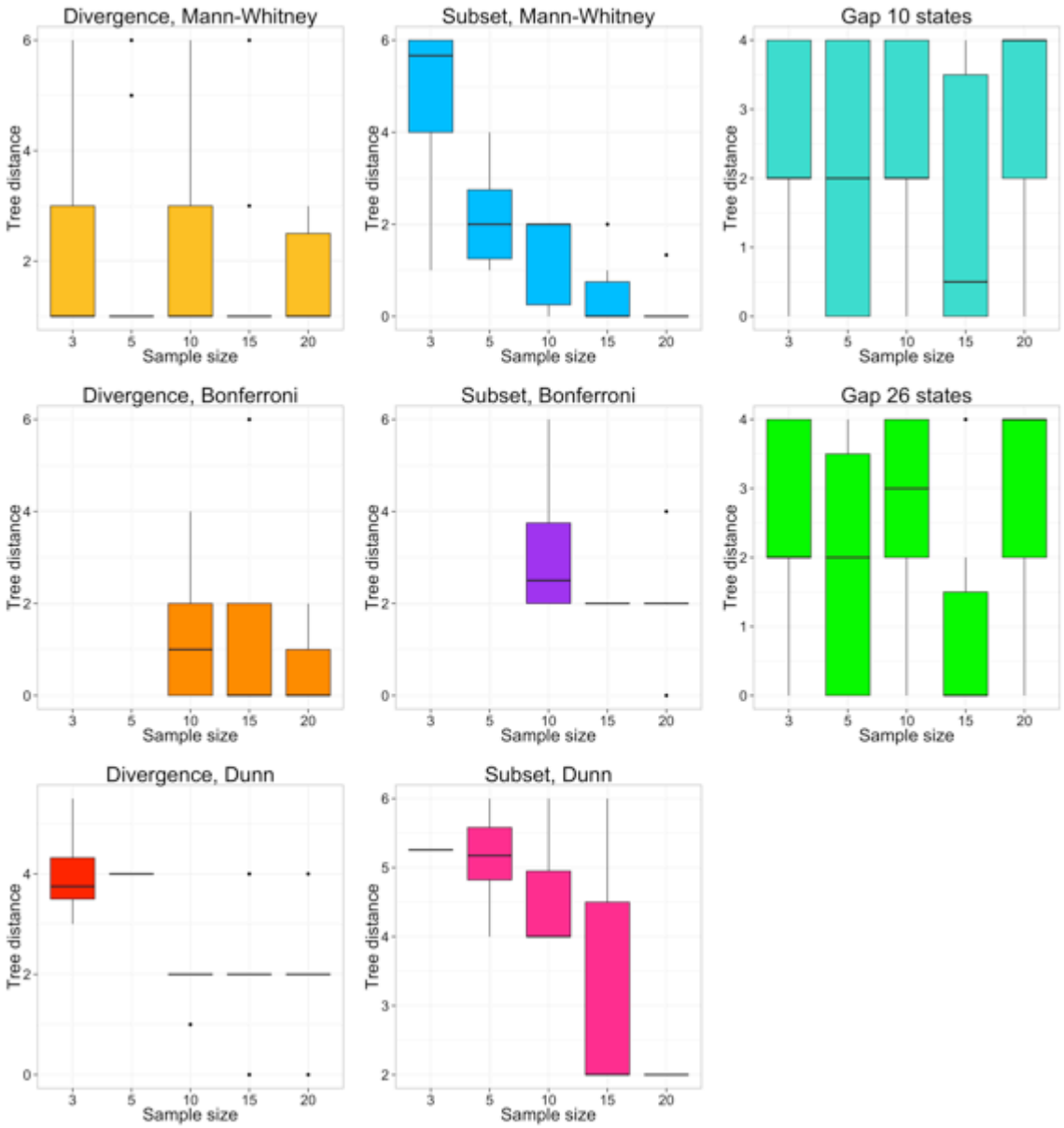

Figure 2.**8** **Boxplots of sample size versus tree distance.**
The scale on the y-axis varies across the different analyses.

2.4. Discussion

Reduced sample size affects the coding of morphological characters in hominoids, and the trees reconstructed, but the effect is strongly dependent on the coding method used. We found that reducing sample size had a major impact on phylogenetic reconstruction generally when divergence coding and subset coding were used but not when gap-weighting was utilized

(Table 2.2). With divergence coding and subset coding methods, reducing sample size led to a decrease in the number of parsimony-informative characters and a corresponding increase in the number of parsimony-uninformative characters. CI values subsequently increased with smaller samples in both of these coding methods. The impact of small samples differed in some cases for divergence coding and subset coding methods where tree length decreased with smaller samples in divergence coding, but increased with smaller samples in subset coding. In contrast, gap-weighting coding method was largely unaffected by reduction in sample size. There were no significant changes in CI and RI with different sample sizes when gap-weighting methods were used to code the character matrices.

Several researchers have preferred coding methods that rely on statistical tests for the rigour and less arbitrary nature of converting continuous measurements into discrete states (Rae 1998; Swiderski et al. 1998; Collard and Wood, 2000, 2001; Humphries 2002; Bjarnason et al. 2010). However, the findings of this study suggest that the reliance on statistical analyses is precisely the reason why divergence coding and homogeneous subset coding were most affected by sample sizes. In particular, when Bonferroni correction for multiple comparisons was carried out, datasets comprised of fewer than ten individuals per species could not be coded. In theory, these coding methods with statistical tests seem more preferable because the state assessment is less arbitrary. However, in order for these coding methods to be effective, there had to be at least ten individuals sampled per species in this dataset.

In contrast, gap-weighting was unaffected by the changes in sample size. Gap weighting divides the observed variation in craniodental measurements among the taxa into predetermined number of character states. Since the mean values of the measurements were taken for the taxa, the number of specimens sampled did not affect how the characters were coded. Given this method of assigning character states, gap-weighting was robust to the changes in the number of sample sizes compared to the master dataset. Garcia-Cruz and Sosa (2006) also found that gap-weighting was the best coding method in terms of overall performance for quantitative characters of plants in a parsimony analysis. They found that this method was preferable in comparison to several other coding methods, including simple gap coding, gap coding, a coding method using ANOVA, and a qualitative assessment of characters. Given this, and the tree distance tests reported above (Table 2.2, last column), gap-weighting may be a more suitable coding method when dealing with morphological data obtained using small samples of fossil hominin specimens.

The impact of the choice of character coding method on the outcome of phylogenetic reconstruction has not been explored in great detail in hominin phylogenetics to date. This issue has been addressed once, in a study conducted by Bjarnason et al. (2010). They found that matrices coded with gap coding produced trees that included clades congruent with the molecular clades of hominoids with higher bootstrap support values when using geometric morphometric data, while divergent coding was preferable when working with linear craniodental measurements. Based on these ambiguous results, Bjarnason et al. (2010) could not determine which of the two coding methods was more reliable to use with craniometric data of hominoids. In this study, we found that the effects of small sample sizes varied depending on the character coding method used. Our results suggest that gap-weighting is most resilient to the effects of small sample sizes, while both divergence and subset coding methods were often greatly affected by small sample sizes. This implies that the choice of character coding methods must be justified in light of the sample sizes and the type of data used in morphological phylogenetics of the fossil hominins.

There are a few implications for morphological phylogenetics in palaeoanthropology based on the results of this study. First, the use of fewer than ten specimens per species in phylogenetic studies is problematic when using divergence and subset coding methods. Hawks (2004) also highlighted small sample size as a potential problem in hominin phylogenetic analyses in a simulation study in which he found that only 12% of the true trees were the shortest when sample sizes varied between one to ten individuals among taxa. Similarly, Smith (2005) cautioned the use of small sample sizes in the context of diagnosing a new species and comparing the new species to small samples of comparative specimens. The reliance on small comparative samples leads to the difficulty in distinguishing between two interpretations: the new specimen represents a new species or an outlier of an existing species. A similar case can be made in the context of phylogenetic analysis especially with the use of three and five specimens per taxon as it became difficult to assess whether the character means were significantly different among taxa compared. There were fewer informative characters to reconstruct the relationships when using small sample sizes, and the consequence of this is that we may potentially lose useful phylogenetic information due to the reliance on small samples of fossil hominin specimens.

The second implication of this study is that the consistency index should not be used to evaluate the reliability of the tree when using small sample sizes. The CI is often reported in

phylogenetic studies of fossil hominins as a measure of how well the data fit the tree, but we were able to elevate the CI value by simply reducing sample sizes with divergence and subset coding methods. The increase in the CI values with small sample sizes was the result of having fewer parsimony-informative characters in the analysis, which reduced the conflicts among characters. In contrast, the Retention Index was not affected by small sample sizes in divergence coding and it dropped significantly with smaller sample sizes with subset coding. As such, the RI values may be better able to signal when analyses are affected by small sample sizes. This is consistent with what is known about these two summary statistics.

The results obtained in the present study indicate that we need to better understand how to use morphometric data when samples are small in palaeoanthropological datasets. Given that the choice of character coding methods strongly affected the impact of small sample sizes, future work should explore the use of morphological characters as continuous variables in phylogenetic analysis. Moreover, many of the craniodental characters used in hominin phylogenetic studies are continuous in nature, but they have been converted into discrete character states such as “small” or “large”. As such, the use of continuous characters directly in phylogenetic inference of hominin taxa should be investigated further. The use of continuous characters is possible in TNT* (Goloboff et al., 2000) under the parsimony framework and in BEAST2 (Drummond et al., 2012) under the Bayesian framework. Recently, a continuous character was used in a Bayesian phylogenetic analysis that was modeled to evolve under Brownian motion along with discrete morphological characters (Lee et al., 2014b). The use of continuous characters directly in phylogenetic analyses should eliminate the problems of using small sample sizes associated with some coding methods in transforming the morphological data into discrete character states. It will, of course, be necessary to evaluate the impact of small sample sizes on continuous-trait phylogenetic inference as well.

2.5. Conclusions

The samples used in hominin phylogenetic studies tend to be small, but it is normally assumed that the small size of the samples does not adversely affect the results of the phylogenetic analysis. Here, small sample sizes were often problematic when reconstructing the phylogenetic relationships of extant hominoids due to their impact on character coding, but this impact differed greatly among coding schemes. Thus, the use of coding methods that rely on

statistical methods to convert continuous measurements into discrete states were problematic, while the use of gap-weighting method was unaffected by changes in sample sizes. This suggests that gap-weighting may be the most suitable coding method when dealing with small samples. The findings of this study have important implications for phylogenetic reconstructions of hominin species. Many hominin taxa are represented by fewer than 20 individuals and it is not uncommon to find sample sizes of fewer than 10 individuals. Until more work is done on reconstructing phylogenies using continuous characters directly, we advocate gap-weighting for conversion, or the scoring of discrete characters directly.

Chapter 3.

Bayesian analysis of a morphological supermatrix sheds light on controversial fossil hominin relationships

This chapter explores the use of dated Bayesian phylogenetic inference to study the fossil hominin evolutionary relationships. It is reproduced with minor modifications from:

Dembo, M, Matzke, NJ, Mooers, AØ. and Collard M. 2015. Bayesian analysis of a morphological supermatrix sheds light on controversial fossil hominin relationships. *Proceedings of the Royal Society B* 282: 20150943.

3.1. Abstract

The phylogenetic relationships of several hominin species remain controversial. Two methodological issues contribute to the uncertainty—use of partial, inconsistent datasets and reliance on phylogenetic methods that are ill-suited to testing competing hypotheses. Here we report a study designed to overcome these issues. We first compiled a supermatrix of craniodental characters for all widely accepted hominin species. We then took advantage of recently developed Bayesian methods for building trees of serially sampled tips to test among hypotheses that have been put forward in three of the most important current debates in hominin phylogenetics—the relationship between *Australopithecus sediba* and *Homo*, the taxonomic status of the Dmanisi hominins, and the place of the so-called hobbit fossils from Flores, Indonesia in the hominin tree. Based on our results, several published hypotheses can be statistically rejected. For example, the data do not support the claim that Dmanisi hominins and all other early *Homo* specimens represent a single species, nor that the hobbit fossils are the remains of small-bodied modern humans one of whom had Down syndrome. More broadly, our study provides a new baseline dataset for future work on hominin phylogeny and illustrates the promise of Bayesian approaches for understanding hominin phylogenetic relationships.

KEY WORDS: human origins, phylogeny, Bayesian morphological analysis

3.2. Introduction

Determining humanity's place in nature has long been an important scientific challenge (Huxley, 1863). As a result of the genetic revolution and the development of formal methods of phylogenetic analysis, the relationship of our tribe (Hominini) to the living apes has been clarified: it is now accepted that hominins are most closely related to chimpanzees and bonobos, and that hominins and panins are more closely related to gorillas than to orangutans (Ruvolo, 1997; Gibbs et al., 2000). By contrast, there remains considerable debate about the relationships among the 20 or so species of hominin. While some relationships seem settled, others continue to be debated—vigorously in some cases (Strait et al., 2015).

Two methodological issues contribute to the uncertainty. One is inconsistency among datasets. Most studies have focused on either early hominins or later hominins (e.g. Kimbel et al. [2004] vs. Martinón-Torres et al. [2007]). Few analyses have included taxa that span the whole period of human evolution. In addition, different studies use different datasets. All studies have relied heavily on craniodental characters, but there is little agreement beyond that (e.g. Strait & Grine [2004] vs. Zeitoun [2009]). The other issue concerns how the datasets are analysed. To date, researchers have relied on parsimony methods to analyse hominin relationships. These methods are useful for generating trees but are not well suited to comparing alternative trees. As a consequence, there have been few attempts to formally evaluate the relative support for competing hypotheses.

Here we report a study of hominin relationships that was designed with both of these issues in mind. We first compiled a "supermatrix" (Kluge, 1989) that includes data for all widely accepted hominin species by collating data from 13 studies (Argue et al., 2009; Berger et al., 2010; Cameron and Groves, 2004; Cameron et al., 2004; Chang, 2005; Gilbert, 2008; Irish et al., 2013; Kimbel et al., 2004; Lordkipanidze et al., 2013; Martinón-Torres et al., 2007; Mounier et al., 2009; Strait and Grine, 2004; Zeitoun, 2009). Using a set of principles to reconcile among-study coding differences (see Material and methods), we amassed scores for 380 craniodental characters for 20 hominin species that span the entire 7 Myr history of our lineage. We also included data for two outgroups: *Pan troglodytes* and *Gorilla gorilla*. To the best of our

knowledge, the supermatrix is the largest qualitative character dataset ever assembled for the hominins.

Subsequently, we tested phylogenetic hypotheses with the supermatrix and a Bayesian method for joint estimation of the relationships of living and dated fossil taxa (Nylander et al., 2004; Pyron, 2011; Ronquist et al., 2012a; Bergsten et al., 2013, Lee et al., 2014a). Bayesian phylogenetic inference estimates the posterior probability distributions of a phylogeny and set of model parameters, given the data and a model of evolution (see Appendix B1). Competing phylogenetic hypotheses were converted into partially-constrained trees with fossil species as dated tips, and the relative support for these trees assessed with Bayes factors, which compare the marginal likelihoods of two sets of partially-constrained trees (Bergsten et al., 2013; Kass and Raftery, 1995). Including dated tips is advantageous because it constrains the search space and allows for more robust estimates of the rate of evolution (Lee et al., 2014a). Importantly for the analysis of fossil hominin taxa—most of which cannot be coded for all characters—ambiguity due to missing data leads to low Bayes factors, which indicate that the data cannot differentiate between trees.

We used Bayes factors to assess the support for the competing hypotheses that have been put forward in three important controversies concerning hominin relationships. The first focuses on whether the recently discovered species *Australopithecus sediba* is the ancestor of the genus *Homo* (Berger et al., 2010; Irish et al., 2013). The second concerns the systematics of the fossil hominins from the site of Dmanisi, Georgia (Gabunia et al., 2000; Gabounia et al., 2002; Rightmire et al., 2006; Martinón-Torres et al., 2008; Lordkipanidze et al., 2013; Bermúdez de Castro et al., 2014; Schwartz et al., 2014). The third is whether or not the so-called “hobbit” fossils from Liang Bua, Indonesia represent a distinct hominin species, and if they do, from which lineage they are descended (Aiello, 2015). For each controversy, we converted the hypotheses into tree models (see Figure B1 in Appendix B) and then compared the models’ marginal likelihoods. Only the relationships of the focal taxa were constrained to conform to their respective hypotheses; other species were allowed to move freely.

Our analyses show that several of the hypotheses that have been put forward regarding *Au. sediba*, the Dmanisi hominins, and the hobbits can be decisively rejected based on the available fossil evidence and the model of evolution employed. More broadly, our study provides

a new baseline dataset for future work on hominin phylogeny and illustrates the promise of Bayesian approaches for understanding hominin phylogenetic relationships.

3.3. Materials and methods

3.3.1. Morphological data

We created a supermatrix of craniodental characters that have been used to study hominin phylogeny (Argue et al., 2009; Berger et al., 2010; Cameron and Groves, 2004; Cameron et al., 2004; Chang, 2005; Gilbert, 2008; Irish et al., 2013; Kimbel et al., 2004; Lordkipanidze et al., 2013; Martinón-Torres et al., 2007; Mounier et al., 2009; Strait and Grine, 2004; Zeitoun, 2009). From the original studies, we recorded the fossil specimens used, the character definitions, any measurements, and the character states assigned to species. In some studies, character states were reported for individual specimens. In these cases, we adopted a 66% majority-rule to code the characters (following Gilbert [2008]). If 66% of the specimens of a given species exhibited a certain character state, that state was assigned to the species. Otherwise, the species was coded as polymorphic for the character.

We then concatenated the matrices. When the same character was used in multiple studies, the character state assessments from those studies were merged. In many cases, character scores were consistent across studies. However, when studies conflicted, we used the following criteria. First, we favoured assessments from studies that used larger samples of fossil specimens. Second, where studies differed, we preferred the more polymorphic designation for the taxon. Third, when the morphological feature was described using different numbers of character states in various studies, we preferred the simpler character scoring system. Lastly, when a conflict among studies could not be resolved based on the above criteria, the state assessments from the conflicted studies were combined and the taxon was coded as polymorphic for the character states in question. This approach to merging character matrices is conservative because it favours ambiguity wherever there is uncertainty in coding.

In total, we collected scores for 380 characters for 20 species of hominins and two outgroup species (*P. troglodytes* and *G. gorilla*).

3.3.2. Geological dates

For each fossil species, the oldest date associated with the specimens providing the morphological data was used. Thus, the dates may not necessarily correspond to the first appearance dates of the species. We dated tips in this manner to better link the scored character states with elapsed time. Dates used in this study are given in Table B1 in Appendix B.

3.3.3. Model selection

Because Bayesian methods of phylogenetic inference are model based, we had to choose a model of evolutionary change prior to testing the competing hypotheses. Starting with a base Markov k-state model (Lewis, 2001), which posits that characters switch among discrete states such that the probability of observing different states in a character is a truncated exponential function of time between observations, we evaluated several model parameters. Best-fit model parameters were identified with Bayes factors associated with the resulting trees. Here, a Bayes factor can be considered a measure of the strength of evidence in favour of one model over another, and is computed as twice the difference of the natural logs of the models' marginal likelihoods (see Appendix B1). Bayes factors are interpreted on the same scale as the log-likelihood ratio test (Kass and Raftery, 1995). Thus, a Bayes factor of 6 is regarded as 'strong evidence' (Kass and Raftery, 1995). It suggests that the better tree fits the data more than 400 times better than the other tree, and is comparable to a *p*-value rejecting the alternative tree of less than 0.02. The model selection procedure was carried out in the program MrBayes 3.2.3 (Ronquist et al., 2012b) via the CIPRES Science Gateway v.3.3 (Miller et al., 2010).

(i) Character sampling

With morphological data, characters chosen for analysis are normally those that are phylogenetically informative (Ronquist et al., 2012b). Characters with no change or change in only one species are often excluded. We corrected for this bias by calculating conditional likelihoods based only on phylogenetically informative characters (Ronquist et al., 2012b). The model with this correction was strongly preferred over the model in which no bias correction was implemented (BF=761.02).

(ii) Rate variation

The craniodental characters used in the present study potentially evolved at different rates. Among-character rate heterogeneity can be modelled by allowing different characters to have different evolutionary rates. Use of a gamma model for rate heterogeneity was favoured over use of a model with no rate variation (BF=11.58).

(iii) Clock rates

Because fossil species are treated as non-contemporaneous tips, the ages of the fossil specimens can be used to calibrate the rate of evolutionary change, resulting in branch lengths that are proportional to time (Ronquist et al., 2012a). There are several options for specifying how the time and rate of evolutionary changes are modelled. A strict clock assumes a constant rate of change throughout the tree (Zuckerkandl and Pauling, 1962). Relaxed-clock models allow the rate of change to vary across the branches. With the autocorrelated relaxed clock (Thorne and Kishino, 2002), the rate of change evolves through time such that the descendant nodes evolve at a rate that is sampled from a distribution centered on the inferred rate of the ancestral branch. With the uncorrelated relaxed clock (Drummond et al., 2006), the rate for each branch is sampled from a distribution specified by the user. In the present study, rates were drawn from an exponential distribution. The uncorrelated relaxed clock model was strongly preferred over the strict clock model (BF=62.88), and the uncorrelated relaxed clock model was preferred over the auto-correlated relaxed clock model clock (BF=33.26).

(iv) Priors on node times

The use of a relaxed-clock model requires a prior distribution on node times. The uniform prior assumes that the time at a particular node has equal probability across the interval between the time of its parent node and its oldest daughter node. The birth-death prior assumes that lineages speciate and go extinct according to a stochastic process with parameters for speciation and extinction. The latter was preferred over the former (BF=11.12).

3.3.4. Analyses

Having evaluated potential model parameters, we proceeded to the analysis of the craniodental data. Based on the results of the model parameter evaluation exercise, characters were modelled to evolve under a Markov-k model with a gamma-distributed among-character rate variation, correcting for the sampling bias for parsimony-informative characters. Of the 380 characters, 281 were treated as unordered and 99 as ordered. The uncorrelated clock-model was implemented to calibrate the tree with fossil hominins as noncontemporaneous tips, and the birth-death model was used as the prior on node times. The oldest dates associated with the specimens in the taxa were assigned as fixed ages for the terminal tips.

To generate a best estimate of hominin phylogeny, we performed four independent runs, each with 10 million Markov chain Monte Carlo (MCMC) generations. Each run consisted of one cold and three heated chains; the cold chain was sampled every 1000 generations. We assessed convergence of the four runs using MrBayes's convergence diagnostics. The first 25% of the sampled trees were discarded as burn-in.

Subsequently, sets of competing trees were constructed (figures B2-4 in Appendix B). Stepping-stone sampling (Fan et al., 2011; Xie et al., 2011) was used to estimate the marginal likelihoods of the tree models. In each 'step', MCMC was conducted for 196 000 generations and samples were taken every 1000 generations. We used a total of 50 steps. The first step was discarded as burn-in, as were the first 49 000 generations from all subsequent steps. For each tree tested, we performed four independent runs, as per the preceding analysis. The marginal likelihoods were used to calculate Bayes factors in a series of tests in which the tree with the best marginal likelihood estimate was compared to the hypothetical trees in a pairwise manner.

The analyses were carried out in the program MrBayes (Ronquist et al., 2012b) via the CIPRES Science Gateway v.3.3 (Miller et al., 2010). Additional background on the analyses is provided in electronic supplementary material in Appendix B.

3.4. Results and discussion

A summary of the best trees we obtained is presented in figure 3.1 (see also figure B4 and table B2 in Appendix B). The tree captures most widely-accepted relationships, and the

posterior probabilities are comparable to those obtained in other Bayesian phylogenetic studies with a high percentage of fossil taxa (Lee et al., 2014a).

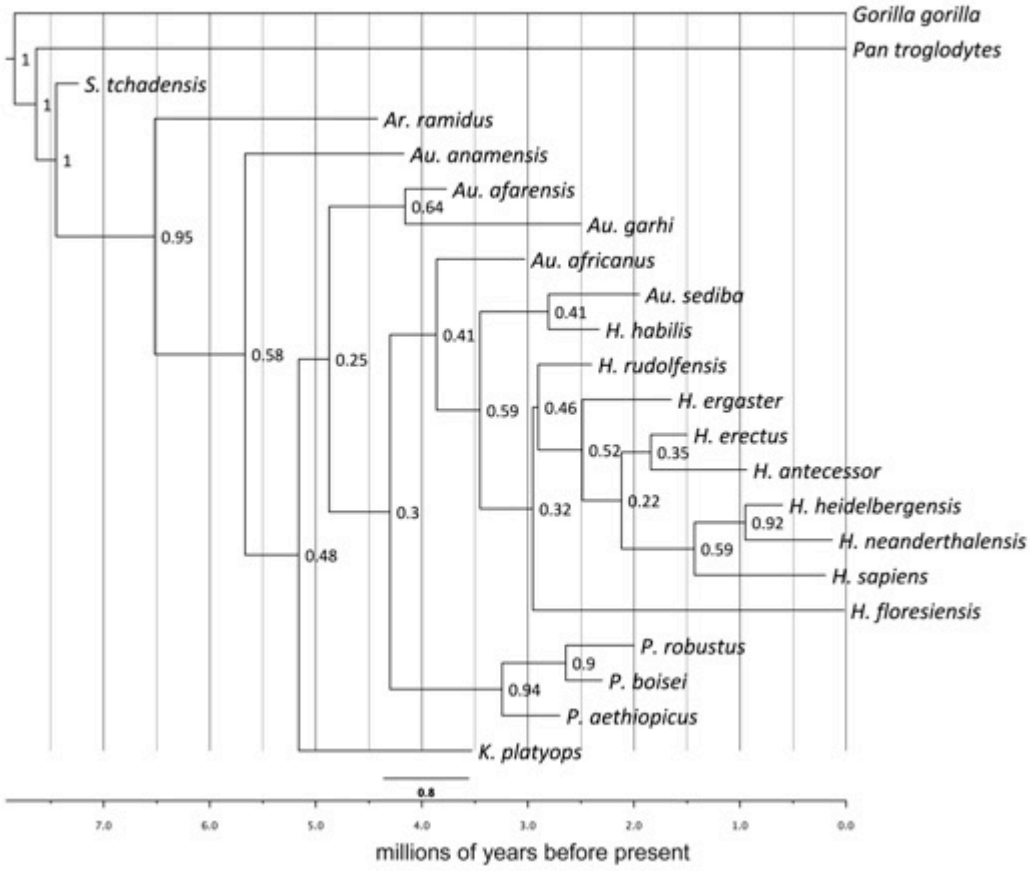

Figure 3.1 Summary of best trees obtained in the dated Bayesian analysis.
The posterior probability values for the clades are indicated. See figure B4 and table B2 in Appendix B for more details.

3.4.1. *Australopithecus sediba* and the origin of genus *Homo*

In 2010, Berger and co-workers (Berger et al., 2010; Pickering et al., 2011) reported the discovery of 1.97 Ma fossil hominins from Malapa, South Africa. These fossils have a unique combination of morphological features, some of which are shared with the australopiths and others with early *Homo*. In light of this, Berger et al. (2010) assigned the fossils to a new species, *Au. sediba*.

Berger et al. (2010) outlined four competing hypotheses regarding the relationships of *Au. sediba*, and then tested them with a parsimony analysis of 69 craniodental characters. The hypotheses differ in how *Au. sediba* is related to the members of genus *Homo*, especially the three earliest members, *H. habilis*, *H. rudolfensis*, and *H. erectus*. Berger et al.'s parsimony analysis yielded a single most parsimonious tree in which *Au. sediba* was the sister taxon of a clade consisting of all the species of *Homo*, which Berger et al. took to be evidence that *Au. sediba* is affiliated with *Homo* and may actually be its ancestor.

Subsequently, several researchers (Balter, 2010; Kimbel, 2013) challenged the putative link between *Au. sediba* and *Homo*. They argued that *Au. sediba* likely arose from the much better known South African australopith *Au. africanus,* and then went extinct without issue. This hypothesis was supported by a parsimony analysis of dental characters conducted by Irish et al. (2013). These authors obtained a single shortest tree in which *Au. sediba* was the sister taxon of *Au. africanus*, and the (*Au. sediba* and *Au. africanus*) clade was the sister taxon of *Homo*.

The partially-constrained trees we used to represent these hypotheses are shown in figure B2 in Appendix B. Three hypotheses have low support and can be rejected (Table 3.1). There is strong evidence to reject the tree in which *Au. sediba* and *Au. africanus* are sister taxa (BF=16.42), the one in which *H. habilis* is the sister taxon of a clade comprising *Au. sediba, H. rudolfensis*, *H. erectus*, and later *Homo* (BF=9.22), and the one in which *H. rudolfensis* is the sister taxon of a clade comprising *Au. sediba, H. habilis, H. erectus*, and later *Homo* (BF=7.68). Of the remaining hypotheses, the best supported is the one in which *Au. sediba* is the sister taxon of a clade comprising all *Homo* species. Thus, our analysis does not support the hypothesis that *Au. sediba* arose from *Au. africanus* and died out without issue (Balter, 2010; Kimbel, 2013; Irish et al., 2013). Rather, it is consistent with Berger et al.'s (2010) conclusion that *Au. sediba* groups with *Homo* and may be its ancestor.

Our best-supported tree has some important implications. To begin with, all genus concepts used in palaeoanthropology agree that genera should be monophyletic (Collard and Wood, 2015), and so *Au. sediba* does not belong in the genus *Australopithecus*. The species could be assigned to *Homo*, or given its own genus name, depending on the importance accorded to maximizing information content in taxonomic names (Collard and Wood, 2015). A second implication is that the current first appearance date for *Au. sediba* is substantially too young. Because sister lineages have to be the same age, the lineage leading to *Au. sediba* must

be either the same age or older than the oldest *Homo* specimen. Currently, the earliest specimen that is widely accepted to belong to *Homo* dates to 2.5-2.3 Ma (Schrenk et al., 2015). A recent discovery may push this date back to 2.8 Ma (Villmoare et al., 2015). Thus, the *Au. sediba* lineage must be at least 300 000-500 000 years older than the current hypodigm suggests, and may be as much as 800 000 years older. Lastly, the best-supported tree has implications for the place of origin of *Homo*. It is widely believed that East Africa was the locus of early hominin evolution, and that species dispersed from there to other regions (Strait, 2013). However, some have argued that genus *Homo* originated in South Africa (Curnoe, 2010). *Australopithecus sediba* is only known from South Africa at the moment, so our best-supported tree is consistent with this alternative hypothesis.

Table 3.1 Results of the Bayes factor analyses regarding *Au. sediba*

Results of Bayes factor analyses carried out to compare phylogenetic hypotheses regarding *Au. sediba* and the species of genus *Homo.* Numbers refer to Appendix B, figure B2.

Hypothesis	Marginal log likelihood	Bayes factor	Interpretation
1a. Ancestor to *H. habilis*	-2122.00	7.68	Strong evidence to reject model
1b. Ancestor to *H. rudolfensis*	-2122.77	9.22	Strong evidence to reject model
1c. Ancestor to *H. erectus*/*ergaster*	-2119.74	3.16	Evidence not strong enough to reject model
1d. Ancestor to genus *Homo*	-2118.16	--	Best model
1e. Descendant of *A. africanus*	-2126.37	16.42	Strong evidence to reject model

3.4.2. Systematics of the Dmanisi hominins

Since the early 1990s, the site of Dmanisi in Georgia has yielded a number of important early *Homo* specimens (Gabunia and Vekua, 1995; Gabunia et al., 2000; Gabounia et al., 2002; Vekua et al., 2002; Lordkipanidze et al., 2005, 2007, 2013). Dating to 1.85 Ma (Ferring et al., 2011), these are the oldest hominin remains outside of Africa.

Several hypotheses regarding the systematics of the Dmanisi hominins have been put forward. These hypotheses differ in relation to the number of species represented among the Dmanisi hominins, and the Dmanisi hominins' relationships with *H. habilis*, *H. rudolfensis*, Asian *H. erectus*, and early African *H. erectus* (sometimes called *H. ergaster*). One suggestion is that the Dmanisi specimens represent an early lineage of *H. erectus* that descended from *H. habilis* or a *H. habilis*-like species and is ancestral to both Asian *H. erectus* and early African *H. erectus* (Rightmire et al., 2006). Another proposal is that the Dmanisi specimens are more closely related to early African *H. erectus* than to *H. habilis*, *H. rudolfensis*, or Asian *H. erectus* (Gabunia et al., 2000). A third hypothesis is that the Dmanisi hominins represent a new species, *Homo georgicus*, that is descended from *H. habilis* and *H. rudolfensis*, and which gave rise to early African *H. erectus* (Gabounia et al., 2000).

More radical proposals have also been made. Lordkipandze et al. (2013) have argued that the taxonomy of early *Homo* needs to be simplified in light of the Dmanisi sample, and have suggested that the Dmanisi hominins, Asian *H. erectus*, early African *H. erectus*, *H. rudolfensis*, and *H. habilis* should all be assigned to a single species. In diametric opposition to Lordkipandze et al. (2013), Martinón-Torres et al. (2008) have argued on the basis of the mandibles from the site, that the Dmanisi sample includes the remains of two *Homo* species. They contend that the small mandibles represent a species that is close to the node from which early African *H. erectus*, Asia *H. erectus*, and later *Homo* species originated, while a large mandible, D2600, belongs to a different species. Bermúdez de Castro et al. (2014) have also suggested that the small mandibles represent one species and D2600 another, but they contend that the species represented by the small mandibles is closely related to just *H. habilis* and early African *H. erectus*.

We tested all of these hypotheses (Appendix B figure B3; Table 3.2). The support for three of them is so low that they can be rejected. There is strong evidence to reject Lordkipanidze et al.'s (2013) hypothesis that there is just one species of early *Homo* (BF=18.98). We can also reject the *H. georgicus* hypothesis (BF=6.28) and Bermúdez de Castro et al.'s (2014) version of the two species hypothesis (BF=9.04). However, the remaining three cannot be rejected. Of these, the one with the highest marginal likelihood is based on Martinón-Torres et al.'s (2008) two species hypothesis.

Lordkipanidze et al.'s (2013) "one species of early *Homo*" hypothesis is based on the results of a geometric morphometrics analysis of overall cranial shape. Their analysis indicated that the variation in the Dmanisi hominin cranial sample exceeds the variation in a combined sample of *H. habilis*, *H. rudolfensis*, early African *H. erectus*, and Asian *H. erectus* crania. Lordkipanidze et al. (2013) argued that this must mean that *H. habilis*, *H. rudolfensis*, early African *H. erectus*, and Asian *H. erectus* belong to the same species as the Dmanisi specimens. This hypothesis was immediately criticized by Spoor (2013), and has since been challenged by other researchers (Schwartz et al., 2014; Collard and Wood, 2015). One concern of the critics is that many of the features that have been used to distinguish *H. habilis*, *H. rudolfensis*, early African *H. erectus*, and Asian *H. erectus* were not captured in Lordkipanidze et al.'s (2013) analysis of overall cranial shape (Schwartz, 2000; Schwartz et al., 2014; Collard and Wood, 2015). Critics have also highlighted the inability of Lordkipanidze et al.'s (2013) landmarks to distinguish between a Neanderthal cranium and Dmanisi Skull 4 in their analysis. Because these specimens are separated in time by more than 1.5 million years and are widely accepted to belong to separate species, it has been argued that the landmarks are inadequate for assessing the limits of fossil hominin species (Collard and Wood, 2015). The results of our analyses also go against Lordkipanidze et al.'s hypothesis.

Table 3.2 Results of the Bayes factor analyses regarding the Dmanisi hominins

Results of Bayes factor analyses carried out to compare phylogenetic hypotheses regarding the Dmanisi fossils. Numbers refer to electronic supplementary material, figure B3.

Hypothesis	Marginal log likelihood	Bayes factor	Interpretation
2a. Rightmire et al. (2006)	-2258.95	4.00	Evidence not strong enough to reject model
2b. Gabunia et al. (2000)	-2259.21	4.52	Evidence not strong enough to reject model
2c. Gabounia et al. (2002)	-2260.09	6.28	Strong evidence to reject model
2d. Lordkipanidze et al. (2013)	-2266.44	18.98	Strong evidence to reject model
2e. Martinón-Torres et al. (2008)	-2256.95	--	Best model
2f. Bermúdez de Castro et al. (2014)	-2261.47	9.04	Strong evidence to reject model

Another implication of our results is that more attention should be paid to the idea that there are two species represented among the Dmanisi hominins. The possibility that the Dmanisi hominin sample includes the remains of more than one species has been raised a number of times (Schwartz, 2000; Skinner et al., 2006; Martinón-Torres et al., 2008; Bermúdez de Castro, 2014; Schwartz et al., 2014), but has not yet been taken seriously (Gabounia et al., 2002; Rightmire et al., 2006; Zollikofer et al., 2014). The Bayes factor support for Martinón-Torres et al.'s (2008) hypothesis suggests the two-species hypothesis deserves closer scrutiny. Skinner et al. (2006) examined height and breadth variation in the Dmanisi mandibles and found that they exhibit more variation in corpus shape, corpus height, and overall mandible size than any extant ape species. Martinón-Torres et al. (2008) noted that the D2600 mandible has the primitive pattern of molar size gradient whereas the rest of the Dmanisi mandibles have the derived pattern. This morphological evidence has generally been viewed as less compelling than the geological evidence, which is usually interpreted as indicating that the fossils recovered at the site were deposited within a few centuries and have not moved very far (Zollikofer et al., 2014). Our results suggest that alternative scenarios should be considered. For example, Bermúdez de Castro et al. (2014) argue that the stratigraphic context of the hominin fossils is more complex than is usually presented, and that the hominin fossils could in fact have been re-deposited from sediments of different age. Even if the fossils have not moved, Schwartz et al. (2014) have argued that a window of several hundred years would provide "ample time" for faunal migration and/or replacement.

3.4.3. What is *H. floresiensis?*

In 2004, a team led by the late Mike Morwood reported the discovery of fossil hominins on Flores, Indonesia (Brown et al., 2004; Morwood et al., 2004). These fossils, dated to 17-74 kya, were discovered at the cave site of Liang Bua, along with fossilized animal remains and stone tools (Morwood et al., 2004; Roberts et al., 2009). The hominins included a relatively complete skeleton, LB1, and the remains of at least nine other individuals (Morwood and Jungers, 2009). These fossils possess a unique combination of primitive and derived features. Like the australopiths, they were small-bodied (estimated stature of 106 cm with body mass of 16-29 kg) and small-brained (380-426 cc) (Brown et al., 2004; Kubo et al., 2013). However, other cranial features resemble *Homo* (Brown et al., 2004; Kaifu et al., 2011). Based on this

mosaic morphology, the team assigned the fossils to a new species called *Homo floresiensis*, and argued that it is a dwarfed descendant of *H. erectus* (Brown et al., 2004).

Debate about the nature of the Liang Bua hominin fossils has raged over the past decade. Immediately following the announcement of the Flores discovery, it was suggested that the Liang Bua hominin fossils do not represent a new species, but rather are a group of small-bodied *H. sapiens*, one of whom, LB1, was afflicted with microcephaly (Henneberg and Thorne, 2004). Several other pathological diagnoses have been put forward since (Aiello, 2015). Most recently, some of the proponents of the original pathological hypothesis have argued that LB1 had Down syndrome (Henneberg et al., 2014). Other researchers have accepted Morwood et al.'s assessment that the fossils represent a new hominin species but have questioned the idea that *H. floresiensis* is descended from *H. erectus* (Argue et al., 2009; Brown and Maeda, 2009). Argue et al. (2009) argue that *H. floresiensis* is a descendant of an early *Homo* species that preceded *H. erectus,* such as *H. habilis* or *H. rudolfensis*. Brown and Maeda (2009) contend that *H. floresiensis* could be descended from an australopith species rather than a species of early *Homo*.

We created six partially-constrained trees to test these hypotheses (Appendix B figure B4; Table 3.3). Based on the Bayes factor tests, we can reject the tree in which *H. floresiensis* is the sister taxon of *H. sapiens* (BF=7.96), and the one in which *H. floresiensis* is the sister taxon of *Au. africanus* and *Paranthropus* (BF=8.74). The remaining trees could not be rejected. Of these trees, the best supported is the one in which *H. floresiensis* is constrained to fall on the branches leading to *H. habilis* and *H. rudolfensis*, but not the branches leading to the other *Homo* species.

The rejection of the tree in which *H. floresiensis* is the sister taxon of *H. sapiens* means our data do not support the latest pathology hypothesis. An obvious potential concern about this is that our *H. sapiens* sample does not include any Down syndrome individuals. However, this is not in fact a problem. Henneberg et al. (2014) used 17 skeletal characters to diagnose LB1 with Down syndrome. None of these characters is among the 43 characters in our supermatrix for which we have data for the Liang Bua hominins. Thus, the results of the Bayes factor tests are independent of Henneberg et al.'s assessment of the health status of LB1. Even if their diagnosis of LB1 were correct, it would not alter our results. This is because the Down syndrome hypothesis contends that the Liang Bua hominin fossils are the remains of modern humans, one

of whom, LB1, had Down syndrome. For this hypothesis to be correct, LB1 must have characters that are diagnostic of Down syndrome, and LB1 and the other Liang Bua hominins must also exhibit characters that align them with *H. sapiens*. Henneberg et al. concentrated on trying to demonstrate that LBI has characters that are diagnostic of Down syndrome (Henneberg et al., 2014), but they failed to identify any characters aligning the fossils to *H. sapiens*. Henneberg et al. are not alone in this. None of the proponents of the pathology hypotheses has identified characters that align the Liang Bua hominins with *H. sapiens* (Henneberg and Thorne, 2004; Hershkovitz et al., 2007; Obendorf et al., 2008). Thus, our results are not particularly surprising. No data support the hypothesis that the Liang Bua hominins are *H. sapiens*, regardless of the health status of LB1.

Table 3.3 Results of Bayes factor analyses regarding *H. floresiensis*

Results of Bayesian factor analyses carried out to compare phylogenetic hypotheses regarding the status of *H. floresiensis*. Numbers refer to electronic supplementary material, figure B4.

Hypothesis	Marginal log likelihood	Bayes factor	Interpretation
3a. Descendant of *H. erectus*	-2118.12	3.70	Evidence not strong enough to reject model
3b. Pathological *H. sapiens*	-2120.25	7.96	Strong evidence to reject model
3c. Descendant of early *Homo*	-2116.27	--	Best model
3d. Descendant of *Australopithecus*	-2120.64	8.74	Strong evidence to reject model
3e. Descendant of early hominin 1	-2118.15	3.76	Evidence not strong enough to reject model
3f. Descendant of early hominin 2	-2119.17	5.80	Evidence not strong enough to reject model

While the data we currently have for *H. floresiensis* are unable to distinguish among the various “the hobbits are early hominins” hypotheses, it is interesting that the best supported of the trees that we tested is the one in which *H. floresiensis* was constrained to fall on the branches leading to *H. habilis,* and *H. rudolfensis*. This suggests that *H. floresiensis* is a descendant of pre-*H. erectus* small-bodied hominins that migrated out of Africa and made it to Southeast Asia (Brown and Maeda, 2009; Morwood and Jungers, 2009). A corollary of this is

that our understanding of hominin colonization of Eurasia may require revision. The current consensus is that *H. erectus* was the first hominin species to migrate out of Africa and did so shortly after 2 Ma. A pre-*H. erectus* origin for *H. floresiensis* implies that an earlier *Homo* was the first species of hominin to leave Africa. A pre-*H. erectus* origin for *H. floresiensis* also raises the possibility that *H. erectus* evolved in Asia rather than in Africa (Dennell, 2009).

3.5. Conclusion

The study reported here is the first to use Bayesian phylogenetic analysis to evaluate competing hypotheses concerning the relationships of the fossil hominins. Based on our results, the utility of the approach for the investigation of hominin phylogeny seems clear. Our analyses show that a number of hypotheses that have been put forward in three important on-going debates can be rejected unequivocally, thereby reducing the scope of the disagreement in each case and moving the field forwards. Given this, we suggest that the Bayesian framework should be adopted to systematically evaluate other phylogenetic debates in palaeoanthropology. The approach improves objectivity because the statistical results are replicable given a dataset and model.

Improved models might well alter confidence in the inferences made here, and this is one place where further research should be focused, as the Bayesian framework also allows alternative (e.g. simpler versus more complex) models to be formally compared. We need fine-grained information on skeletal development such that covariation among characters due to common developmental pathways and allometric constraints can be tested for and accommodated. With such data, more complex scenarios of character evolution—such as rates that (co-)vary not only among characters, but also in different parts of the tree (Pagel and Meade, 2008)—can also be modelled.

Although improved models are necessary, our primary recommendation concerns the data used to evaluate fossil hominin phylogenetic relationships. While we believe our supermatrix is the largest qualitative dataset ever compiled for the fossil hominins, it only contains characters of the skull. The omission of postcranial data needs to be rectified. Given that morphological analyses of the postcranial remains of *H. floresiensis* have found similarities to extant apes, australopiths, and early *Homo* (Tocheri et al., 2007; Jungers et al., 2009), there

is reason to believe that the inclusion of postcranial data may allow us to discriminate between the various “the hobbits are early hominins” hypotheses for *H. floresiensis*. Including postcranial data should also improve our ability to test between the remaining hypotheses concerning *Au. sediba* and the Dmanisi hominins. More generally, there is a need for palaeoanthropologists to develop, and commit to using, a common character state dataset for the investigation of fossil hominin phylogeny, as has been achieved in various “Tree of Life” projects. This dataset must include data for all generally accepted species and all widely used characters. In addition, characters and their states must be rigorously defined, and the relationship between the states assigned to species and the hypodigms of the species must be clear. Continued use of partial, poorly defined character state data matrices should be avoided.

3.6. Acknowledgements.

We thank the members of HESP and FAB* at SFU, as well as Yoel Rak, Charles Roseman, and Bernard Wood for helpful comments and suggestions. We are grateful to Norman Macleod, Marta Mirazon Lahr, Kieran McNulty, and an anonymous reviewer for constructive comments on an earlier version of this manuscript. Our work was supported by the Canada Research Chairs Program, the Canada Foundation for Innovation, the British Columbia Knowledge Development Fund, NSERC Canada, the National Institute for Mathematical and Biological Synthesis, NSF, the University of Tennessee, Knoxville, and Simon Fraser University.

Chapter 4.

The evolutionary relationships and age of *Homo naledi*: an assessment using dated Bayesian phylogenetic methods

This chapter explores the phylogenetic placement of a newly discovered species, *Homo naledi*. It is reproduced from a manuscript accepted for publication in *Journal of Human Evolution*:

Dembo, M., Radovčić, D., Garvin, H.M., Laird, M.F., Schroeder, L., Scott, J.E., Brophy, J., Ackermann, R.R., Musiba, C.M., de Ruiter, D.J., Mooers, A. Ø., Collard, M. The evolutionary relationships and age of *Homo naledi*: an assessment using dated Bayesian phylogenetic methods. Journal of Human Evolution. In press.

4.1. Abstract

Homo naledi is a recently discovered species of fossil hominin from South Africa. A considerable amount is already known about *H. naledi* but some important questions remain unanswered. Here we report a study that addressed two of them: "Where does *H. naledi* fit in the hominin evolutionary tree?" and "How old is it?" We used a large supermatrix of craniodental characters for both early and late hominin species and Bayesian phylogenetic techniques to carry out three analyses. First, we performed a dated Bayesian analysis to generate estimates of the evolutionary relationships of fossil hominins including *H. naledi*. Then we employed Bayes factor tests to compare the strength of support for hypotheses about the relationships of *H. naledi* suggested by the best-estimate trees. Lastly, we carried out a resampling analysis to assess the accuracy of the age estimate for *H. naledi* yielded by the dated Bayesian analysis. The analyses strongly supported the hypothesis that *H. naledi* forms a clade with the other *Homo* species and *Australopithecus sediba*. The analyses were more ambiguous regarding the position of *H. naledi* within the (*Homo*, *Au. sediba*) clade. A number of hypotheses were

rejected, but several others were not. Based on the available craniodental data, *Homo antecessor*, Asian *Homo erectus*, *Homo habilis*, *Homo floresiensis*, *Homo sapiens*, and *Au. sediba* could all be the sister taxon of *H. naledi*. According to the dated Bayesian analysis, the most likely age for *H. naledi* is 912 ka (thousands of years ago). This age estimate was supported by the resampling analysis. Our findings have a number of implications. Most notably, they support the assignment of the new specimens to *Homo*, cast doubt on the claim that *H. naledi* is simply a variant of *H. erectus*, and suggest *H. naledi* is younger than has been previously proposed.

Keywords: Dinaledi hominins; Bayesian phylogenetic analysis; morphological clock; genus *Homo*

4.2. Introduction

In late 2013 the fossilized remains of several hominin individuals were recovered from the Dinaledi chamber of the Rising Star cave system in the Cradle of Humankind World Heritage Site near Johannesberg, South Africa (Berger et al., 2015). Analyses of the craniodental and postcranial morphology of these individuals suggest that they share similarities with several species of *Homo*, including *Homo habilis*, *Homo rudolfensis, Homo erectus*, and *Homo heidelbergensis*, but are distinct enough to be assigned to a new species, which Berger et al. (2015) have named *Homo naledi*. So far it has not proved possible to obtain a radiometric or biostratigraphic date for *H. naledi* (Berger et al., 2015).

The discovery of a new hominin species raises a number of questions. One of the most important of these is “Where does the new species fit in the hominin evolutionary tree?” The answer to this question has the potential to not only shed new light on which species are our direct ancestors and which are our collateral relatives, but also illuminate the processes involved in hominin evolution. For example, phylogenetic analyses have shown that convergence has been an important factor in the evolution of the hominin skull (see e.g., Skelton and McHenry, 1992). In addition, the placement of a new species in the hominin evolutionary tree has taxonomic implications because most genus concepts hold that genera should be monophyletic (Collard and Wood, 2015).

Here, we report the first analysis of the phylogenetic relationships of *H. naledi*. Normally, palaeoanthropologists rely on maximum parsimony analysis to reconstruct hominin phylogenetic relationships (see e.g., Skelton and McHenry, 1992; Strait et al., 1997; Smith and Grine, 2008). However, while maximum parsimony analysis is useful for generating trees, it is not well suited to formally evaluating the relative support for different hypotheses of phylogenetic relationships, especially when fossil taxa are involved. With this in mind, we employed a relatively new, Bayesian inference-based method of phylogenetic analysis that allows phylogenetic hypotheses to be compared in a straightforward manner and with statistical rigor (Nylander et al., 2004; Pyron, 2011; Bergsten et al., 2013; Lee et al., 2014a; Dembo et al., 2015). The Bayesian method of phylogenetic analysis (Rannala and Yang, 1996; Yang and Rannala, 1997) has been increasingly widely used over the last two decades to infer the relationships of extant organisms (see review by Huelsenbeck et al., 2008). Recently, its use has been extended to the study of the phylogenetic relationships of extinct taxa (Lee et al., 2014a), including fossil hominins (Dembo et al., 2015).

The Bayesian method of phylogenetic analysis differs from maximum parsimony analysis in several respects. One difference concerns the treatment of character state changes. Maximum parsimony assumes that each character evolves via its own evolutionary process and therefore has its own rate of change along every branch of the tree (Steel and Penny, 2000). In contrast, common Bayesian methods require a single explicit model of character state change for all characters. The approaches also differ in relation to geological dates. In the maximum parsimony framework, geological dates can only be used a posteriori, by comparing the congruence of candidate trees and the stratigraphic record (Fisher, 2008). In contrast, geological dates can be used in the Bayesian framework to inform the expected amount of change leading to dated taxa at the inference stage (Ronquist et al., 2012a). A third crucial difference is the way in which trees are evaluated. Maximum parsimony relies on a single number—the minimum number of changes required to explain the observed differences. In the Bayesian approach, in contrast, trees are assessed and compared based on their posterior probability of being true given the data and the assumptions of the model of evolutionary change, with trees of higher probability being preferred. A recent simulation study showed that the Bayesian phylogenetic approach outperforms maximum parsimony when applied to discrete characters that are evolving at a high rate and when there are missing data (Wright and Hillis, 2014). Therefore, while further work is required to improve the model of the evolution of morphological data (see

Discussion), Bayesian analysis can be expected to often produce more reliable hypotheses of relationship than maximum parsimony analysis.

Within the Bayesian framework, obtaining the posterior probability of a tree involves solving the following equation:

$$P(T,\theta|\,X) = \frac{P(X|T,\theta)P(T,\theta)}{P(X)} \quad \text{(Equation 1)}$$

where P(T,θ|X) represents the posterior probability of a particular tree (T) and the parameters (θ) given the data (X). The first term on the right, P(X|T,θ), is the likelihood function, which is the probability of observing the data given the candidate tree (T) and attendent parameters (θ). The second term, P(T,θ), is the prior probability of the tree and the parameters. P(X) is the probability of the data across all possible trees and parameter values. For the second term in the numerator, we usually have few prior beliefs, and so most candidate trees and parameter values will be given equal prior probabilities. The term in the denominator is required because a Bayesian phylogenetic analysis returns a point probability for each tree and set of parameter values. The sum of these point probabilities across all possible trees and parameter values must equal 1.0. Unfortunately, we cannot calculate the overall probability of the data needed to calculate the posterior probabilities, because there is a near infinite number of possible combinations of trees and parameter values. Therefore, the posterior probabilities needed to evaluate trees (i.e., the entire right-hand side of equation 1) are approximated using a sampling procedure known as the Markov chain Monte Carlo (MCMC) method (Yang and Rannala, 1997).

The MCMC method estimates the posterior probability of a tree as its frequency in a distribution of trees. Trees are evaluated and retained in this distribution in an iterative manner: a new tree or set of parameter values is proposed, and the resulting likelihood is multiplied by the prior probability of the tree and associated parameter values. The product is then compared to the corresponding value of the previously retained tree. If the fit to the data is better than that of the previous tree, the new tree and/or set of parameter values is retained. If it is worse, it is retained in proportion to how much worse it is (e.g., a topology that is 10X worse would only have a one in ten chance of being retained). Every time a new or unchanged tree is retained, the process is said to have produced a “generation” in a “chain” and the retained tree becomes the tree for comparison in a subsequent step. This is usually done over millions of steps, with good

combinations of trees and parameter values being retained at high frequencies in the sample, suboptimal ones retained at lower frequency, and very poor ones ignored. Multiple chains can be constructed and compared in parallel, with some ("hot") chains being less likely to reject new candidate trees and parameters in the hope of sampling more broadly in search of optimal solutions (Beiko et al., 2006). Early on in a chain all trees may fit the data poorly, and so these early generations are usually discarded as "burn-in." Generally, while many millions of trees are evaluated and some large proportion retained, the distributions used in analyses are usually composed of trees from a smaller subsample, such as every 1000th tree in a chain. Known as the "posterior MCMC distribution," the retained subsample of trees and their attendant parameter values, prior probabilities, and likelihoods allow the strength of support for individual clades to be evaluated and specific hypotheses to be compared (Bergsten et al., 2013).

In the study reported here, we employed two forms of Bayesian phylogenetic analysis. First, we conducted a dated Bayesian analysis. Developed over the last decade, this form of analysis is designed to work with samples that include fossil taxa (Pyron, 2011; Lee et al., 2014a; Dembo et al., 2015). It uses geological dates associated with fossil specimens to constrain the branch lengths of non-contemporaneous[1] taxa (Lee et al., 2014a) and therefore improve estimates of the rate of evolution. The trees sampled in a dated Bayesian analysis are summarized in a maximum clade credibility (MCC) tree, which shows the posterior probability for each clade. A clade's posterior probability is just the proportion of times the clade appears in trees in the MCMC sample. This means that the posterior probabilities of the MCC tree are coarse analogues of bootstrap values in the maximum parsimony framework.

Subsequently, we carried out a series of Bayes factor tests. A Bayes factor is a ratio of marginal likelihoods of two different hypotheses, and is interpreted as the relative ability of each hypothesis to predict the data (Kass and Raftery, 1995). A hypothesis that is more likely to lead to the observed dataset will produce a higher marginal likelihood than one that is less likely to have given rise to the observed dataset, and this will result in a high Bayes factor. In Bayes factor tests, competing hypotheses are represented as differing topological constraints on trees, and the aforementioned procedure for inferring trees is employed to produce the best fully defined hypotheses of relationship consistent with each constraint. The fits of these constrained

[1]The term "non-contemporaneous" is used in the phylogenetics literature to refer to branches of the phylogeny that do not extend to the present (see e.g., Wood et al., 2013).

trees to the data can then be compared. An advantage of this approach for palaeoanthropology is that ambiguity due to missing data simply leads to low Bayes factors, which indicates that the data cannot differentiate among trees (Dembo et al., 2015). In the present study, we used Bayes factor tests to compete hypotheses about the phylogenetic position of *H. naledi* suggested by the MCC tree. The hypotheses were converted into trees in the manner shown in Figure 4.1, and then the trees' marginal likelihoods were compared (Bergsten et al., 2013; Dembo et al., 2015).

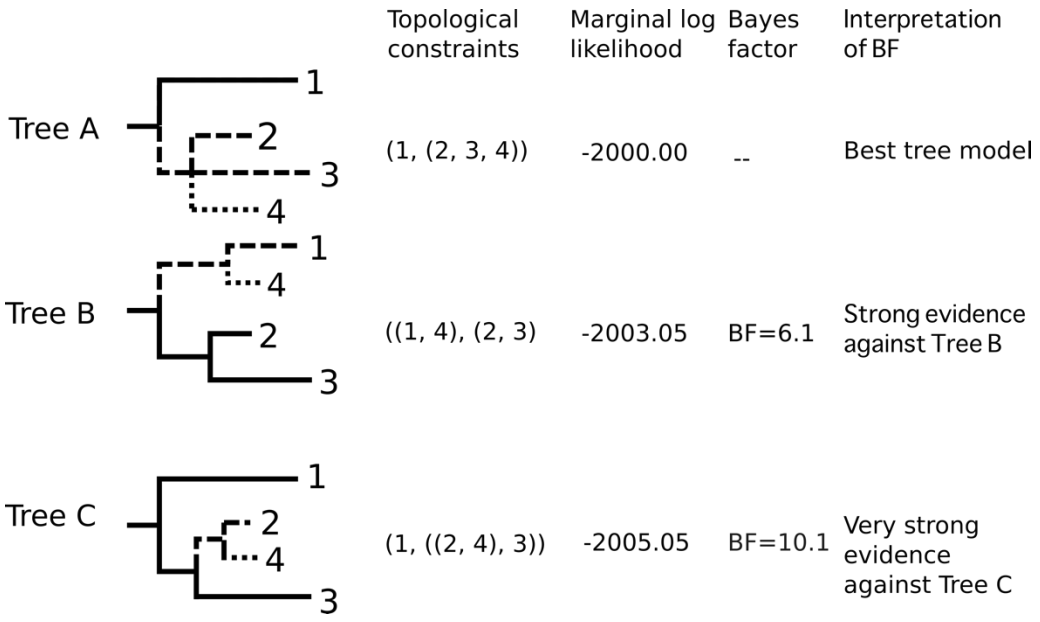

Figure 4.1 An illustration of how trees were constrained in the Bayes Factor tests, and how we interpreted the Bayes factors yielded by the tests.

Dotted edges are where the target species (4) can enter the corresponding model tree. For each hypothesis, we show one possible position after the data are analyzed. Bayes factor tests are carried out by comparing the marginal log likelihood of the best model tree to the other model trees. This figure is adapted from Dembo et al.'s (2015) Figure S1.

The final part of our study focused on the age of the Dinaledi fossils. An unintended but useful byproduct of dated Bayesian analysis is a "morphological clock" estimate of the age of any undated terminal node. Such ages are produced by combining the rate of change for each character derived from the underlying model, the inferred tree, and the ages of geologically-dated terminal tips on the one hand with the character states exhibited by the undated tip on the other. While morphological data have been used in concert with molecular data to estimate the age of taxa without geological dates in a number of dated Bayesian analyses (e.g., Pyron, 2011;

Ronquist et al., 2012a; Wood et al., 2013), we believe the exclusive use of morphological data to generate age estimates is novel, and remains untested (see discussion in Beck and Lee, 2014; Lee et al., 2014a). With this in mind, we used a jackknife resampling procedure to assess the reliability of the morphological clock age for the Dinaledi fossils yielded by the dated Bayesian analysis.

4.3. Materials

4.3.1. Morphological data

Most of the data used in the study were taken from Dembo et al. (2015), who compiled a supermatrix from craniodental matrices used in 13 previous studies (Cameron and Groves, 2004; Cameron et al., 2004; Kimbel et al., 2004; Strait and Grine, 2004; Chang, 2005; Martinón-Torres et al., 2007; Gilbert, 2008; Argue et al., 2009; Mounier et al., 2009; Zeitoun, 2009; Berger et al., 2010; Irish et al., 2013; Lordkipanidze et al., 2013). When character state codes for a given character differed among studies, Dembo et al. (2015) resolved the disagreement by favoring codes from studies that used larger samples of fossils, that recognized more polymorphic states, and that employed simpler character scoring systems. When a conflict could not be resolved via these criteria, the taxon was coded as polymorphic for that character. For studies that reported character states for individual fossil specimens, Dembo et al. (2015) used a 66% majority-rule to code characters. If less than 66% of the specimens exhibited a given character state, the species was coded as polymorphic. This approach to merging matrices is conservative because it favors ambiguity whenever there is disagreement among studies. In total, Dembo et al. (2015) assembled scores for 380 characters for 20 hominin taxa plus two extant hominoids, the gorilla (*Gorilla gorilla*), and the common chimpanzee (*Pan troglodytes*).

We made a number of alterations to Dembo et al.'s (2015) supermatrix for the purposes of the present study. First, we merged two zygoma-related characters that we deemed too similar to be treated as independent characters. Second, we amended some of the codes for two characters related to the articular eminence. Third, we added codes for 12 additional characters for as many taxa as possible (characters 12, 46, 69, 105, 134, 258, 261, 272, 276-279 and 334 in Table C1 in Appendix C). Seven of these characters relate to the cranium, five to the dentition, and one to the mandible. The additional characters were scored on original

specimens and casts. Fourth, we added *H. naledi* to the matrix. We were able to score *H. naledi* for 123 of the characters, 73 cranial characters, 31 dental characters, and 19 mandibular characters. All 123 characters were scored on original specimens during a workshop held at the University of the Witwatersrand in May 2014. Where necessary, we adopted the 66% majority-rule to code *H. naledi*. Lastly, we used original specimens and casts to score several taxa for characters that were missing codes in Dembo et al.'s (2015) supermatrix, paying particular attention to the 123 characters preserved in *H. naledi.* In total, the character state data matrix used in the present study contains scores for 391 craniodental characters for 22 hominin taxa and two extant hominoids (details of the fossil hypodigms are given in Table C2). This means that, to our knowledge, the dataset is the most comprehensive qualitative character state data matrix ever assembled for the tribe Hominini. The matrix and accompanying tables are provided in Appendix C. They have also been deposited in the Dryad database (doi:10.5061/dryad.d7r4g).

4.3.2. Geological dates

We used the oldest dates associated with the specimens that provided the morphological data to constrain the branch lengths for the non-*H. naledi* hominin taxa. Consequently, the dates used in this study (Table C3) do not necessarily correspond to the first appearance dates (FADs) of the taxa in the fossil record. In theory, dating the taxa on the basis of the oldest date associated with the specimens that provide the morphological data should link the scored character states with elapsed time more accurately than dating the taxa on the basis of the oldest known specimen in each hypodigm. This should, in turn, improve the estimates of the rate of evolutionary change for the characters (Ronquist et al., 2012a).

As we explained earlier, *H. naledi* has not been geologically dated (Berger et al., 2015). Consequently, we had to assign a date to it in a different manner. The analysis we carried out to do this is described below.

4.4. Analyses and results

4.4.1. Model parameter selection

Bayesian phylogenetic analyses are model based, so several decisions needed to be made before reconstructing the phylogeny of the hominins and evaluating the competing phylogenetic hypotheses concerning *H. naledi*. Specifically, we had to choose a model of character state evolution, and we had to select an appropriate clock model to infer the rate of change on the tree. Also, because *H. naledi* is currently undated, we had to decide how best to constrain it temporally.

We used a two-step procedure to choose the model of character state evolution, select a clock model, and temporally constrain *H. naledi*. First, we estimated the model likelihoods for the available options using MCMC simulation. We then compared the options using Bayes factors. A Bayes factor is calculated as twice the difference in natural logarithms of marginal likelihoods, and is interpreted on the same scale as the log-likelihood ratio test (Kass and Raftery, 1995). It is generally accepted that a Bayes factor greater than six suggests strong evidence in favor of one model over another; a Bayes factor greater than six indicates that the preferred model fits the data more than 400 times better than the alternative model (Kass and Raftery, 1995), and so is comparable to rejecting the alternative model at a *p*-value of less than 0.02. These analyses were conducted in MrBayes 3.2.4 (Ronquist et al., 2012b).

Process model Currently, only one widely-used model of character state change is available for discrete morphological data—Lewis's (2001) Markov k (Mk) state model. In the Mk model, characters switch among discrete states such that the probability of observing different states in a character is a truncated exponential function of time between observations.

Several of the parameters of the Mk model can be varied, and we assessed these parameters using Bayes factors before proceeding to tree generation and hypothesis comparison. One such parameter concerns characters that are phylogenetically uninformative. Morphological character state data matrices frequently include just those characters that have the potential to be informative regarding phylogenetic relationships. Characters that do not vary among the taxa and autapomorphic characters are often omitted. This sampling bias can be corrected in MrBayes by calculating conditional likelihoods based only on the parsimony-

informative characters or characters with variable character states (Lewis, 2001; Nylander et al., 2004). Bayes factors indicated that the model with parsimony-informative correction was strongly preferred over both the model in which no sampling bias correction was implemented (BF=723.28) and the model that assumed all variable characters were included (BF=495.56). Thus, we opted to utilize the parsimony-informative correction option.

Another decision that needs to be made when implementing the Mk model is whether or not to allow characters to evolve at different rates. Heterogeneity in among-character rate of evolution can be modeled such that the rate of change for a given character can be sampled from a statistical distribution. Bayes factors strongly favored the implementation of a gamma model of rate heterogeneity (Yang, 1994) over a model with a single rate of change assigned to all of the characters (BF=24.84). Consequently, we implemented the model with a gamma distribution of rate heterogeneity.

Clock model In a dated Bayesian analysis, dates associated with fossil specimens are used to calibrate the rate of evolutionary change. This produces branch lengths that are proportional to time (Heath et al., 2014). MrBayes offers several clock models that differ in the assumptions they make about the rate of evolutionary change. The strict clock model assumes a constant rate of change throughout the tree (Zuckerkandl and Pauling, 1962). In contrast, in the relaxed clock model, the rate of change evolves through time. In the autocorrelated relaxed clock model (Thorne and Kishino, 2002), the descendant nodes evolve at a rate that is sampled from a distribution centered on the inferred rate of the ancestral branch. In the uncorrelated relaxed clock model (Drummond et al., 2006), the rate for each branch is sampled from an exponential distribution. Bayes factors indicated that the uncorrelated relaxed clock model was strongly preferred over the strict clock model (BF=79.56), and that the uncorrelated relaxed clock model was better than the autocorrelated relaxed clock model (BF=42.54). Based on these results, we decided to use the uncorrelated relaxed clock model in the main analyses.

The use of a relaxed clock model requires an additional parameter to model how nodes appear throughout the tree. A uniform prior on node times assumes that a node has equal probability of appearing across the interval between the time of its parent node and its oldest daughter node. A birth-death prior assumes that lineages arise and go extinct according to a stochastic process with parameters for speciation and extinction. Based on Bayes factors, the use of birth-death prior on node times was preferred over a uniform prior on node times

(BF=17.58), and we therefore included the prior probability of birth-death trees in our evaluation of candidate trees (see discussion of Equation 1 above).

Because *H. naledi* does not currently have an independent geological date, we used Bayes factor tests to assess four different potential age priors for this taxon. In the first model, we assumed that *H. naledi* could be as old as the oldest hominin species, and so *H. naledi* was assigned a uniform prior from 7.24 Ma (millions of years ago) to the present. In the second model, *H. naledi* was allowed to be as old as the oldest *Australopithecus* specimen in the sample, and thus the *H. naledi* node was given a uniform prior from 4.17 Ma to the present. In the third model, we assumed that *H. naledi* could be as old as the oldest specimen of the genus *Homo* for which we had morphological data. The age of the *H. naledi* terminal node was therefore assigned a uniform prior from 2.33 Ma to the present. In the last model, we treated *H. naledi* as a modern taxon. This model assumed that the *H. naledi* tip could not be older than the present. The Bayes factor tests indicated that there were no significant differences in the marginal likelihood values among the four models (Table 4.1 and Figures C1-C4). Given this, we opted to use the "7.24 Ma to present" prior because it was the least likely to bias the placement of *H. naledi*.

Table 4.1 Different age prior settings for *H. naledi* used in this study.

The marginal likelihoods and Bayes factors of the different age prior models evaluate the fit between the model and the data. The terminal date for the *H. naledi* branch is presented as the tip date along with the 95% high posterior density (HPD) interval.

Models	Age prior (Ma)	Marginal likelihood	Bayes factor	Tip date (kya)	95% HPD on tip date (Ma)
As old as the oldest hominin	Uniform (0, 7.24)	-2563.66	BF=1.52 No evidence to reject model	912	0-2.39
As old as the oldest australopith	Uniform (0, 4.17)	-2563.54	BF=1.28 No evidence to reject model	909	0-2.37
As old as the oldest *Homo*	Uniform (0, 2.33)	-2563.10	BF=0.40 No evidence to reject model	801	0-1.94
As extant species	Fixed (0)	-2562.90	Best model	0	-

4.4.2. Dated Bayesian analysis

Based on results of the preliminary analyses, we inferred trees using characters modeled to evolve under the Markov k model with a gamma-distributed among-character rate variation, correcting for the sampling bias for parsimony-informative characters. Of the 391 characters, 288 were treated as unordered and 103 as ordered. The polymorphic characters were treated as uncertainty in the character coding in the dated Bayesian analysis. The uncorrelated clock-model was employed to calibrate the tree, and the birth-death model was used as the prior on node times. We used a normally distributed clock rate prior with a mean of 0.2 and a standard deviation of 0.02. The hominin taxa were treated as non-contemporaneous tips to calibrate the clock, and the oldest dates associated with the specimens in the hypodigms used in this study were assigned as fixed ages for those terminal tips, except for the terminal node of *H. naledi*, which as explained above was assigned a uniform age prior between 7.24 Ma and the present.

We ran the Bayesian analysis in MrBayes 3.2.4. To estimate the posterior probability distribution of the trees and the parameters, we completed four independent runs, each with 20 million MCMC generations for each analysis. Each run consisted of one cold and three heated chains that could contribute to the cold chain, and we sampled the cold chain every 1000 generations. Convergence in the runs was assessed using MrBayes's convergence diagnostics and Tracer v.1.6 (Rambaut et al., 2014). All the standard test criteria were met (Tables C4-C7), indicating that convergence was achieved. We discarded the first 25% of the sampled trees in each run as burn-in.

The MCC tree, which summarizes the 60,000 post-burnin trees sampled during the Bayesian analysis, is presented in Figure 2. Several of the widely accepted relationships among the fossil hominins feature in this summary tree. For example, *Australopithecus anamensis* is the most basal species of the genus *Australopithecus* followed by *Australopithecus afarensis*. Similarly, the three *Paranthropus* species form a clade to the exclusion of all other hominin species, and *H. heidelbergensis*, *Homo neanderthalensis,* and *Homo sapiens* form a clade to the exclusion of other *Homo* species. The posterior probabilities for most of the relationships are low, but they are comparable to those obtained in other Bayesian phylogenetic studies involving morphological characters and a large percentage of fossil taxa with missing data (e.g., Lee et al., 2014a).

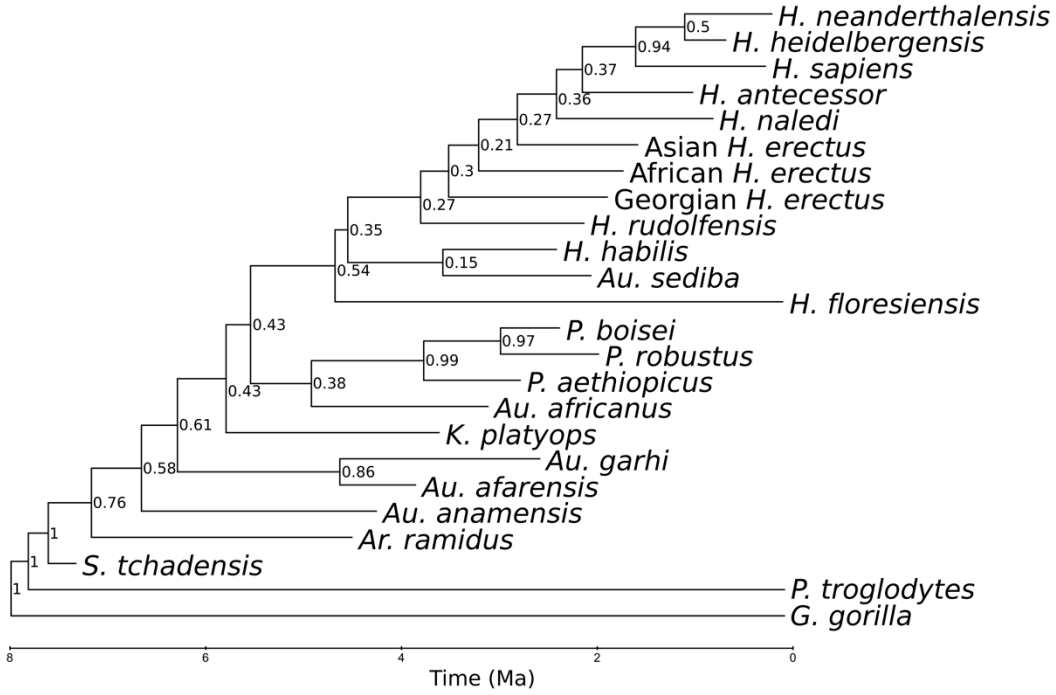

Figure 4.2 Summary of the best trees obtained in the dated Bayesian analysis.
The posterior probability values for the clades are indicated.

In the MCC tree, *H. naledi* is found in a clade with the other *Homo* species and *Australopithecus sediba*. Within this clade, there is a split between *Homo floresiensis* and all the other species. There is then a split between a clade formed by *H. habilis* and *Au. sediba*, and one formed by the remaining *Homo* species. Within the latter clade, *Homo naledi* is positioned as a member of a clade that also includes *Homo antecessor, H. heidelbergensis, H. neanderthalensis,* and *H. sapiens.* Thus, the MCC tree topology suggests that *H. naledi* is most closely related to *H. antecessor*, *H. heidelbergensis*, *H. neanderthalensis*, and *H. sapiens*, and that the closest relatives of the (*H. antecessor*, *H. heidelbergensis*, *H. naledi*, *H. neanderthalensis*, *H. sapiens*) clade are *H. erectus*, then *H. rudolfensis*, and then (*Au. sediba* plus *H. habilis*). The MCC tree topology also suggests that the closest relative of the (*H. antecessor*, *H. erectus*, *H. habilis*, *H. heidelbergensis*, *H. naledi, H. neanderthalensis*, *H. rudolfensis*, *H. sapiens*, *Au. sediba*) clade is *H. floresiensis*.

4.4.3. Comparison with maximum parsimony and undated Bayesian analyses

Given that the Bayesian Mk method outperforms maximum parsimony when applied to discrete characters that are evolving at a high rate and when there are missing data (Wright and Hillis, 2014), it seems likely that a Bayesian analysis will produce more accurate reconstructions of fossil hominin phylogenetic relationships than a maximum parsimony analysis. As a check, we carried out two additional analyses: an undated Bayesian analysis and a maximum parsimony analysis. These analyses are reported in detail in Appendix C5. Briefly, the topological differences among the summary trees yielded by the three analyses (Figures 4.2, C5 and C7) are consistent with what we expect based on the differences among the methods (e.g., the use of a model of character evolution in the Bayesian analyses versus no model of character evolution in maximum parsimony analysis, and the use of FAD-constrained rates of evolutionary change in the dated Bayesian analysis versus unconstrained rates of evolutionary change in the undated Bayesian analysis). Such consistency lends further support to the Bayesian results. Less theoretically compelling but perhaps more intuitively satisfying, all three analyses place *H. naledi* in a clade with the widely recognized species of genus *Homo*.

4.4.4. Bayes factor tests

We carried out two Bayes factor tests. The goal of the first was to evaluate the strength of support for the hypothesis that *H. naledi* forms a clade with the other species of *Homo* and *Au. sediba*, as suggested by the MCC tree topology. Using the approach discussed earlier, we compared two hypothetical trees (Figure C8). In one, the topology was constrained so that *H. naledi* was part of a clade that included the other *Homo* taxa (i.e., *H. antecessor*, African *H. erectus*, Asian *H. erectus*, Georgian *H. erectus*, *H. floresiensis*, *H. habilis*, *H. heidelbergensis*, *H. neanderthalensis*, *H. rudolfensis*, and *H. sapiens*) and *Au. sediba.* In the other, the topology was constrained in such a way that *H. naledi* was excluded from a clade containing the other *Homo* taxa and *Au. sediba*.

In the second Bayes factor test, we assessed the strength of support for the potential sister group relationships of *H. naledi* within the (*Homo*, *Au. sediba*) clade (Figure C9). To accomplish this we constructed hypothetical trees in which *H. naledi* was constrained to be the

sister taxon of each of the other species in the (*Homo*, *Au. sediba*) clade, and then compared the strength of support for these trees in turn.

Some frequently used methods of estimating marginal likelihoods, such as the harmonic mean method (Newton and Raftery, 1994), are known to be biased and to overestimate marginal likelihoods (Xie et al., 2011; Baele et al., 2013). With this in mind, we took advantage of a new method (Stepping stone Importance Sampling) that allow for a broader sampling of the MCMC and provides a more accurate estimate of the marginal likelihoods (Fan et al., 2011; Xie et al., 2011). We used 50 steps, each consisting of 392,100 generations, with samples taken every 100 generations. The 3920 samples from the first of 50 steps were discarded as burn-in. The first 980 samples from all subsequent steps were also discarded for the same reason. For each stepping-stone sample, we conducted four independent runs. Each run involved one cold chain and three heated chains. The marginal likelihood was computed as the arithmetic mean of the four runs. The marginal likelihoods were then used to calculate the Bayes factor. Once again, the analyses were carried out in MrBayes 3.2.4.

The results of the first Bayes factor test were unambiguous (Table 4.2): they strongly support the indication from the MCC tree that *H. naledi* is nested within a clade consisting of the other *Homo* taxa and *Au. sediba* (BF=10.22).

In the second set of Bayes factor tests, the tree in which *H. naledi* was constrained to be the sister of *Au. sediba* had the highest marginal likelihood. Compared to this tree, we were able to reject the trees in which *H. naledi* was constrained to be the sister taxon of African *H. erectus* (BF=7.52), Georgian *H. erectus* (BF=8.44), *H. heidelbergensis* (BF=11.54), *H. neanderthalensis* (BF=10.06), or *H. rudolfensis* (BF=9.50). However, we could not reject the trees in which *H. naledi* was constrained to be the sister taxon of *H. antecessor*, Asian *H. erectus*, *H. habilis*, *H. floresiensis*, or *H. sapiens* (all BF<6). Thus, the Bayes factor tests narrowed down the possibilities but did not identify the sister taxon of *H. naledi* within the (*Homo*, *Au. sediba*) clade. They indicated that *H. antecessor*, Asian *H. erectus*, *H. habilis*, *H. floresiensis*, *H. sapiens*, and *Au. sediba* could all be the sister taxon of *H. naledi*.

Table 4.2 Results of the Bayes factor tests.

A Bayes factor greater than 6 indicates strong evidence against a tree model compared to the best model.

	Marginal likelihood	Bayes factor	Interpretation
Is *H. naledi* nested in the clade of *Homo* + *Au. sediba*?			
Inside the clade	-2550.84	–	Best model
Outside the clade	-2555.95	10.22	Strong evidence to reject model
Does *H. naledi* form a sister taxon to other members of the genus *Homo* or *Au. sediba*?			
Sister to *H. antecessor*	-2556.04	0.24	Evidence not strong enough to reject model
Sister to African *H. erectus*	-2559.68	7.52	Strong evidence to reject model
Sister to Asian *H. erectus*	-2558.91	5.98	Evidence not strong enough to reject model
Sister to Georgian *H. erectus*	-2560.14	8.44	Strong evidence to reject model
Sister to *H. floresiensis*	-2557.68	3.52	Evidence not strong enough to reject model
Sister to *H. habilis*	-2558.90	5.96	Evidence not strong enough to reject model
Sister to *H. heidelbergensis*	-2561.69	11.54	Strong evidence to reject model
Sister to *H. neanderthalensis*	-2560.95	10.06	Strong evidence to reject model
Sister to *H. rudolfensis*	-2560.67	9.50	Strong evidence to reject model
Sister to *H. sapiens*	-2557.35	2.86	Evidence not strong enough to reject model
Sister to *Au. sediba*	-2555.92	-	Best model

4.4.5. Estimating the age of *H. naledi*

Using the “7.24 Ma to present” prior, the dated Bayesian analysis placed the age of *H. naledi* at 912 ka (thousands of years ago), with a 95% high posterior density (HPD) interval between 0.000 and 2.388 Ma (Table 4.1).

To evaluate the accuracy of this estimate, we used a jackknife resampling procedure. This involved iteratively removing the geological dates associated with non-*H. naledi* hominin taxa to mimic the situation with regard to *H. naledi*, and then estimating the ages of non-*H. naledi* hominin taxa by dated Bayesian phylogenetic analysis. Subsequently, the estimated ages were statistically compared with the geological dates to assess the overall accuracy of the morphological clock.

Twenty hominin and two outgroup taxa were included in the jackknife analysis. The two hominin taxa that were excluded were *Sahelanthropus tchadensis* and *H. naledi.* Because we used the geological date associated with *S. tchadensis* as the upper limit of a uniform distribution for the root age of the hominins, there was reason to expect its morphological clock date would be biased towards younger ages. *H. naledi* had to be excluded because it lacks a geological date.

Four independent, 20 million MCMC-generation runs were performed in each jackknife iteration. A "7.24 Ma to present" prior was used for the focal taxon in the MCMC analyses. Each MCMC run consisted of one cold and three heated chains that could contribute to the cold chain, and we sampled the cold chain every 1000 generations. Convergence in the runs was assessed using MrBayes's convergence diagnostics and Tracer v.1.6 (Rambaut et al., 2014). We discarded the first 25% of the sampled trees in each run as burn-in. Once the MCMC analyses were conducted, the tip date for the focal taxon was recorded. Subsequently, we used correlation analysis to compare all the morphological clock dates to the geological dates associated with the fossil taxa. The dated Bayesian analyses were carried out in MrBayes 3.2.4, while the inferred and geological ages were compared using Pearson correlation in the base R package (R Core Team, 2015).

The results of the morphological clock resampling analyses are presented in Figure 4.3 and Table 4.3. The dates estimated from the calibrated morphological clock are strongly correlated with the geological dates associated with the geological FADs for the hominin species (r^2=0.56). This supports the morphological clock age estimate of 912 ka for *H. naledi*.

It should be noted that the jackknife analysis was conducted prior to the publication of the new dates for *H. floresiensis* (Sutikna et al., 2016). As such, the geological date associated with *H. floresiensis* is 19 kya (Table 4.3). Using the new date for *H. floresiensis* in the correlation analysis did not have a significant impact on the r^2 value (it increased by just 0.004, from 0.564 to 0.568). This suggests that the new date is very unlikely to change the key findings of the present study.

Table 4.3 Results of the resampling analysis to evaluate the accuracy of the morphological clock.

Dates were estimated from the calibrated morphological clock for each of the fossil hominin species. The difference between the geological date and the morphological clock date is calculated. Positive values indicate a date overestimated by the morphological clock while the negative values indicate a date underestimated by the morphological clock.

Species	Geological date (Ma)	Morphological clock date (Ma)	Difference (millions of years)
Ardipithecus ramidus	4.419	4.463	0.044
Australopithecus anamensis	4.170	3.508	-0.662
Australopithecus afarensis	3.770	2.111	-1.659
Kenyanthropus platyops	3.500	1.159	-2.341
Australopithecus africanus	3.030	3.732	0.702
Paranthropus aethiopicus	2.700	2.210	-0.490
Australopithecus garhi	2.500	3.712	1.212
Homo habilis	2.330	2.773	0.443
Paranthropus boisei	2.300	1.101	-1.199
Homo rudolfensis	2.050	1.619	-0.431
Australopithecus sediba	1.977	1.486	-0.491
Paranthropus robustus	1.900	1.366	-0.534
Georgian *Homo erectus*	1.810	1.157	-0.653
African *Homo erectus*	1.650	1.257	-0.393
Asian *Homo erectus*	1.500	1.047	-0.453
Homo antecessor	0.938	0.969	0.031
Homo heidelbergensis	0.600	0.550	-0.050
Homo sapiens	0.195	0.491	0.296
Homo neanderthalensis	0.130	0.512	0.382
Homo floresiensis	0.019	1.354	1.335

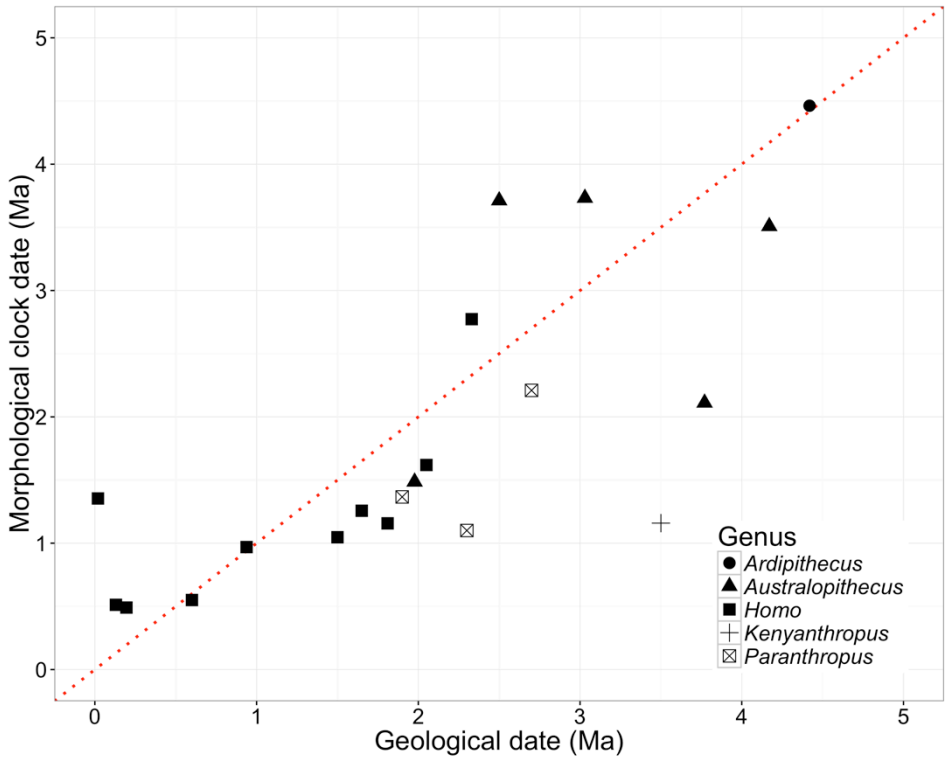

Figure 4.3 A plot of the geological dates associated with the fossil taxa compared with the dates estimated with the morphological clock.
Points above the dotted line of equality represent species with dates that are overestimated by the morphological clock while points beneath the dotted line are species whose dates are underestimated by the morphological clock.

4.5. Discussion and conclusions

We investigated the phylogenetic relationships of the recently announced species *H. naledi* using a large supermatrix of craniodental characters and Bayesian phylogenetic methods. We began by inferring the phylogeny of all the fossil hominins. The 60,000 trees sampled during this analysis suggest that *H. naledi* is sister to a clade that includes *H. antecessor, H. heidelbergensis, H. neanderthalensis,* and *H. sapiens*, and that these species are nested within a clade formed by *Homo* species and *Au. sediba* (Figure 4.2). Subsequently, we used Bayes factor tests to evaluate the hypothesis that *H. naledi* forms a clade with the other *Homo* taxa and *Au. sediba*, and to evaluate which taxon within this clade is most likely to be the sister of *H. naledi.* The Bayes factor tests supported the inclusion of *H. naledi* in a clade formed by the other *Homo* taxa and *Au. sediba*, but they did not support any particular sister taxon relationship

between *H. naledi* and any of the other taxa in that clade. Rather, they indicated that *H. antecessor*, Asian *H. erectus*, *H. habilis*, *H. floresiensis*, *H. sapiens*, and *Au. sediba* could all be the sister taxon of *H. naledi*.

Berger et al. (2015) found that *H. naledi* shares craniodental features with several species of *Homo*, including *H. habilis*, *H. rudolfensis,* and *H. erectus*. Our results are consistent with this assessment to the extent that they support a close relationship between *H. naledi* and the other *Homo* taxa without linking *H. naledi* exclusively with any particular species within the *Homo* clade. However, our results depart from Berger et al.'s (2015) evaluation in some ways. The most obvious of these is that our Bayes factor analyses suggest that *H. naledi* is as closely related to *Au. sediba* as it is to some of the existing species of *Homo*. Our results are also inconsistent with a proposal that was put forward immediately following the publication of the initial description of the *H. naledi* fossils—namely that they do not represent a distinct species but instead belong to *H. erectus* (e.g., Zollikofer quoted in Randolph-Quinney, 2015). This hypothesis predicts that *H. naledi* should be either most closely related to African *H. erectus* or equally closely related to African *H. erectus*, Georgian *H. erectus*, and Asian *H. erectus*. However, the Bayes factor tests rejected the possibility that *H. naledi* is the sister taxon of African *H. erectus* and the possibility that it is the sister taxon of Georgian *H. erectus.* Thus, neither prediction of the "*H. erectus* hypothesis" is met. The most reasonable conclusion to draw from our phylogenetic results, we think, is that the position of *H. naledi* within the clade formed by *Homo* and *Au. sediba* is currently ambiguous. Improving the power of the supermatrix to discriminate among the various hypotheses should be a priority for future research.

The most likely age for *H. naledi* yielded by the dated Bayesian analysis (912 ka) was surprisingly well supported by the resampling procedure. This age estimate is considerably younger than has been proposed by Thackeray (2015) on the basis of the cranial characteristics of *H. naledi*. While our morphological clock date has to be treated with caution, there are interesting implications if *H. naledi* is indeed less than one million years old. Most obviously, it adds to the diversity of hominin species that persisted into more recent times. In addition, it expands the range of morphological variation observed among these later hominin species. Such a recent date for *H. naledi* suggests that small-brained *Homo* species lived contemporaneously with larger-brained *Homo* species in Africa, similar to the case in southeast Asia, with *H. floresiensis,* Asian *H. erectus*, and *H. sapiens* possibly all living contemporaneously (Brown et al., 2004).

The results of the present study have implications beyond the inclusion of *H. naledi* in a clade formed by *Homo* and *Au. sediba*, and the estimate of its age. Perhaps the most obvious of these concerns the genera to which *H. floresiensis* and *Au. sediba* are assigned. Given that the MCC tree recovered a clade formed by the various species of *Homo* and *Au. sediba*, with *H. floresiensis* as the most basal lineage, the species in the genus *Homo* may form a paraphyletic group. Since all of the genus concepts that are currently in use in palaeoanthropology agree that genera should be monophyletic (Collard and Wood, 2015), such a placement would suggest that either *Au. sediba* should be included in the genus *Homo* or *H. floresiensis* should be excluded from the genus. However, given that we only used cranial characters in our analyses it would be sensible to revisit this issue after carrying out a phylogenetic analysis using a broader range of characters.

We conclude with a short list of suggestions for future research. One task concerns the low posterior probability values for parts of the MCC tree (Figure 4.2). This may be due to the fact that the dataset has numerous empty cells and a large number of polymorphic characters. Alternatively, the low posterior values may be caused by the presence of "wildcard" taxa that move around in the trees. In addition, the dataset likely contains conflicting signals as a result of convergence, parallelism, and/or homoiology (Lieberman, 1999; Lockwood and Fleagle, 1999; Collard and Wood, 2001). Determining the influence of these contributors to low clade support will require further work. Reducing the numbers of empty cells in a data matrix that contains numerous fossil species is always going to be difficult. However, reducing the number of polymorphic characters should be easier, given that many arise because of disagreements among the datasets that were used to compile the supermatrix, and thus are likely due to differences of opinion among researchers. It should be possible to resolve many of these coding disagreements through quantification and statistical analysis. For those that cannot be resolved in this manner, the use of a panel of coders offers an interim way forward. If the MCC tree still has numerous low posterior probability values after the number of polymorphic characters has been reduced, it will be reasonable to conclude that conflicting signal among characters is the cause, with all that that implies.

A second avenue for future research is to add postcranial characters to the supermatrix. While our supermatrix is the largest qualitative dataset assembled to date, it only contains characters of the skull. The omission of postcranial data is problematic and these data should be added in future phylogenetic studies in order to assess total morphological pattern. The fossil material recovered from the Dinaledi chamber includes well-preserved postcranial remains with

a unique combination of *Australopithecus*-like and *Homo*-like features (Berger et al., 2015; Harcourt-Smith et al., 2015; Kivell et al., 2015). As such, additional data on postcranial morphology may improve the power to discriminate among the hypotheses evaluated in the second part of this study.

Lastly, we need to develop better models of diversification and morphological character evolution. This process has already begun (e.g., Gavryushkina et al., 2014), but considerably more work is required. With regard to models of morphological character evolution, we know that various regions of the hominin cranium are integrated and so we expect covariation among cranial characters due to genetic, developmental, and functional constraints (Mitteroecker and Bookstein, 2008). But we do not have the relevant information to accomodate this in any phylogenetic inference framework at present. Fine-grained information on how shared developmental pathways influence covariation among craniodental characters would allow for a more complex model of character evolution in which the rates of evolution covary among characters and in different parts of the tree, analogous to the covarion models available for molecular data (Pagel and Meade, 2008). We suspect that models based on developmental data would significantly improve the support for hominin evolutionary relationships.

4.6. Acknowledgements

We wish to express our gratitude to the National Geographic Society and the National Research Foundation of South Africa for funding the discovery, recovery, and analysis of the *H. naledi* material. The study reported here was also made possible by grants from the Social Sciences and Humanities Research Council of Canada, the Canada Foundation for Innovation, the British Columbia Knowledge Development Fund, the Canada Research Chairs Program, Simon Fraser University, the DST/NRF Centre of Excellence in Palaeosciences (COE-Pal), as well as by a Discovery Grant from the Natural Sciences and Engineering Research Council of Canada, a Young Scientist Development Grant from the Paleontological Scientific Trust (PAST), a Baldwin Fellowship from the L.S.B. Leakey Foundation, and a Seed Grant and a Cornerstone Faculty Fellowship from the Texas A&M University College of Liberal Arts. We would like to thank the South African Heritage Resource Agency for the permits necessary to work on the Rising Star site; the Jacobs family for granting access; Wilma Lawrence, Bonita De Klerk, Merrill Van der Walt, and Justin Mukanku for their assistance during all phases of the project; Lucas Delezene for valuable discussion on the dental characters of *H. naledi*. We would also like to

thank Peter Schmid for the preparation of the Dinaledi fossil material; Yoel Rak for explaining in detail some of the characters used in previous studies; William Kimbel for drawing our attention to the possibility that there might be a problem with Dembo et al.'s (2015) codes for the two characters related to the articular eminence; Will Stein for helpful discussion about the Bayesian analyses; Mike Lee for his comments on this manuscript; John Hawks for his support in organizing the Rising Star workshop; and the associate editor and three anonymous reviewers for their valuable comments. We are grateful to S. Potze and the Ditsong Museum, B. Billings and the School of Anatomical Sciences at the University of the Witwatersrand, and B. Zipfel and the Evolutionary Studies Institute at the University of the Witwatersrand for providing access to the specimens in their care; the University of the Witwatersrand, the Evolutionary Studies Institute, and the South African National Centre of Excellence in PalaeoSciences for hosting a number of the authors while studying the material; and the Western Canada Research Grid for providing access to the high-performance computing facilities for the Bayesian analyses. Last but definitely not least, we thank the head of the Rising Star project, Lee Berger, for his leadership and support, and for encouraging us to pursue the study reported here.

Chapter 5.

Investigating the impact of cranial modularity on hominin phylogenetics using dated Bayesian analysis

5.1. Introduction

A reliable phylogeny is necessary for both proposing and evaluating evolutionary scenarios that might account for the morphology of fossil hominins (Tattersall and Eldredge, 1977), including adaptive changes linking events in human evolution with changes in the environment and with wider patterns of faunal evolution (Tattersall and Eldredge, 1977). That said, there is an ongoing debate on the reliability of the craniodental data used to reconstruct phylogenetic relationships of fossil hominins (Skelton and McHenry, 1992; McCollum 1999; Collard and Wood, 2001).

At the centre of this debate is the argument that certain regions of the hominin skull are more reliable than others as sources of phylogenetic information. Some authors have asserted that the basicranium can be expected to preserve a strong phylogenetic signal because it is under strict developmental constraints and therefore is less influenced by activity (Olson, 1981; Lieberman et al., 1996; Wood and Lieberman 2001). In contrast, the face has been argued to be a less reliable indicator of phylogeny because it is developmentally more flexible and thus responds to both selection and activity during development (Lieberman, 1999; Harvati and Weaver 2006a, b). For instance, Harvati and Weaver (2006a, b) found that the facial shape correlated strongly to climatic variables in modern human crania. Thus, the ongoing debate has questioned the reliability of phylogenies of fossil hominins reconstructed using a large proportion of facial characters (Skelton and McHenry, 1992; McCollum 1999) and this has led others to suggest that phylogenetic analyses should be conducted based solely on more reliable characters from the temporal bone (Lockwood et al., 2004).

A number of recent studies have approached the problem at different temporal scales. Several authors (Roseman, 2004; Harvati and Weaver, 2006a, b; Betti et al., 2009; Smith, 2009; von Cramon-Taubadel, 2009a, 2011) have used a quantitative genetics approach to investigate whether the variation in modern human crania can be explained by various microevolutionary processes. These studies assessed the correlation between the variation in the cranial regions among modern human populations and the genetic distances among these populations to identify cranial regions that deviate from the neutral evolution model. The results of these studies have suggested that some of the variation in the cranial regions can be explained by neutral processes like mutation, gene flow, and genetic drift, and these regions are not strongly influenced by natural selection (Harvati and Weaver, 2006a, b; Smith, 2009; von Cramon-Taubadel, 2009a, 2011). The results have not been entirely consistent; Harvati and Weaver (2006a, b) reported that temporal and vault shapes correlated significantly with genetic distances but not the facial shape, while Smith (2009) found that shapes of upper face and basicranium did correlate with the genetic distances, but the vault shape did not. The findings in both of these studies differed from the study reported by von Cramon-Taubadel (2009a), in which the shape variations in all three regions of the cranium (chondrocranium, face, and vault) were significantly correlated with the genetic distances. Despite these inconsistent findings, the argument has been made that if the cranial regions are identified as neutrally evolving then they are useful for inferring phylogenetic relationships or population structure in modern humans (von Cramon-Taubadel, 2009a; Smith, 2009). A similar study has been conducted at a deeper time scale, contrasting the shape variations in the cranial regions and genetic distances among extant hominoids (von Cramon-Taubadel and Smith, 2012). In this study, they found that the shape variations in the chondrocranium, face and vault were all correlated with genetic distances among extant hominoids. Moreover, the face was more strongly correlated with the genetic distance matrix than the vault, neurocranium, or the entire cranium. Here, the pattern and strength of correlation between cranial regions and genetic distances among extant hominoids differed from the patterns of genetic-craniometric congruence among modern human crania. In light of these contradictory findings, more work seems necessary to explore the utility of different cranial regions in phylogenetic reconstructions for fossil hominins.

This issue sits in a broader context in systematics. The heterogeneity in the evolutionary processes operating on different sets of characters has been the focus of a debate that took place among evolutionary biologists several decades ago. Different molecular datasets may yield incongruent phylogenies because the underlying evolutionary processes may differ among

genes due to different rates of mutational input and different selective regimes. Some researchers advocated for a total evidence approach in which all available evidence should be combined and used regardless of potentially conflicting signals from different datasets (Kluge, 1989). Other scientists argued against combining different datasets *a priori*, and instead advocated that that independent phylogenetic analyses should be conducted for each of the datasets and then assessed as to whether there are inconsistencies in the phylogenetic estimates (Miyamoto and Fitch, 1995). Still others suggested that the datasets should be combined only if they are tested to produce homogeneous tree estimates, but if the datasets produce significantly different estimates, they should not be combined in phylogenetic analysis (Bull et al., 1993). A mixed model approach has been developed to account for heterogeneous evolutionary processes underlying different gene sequences and this approach has been used in many recent phylogenetic analyses (Ronquist and Huelsenbeck, 2003; Nylander et al., 2004).

The approach taken in phylogenetic analyses of fossil hominins hitherto mirrors the total evidence approach (Kluge, 1989) without test: datasets from different regions of the hominin skull have been included *a priori*. If it is true that different cranial regions are influenced by heterogeneous evolutionary processes, it may be that these regional datasets produce significantly different phylogenetic estimates. If so, the decision to include all characters from the skull *a priori* to conduct phylogenetic analyses may be problematic.

To test this end, we divide the skull into four functional regions–basicranium, face, neurocranium, and dentition– and conduct a series of tip-dated Bayesian phylogenetic analyses. Bayesian phylogenetic inference is a method commonly used by evolutionary biologists to reconstruct phylogenetic trees, and the Bayesian inference method estimates the posterior probability distributions of a phylogeny and set of model parameters, given the data and a model of evolution. We use the recently developed tip-dating method to constrain the branches of the fossil hominin taxa using the geological dates associated with the fossil specimens (Pyron, 2011; Ronquist et al., 2012a; Lee et al., 2014a; Dembo et al., 2015). The aim of this study is to evaluate whether the phylogenetic signals from the four functional regions of the skull vary and to test if the trees produced from the functional regions are significantly different from each other. Based on these results, we evaluate whether it is problematic to combine the data from these functional regions to reconstruct the phylogeny of fossil hominins as it has been done previously.

5.2. Materials and methods

5.2.1. Morphological data

The morphological data were taken from the supermatrix compiled by Dembo et al. (2015). This matrix has combined 13 previously published studies and contains 380 craniodental characters on 20 hominin species and 2 extant hominoids (Argue et al., 2009; Berger et al., 2010; Cameron and Groves, 2004; Cameron et al., 2004; Chang, 2005; Gilbert, 2008; Irish et al., 2013; Kimbel et al., 2004; Lordkipanidze et al., 2013; Martinón-Torres et al., 2007; Mounier et al., 2009; Strait and Grine, 2004; Zeitoun, 2009). The details of the supermatrix can be found in Dembo et al. (2015).

The 380 craniodental characters were assigned to one of four regions: face, basicranium, dentition and neurocranium (Figure 5.1). Previous studies have delineated the cranial regions using a functional-developmental concept for humans and extant hominoids (von Cramon-Taubadel, 2009a; von Cramon-Taubadel and Smith, 2012). The cranial structures differ in how they ossify during embryonic development. Chondrocranial structure (i.e., basicranium) undergoes endochondral ossification where bones form from cartilaginous precursors in the embryo, while dermatocranial structures, such as the neurocranium and the face, develop through intramembranous ossification where bones develop within or on fibrous connective tissue membranes (Cohen, 2000). The dermatocranial structures have been further delineated into the neurocranium and the face based on different functions of these structures (von Cramon-Taubadel, 2009a). In this study, we modified the functional-developmental concept used elsewhere to accommodate the data used here. First, we included the mandibular characters into the face partition based on their involvement in the masticatory function. Second, we created a fourth functional developmental module, extending the three modules used by von Cramon-Taubadel (2009a) and von Cramon-Taubadel and Smith (2012) to include dental characters. We treated the dental characters separately from the face because dentition has a different developmental pathway from the bony structures of the skull (Tucker and Sharpe, 2004), and more importantly, teeth do not remodel through life.

In this study, we assigned 63 characters to the basicranium partition, and included characters inferior to the nuchal line on the occipital bone, the mastoid process and characters posterior to it on the temporal bone, and characters posterior to the spheno-occipital suture. The dental partition included 79 characters of the maxillary and mandibular dentition. There were 138

characters assigned to the face partition, which included facial characters up to and including the supraorbital region, extending laterally to the zygomaticotemporal suture, and the mandibular characters. Finally, the neurocranium partition contained 100 characters from the cranial vault superior to the glabella anteriorly, superior to the nuchal line posteriorly, the zygomaticotemporal suture to the external auditory meatus laterally.

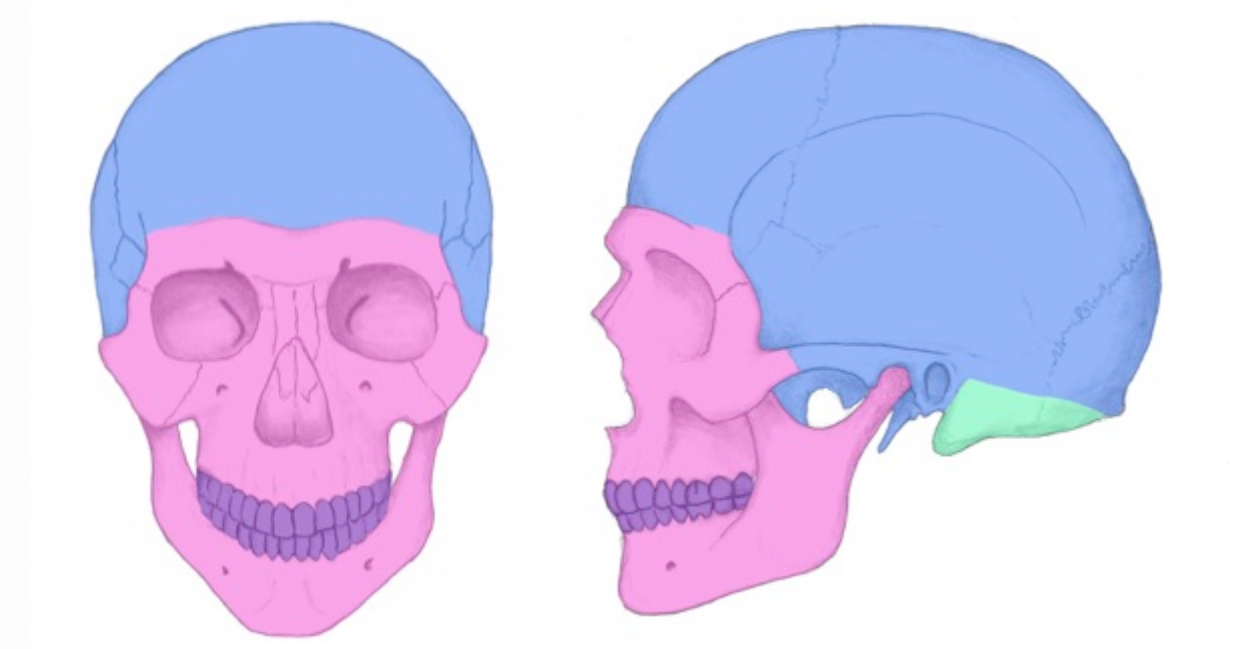

Figure 5.1 Anterior (left) and lateral (right) views of the skull and the four functional-developmental regions

The neurocranium partition is represented by the region in blue, the face partition is in pink, the dental partition is purple, and the basicranium partition is coloured greed.

5.2.2. Geological dates

The hominin taxa were used as non-contemporaneous tips in the dated Bayesian analysis. The dates we used to fix the ages of the hominin taxa are presented in Table D1 in Appendix B. The dates of the hominin taxa were taken from the oldest specimen for which we had morphological data. Thus, there may not be congruence between the dates used here and the oldest known dates associated with the hominin species in the paleontological record. However, we chose to date the hominin species in this manner in order to improve the estimate the rates of evolutionary change (Ronquist et al., 2012a).

5.2.3. Dated Bayesian analysis

Since the Bayesian analysis is a model-based method, we explored the choice of parameters for the best-fit model prior to conducting analyses. We report the results of these model selection analyses in the supplementary material (Appendix D2). The characters were modelled to evolve under Markov k-state (Mk) model (Lewis, 2001) with a gamma-distributed among-character rate variation, correcting for the sampling bias for parsimony-informative characters (Lewis, 2001). The uncorrelated relaxed clock-model (Drummond et al., 2006) was implemented to calibrate the tree with fossil hominins as dated tips and the birth-death model was used as the prior on node times. We used a normally distributed clock rate prior with a mean of 0.2 and a standard deviation of 0.02. The oldest dates associated with the specimens in this study were assigned as fixed ages of those terminal tips.

First, we conducted five separate dated Bayesian analyses: one for each of the four functional regions and one for a dataset that combined all of the functional regions. In each analysis, we ran four independent runs, each with 20 million Markov chain Monte Carlo (MCMC) generations. Each run consisted of one cold and three heated chains; the cold chain was sampled every 1000 generations. We assessed convergence of the four runs using MrBayes's convergence diagnostics and Tracer v.1.6 (Rambault et al., 2006). The first 25% of the sampled trees were discarded as burn-in. All of the analyses were conducted in MrBayes 3.2.4 (Ronquist et al., 2012b) installed on the Bugaboo cluster of the Western Canada Research Grid (www.westgrid.ca).

The dated Bayesian analyses produced a posterior distribution of 60, 000 trees from each of the five analyses. From each posterior distribution, we randomly sampled 10 000 pairs of trees and computed the tree distances to produce a null distribution of tree distances within each of the functional regions. We used the branch score distance (Kuhner & Felsenstein, 1994) as the tree distance measure and it is calculated by considering the topologies and the branch length differences of the two trees. A branch score distance closer to zero indicate that two trees are similar in topology and branch lengths, while the distance increases as the two trees become more incongruent in topology and branch lengths. The branch score distances were rescaled by 12 to make all tree distances across the five posterior distributions comparable.

Next, we sampled 10 000 trees from each of the five posterior distributions and compared these trees to the trees sampled from all other distributions to compute the between-

region tree distances. The tree distances were computed using the phangorn package (Schliep, 2011) in R. The branch score distances of the between-region comparisons were compared to the null distributions of the within-region comparisons using Welch's one-tailed t-test with Bonferroni correction for multiple unplanned comparisons in R (R Core Team, 2015). We reasoned that if the reconstructed trees from the five datasets are different, the branch score distances between the tree from its region and other regional trees should be significantly larger than the branch score distances computed between two trees drawn at random from its own region.

5.3. Results

5.3.1. Dated Bayesian analyses

The posterior distributions of trees from the five Bayesian analyses are summarized in maximum clade credibility (MCC) trees presented in Figure 5.2-5.6 and the convergence diagnostics for all of the analyses are presented in Table D2-D6 in Appendix D.

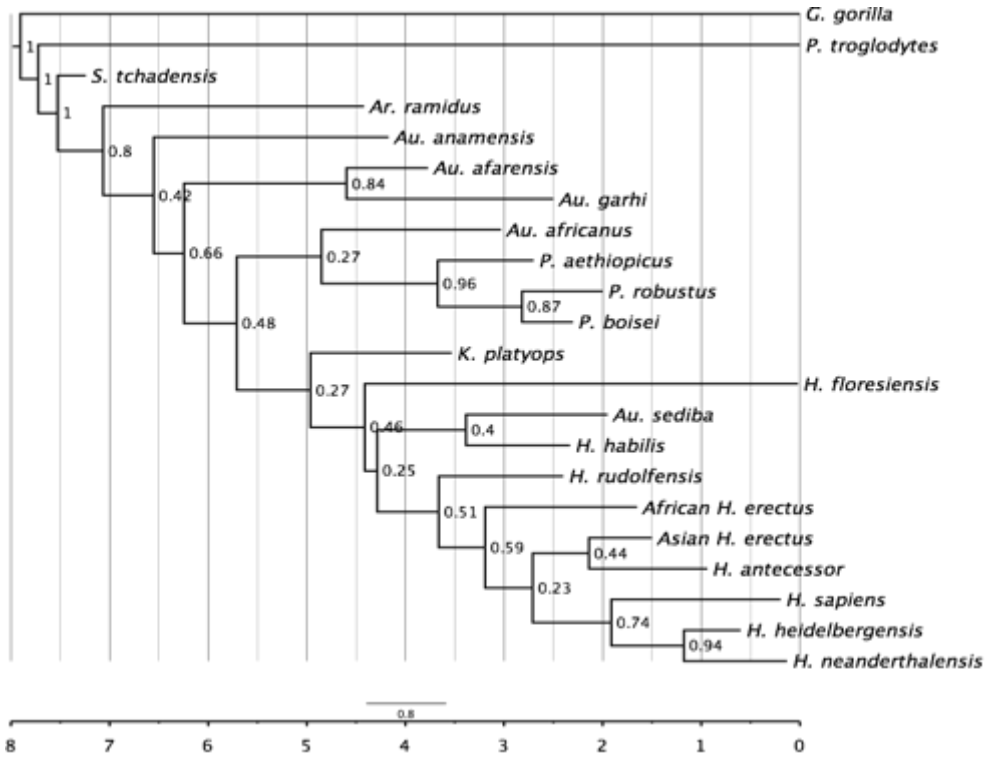

Figure 5.2 MCC tree of the combined dataset.

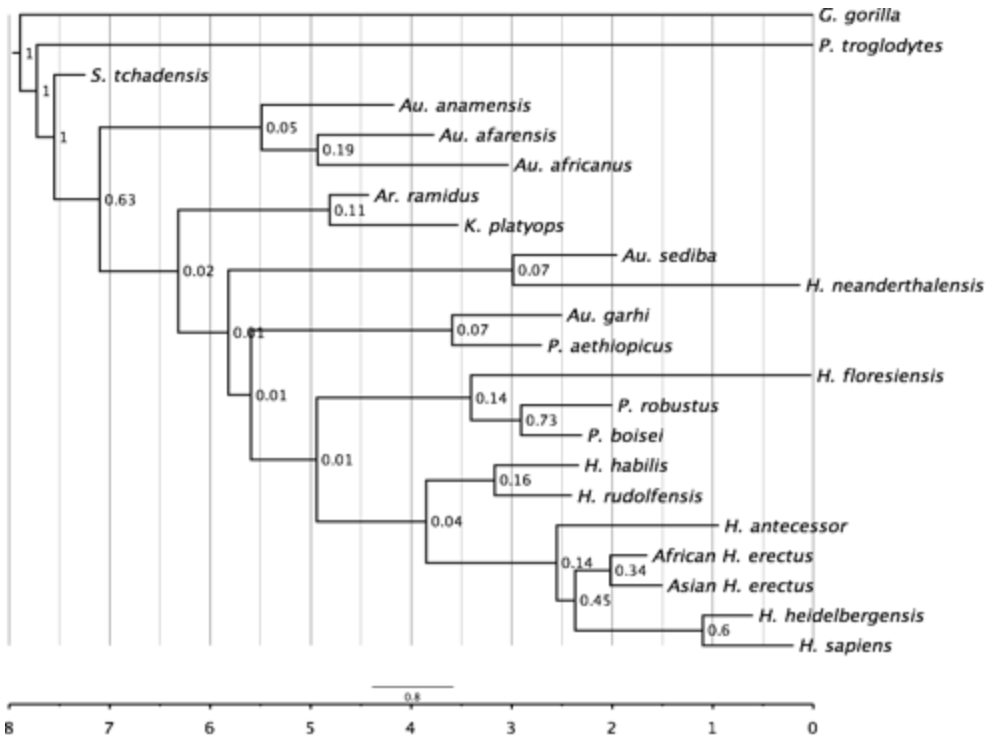

Figure 5.3 MCC tree of the basicranium dataset.

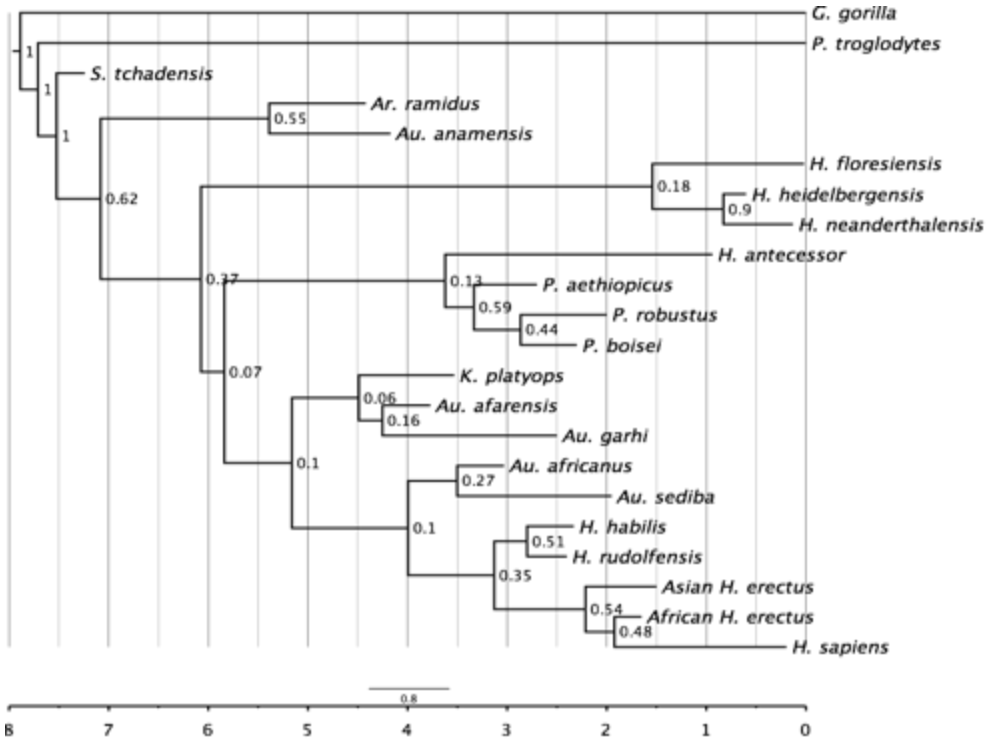

Figure 5.4 MCC tree of the dentition dataset.

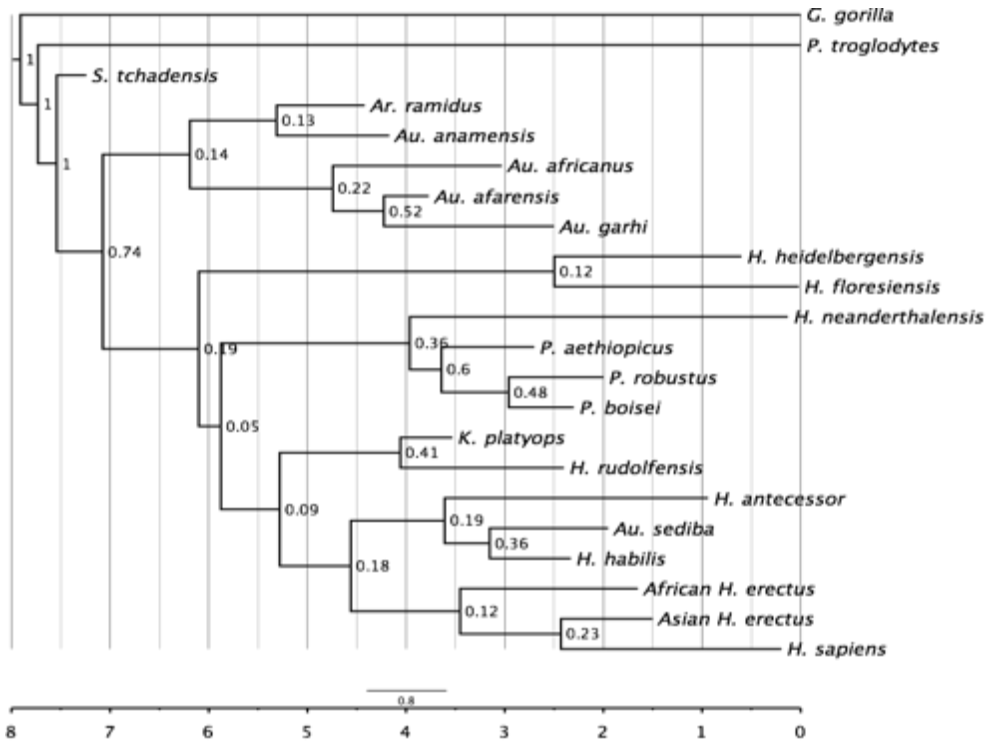

Figure 5.5 MCC tree of the face dataset.

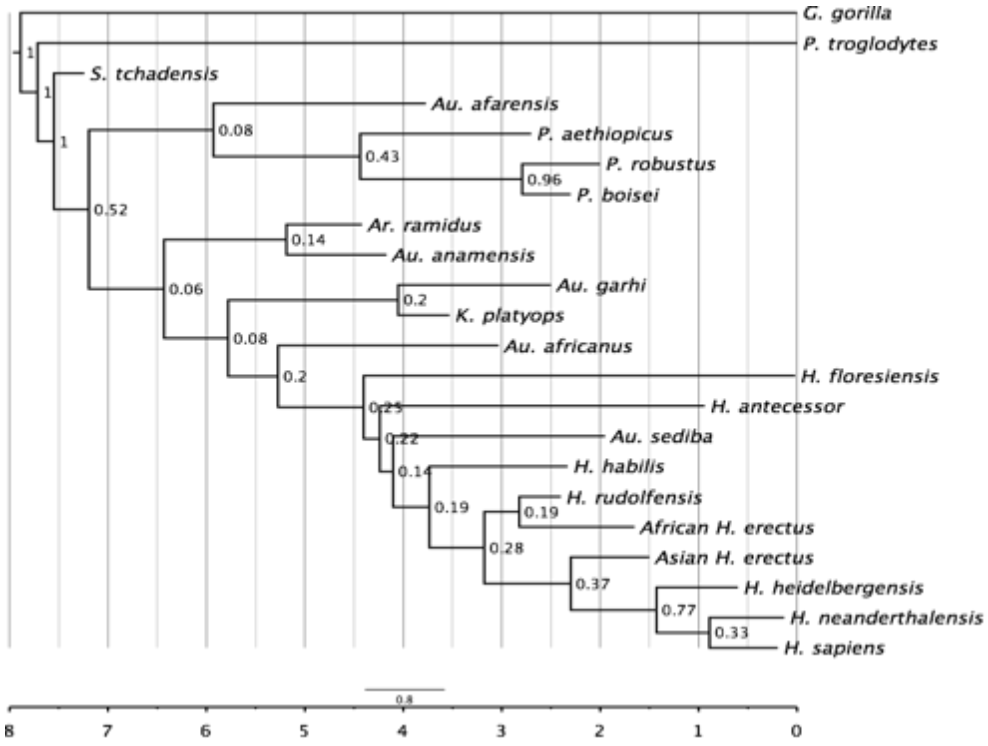

Figure 5.6 MCC tree of the neurocranium dataset.

There are two particularly noteworthy observations. First, all of the regional trees vary from one another to different degrees. Second, all four of the regional trees have low posterior probability values on many of the nodes, while the posterior probabilities of the combined tree (Figure 5.2) are generally much higher.

5.3.2. Are the trees from different functional regions significantly different from one another?

The density distributions of the tree distances for each functional region are presented in Figure 5.7 and Figure 5.8. Within each plot, the focal trees are compared against trees from four other posterior distributions. The results of the Welch's t-tests are presented in Table 5.1.

The trees sampled from each functional region were indeed different from trees sampled from the other four regions (including all regions combined). When the basicranium trees were compared to four other regions, the tree distances were significantly longer ($p=0.00$ in all comparisons) than the tree distances computed among any two basicranium trees. The tree distances between any two dentition trees were significantly shorter than the distances computed between the dentition trees and trees from basicranium, face, and neurocranium datasets ($p=0.00$ for all three comparisons). However, the tree distances computed between the dentition trees and the combined trees were not significantly different ($p=0.21$) from tree distances between any two dentition trees. The tree distances between face trees were significantly shorter than the tree distances calculated between face trees and trees from other four regions ($p=0.00$ in all comparisons). When the neurocranium trees were compared to the other regions, the tree distances were significantly longer ($p=0.00$ in all comparisons) than the tree distances computed between any two neurocranium trees.

Table 5.1 The results of Welch's t-test comparing the tree distances

Trees compared	P-value	Trees compared	P-value	Trees compared	P-value	Trees compared	P-value
Basicranium vs Dentition	0.00	Dentition vs Basicranium	0.00	Face vs Basicranium	0.00	Neurocranium vs Basicranium	0.00
Basicranium vs Face	0.00	Dentition vs Face	0.00	Face vs Dentition	0.00	Neurocranium vs Dentition	0.00
Basicranium vs Neurocranium	0.00	Dentition vs Neurocranium	0.00	Face vs Neurocranium	0.00	Neurocranium vs Face	0.00
Basicranium vs Combined	0.00	Dentition vs Combined	0.21	Face vs Combined	0.00	Neurocranium vs Combined	0.00

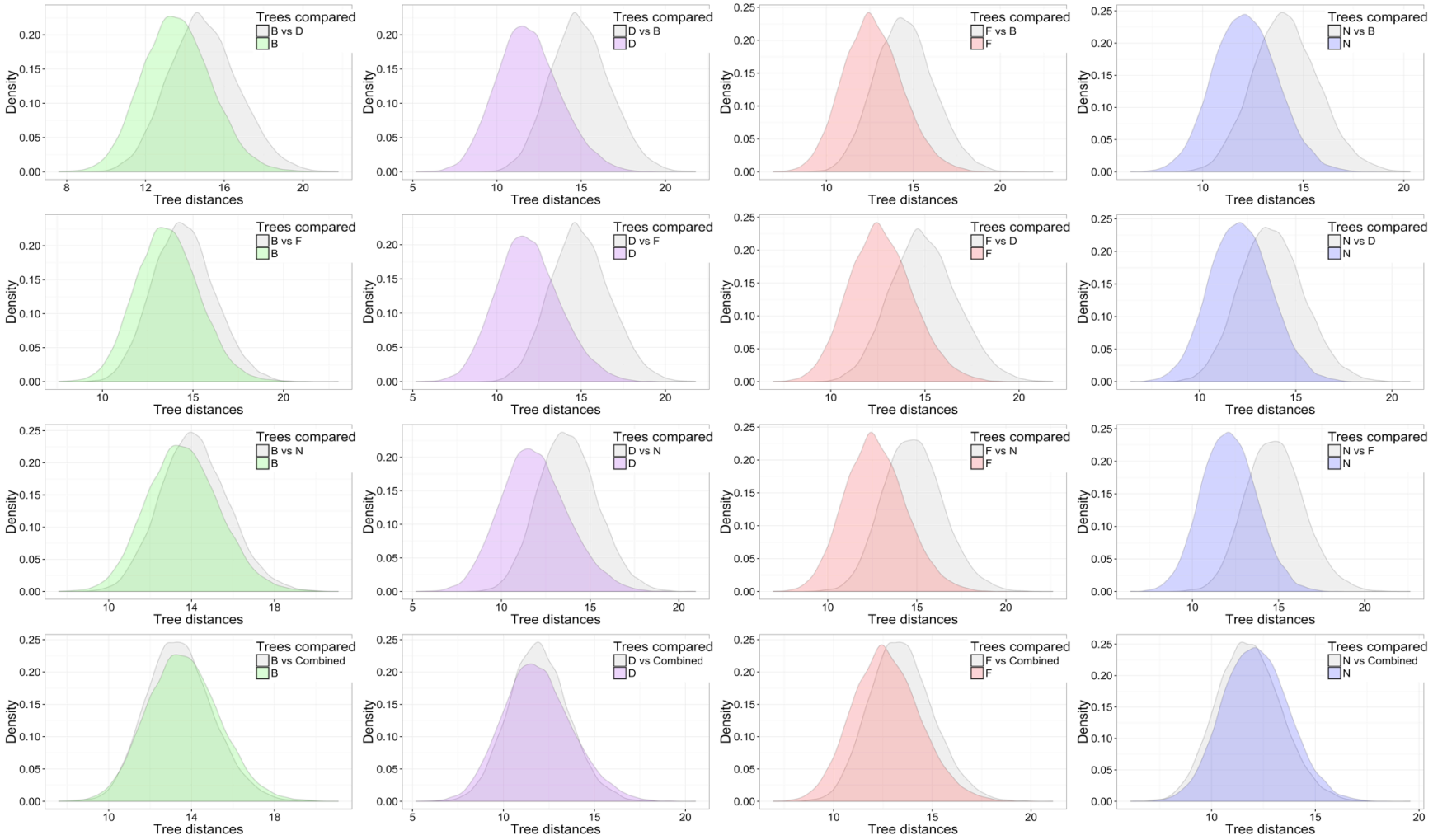

Figure 5.7 The distribution of tree distances comparing trees from four functional regions and the combined dataset.

The distribution of tree distances from Basicranium (B) in plotted in green, Dentition (D) in purple, Face (F) in red, and Neurocranium (N) in blue.

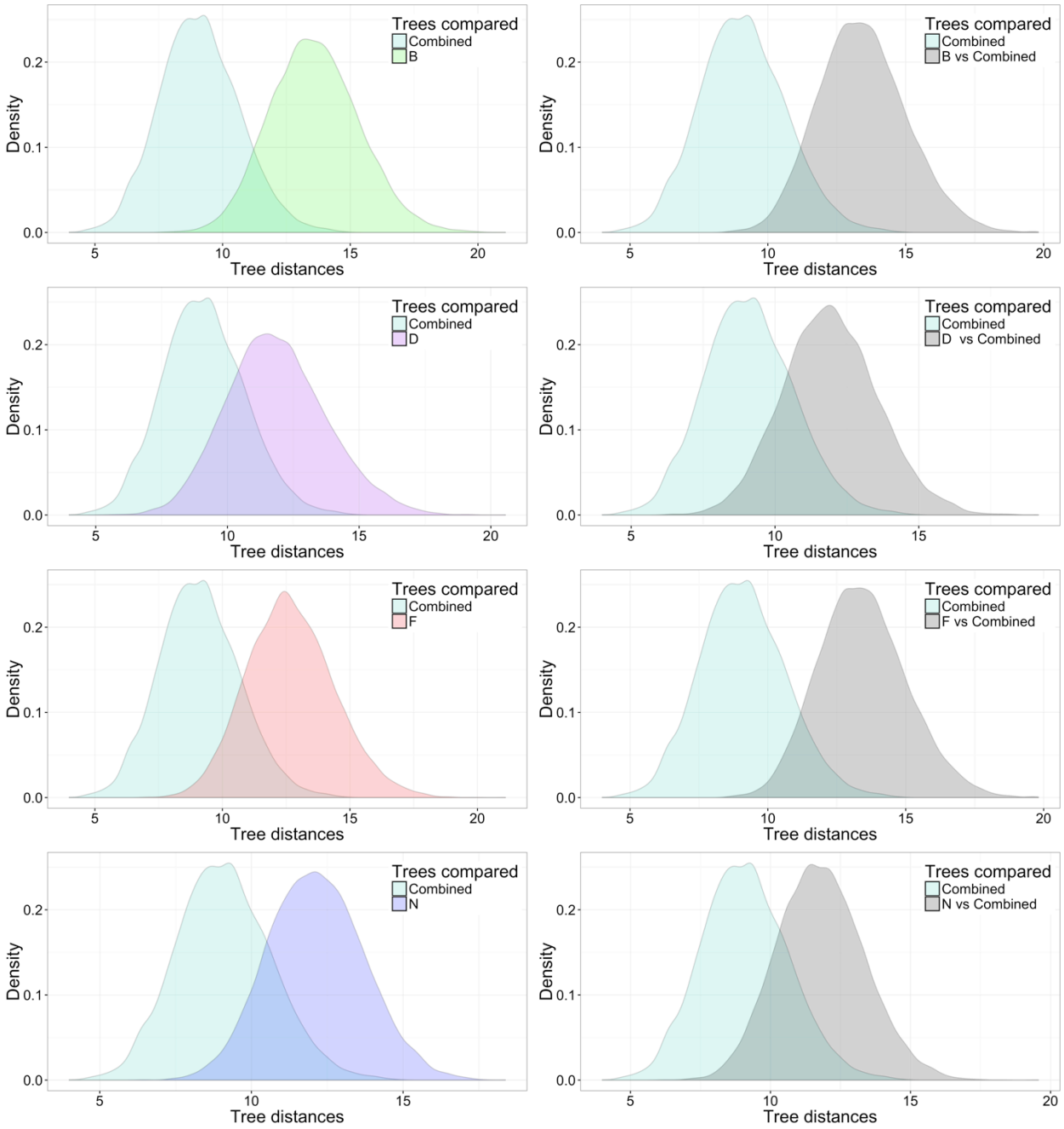

Figure 5.8 The distribution of tree distances comparing trees from four regions and the combined dataset.

The distribution of tree distances from Basicranium (B) in plotted in green, Dentition (D) in purple, Face (F) in red, and Neurocranium (N) in blue and the Combined dataset in light blue.

5.4. Discussion

In this study, we evaluated whether the phylogenetic signals of the four regions of the skull—the basicranium, the dentition, the face, and the neurocranium—are significantly different from each other. The results here suggest that the characters from the four regions do indeed produce significantly different phylogenetic estimates.

Conflicting phylogenetic signals from different sources of data is not uncommon. It has been documented in the gene tree versus species tree discussion in phylogenetics (Maddison, 1997). In the case of morphological datasets, we know that these functional regions should produce one true tree since these characters are scored on species that have a single evolutionary history. The fact that the characters from the four functional regions produce incongruent trees indicates that there is conflict in phylogenetic signals among these regions. When the MCC trees are compared, the phylogenetic relationships are not all inconsistent. There are certain relationships that are recovered in all the four regions and we can place some degree of confidence in the reliability of these inferences. However, when one tree suggests a particular set of relationships that is not supported by trees from other regions, there is a high likelihood that this is a false phylogenetic signal from a particular region of the cranium. The false signal may be due to convergence or correlated change in some characters in a particular cranial region among certain taxa. In order to avoid being misled by these false signals, it is best to use as many characters from various regions of the skull.

The results of this study suggest that combining all characters from the skull *a priori* is a good approach to study hominin phylogenetic relationships. The tree distances between any two combined trees were significantly shorter than the within-region tree distances from other regions (right panels of Figure 5.8). This implies that the combined trees were more similar to each other than the trees from the functional regions. The corollary to this is that using all available characters produce trees that are better estimated during the Bayesian analysis than relying on smaller subsets of craniodental data. This observation is also supported by the posterior probability values reported on the MCC trees in which the posteriors are much higher in the combined tree than any of the regional trees. Therefore, these findings suggest that it is better to combine all data from the skull to infer hominin phylogenetic relationships as this produces trees that are more strongly supported. When morphological data are noisy and

contain weak but conflicting phylogenetic signals, we think it is preferable to include as many characters as possible to overwhelm the incongruent and potentially false signals.

Face, neurocranium, and basicranium have been identified to constitute evolutionary modules in the cranium of primates (e.g., Cheverud, 1995; Mitteroeker and Bookstein, 2008; Singh et al., 2012). We found that cranial modularity did affect the outcome of this study to some degree as different regions of the hominin skull produced significantly different phylogenetic estimates. Some of the phylogenetic relationships recovered from each of these functional modules recovered relationships consistent with the combined tree as inferred from the overlap of the tree distance distributions in Figure 5.7. However, in each dataset, some of the inferred relationships were inconsistent with the combined tree or trees from other functional modules. These findings suggest that characters in each functional developmental module of the skull may be under independent morphological evolution to some extent. This implies that the characters assigned to a particular module are covarying strongly enough to suggest specific sets of phylogenetic relationships that are incongruent with trees from other functional modules.

The level of integration among characters within these cranial modules, however, may not be that strong. For instance, studies of basicranial integration have found fewer basicranial features that were actually integrated than it was previously hypothesized (Strait, 2001), and that there were lower levels of integration between midline and lateral features of the basicranium than predicted (Bastir and Rosas, 2005). Within the face module, Villmoare et al. (2014) recently identified premaxilla as an independent evolutionary module within the palate of primates. Thus, while some characters within a module do appear to be strongly integrated, these integrated characters do not retain strong phylogenetic signals that overwhelm the common phylogenetic signal of a module or the entire skull.

The basicranial morphology, in particular the temporal bone morphology, has been suggested to be more reliable for phylogenetic reconstruction due to its developmental constraints and its involvement in various functions for fossil hominins (Olson, 1981; Wood and Lieberman 2001; Lockwood et al., 2004). In contrast, it has been suggested that the facial morphology was less reliable because gnathic characters are more likely to contain homoplasies due to convergent evolution (Skelton and McHenry, 1992; McCollum 1999). Based on these suggestions, it is predicted that the basicranial characters under strict developmental constraints

should evolve slowly while the facial characters that arise due to convergent evolution should evolve more quickly on a tree.

Interestingly, and contrary to simple expectations that constrained regions like the basicranium might evolve more slowly than the face, the rates of evolutionary change did not vary significantly across different functional regions (Table D7 in Appendix D). The rate parameter for the combined dataset was estimated at 0.192. The face dataset was the slowest region to evolve, with a rate lower than the combined dataset at 0.185. The rate parameter estimated based on the neurocranium characters had an intermediate rate among the datasets of four functional regions at 0.191. The rate parameters estimated using the basicranium and dentition datasets were slightly faster (clock rate=0.204 and clock rate=0.206 respectively). If it were true that the hominin facial morphology contained more homoplasies than the basicranial region, the rates of evolution of facial characters would be increased since these characters would change states more frequently in different parts of the tree. The basicranial characters, in contrast, would have slower rates of change to reflect stronger functional or developmental constraints. However, the rates of evolutionary change estimated for each dataset were not greatly different from one another; none of the regions exhibited rates that doubled or tripled the rates of other regions. Thus, we failed to find evidence that the rates of evolution of these regions were markedly different to support the claim that the basicranial characters evolve slower than the facial characters.

Based on the rates of character evolution and the tree distances compared, the characters of the hominin face were no more problematic for phylogenetic reconstructions than the characters from other functional modules of the skull. This is in keeping with findings reported by von Cramon-Taubadel and Smith (2012) in which the facial morphology was most strongly correlated with the genetic distances of extant hominoids in their geometric morphometric analysis of the shapes of cranial regions. They found that morphological distances of various cranial regions and the genetic distances were generally strongly correlated among extant hominoids, which led to their conclusion that there is no single cranial region that is significantly better at retaining phylogenetic signal. Our study also suggests a similar case for fossil hominins that no one region of the skull has an especially strong and reliable phylogenetic signal.

In addition, we find no support for the argument that has been put forth that the overabundance of the gnathic characters bias the phylogenetic reconstruction of fossil hominins (Skelton and McHenry, 1992; McCollum 1999). This is based on our finding that the combined dataset is not strongly biased by any one particular region of the hominin skull. If the gnathic characters were biasing the hominin phylogenetic reconstruction, we would expect the tree distances between the face trees and the combined trees as well as the dentition trees and combined trees to be more similar to the tree distances computed between any two combined trees. This prediction is not consistent with our findings (right panels of Figure 5.8). We did find that the tree distances between dentition trees and combined trees were not significantly different from the tree distances between any two dentition trees implying that dental characters recover phylogenetic relationships that are more congruent with the combined tree than characters from the basicranium, the face or the neurocranium. That said, however, we did not find the same pattern for the tree distance comparisons of the face trees and the combined trees. While there are different numbers of characters assigned to each of the functional regions, the number of characters or the strength of phylogenetic signal from each of the datasets do not seem to strongly influence the combined tree topology.

In this study, the characters from the skull were partitioned into four functional developmental modules. The modules of basicranium, face, and neurocranium were used to remain consistent with previous studies conducted by von Cramon-Taubadel (2009a) and von Cramon-Taubadel and Smith (2012). In addition, we decided to create an extra partition for dental characters because the developmental pathway differs from the bony structures of the skull (Tucker and Sharpe, 2004). We also decided to include the mandibular characters in the face module because of their involvement in masticatory function. However, the decision to merge the mandibular characters into the face partition may need to be reconsidered given that mandibular morphology, but not the palatomaxillary or the zygomaticotemporal morphology, reflects adaptations to different subsistent strategies in modern humans (von Cramon-Taubadel, 2011). The inclusion of mandibular characters with the cranial characters of the face may have produced conflicting signals within this partition, potentially giving rise to more ambiguous trees.

The partitioning scheme adopted in this study has also contributed to producing greater ambiguity among basicranial trees. There were no basicranial characters scored for *Australopithecus garhi* and *Australopithecus sediba* in the supermatrix. As a result, these two species float around in the phylogeny produced by the basicranial characters as indicated by the

very low posterior probabilities associated with these taxa in the MCC tree. The uncertainty in their phylogenetic placements has undoubtedly contributed to the greater tree distances calculated between any two basicranium trees (Figure 5.7).

The functional developmental modules employed here are obviously not the only option to partition the characters of the skull. In future studies, it is worth exploring other partitioning scheme based on other factors that may affect hominin cranial morphology such as the homoiology hypothesis (Lieberman, 1995; Lieberman et al., 1996; Lycett and Collard, 2005; Collard and Wood, 2007; von Cramon-Taubadel, 2009b). Homoiology hypothesis predicts that bony regions that are affected by mechanical stress will be more variable, and thus, may attract more homoplasies. To evaluate this hypothesis, the characters in the supermatrix can be partitioned into three groups delineating those that experience high-strain, those that experience low-strain, or those that are not phenotypically plastic. The method outlined in this study can be applied to address various hypotheses on the craniodental evolution of fossil hominins.

5.5. Conclusions

The characters from different functional regions of the skull suggest different evolutionary relationships among hominin species. While heterogeneous evolutionary processes may affect cranial regions due to different functional and developmental constraints, these factors appear to not overwhelm the common phylogenetic signal. There have been attempts to identify and eliminate problematic characters that may jeopardize the reliability of phylogenetic reconstructions *a priori.* However, there is no evidence to suggest that there is one particular cranial region that yields strongly misleading phylogenetic signal and that there is no golden character or cranial region that reliably gives us a true phylogenetic signal. The total evidence approach employed in previous phylogenetic studies of fossil hominins seems not to be particularly problematic. That said, we found evidence to suggest that characters within a functional developmental module are correlated to some degree and this should be addressed in future phylogenetic studies by employing a more complicated model of character evolution that accommodates covariation in rates among characters.

Chapter 6.

General discussion and conclusions

In this dissertation, I explored three topics pertaining to hominin phylogenetic analyses. I explored the effects of small sample sizes in Chapter 2. I used a new method, tip-dated Bayesian analyses for the first time in palaeoanthropology to evaluate various phylogenetic hypotheses that have been presented in the last ten years in Chapter 3. I once again used the tip-dated Bayesian framework to evaluate the phylogenetic placement of a newly discovered species, *Homo naledi* in Chapter 4. The effects of cranial integration and the choice of character selection was evaluated in Chapter 5. While specific issues related to each of these studies have been discussed in their respective chapters, there are limitations and areas of future improvements to these studies in a broader context, and I will discuss each in turn. I will first outline the contributions of these studies to palaeoanthropology and then discuss the future directions based on the findings of the present research.

6.1. Contributions of the present research

The present research makes a number of important contributions to palaeoanthropology. First, while there are several limitations to the dataset as outlined below, the supermatrix that I compiled for the fossil hominins is the largest qualitative character state data matrix assembled to date. This supermatrix includes data for 21 hominin species–including the most recently discovered *Homo naledi* (Berger et al., 2015)–from the last seven million years of hominin evolution. I attempted to bring together previously published character matrices to include all generally accepted species and as many craniodental characters as possible. The supermatrix in its current form is by no means complete. There are many missing cells in the matrix that can be filled and data from postcrania of fossil hominins should be added. Therefore, I hope that this supermatrix can act as a starting point for standardizing morphological data collected for fossil hominins in future phylogenetic studies in palaeoanthropology.

Second, several studies in this dissertation involve the application of Bayesian phylogenetic methods to evaluate fossil hominin phylogenetic relationships. It is the first time in palaeoanthropology that a Bayesian framework was used to study fossil hominin phylogenetic relationships. While the Bayesian phylogenetic methods have been widely used in evolutionary biology (Huelsenbeck et al., 2008), it had not been taken up by palaeoanthropologists. However, there are obvious advantages to adopting the Bayesian framework. Instead of simply generating weakly supported phylogenies of fossil hominins using maximum parsimony, we can now explicitly evaluate competing phylogenetic hypotheses by comparing the posterior probabiliies of these hypotheses of being true given the data and the assumptions of the model of evolutionary change. Using this approach, a number of hypotheses that have been proposed in three recent debates were evaluated in Chapter 3, and several of these hypotheses were unambiguously refuted. By comparing the strength of support of various phylogenetic hypotheses, we can systematically narrow the range of possibilities based on fossil data and move the debates on hominin phylogenetic relationships forward.

Third, the adoption of the Bayesian framework allows us to incorporate geological dates associated with hominin species directly in the analysis to simultaneously infer the tree topology and to date the tree by calibrating the morphological clock. The extension of this tip-dated Bayesian method is that we can infer a date for *Homo naledi* using the calibrated morphological clock as reported in Chapter 4. Based on the rate of morphological evolution, I tentatively date *H. naledi* to 912 kya, which is much younger than what some have suggested based on its morphology (Thackeray, 2015). This species currently lacks geological dates associated with the fossil material and the temporal information based on the phylogenetic analysis is important in fully understanding the evolutionary significance of *Homo naledi*.

Fourth, the application of the tip-dated Bayesian methods permits the comparisons of the rates of evolutionary change of various craniodental characters as reported in Chapter 5. It has previously been suggested that certain cranial regions contain homoplasies, and thus, these characters are less reliable for phylogenetic reconstructions. However, it has not been possible within the parsimony framework to evaluate the rates of change of these potentially problematic characters. The adoption of a likelihood-based phylogenetic method that uses an explicit model of character state change allows us to explore hypotheses on the rates of craniodental evolution in fossil hominins. This method can be applied more widely to evaluate other key evolutionary

event in the course of hominin evolution, such as the rates of brain size and body size evolution in future studies.

6.2. Future directions

The findings presented in this dissertation raise questions about how best to proceed in the future. There are several recommendations and outstanding issues that need to be addressed in future studies.

6.2.1. Data

The outcomes of the phylogenetic analyses are largely influenced by the data used. In the present research, I used two datasets. The first dataset from Chapter 2 contains craniodental measurements taken on extant hominoids, and the second dataset is the supermatrix of fossil hominins and extant African apes used in Chapters 3 to 5. Several limitations of these datasets and how to build upon these datasets for future studies will be discussed in this section.

The data on hominoid craniodental measurements were taken from Wood (1975) and this dataset has been used in several previously published studies (Wood et al., 1991; Collard and Wood, 2000, 2001, 2007; Collard and Lycett, 2009). The limitations do not concern the measurements themselves, but the manner in which they were used in the phylogenetic context. The aim of Chapter 2 was to investigate the effects of small sample sizes comparable to the number of fossil specimens actually used in palaeoanthropology. The dataset contained 76 measurements taken on the primate crania, which capture the cranial shape differences among the extant hominoids. Each of these measurements was used as a character in the maximum parsimony analysis and it is debatable whether each character retains a strong phylogenetic signal. It is not unreasonable to predict that some of these measurements covary due to developmental and/or functional constraints in the primate skull (e.g., Cheverud, 1995). The lack of independence among characters may be a problem for phylogenetic studies. Despite the issue of covariation, I chose to employ the data because covariation among characters is an issue independent of sample size, which was the main focus of this study. The issue of covariation does, however, highlight the problem of how non-independent characters should be modeled in phylogenetic analyses. If characters are covarying due to the underlying

developmental and/or functional processes, then these characters do not provide independent estimates of evolutionary change. We need to first determine whether these craniodental measurements are covarying with one another using methods such as discriminant function analysis and if they are indeed covarying, then a model that allows joint evolution of these characters on a phylogeny should instead be used (e.g., Pagel and Meade, 2006).

The second dataset used in this dissertation was a supermatrix that I compiled from 13 previously published studies on fossil hominin morphology (Argue et al., 2009; Berger et al., 2010; Cameron and Groves, 2004; Cameron et al., 2004; Chang, 2005; Gilbert, 2008; Irish et al., 2013; Kimbel et al., 2004; Lordkipanidze et al., 2013; Martinón-Torres et al., 2007; Mounier et al., 2009; Strait and Grine, 2004; Zeitoun, 2009). I attempted to bring together character matrices on all widely accepted species for as many craniodental characters as possible. When the same character was used in multiple studies, the character state assessments from those studies were merged. In many cases, character scores were consistent across studies. However, when studies conflicted, I devised a set of criteria to resolve the disagreements as systematically as possible. First, I favoured character state assessments that were based on larger samples of fossil specimens. Second, if a study reported polymorphic states for a species for a particular character, I used that state assessment in the supermatrix. Third, when studies differed in the number of states used to score a character, I chose the character scoring system with the fewest number of states. Lastly, if the conflict could not be resolved via these criteria, I coded the taxon as polymorphic. In the end, there were many cells in the supermatrix with polymorphic state assessments, which is not ideal. However, this approach to merging matrices was justified because it is a conservative approach that favours ambiguity whenever there is disagreement among studies.

The level of ambiguity can be lowered in future phylogenetic studies if palaeoanthropologists can commit to using a common character matrix for investigating hominin phylogeny. This character matrix should include all widely used characters that are clearly defined. There were a handful of cases in which the same anatomical feature was defined using different anatomical landmarks by various researchers in previous studies. For instance, postorbital constriction, which describes the narrowing of the anterior portion of the cranium just behind the orbits, has been defined in different ways. Gilbert (2008) evaluates this character by calculating an index of the minimum frontal breadth by the maximum cranial breadth. Strait and Grine (2004) compute an index of the minimum frontal breadth by the superior upper facial

breadth measured at the frontotemporale. Kimbel et al. (2004) take an index of the minimum frontal breadth by the bi-zygomatic distance. Lordkipanidze et al. (2013) calculate an index of the bi-pterionic distance by the bi-frontotemporale distance. Therefore, it is recommended that the palaeoanthropologists agree on definitions of morphological features so that the character definitions can be standardized across future studies of fossil hominin phylogenetics.

The common character matrix should also include character states that are based on numerical indices wherever possible with each state representing an explicit range of the index like many characters in Strait and Grine (2004)'s matrix. There should also be a consensus among palaeoanthropologists on what the character states represent. For example, cranial capacity, which is a character used in most phylogenetic studies, has been transformed into three to five character states with each state representing an inconsistent range of endocranial volume estimates. In Berger et al.'s (2010) matrix, the "small" state is assigned to species with less than 600 cc of endocranial volume, the "intermediate" state is assigned to those with endocranial volume of 600-700 cc, and the "large" state is assigned to those with endocranial volume of greater than 700 cc. Strait et al. (1997) score this character using five states: "small" for those less than 500 cc, "intermediate" for those about 500 cc, "large" for those between 509-680 cc, "larger" for those between 750-875 cc, and finally "very large" for those greater than 1400 cc. The variation in the character scoring system can be attributed in part to the species that are included in these studies. If the focus of the study is early hominin phylogenetic relationships, there is no need to have a "very large" state to describe a brain size greater than 1400 cc. Yet, the reason for employing a particular scoring system is never discussed in the literature, and it is recommended that character states used in future studies should be explicitly defined. When the character states cannot be expressed as numerical indices, the character states need to be clearly described in a manner similar to Lahr (1996)'s work that outlined and depicted the morphology associated with each state for characters employed in the debate of the modern human origins.

It is also recommended that the character state assessments be reported for each specimen evaluated. There are ongoing debates about the species designation of some fossil specimens. For instance, a South African specimen, SK 847 has been assigned to *H. ergaster* in Berger et al. (2010)'s study, while Strait and Grine (2004) assigned the same specimen to *H. habilis*. Likewise, there is a disagreement over the status of the specimen, Stw 53, which has been attributed to *Au. africanus* by Berger et al. (2010) and to *H. habilis* by Strait and Grine

(2004). If the character states were reported for each fossil specimen, then we can address these disputes over alpha taxonomy of hominin species by investigating the effects of variable composition of specimens for each species in question.

Perhaps the most obvious recommendation for the data used in future hominin morphological phylogenetic studies concerns the missing data in the current supermatrix. As mentioned previously, there are many empty cells in the supermatrix and future work should focus on reducing the amount of missing data by including additional studies, and by evaluating new fossil specimens and revisiting pre-existing specimens. The supermatrix presently includes only the craniodental characters and this needs to be rectified by using all available evidence from the fossil record. In the last two decades, palaeoanthropologists have discovered seven new hominin species. These species, namely *Ardipithecus ramidus, Australopithecus anamensis, Au. sediba, Homo antecessor, H. floresiensis, H. naledi,* and *Orrorin tugenensis* (White et al., 2009; Leakey et al., 1995; Berger et al., 2010; Bermúdez de Castro et al., 1997; Brown et al., 2004; Berger et al., 2015; Senut et al., 2001), have associated postcranial remains. Furthermore, new postcranial specimens have been recovered from several important sites such as Dmanisi in Georgia (Lordkipanidze et al., 2007), Olduvai Gorge in Tanzania (Domingo-Rodriguez et al., 2013) and Ileret in Kenya (Jungers et al., 2015). There is now a substantial collection of postcranial specimens for various fossil hominin species that can be utilized to infer their phylogenetic relationships. Therefore, it has become clear that we have no reason to keep excluding postcranial data of fossil hominins in phylogenetic analyses.

Aside from postcranial data, characters that are often omitted in maximum parsimony analysis should also be included in the supermatrix. Morphological character matrices frequently include just those characters that have the potential to be informative regarding phylogenetic relationships. Characters that do not vary among the taxa and autapomorphic characters are often omitted. However, these parsimony-uninformative characters are necessary for more accurate estimates of rates of morphological change and more accurate estimates of divergence times (Lee and Palci, 2015). The rates of evolution estimated from a dataset that only includes parsimony-informative characters will be faster than the rates estimated if the unchanging and slowly changing characters are also included. This sampling bias for parsimony-informative characters has been corrected in the Bayesian analysis by calculating conditional likelihoods based only on the parsimony-informative characters (Lewis, 2001; Nylander et al., 2004). However, this sampling correction is not ideal. It is preferable to include all characters regardless

of whether they are parsimony-informative since these data are readily available on fossil specimens despite the fact that they have been ignored until now.

6.2.2. Analysis

There are many avenues for future improvements in the analyses presented here. It is only in the last few years that tip-dated Bayesian analyses have been conducted using only morphological data (e.g., Lee et al., 2014a; Dembo et al., 2015). Therefore, there are many outstanding issues that remain underexplored.

The first issue concerns the process model used for morphological characters. Currently, the only evolutionary model available for discrete morphological characters is the Markov k-state model (Lewis, 2001) where a character can change states instantaneously along a branch, and the probability of a state change is independent of other instances of state changes. However, the Mk model may be too simple to capture the underlying processes involved in morphological evolution (Lee and Palci, 2015). Researchers are beginning to test the applicability of the Mk model (e.g., Wright and Hillis, 2014) and other parameters associated with the Mk model with morphological data. For instance, a recent simulation study conducted by Wright and Hillis (2014) demonstrated that the Mk model outperformed maximum parsimony when characters are evolving at a high rate and when there are data missing in the character matrix. Moreover, Harrison and Larsson (2015) suggest that a lognormal distribution, rather than the commonly used gamma distribution, may be a more suitable prior to estimate among-character rate variation for some morphological datasets. Wright et al. (2015) explore the use of an asymmetrical rate of transition between states by changing the prior setting of the Mk model for characters that are unlikely to re-evolve a state once it has been lost. These efforts will undoubtedly bring us closer to developing more realistic process models for describing evolutionary changes in morphological characters.

A more realistic model for morphological evolution should incorporate insights from other fields such as developmental biology to identify characters that may be integrated. Such an attempt was made in a study conducted by Villmoare et al. (2014), who looked at the developmental and evolutionary origins of the premaxilla, which is derived from the frontal nasal processes during development, and the rest of the palate (maxilla and palatine bones), which is derived from the first brachial arch. Because the premaxilla is an independent module within the

palate, Villmoare et al. (2014) suggest that two characters of the premaxilla, the nasal clivus angle and the incisor alveolar angle, should be treated as integrated features and not as independent characters to study hominin facial evolution. Non-independence of characters is not an issue unique to morphological data. There are process models for molecular data that allow for evolutionary dependency among sites, such as codon models that allow sites within a codon to be dependent. Insights from developmental biology could then be applied to partition integrated characters to evolve under their own model that allows for evolutionary dependency separate from other characters. However, in order to systematically evaluate covariation among all morphological characters due to modularity and integration, we need detailed information from developmental studies. This may allow us to effectively deal with non-independence of morphological characters.

In addition, there is now the ability to include continuous traits along with discrete characters to infer phylogenetic relationships. Lee et al. (2014b) used over 1500 discrete characters and a continuous body size measure of theropods to simultaneously reconstruct the phylogeny, date the phylogeny, and infer the ancestral states for the discrete and continuous characters using BEAST (Drummond et al., 2012). The discrete characters were modeled using the Mk model and the continuous character was modeled using a Brownian motion process (Lemey et al., 2010). The ability to incorporate continuous characters to infer the phylogeny should be of great interest to palaeoanthropologists. The current approach is to transform continuous measurements of craniodental features into discrete character states to reconstruct phylogenies (Mickevich and Johnson, 1976; Colless, 1980; Thorpe, 1984; Archie, 1985; Thiele, 1993; Wiens, 2001; Gilbert and Rossie, 2007; Gilbert et al., 2009). While this approach continues to be used, it would be preferable to employ continuous traits, such as the estimates of endocranial volume, directly as a quantitative trait for inferring phylogenetic relationships. This will undoubtedly resolve some existing issues with converting continuous variables into discrete states that may sometimes be ambiguously defined.

6.3. Conclusions

In this dissertation, several issues concerning morphological phylogenetics in palaeoanthropology were explored. In particular, I evaluated 1) the effects of using small

samples, 2) the utility of a new technique called dated Bayesian analysis and 3) the impact of cranial modularity and integration. Several key findings are highlighted below.

Small sample sizes were often problematic when reconstructing the phylogenetic relationships of extant hominoids. The results of the phylogenetic analyses were much more variable with small samples and the trees reconstructed were often incongruent with trees reconstructed using larger sample sizes. This effect was most noticeable when samples included less than ten individuals per taxon. However, the effects of small sample sizes were greatly mediated by the choice of character coding methods. Thus, these results suggest the number of fossil hominin specimens used to reconstruct hominin phylogeny greatly affects the reliability of the inferred phylogeny, and we need to carefully consider how the morphological data are used in phylogenetic analyses of fossil hominins.

The use of Bayesian phylogenetic methods is promising for palaeoanthropology. Palaeoanthropologists can now directly test several competing phylogenetic hypotheses by evaluating the strength of support based on the current fossil evidence. The ability to demonstrate which hypotheses are more likely is useful in narrowing the scope of discussion in palaeoanthropology. By using these Bayesian methods to test competing hypotheses, we can highlight where ambiguities in the data and the model exist and demonstrate the limit of the interpretation of the current fossil evidence, like the case with *H. naledi.* The adoption of the Bayesian methods also allows palaeoanthropologists to revisit these hypotheses as new data and new models of morphological evolution become available. These new tools should help us gain a better understanding of hominin evolution.

It appears that heterogeneous evolutionary processes may affect cranial regions due to different functional and developmental constraints, and the results reported in Chapter 5 are consistent with this idea. However, there is no evidence to suggest that there is one particular cranial region that yields a strongly reliable phylogenetic signal and that there is no golden character or cranial region that we should seek. The characters from the skull appear to retain weak but conflicting phylogenetic signals, and thus, these results suggest that we should not eliminate characters *a priori* that have been assumed to be problematic.

Further work is necessary to improve the data and methods currently used in morphological phylogenetics of fossil hominins. Expanding the character matrix to include as

many characters of the whole skeleton as possible would be ideal. We also need to add characters that have been omitted in phylogenetic studies, such as those that are not parsimony-informative. There are also data available that have not been scored on existing specimens, and this will reduce the proportion of missing data in the current supermatrix. The use of continuous characters should be reconsidered and perhaps the correct approach might be to use these characters directly in the inference stage of the phylogenetic analysis. Finally, more complex evolutionary models for morphological characters should be developed for Bayesian analyses that allow characters to covary with rates that differ across the tree. As we start to tackle these issues, the applicability of the Bayesian framework to fossil hominins should improve, and the future of morphological phylogenetics in palaeoanthropology should be encouraging.

References

Aiello, L.C., 2015. *Homo floresiensis*. In: Henke, W., Tattersall, I. (Eds.), Handbook of Paleoanthropology 2nd edition, Springer Reference, New York, pp 2281-2297.

Archie, J.W., 1985. Methods for coding variable morphological features for numerical taxonomic analysis. Systematic Zoology 34, 326–345.

Argue, D., Morwood, M.J., Sutikna, T., Jatmiko, Saptomo, W., 2009. *Homo floresiensis*: a cladistic analysis. Journal of Human Evolution 57, 623–639.

Asfaw, B., White, T.D., Lovejoy, O., Latimer, B., Simpson, S.W., Suwa, G., 1999. *Australopithecus garhi*: a new species of early hominid from Ethiopia. Science 284, 629–635.

Baele, G., Lemey, P., Vansteelandt, S., 2013. Make the most of your samples: Bayes factor estimators for high-dimensional models of sequence evolution. BMC Bioinformatics 14, 85.

Balter, M., 2010. Candidate human ancestor from South Africa sparks praise and debate. Science 328, 154–155.

Bastir, M., Rosas, A., 2005. Hierarchical nature of morphological integration and modularity in the human posterior face. American journal of Physical Anthropology 128, 26–34.

Beck, R.M.D., Lee, M.S.Y., 2014. Ancient dates or accelerated rates? Morphological clocks and the antiquity of placental mammals. Proceedings of the Royal Society B 281, 20141278.

Berger, L.R., de Ruiter, D.J., Churchill, S.E., Schmid, P., Carlson, K.J., Dirks, P.H.G.M., Kibii, J.M., 2010. *Australopithecus sediba*: a new species of *Homo*-like australopith from South Africa. Science 328, 195–204.

Berger, L.R., Hawks, J., de Ruiter, D.J., Churchill, S.E., Schmid, P., Delezene, L.K., Kivell, T.L., Garvin, H.M., Williams, S. a, DeSilva, J.M., Skinner, M.M., Musiba, C.M., Cameron, N., Holliday, T.W., Harcourt-Smith, W., Ackermann, R.R., Bastir, M., Bogin, B., Bolter, D., Brophy, J., Cofran, Z.D., Congdon, K.A, Deane, A.S., Dembo, M., Drapeau, M., Elliott, M.C., Feuerriegel, E.M., Garcia-Martinez, D., Green, D.J., Gurtov, A., Irish, J.D., Kruger, A., Laird, M.F., Marchi, D., Meyer, M.R., Nalla, S., Negash, E.W., Orr, C.M., Radovcic, D., Schroeder, L., Scott, J.E., Throckmorton, Z., Tocheri, M.W., VanSickle, C., Walker, C.S., Wei, P., Zipfel, B., 2015. *Homo naledi*, a new species of the genus *Homo* from the Dinaledi Chamber, South Africa. eLife 4, 1–35.

Bergsten, J., Nilsson, A.N., Ronquist, F., 2013. Bayesian tests of topology hypotheses with an example from diving beetles. Systematic Biology 62, 660-673.

Bermúdez de Castro, J.M., Arsuaga, J.L., Carbonell, E., Rosas, A., Martinez, I., Mosquera, M., 1997. A hominid from the Lower Pleistocene of Atapuerca, Spain: Possible ancestor to Neandertals and modern humans. Science 276, 1392–1395.

Bermúdez de Castro, J.M., Martinón-Torres, M., Sier, M.J., Martín-Francés, L., 2014. On the variability of the Dmanisi mandibles. PLoS One 9, e88212.

Betti, L., Balloux, F., Amos, W., Hanihara, T., Manica, A., 2009. Distance from Africa, not climate, explains within-population phenotypic diversity in humans. Proceedings of the Royal Society B 276, 809–814.

Bjarnason, A., Chamberlain, A.T., Lockwood, C.A., 2010. A methodological investigation of hominoid craniodental morphology and phylogenetics. Journal of Human Evolution 60, 47–57.

Brown, P., Maeda, T., 2009. Liang Bua Homo floresiensis mandibles and mandibular teeth: a contribution to the comparative morphology of a new hominin species. Journal of Human Evolution 57, 571–596.

Brown, P., Sutikna, T., Morwood, M.J., Soejono, R.P., Jatmiko, Saptomo, E.W., Due, R.A., 2004. A new small-bodied hominin from the Late Pleistocene of Flores, Indonesia. Nature 431, 1055–1061.

Brunet, M., Beauvilain, A., Coppens, Y., Heintz, E., Moutaye, A.H.E., Pilbeam, D., 1995. The first australopithecine 2,500 kilometres west of the Rift Valley (Chad). Nature 378, 783–785.

Brunet, M., Guy, F., Pilbeam, D.R., Mackaye, H.T., Likius, A., Ahounta, D., Beauvilain, A., Fronty, P., Geraads, D., Lehmann, T., Lihoreau, F., Duringerq, P., Louchart, A., Mahamat, A., Merceron, G., Mouchelin, G., Otero, O., Campomanes, P.P., Leon, M.P. De, Rage, J., Sapanetkk, M., Schuster, M., Sudrek, J., Tassy, P., Valentin, X., Vignaud, P., Viriot, L., Zazzo, A., Zollikofer, C.P.E., 2002. A new hominid from the Upper Miocene of Chad, Central Africa. Nature 418, 145–152.

Bull, J.J., Cunningham, C.W., Molineux, I.J., Badget, M.R., Hillis, D.M., 1993. Experimental molecular evolution of bacteriophage T7. Evolution 47, 993–1007.

Cameron, D.W., Groves, C.P., 2004. Bones, Stones and Molecules: Out of Africa and Human Origins. Elsevier, San Diego.

Cameron, D., Patnaik, R., Sahni, A., 2004. The phylogenetic significance of the Middle Pleistocene Narmada hominin cranium from central India. International Journal of Osteoarchaeology 14, 419–447.

Cardini, A., Elton, S., 2007. Sample size and sampling error in geometric morphometric studies of size and shape. Zoomorphology 126, 121-134.

Chamberlain, A.T., Wood, B.A., 1987. Early hominid phylogeny. Journal of Human Evolution 16, 119–133.

Chang, M.L., 2005. Neandertal origins, Middle Pleistocene systematics, and tests of current taxonomic and phylogenetic hypotheses. Ph.D. Dissertation, University of Pennsylvania.

Chappill, J.A., 1989. Quantitative characters in phylogenetic analysis. Cladistics 5, 217-234.

Cheverud, J.M., 1995. Morphological integration of the saddle-back tamarin (*Saguinus fuscicollis*) cranium. The American Naturalist 145, 63–89.

Cobb, S.N., O'Higgins, P., 2004. Hominins do not share a common postnatal facial ontogenetic shape trajectory. Journal of Experimental Zoology 302, 302–21.

Cohen, M.M.J., 2000. Merging the old skeletal biology wiht the new. I. Intramembranous ossification, endochondral ossification, ectopic bone, secondary cartilage, and pathologic considerations. Journal of Craniofacial Genetics and Developmental Biology 20, 84–93.

Collard, M., Lycett, S.J., 2009. An assessment of the likely impact of strain-related phenotypic plasticity on hominin fossil species identification. South African Journal Of Science 312–316.

Collard, M., Wood, B.A., 2000. How reliable are human phylogenetic hypotheses? Proceedings of the National Academy of Sciences 97, 5003–5006.

Collard, M., Wood, B.A., 2001. Homoplasy and the early hominid masticatory system: inferences from analyses of extant hominoids and papionins. Journal of Human Evolution 41, 167–194.

Collard, M., Wood, B.A., 2007. Hominin homoiology : An assessment of the impact of phenotypic plasticity on phylogenetic analyses of humans and their fossil relatives. Journal of Human Evolution 52, 573–584.

Collard, M., Wood, B., 2015. Defining the genus *Homo.* In: Henke, W., Tattersall, I. (Eds.), Handbook of Paleoanthropology 2nd edition, Springer Reference, New York, pp 2107-2144.

Colless, D.H., 1980. Congruence between morphologic and allozyme data for Menidia species: a reappraisal. Systematic Zoology 29, 288–299.

Corruccini, R.S., 1994. How certain are hominoid phylogenies ? The role of confidence intervals in cladistics. In: Corruccini, R.S., Ciochon, R.L. (Eds.), Integrative Paths to the Past: Paleoanthropological Advances in Honor of F. Clark Howell. Prentice-Hall, New York, pp. 167–183.

Curnoe, D., 2003. Problems with the use of cladistic analysis in palaeoanthropology. Homo 53, 225–234.

Curnoe, D., 2010. A review of early *Homo* in southern Africa focusing on cranial, mandibular and dental remains, with the description of a new species (*Homo gautengensis* sp. nov.). Homo 61, 151–77.

Delson, E., Eldredge, N., Tattersall, I., 1977. Reconstruction of hominid phylogeny: a testable framework based on cladistic analysis. Journal of Human Evolution 6, 263–278.

Dembo, M., Matzke, N.J., Mooers, A.Ø., Collard, M., 2015. Bayesian analysis of a morphological supermatrix sheds light on controversial fossil hominin relationships. Proceedings of the Royal Society B 282, 20150943.

Dennell, R., 2009. The Palaeolithic Settlement of Asia. Cambridge University Press, New York.

Domínguez-Rodrigo, M., Pickering, T.R., Baquedano, E., Mabulla, A., Mark, D.F., Musiba, C., Bunn, H.T., Uribelarrea, D., Smith, V., Diez-Martin, F., Pérez-González, A., Sánchez, P., Santonja, M., Barboni, D., Gidna, A., Ashley, G., Yravedra, J., Heaton, J.L., Arriaza, M.C., 2013. First partial skeleton of a 1.34-million-year-old *Paranthropus boisei* from Bed II, Olduvai Gorge, Tanzania. PLoS ONE 8, e80347.

Drummond, A.J., Ho, S.Y.W., Phillips, M.J., Rambaut, A., 2006. Relaxed phylogenetics and dating with confidence. PLoS Biology 4, e88.

Drummond, A.J., Suchard, M.A, Xie, D., Rambaut, A., 2012. Bayesian phylogenetics with BEAUti and the BEAST 1.7. Molecular Biology and Evolution 29, 1969–1973.

Eldredge, N., Gould, S.J., 1972. Punctuated equilibria: an alternative to phyletic gradualism. In: Schopf, T.J. (Ed.), Models in Paleobiology. Freeman, Cooper and Company, San Francisco, pp. 82–115.

Eldredge, N., Tattersall, I., 1975. Evolutionary models of phylogenetic reconstruction and another look at hominid phylogeny. In: Szalay, F. (Ed.), Approaches to Primate Paleobiology. Karger, Basel, pp. 218–242.

Fan, Y., Wu, R., Chen, M.H., Kuo, L., Lewis, P.O., 2011. Choosing among partition models in Bayesian phylogenetics. Molecular Biology and Evolution 28, 523-532.

Farris, J.S., 1989. The retention index and the rescaled consistency index. Cladistics 5, 417–419.

Ferring, R., Oms, O., Agustí, J., Berna, F., Nioradze, M., Shelia, T., Tappen, M., Vekua, A., Zhvania, D., Lordkipanidze, D., 2011. Earliest human occupations at Dmanisi (Georgian Caucasus) dated to 1.85-1.78 Ma. Proceedings of the National Academy of Sciences 108, 10432–6.

Fisher, D.C., 2008. Stratocladistics: integrating stratigraphic and morphologic data in phylogenetic inference. Annual Review of Ecology, Evolution, and Systematics 39, 365–385.

Gabounia, L., de Lumley, M.-A., Vekua, A., Lordkipanidze, D., de Lumley, H., 2002. Découverte d'un nouvel hominidé à Dmanissi (Transcaucasie, Géorgie). Comptes Rendus Palevol 1, 243–253.

Gabunia, L., Vekua, A., 1995. A Plio-Pleistocene hominid from Dmanisi, East Georgia, Caucasus. Nature 373, 509–512.

Gabunia, L., Vekua, A., Lordkipanidze, D., Swisher III, C.C., Ferring, R., Justus, A., Nioradze, M., Tvalchrelidze, M., Antón, S.C., Bosinski, G., Joris, O., de Lumley, M.-A., Majsuradze, G., Mouskhelishvili, A., 2000. Earliest Pleistocene hominid cranial remains from Dmanisi, Republic of Georgia: taxonomy, geological setting, and age. Science 288, 1019–1025.

Garcia-Cruz, J., Sosa, V., 2006. Coding quantitative character data for phylogenetic analysis: A comparison of five methods. Systematic Botany 31, 302–309.

Gavryushkina, A., Welch, D., Stadler, T., Drummond, A.J., 2014. Bayesian inference of sampled ancestor trees for epidemiology and fossil calibration. PLoS Computational Biology 10, e1003919.

Gibbs, S., Collard, M., Wood, B.A., 2000. Soft-tissue characters in higher primate phylogenetics. Proceedings of the National Academy of Sciences 97, 11130–11132.

Gilbert, C.C., Frost, S.R., Strait, D.S., 2009. Allometry, sexual dimorphism, and phylogeny: a cladistic analysis of extant African papionins using craniodental data. Journal of Human Evolution 57, 298–320.

Gilbert, C.C., Rossie, J.B., 2007. Congruence of molecules and morphology using a narrow allometric approach. Proceedings of the National Academy of Sciences 104, 11910–11914.

Gilbert, W.H., 2008. *Homo erectus* cranial anatomy. In: Gilbert, W.H., Asfaw, B. (Eds), *Homo erectus*: Pleistocene evidence from the Middle Awash, Ethiopia, University of California Press , Berkeley, pp 265–311.

Goloboff, P., 1999. NONA (NO NAME) ver. 2 Published by the author, Tucumán, Argentina.

Goloboff, P., Farris, S., Nixon, K., 2000. TNT (Tree analysis using New Technology) (BETA) ver. 1.5 Published by the author, Tucumán, Argentina.

González-José, R., Escapa, I., Neves, W.A., Cúneo, R., Pucciarelli, H.M., 2008. Cladistic analysis of continuous modularized traits provides phylogenetic signals in *Homo* evolution. Nature 453, 775–778.

Haile-Selassie, Y., 2001. Late Miocene hominids from the Middle Awash, Ethiopia. Nature 412, 178–181.

Haile-Selassie, Y., Gibert, L., Melillo, S.M., Ryan, T.M., Alene, M., Deino, A., Levin, N.E., Scott, G., Saylor, B.Z., 2015. New species from Ethiopia further expands Middle Pliocene hominin diversity. Nature 521, 483–488.

Harcourt-Smith, W.E.H., Throckmorton, Z., Congdon, K.A., Zipfel, B., Deane, A.S., Drapeau, M., Churchill, S.E., Berger, L.R., DeSilva, J.M., 2015. The foot of *Homo naledi.* Nature Communication 6, 8432.

Harrison, L.B., Larsson, H.C.E., 2015. Among-character rate variation distributions in phylogenetic analysis of discrete morphological characters. Systematic Biology 64, 307–324.

Harvati, K., Weaver, T.D., 2006a. Human Cranial Anatomy and the Differential Preservation of Population History and Climate Signatures. The Anatomical Record Part A 1233, 1225–1233.

Harvati, K., Weaver, T.D., 2006b. Reliability of cranial morphology in reconstructing Neanderthal phylogeny. In: Harvati, K., Harrison, T. (Eds.), Neanderthals Revisited: New Approaches and Perspectives. Springer, Dordrecht, pp. 239–254.

Hawks, J.D., 2004. How much can cladistics tell us about early hominid relationships? American Journal of Physical Anthropology 125, 207–219.

Heath, T.A., Huelsenbeck, J.P., Stadler, T., 2014. The fossilized birth–death process for coherent calibration of divergence-time estimates. Proceedings of the National Academy of Sciences 111, E2957–E2966.

Henneberg, M., Eckhardt, R.B., Chavanaves, S., Hsu, K.J., 2014. Evolved developmental homeostasis disturbed in LB1 from Flores, Indonesia, denotes Down syndrome and not diagnostic traits of the invalid species Homo floresiensis. Proceedings of the National Academy of Sciences 111, 11967–11972.

Henneberg, M., Thorne, A., 2004. Flores human may be a pathological *Homo sapiens*. Before Farming 4, 2–4.

Hershkovitz, I., Kornreich, L., Larson, Z., 2007. Comparative skeletal features between *Homo floresiensis* and patients with primary growth hormone insensitivity (Laron syndrome). American Journal of Physical Anthropology 132, 535–544.

Hothorn, T., Hornik, K., van de Wiel, M., Zeileis, A., 2008. Implementing a Class of Permutation Tests: The coin Package. Journal of Statistical Software 28, 1 – 23.

Huelsenbeck, J.P., Ronquist, F., Nielsen, R., Bollback, J.P., 2008. Bayesian inference of phylogeny and its impact on evolutionary biology. Science 294, 2310–2314.

Humphries, C.J., 2002. Homology , characters and continuous variables. In: MacLeod, N., Forey, P.L., (Eds.), Morphology, shape and phylogeny, Taylor & Francis, London, pp. 8-26.

Huxley, T.H., 1863. Evidence as to Man's Place in Nature. D. Appleton and company, New York.

Irish, J.D., Guatelli-Steinberg, D., Legge, S.S., de Ruiter, D.J., Berger, L.R., 2013. Dental morphology and the phylogenetic “place” of *Australopithecus sediba*. Science 340, 1233062–1233062.

Jolly, C.J., 2001. A Proper Study for Mankind: Analogies From the Papionin Monkeys and Their Implications for Human Evolution. Yearbook of Physical Anthropology 44, 177–204.

Jungers, W.L., Falsetti, A.B., Wall, C.E., Size, R., 1995. Shape, relative size, and size-adjustments in morphometrics. American Journal of Physical Anthropology 38, 137–161.

Jungers, W.L., Grine, F.E., Leakey, M.G., Leakey, L., Brown, F., Yang, D., Tocheri, M.W. 2015. New Hominin fossils from Ileret (Kolom Odiet), Kenya. American Journal of Physical Anthropology Supplement 60, 181.

Jungers, W.L., Harcourt-Smith, W.E.H., Wunderlich, R.E., Tocheri, M.W., Larson, S.G., Sutikna, T., Due, R.A., Morwood, M.J., 2009. The foot of *Homo floresiensis.* Nature 459, 81–84.

Kaifu, Y., Baba, H., Sutikna, T., Morwood, M.J., Kubo, D., Saptomo, E.W., Jatmiko, Awe, R.D., Djubiantono, T., 2011. Craniofacial morphology of *Homo floresiensis*: description, taxonomic affinities, and evolutionary implication. Journal of Human Evolution 61, 644–682.

Kass, R.E., Raftery, A.E., 1995. Bayes Factors. Journal of American Statistical Association 90, 773-795.

Kimbel, W.H., 2013. Hesitation on hominin history. Nature 497, 573–574.

Kimbel, W.H., Rak, Y., Johanson, D.C., 2004. The skull of *Australopithecus afarensis*, Oxford University Press, New York.

Kivell, T.L., Deane, A.S., Tocheri, M.W., Orr, C.M., Schmid, P., Hawkes, J., Berger, L.R., Churchill, S.E., 2015. The hand of *Homo naledi.* Nature Communication 6, 8431.

Kluge, A.G., 1989. A concern for evidence and a phylogenetic hypothesis of relationships among Epicrates (Boidae, Serpentes). Systematic Zoology 38, 7-25.

Kluge, A.G., Farris, J.S., 1969. Quantitative phyletics and the evolution of Anurans. Cladistics 18, 1–32.

Kramer, A., Crummett, T.L., Wolpoff, M.H., 2001. Out of Africa and into the Levant: replacement or admixture in Western Asia? Quaternary International 75, 51–63.

Kubo, D., Kono, R.T., Kaifu, Y., 2013. Brain size of *Homo floresiensis* and its evolutionary implications. Proceedings of the Royal Society B 280, 20130338.

Kuhner, M.K., Felsenstein, J., 1994. A simulation comparison of phylogeny algorithms under equal and unequal evolutionary rates. Molecular Biology and Evolution 11, 459–468.

Lahr, M.M., 1996. The evolution of modern human diversity: a study of cranial variation. Cambridge University Press, Cambridge.

Leakey, M.G., Feibel, C.S., McDougall, I., Walker, A., 1995. New four-million-year-old hominid species from Kanapoi and Allia Bay, Kenya. Nature 376, 565–571.

Leakey, M.G., Spoor, F., Brown, F.H., Gathogo, P.N., Kiarie, C., Leakey, L.N., McDougall, I., 2001. New hominin genus from eastern Africa shows diverse middle Pliocene lineages. Nature 410, 433–440.

Lee, M.S.Y., Cau, A., Naish, D., Dyke, G.J., 2014a. Morphological clocks in palaeontology, and a mid-Cretaceous origin of crown Aves. Systematic Biology 63, 442–449.

Lee, M.S.Y., Cau, A., Naish, D., Dyke, G.J., 2014b. Sustained miniaturization and anatomical innovation in the dinosaurian ancestors of birds. Science 345, 562–566.

Lee, M.S.Y., Palci, A., 2015. Morphological Phylogenetics in the Genomic Age. Current Biology 25, R922–R929.

Lemey, P., Rambaut, A., Welch, J.J., Suchard, M.A., 2010. Phylogeography takes a relaxed random walk in continuous space and time. Molecular Biology and Evolution 27, 1877–1885.

Lewis, P.O., 2001. A likelihood approach to estimating phylogeny from discrete morphological character data. Systematic Biology 50, 913–925.

Lieberman, D.E., 1995. Testing hypotheses about recent human evolution from skulls: integrating morphology, function, development, and phylogeny. Current Anthropology 36, 159–197.

Lieberman, D.E., 1999. Homology and hominid phylogeny: problems and potential solutions. Evolutionary Anthropology 7, 142–151.

Lieberman, D.E., Wood, B.A., Pilbeam, D.R., 1996. Homoplasy and early *Homo*: an analysis of the evolutionary relationships of *H. habilis sensu stricto* and *H. rudolfensis*. Journal of Human Evolution 30, 97–120.

Lockwood, C.A., Fleagle, J.G., 1999. The recognition and evaluation of homoplasy in primate and human evolution. Yearbook of Physical Anthropology 42, 189–232.

Lockwood, C.A., Kimbel, W.H., Lynch, J.M., 2004. Morphometrics and hominoid phylogeny: support for a chimpanzee-human clade and differentiation among great ape subspecies. Proceedings of the National Academy of Sciences 101, 4356–4360.

Lordkipanidze, D., Jashashvili, T., Vekua, A., Leo, M.S.P. De, Rightmire, G.P., Pontzer, H., Ferring, R., Oms, O., Tappen, M., Bukhsianidze, M., Agusti, J., Kahlke, R., Kiladze, G., Martinez-navarro, B., Mouskhelishvili, A., 2007. Postcranial evidence from early *Homo* from Dmanisi, Georgia. Nature 449, 305–310.

Lordkipanidze, D., Ponce de León, M.S., Margvelashvili, A., Rak, Y., Rightmire, G.P., Vekua, A., Zollikofer, C.P.E., 2013. A complete skull from Dmanisi, Georgia, and the evolutionary biology of early *Homo*. Science 342, 326–331.

Lordkipanidze, D., Vekua, A., Ferring, R., Rightmire, G.P., Agusti, J., Kiladze, G., Mouskhelishvili, A., Nioradze, M., Ponce de León, M.S., Tappen, M., Zollikofer, C.P.E., 2005. The earliest toothless hominin skull. Nature 434, 717–718.

Lycett, S.J., Collard, M., 2005. Do homoiologies impede phylogenetic analyses of the fossil hominids? An assessment based on extant papionin craniodental morphology. Journal of Human Evolution 49, 618–642.

Maddison, W.P., 1997. Gene trees in species trees. Systematic Biology 46, 523–536.

Manzi, G., Mallegni, F., Ascenzi, A., 2001. A cranium for the earliest Europeans: phylogenetic position of the hominid from Ceprano, Italy. Proceedings of the National Academy of Sciences 98, 10011–6.

Martinón-Torres, M., Bermúdez de Castro, J.M., Gomez-Robles, A., Arsuaga, J.L., Carbonell, E., Lordkipanidze, D., Manzi, G., Margvelashvili, A., 2007. Dental evidence on the hominin dispersals during the Pleistocene. Proceedings of the National Academy of Sciences 104, 13279–13282.

Martinón-Torres, M., Bermúdez de Castro, J.M., Gómez-Robles, A., Margvelashvili, A., Prado, L., Lordkipanidze, D., Vekua, A., 2008. Dental remains from Dmanisi (Republic of Georgia): Morphological analysis and comparative study. Journal of Human Evolution 55, 249–273.

McCollum, M.A., 1999. The robust australopithecine face : A morphogenetic perspective. Science 284, 301–305.

Mickevich, M.F., Johnson, M.S., 1976. Congruence between morphological and allozyme data in evolutionary influence and character evolution. Systematic Zoology 25, 260–270.

Miller, M.A., Pfeiffer, W., Schwartz, T., 2010. Creating the CIPRES Science Gateway for inference of large phylogenetic trees. Proceedings of the Gateway Computing Environments Workshop *(GCE) 14 Nov. 2010* (New Orleans, LA), 1–8.

Mitteroecker, P., Bookstein, F., 2008. The evolutionary role of modularity and integration in the hominoid cranium. Evolution 62, 943–958.

Miyamoto, M.M., Fitch, W.M., 1995. Testing species phylogenies and phylogenetic methods with congruence. Systematic Biology 44, 64–76.

Morwood, M.J., Soejono, R.P., Roberts, R.G., Sutikna, T., Turney, C.S.M., Westaway, K.E., Rink, W.J., Due, R.A., Hobbs, D.R., Moore, M.W., Bird, M.I., Fifield, L.K., 2004. Archaeology and age of a new hominin from Flores in eastern Indonesia. Nature 431, 1087–1091.

Morwood, M.J., Jungers, W.L., 2009. Conclusions: implications of the Liang Bua excavations for hominin evolution and biogeography. Journal of Human Evolution 57, 640–648.

Mounier, A., Balzeau, A., Caparros, M., Grimaud-Hervé, D., 2016. Brain, calvarium, cladistics: A new approach to an old question, who are modern humans and Neandertals? Journal of Human Evolution 92, 22–36.

Mounier, A., Caparros, M., 2015. The phylogenetic status of *Homo heidelbergensis* – a cladistic study of Middle Pleistocene hominins. Bulletins et Mémoires de la Société d'Anthropologie de Paris 27, 110–134.

Mounier, A., Marchal, F., Condemi, S., 2009. Is *Homo heidelbergensis* a distinct species? New insight on the Mauer mandible. Journal of Human Evolution 56, 219–246.

Nadal-Roberts, M., Collard, M., 2005. Impact of methodological choices on assessments of the reliability of fossil primate phylogenetic hypotheses. Folia Primatologica 76, 207–221.

Newton, M.A., Raftery, A.E., 1994. Approximante Bayesian Inference with the Weights Likelihood Bootstrap. Journal of the Royal Statistical Society B 56, 3-48.

Nylander, J., Ronquist, F., Huelsenbeck, J.P., Nieves-Aldrey, J., 2004. Bayesian phylogenetic analysis of combined data. Systematic Biology 53, 47–67.

Obendorf, P.J., Oxnard, C.E., Kefford, B.J., 2008. Are the small human-like fossils found on Flores human endemic cretins? Proceedings of the Royal Society B 275, 1287–1296.

Olson, T.R., 1981. Basicranial morphology of the extant hominoids and Pliocene hominids: the new material from the Hadar Formation, Ethiopia, and its significance in early human evolution and taxonomy. In: Stringer, C.B. (Ed.), Aspects of Human Evolution. Taylor & Francis Lt, London, pp. 99–128.

Pagel, M., Meade, A., 2006. Bayesian Analysis of Correlated Evolution of Discrete Characters by Reversible-Jump Markov Chain Monte Carlo. The American Naturalist 167, 808–825.

Pagel, M., Meade, A., 2008. Modelling heterotachy in phylogenetic inference by reversible-jump Markov chain Monte Carlo. Philosophical Transactions of Royal Society B 363, 3955-3964.

Pickering, R., Dirks, P.H.G.M., Jinnah, Z., de Ruiter, D.J., Churchil, S.E., Herries, A.I.R., Woodhead, J.D., Hellstrom, J.C., Berger, L.R., 2011. *Australopithecus sediba* at 1.977 Ma and implications for the origins of the genus *Homo*. Science 333, 1421–3.

Pimentel, R.A., Riggins, R., 1987. The nature of cladistic data. Cladistics 3, 201–209.

Pyron, R.A., 2011. Divergence time estimation using fossils as terminal taxa and the origins of Lissamphibia. Systematic Biology 60, 466-481.

R Core Team, 2015. R: A language and environment for statistical computing. R Foundation for Statistical Computing, Vienna, Austria. URL http://www.R-project.org/.

Rae, T., 1998. The Logical Basis for the use of Continuous Characters in Phylogenetic Systematics. Cladistics 14, 221–228.

Rambaut, A., Suchard, M.A., Xie, D., Drummond, A.J., 2014. Tracer v1.6, Available from http://beast.bio.ed.ac.uk/Tracer.

Randolph-Quinney, P.S. 2015. The mournful ape: conflating expression and meaning in the mortuary behaviour of *Homo naledi*. South African Journal of Science 111, 1-5.

Rannala, B., Yang, Z., 1996. Probability distribution of molecular evolutionary trees: a new method of phylogenetic inference. Journal of Molecular Evolution 43, 304-311.

Rightmire, G.P., Lordkipanidze, D., Vekua, A., 2006. Anatomical descriptions, comparative studies and evolutionary significance of the hominin skulls from Dmanisi, Republic of Georgia. Journal of Human Evolution 50, 115–141.

Roberts, R.G., Westaway, K.E., Zhao, J., Turney, C.S.M., Bird, M.I., Rink, W.J., Fifield, L.K., 2009. Geochronology of cave deposits at Liang Bua and of adjacent river terraces in the Wae Racang valley, western Flores, Indonesia: a synthesis of age estimates for the type locality of *Homo floresiensis*. Journal of Human Evolution 57, 484–502.

Rogers, J., Gibbs, R.A., 2014. Comparative primate genomics: emerging patterns of genome content and dynamics. Nature Reviews Genetics 15, 347–59.

Ronquist, F., Huelsenbeck, J.P., 2003. MrBayes 3: Bayesian phylogenetic inference under mixed models. Bioinformatics 19, 1572–1574.

Ronquist, F., Klopfstein, S., Vilhelmsen, L., Schulmeister, S., Murray, D.L., Rasnitsyn, A.P., 2012a. A total-evidence approach to dating with fossils, applied to the early radiation of the hymenoptera. Systematic Biology 61, 973-999.

Ronquist, F., Teslenko, M., van der Mark, P., Ayres, D.L., Darling, A., Höhna, S., Larget, B., Liu, L., Suchard, M.A., Huelsenbeck, J.P., 2012b. MrBayes 3.2: efficient Bayesian phylogenetic inference and model choice across a large model space. Systematic Biology 61, 539-542.

Roseman, C.C., 2004. Detecting interregionally diversifying natural selection on modern human cranial form by using matched molecular and morphometric data. Proceedings of the National Academy of Sciences 101, 12824–12829.

Ruvolo, M., 1997. Molecular phylogeny of the hominoids: inferences from multiple independent DNA sequence data sets. Molecular Biology and Evolution 14, 248–265.

Schliep, K.P., 2011. Phangorn: Phylogenetic analysis in R. Bioinformatics 27, 592–593.

Schols, P., D'hondt, C., Geuten, K., Merckx, V., Janssens, S., Smets, E., 2004. MorphoCode : coding quantitative data for phylogenetic analysis. PhyloInformatics 4, 1–4.

Schrenk, F., Kullmer, O., Bromage, T., 2015. The earliest putative *Homo* fossils. In: Henke, W., Tattersall, I. (Eds.), Handbook of Paleoanthropology 2nd edition, Springer Reference, New York, pp 2145-2166.

Schwartz, J.H., 2000. Taxono of the Dmanisi Crania. Science 289, 55–56.

Schwartz, J.H., Tattersall, I., Chi, Z., 2014. Comment on 'A complete skull from Dmanisi, Georgia, and the evolutionary biology of early *Homo*'. Science 344, 360.

Scotland, R.W., Olmstead, R.G., Bennett, J.R., 2003. Phylogeny reconstruction: the role of morphology. Systematic Biology 52, 539–548.

Senut, B., Pickford, M., Gommery, D., Mein, P., Cheboi, K., Coppens, Y., 2001. First hominid from the Miocene (Lukeino Formation, Kenya). Comptes Rendus de l'Académie des Sciences - Series IIA - Earth and Planetary Science 332, 137–144.

Simon, C., 1983. A new coding procedure for morphometric data with an example from periodical Cicada wing veins. In: Felsenstein, J. (Ed.), Numerical Taxonomy NATO Advanced Science Institute. Springer, Berlin, pp. 378–382.

Singh, N., Harvati, K., Hublin, J.-J., Klingenberg, C.P., 2012. Morphological evolution through integration: a quantitative study of cranial integration in *Homo, Pan, Gorilla* and *Pongo*. Journal of Human Evolution 62, 155–64.

Skelton, R.R., McHenry, H.M., 1992. Evolutionary relationships among early hominids. Journal of Human Evolution 23, 309–349.

Skelton, R.R., McHenry, H.M., Drawhorn, G.M., 1986. Phylogenetic analysis of early hominids. Current Anthropology 27, 21–43.

Skinner, M.M., Gordon, A.D., Collard, N.J., 2006. Mandibular size and shape variation in the hominins at Dmanisi, Republic of Georgia. Journal of Human Evolution 51, 36–49.

Smith, H.F., 2009. Which cranial regions reflect molecular distances reliably in humans? Evidence from three-dimensional morphology. American Journal of Human Biology 47, 36–47.

Smith, H.F., Grine, F.E., 2008. Cladistic analysis of early *Homo* crania from Swartkrans and Sterkfontein, South Africa. Journal of Human Evolution 54, 684–704.

Smith, N.D., Turner, A.H., 2005. Morphology's role in phylogeny reconstruction: perspectives from paleontology. Systematic Biology 54, 166–173.

Smith, R.J., 2005. Species recognition in paleoanthropology; implications of small sample sizes. In: Lieberman, D.E., Smith, R.J., Kelley, J., (Eds.), Interpreting the past: essays on human, primate, and mammal evolution in honor of David Pilbeam. Boston: Brill Academic Publishers. p 207–219.

Sokal, R.R., Rohlf, F.J., 1995. Biometry: the principles and practice of statistics in biological research. 3rd ed. W.H. Freeman, New York.

Spoor, F., 2013. Small-brained and big-mouthed. Nature 502, 452–453.

Steel, M., Penny, D., 2000. Parsimony, likelihood, and the role of models in molecular phylogenetics. Molecular Biology and Evolution 17, 839–850.

Stevens, P.F., 1991. Character states, morphological variation, and phylogenetic analysis: a review. Systematic Botany 16, 553.

Strait, D.S., 2001. Integration, phylogeny, and the hominid cranial base. American Journal of Physical Anthropology 114, 273–297.

Strait, D.S., 2013. The biogeographic implications of early hominin phylogeny. In: Reed, K.E., Fleagle, J.G., Leakey, R.E. (Eds.), The paleobiology of *Australopithecus*, Springer, New York, pp 183-194.

Strait, D.S., Grine, F.E., 2004. Inferring hominoid and early hominid phylogeny using craniodental characters: the role of fossil taxa. Journal of Human Evolution 47, 399–452.

Strait, D.S., Grine, F.E., Moniz, M.A., 1997. A reappraisal of early hominid phylogeny. Journal of Human Evolution 32, 17–82.

Strait, D., Grine, F.E., Fleagle, J.G., 2015. Analyzing hominin phylogeny: cladistic approach. In: Henke, W., Tattersall, I. (Eds.), Handbook of Paleoanthropology 2nd edition, Springer Reference, New York, pp 1989-2014.

Strait, D.S., Wood, B.A, 1999. Early hominid biogeography. Proceedings of the National Academy of Sciences 96, 9196–9200.

Stringer, C.B., 1987. A numerical cladistic analysis for the genus *Homo*. Journal of Human Evolution 16, 135–146.

Swiderski, D.L., Zelditch, M.L., Fink, W.L., 1998. Why morphometrics is not special: coding quantitative data for phylogenetic analysis. Systematic Biology 47, 508–519.

Swofford DL. 2003. PAUP*. Phylogenetic Analysis Using Parsimony (*and Other Methods). Version 4. Sunderland, Sinauer Associates.

Tattersall, I., Eldredge, N., 1977. Fact, theory and fantasy in human paleontology. American Scientist 65, 204–211.

Thackeray, J.F., 2015. Estimating the age and affinities of *Homo naledi*. South African Journal of Science 111, 11–12.

Thiele, K., 1993. The Holy Grail of the perfect character: the cladistic treatment of morphometric data. Cladistics 9, 275–304.

Thorne, J.L., Kishino, H., 2002. Divergence time and evolutionary rate estimation with multilocus data. Systematic Biology 51, 689–702.

Thorpe R.S., 1984. Coding morphometrics characters for constructing distance Wagner networks. Evolution 38, 244 –255.

Tocheri, M.W., Orr, C.M., Larson, S.G., Sutikna, T., Jatmiko, Saptomo, E.W., Due, R.A., Djubiantono, T., Morwood, M.J., Jungers, W.L., 2007. The primitive wrist of Homo floresiensis and its implications for hominin evolution. Science 317, 1743–1745.

Trinkaus E. 1990. Cladistics and the hominid fossil record. American Journal of Physical Anthropology 83, 1–11.

Tucker, A., Sharpe, P., 2004. The cutting-edge of mammalian development; how the embryo makes teeth. Nature Reviews Genetics 5, 499–508.

Vekua, A., Lordkipanidze, D., Rightmire, G.P., Agusti, J., Ferring, R., Maisuradze, G., Mouskhelishvili, A., Nioradze, M., De Leon, M.P., Tappen, M., Tvalchrelidze, M., Zollikofer, C.P.E., 2002. A new skull of early Homo from Dmanisi, Georgia. Science 297, 85–89.

Venn, O., Turner, I., Mathieson, I., de Groot, N., Bontrop, R., McVean, G., 2014. Strong male bias drives germline mutation in chimpanzees. Science 344, 1272–1275.

Villmoare, B. A., Dunmore, C., Kilpatrick, S., Oertelt, N., Depew, M.J., Fish, J.L., 2014. Craniofacial modularity, character analysis, and the evolution of the premaxilla in early African hominins. Journal of Human Evolution 77, 143–154.

Villmoare, B., Kimbel, W.H., Seyoum, C., Campisano, C.J., Dimaggio, E.N., Rowan, J., Braun, D.R., Arrowsmith, J.R., Reed, K.E., 2015. Early *Homo* at 2.8 Ma from Ledi-Geraru, Afar, Ethiopia. Science 347, 1352–1355.

von Cramon-Taubadel, N., 2009a. Congruence of individual cranial bone morphology and neutral molecular affinity patterns in modern humans. American Journal of Physical Anthropology 140, 205–215.

von Cramon-Taubadel, N., 2009b. Revisiting the homoiology hypothesis : the impact of phenotypic plasticity on the reconstruction of human population history from craniometric data. Journal of Human Evolution 57, 179–190.

von Cramon-Taubadel, N., Cramon-taubadel, N. Von, 2011. Global human mandibular variation reflects differences in agricultural and hunter-gatherer subsistence strategies. Proceedings of the National Academy of Sciences 108, 19546–19551.

von Cramon-Taubadel, N., Smith, H.F., 2012. The relative congruence of cranial and genetic estimates of hominoid taxon relationships: Implications for the reconstruction of hominin phylogeny. Journal of Human Evolution 62, 640–53.

White, T.D., Asfaw, B., Beyene, Y., Haile-Selassie, Y., Lovejoy, C.O., Suwa, G., WoldeGabriel, G., 2009. *Ardipithecus ramidus* and the paleobiology of early hominids. Science 326, 75–86.

Wiens, J.J., 2001. Character analysis in morphological phylogenetics: problems and solutions. Systematic Biology 50, 689–699.

Wiens, J.J., 2004. The role of morphological data in phylogeny reconstruction. Systematic Biology 53, 653–61.

Wiens, J.J., Servedio, M.R., 1998. Phylogenetic analysis and intraspecific variation: performance of parsimony, likelihood, and distance methods. Systematic Biology 47, 228–253.

Wood BA. 1975. An analysis of sexual dimorphism in primates. Ph.D. Dissertation. University of London.

Wood, B.A., 1991. A palaeontological model for determining the limits of early hominid taxonomic variability. Palaeontologica Africana 28, 71–77.

Wood, B.A., 1992. Origin and evolution of the genus *Homo*. Nature 355, 783–90.

Wood, B.A., Boyle, E.K., 2016. Hominin taxic diversity: Fact or fantasy? Yearbook of Physical Anthropology 159, S37–S78.

Wood, B.A., Chamberlain, A.T., 1987. The nature and affinities of the “robust” australopithecines: a review. Journal of Human Evolution 16, 625–641.

Wood, B.A., Collard, M., 1999. The human genus. Science 284, 65–71.

Wood, B.A., Lieberman, D.E., 2001. Craniodental variation in *Paranthropus boisei*: a developmental and functional perspective. American Journal of Physical Anthropology 116, 13–25.

Wood, B.A., Li, Y., Willoughby, C., 1991. Intraspecific variation and sexual dimorphism in cranial and dental variables among higher primates and their bearing on the hominid fossil record. Journal of Anatomy 174, 185–205.

Wood, H.M., Matzke, N.J., Gillespie, R.G., Griswold, C.E., 2013. Treating fossils as terminal taxa in divergence time estimation reveals ancient vicariance patterns in the palpimnoid spiders. Systematic Biology 62, 264-284.

Wright, A.M., Hillis, D.M., 2014. Bayesian analysis using a simple likelihood model outperforms parsimony for estimation of phylogeny from discrete morphological data. PloS One 9, e109210.

Wright, A.M., Lloyd, G.T., Hillis, D.M., 2015. Modeling character change heterogeneity in phylogenetic analyses of morphology through the use of priors. Systematic Biology. Advance Access published December 28, 2015, doi:10.1093/sysbio/syv122.

Xie, W., Lewis, P.O., Fan, Y., Kuo, L., Chen, M.H., 2011. Improving marginal likelihood estimation for Bayesian phylogenetic model selection. Systematic Biology 60, 150–160.

Yang, Z., 1994. Maximum likelihood phylogenetic estimation from DNA sequences with variable rates over sites: approximate methods. Journal of Molecular Evolution 39, 306–314.

Yang, Z., Rannala, B., 1997. Bayesian phylogenetic inference using DNA sequences: a Markov chain Monte Carlo method. Molecular Biology and Evolution 14, 717–724.

Zeitoun, V., 2009. The Human Canopy: *Homo erectus*, *Homo soloensis*, *Homo pekinensis* and *Homo floresiensis*. J. and E. Hedges, Oxford.

Zollikofer, C.P.E., Ponce de León, M.S., Margvelashvili, A., Rightmire, G.P., Lordkipanidze, D., 2014. Response to comment on 'A complete skull from Dmanisi, Georgia, and the evolutionary biology of early Homo'. Science 344, 360.

Zuckerkandl, E., Pauling, L., 1962. Molecular disease, evolution, and genetic heterogeneity. In: Kasha, M., Pullman, B. (Eds), Horizons in Biochemistry, Academic Press, New York, pp 189-225.

Appendix A.

Supplementary material for Chapter 2

Table A1 List of 76 characters used in Study 1 taken from Wood (1975) and Wood et al. (1991).

Palatal traits	Mandibular traits	Craniofacial traits
I^1 labiolingual diameter	I_1 labiolingual diameter	Right orbital breadth
I^1 mesiodistal diameter	I_1 mesiodistal diameter	Right orbital height
I^2 labiolingual diameter	I_2 labiolingual diameter	Interorbital breadth
I^2 mesiodistal diameter	I_2 mesiodistal diameter	Biorbital breadth
C labiolingual diameter	C labiolingual diameter	Nasion-rhinion
C mesiodistal diameter	C mesiodistal diameter	Nasion-nasospinale
C labial height	C labial height	Maximum nasal width
P^3 buccolingual diameter	P_3 buccolingual diameter	Nasospinale-prosthion
P^3 mesiodistal diameter	P_4 buccolingual diameter	Bijugal breadth
P^4 buccolingual diameter	P_4 mesiodistal diameter	Bizygomatic breadth
P^4 mesiodistal diameter	M_1 buccolingual diameter	Glabella-opisthocranion
M^1 buccolingual diameter	M_1 mesiodistal diameter	Minimum post-orbital breadth
M^1 mesiodistal diameter	M_2 buccolingual diameter	Basion-bregma
M^2 buccolingual diameter	M_2 mesiodistal diameter	Maximum bi-parietal breadth
M^2 mesiodistal diameter	M_3 buccolingual diameter	Biporionic width
M^3 buccolingual diameter	M_3 mesiodistal diameter	Mastoid length
M^3 mesiodistal diameter	Maximum cusp height	Coronale-coronale
Outer alveolar breadth at M^3	Condylar height	Bimastoid width
Inter upper canine breadth	Opisthion-inion	Posterior skull length
Palate length	Bicondylar height	Breadth of infratemporal fossa
Inner alveolar breadth at M^3	Coronoid height	
Palate depth at up M1	Bicoronoid height	
Prosthion to plane of M^3	Right condylar head width	
	Right condylar head AP breadth	
	Ramal breadth	
	Bigonial width	
	Height of mandibular body at M_1	
	Thickness of mandibular body at M_1	
	Symphyseal height	

	Symphyseal thickness	
	Inner alveolar breadth at M_3	
	Maximum mandibular length	
	Inter lower canine distance	

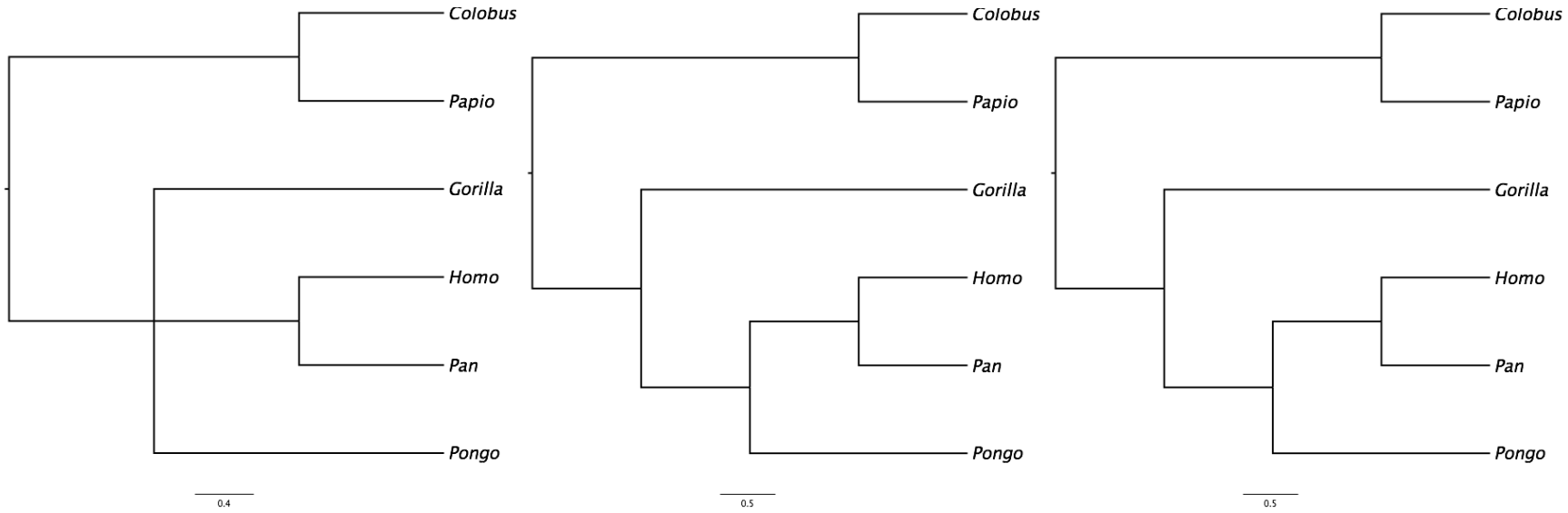

Figure A1 MP strict consensus trees using divergence coding.
Data coded using standard divergence coding (left), divergence coding with Bonferroni correction (middle), and divergence coding with Dunn's test (right).

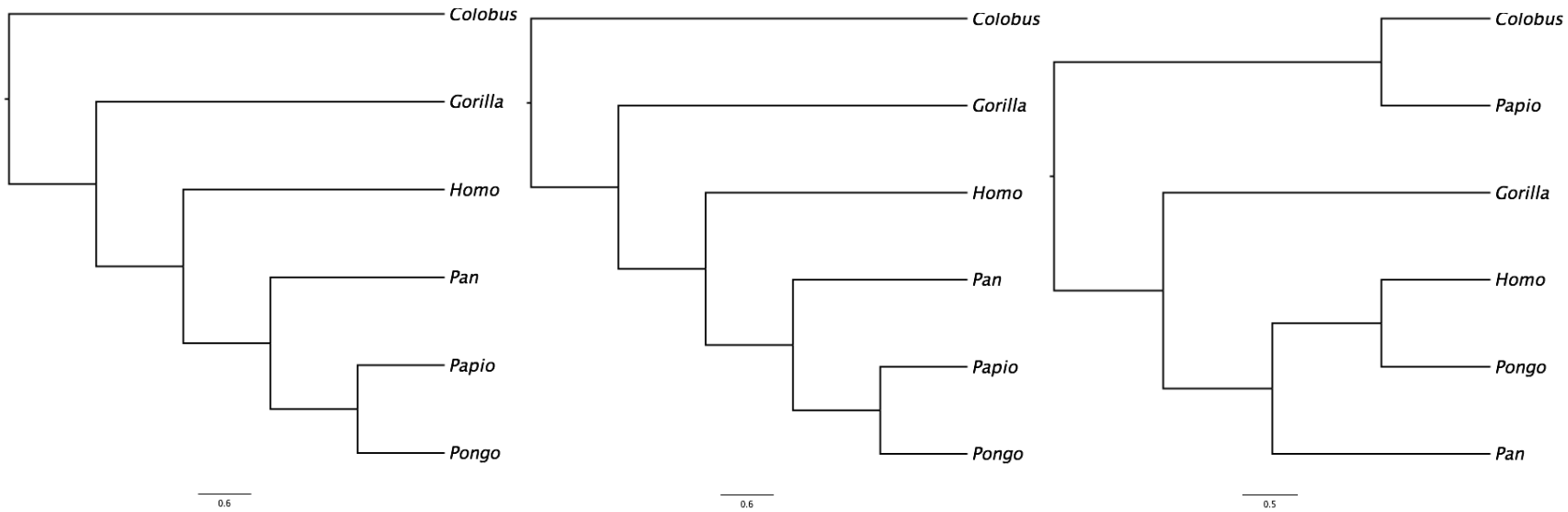

Figure A2 MP strict consensus trees using subset coding.
Data coded using standard subset coding (left), subset coding with Bonferroni correction (middle), and subset coding with Dunn's test (right).

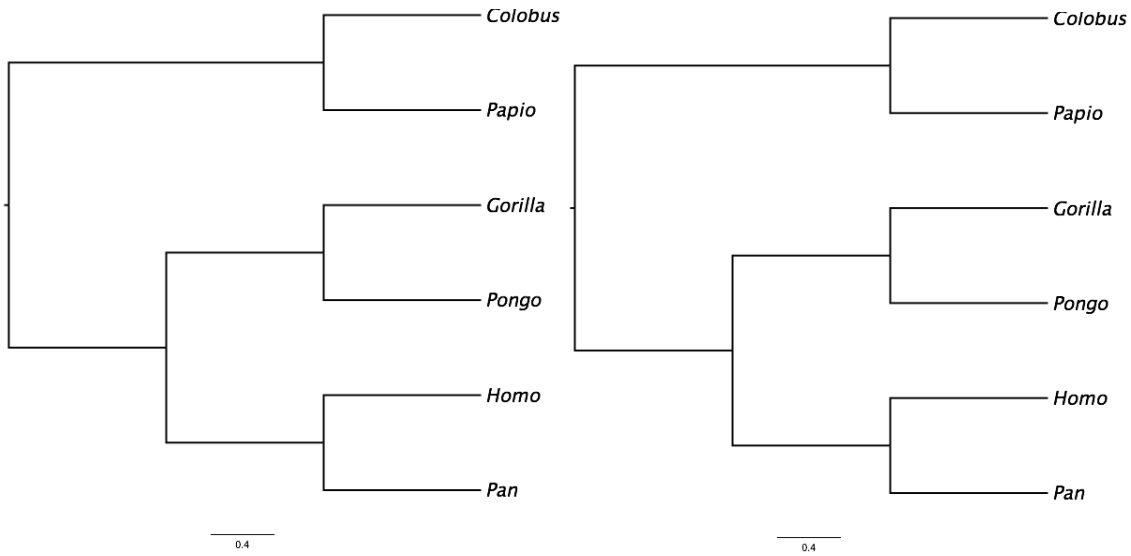

Figure A3 MP strict consensus trees using gap coding.
Data coded using 10 states (left) and 26 states (right).

Appendix B.

Supplementary material for Chapter 3

B1. Analysing phylogenetic hypotheses using Bayes factors.

We combined Bayesian methods for estimating phylogenetic relationships from morphological data [1, 2] with techniques that allow the relative support for phylogenetic hypotheses to be formally compared [3]. Here, we provide a brief, non-technical primer for these approaches. More in-depth discussion and comparisons with, e.g. distance and parsimony methods, can be found in Holder and Lewis [4], while Kass and Raftery [5] is an accessible and authoritative discussion of Bayes factors.

Though supported by a different philosophical camp, Bayesian phylogenetic inference is closely allied to the maximum likelihood (ML) approach to phylogenetic reconstruction. Under ML, one first specifies a model of evolution for characters (e.g. Lewis' Markov-k model [6]). One then evaluates candidate trees (topologies and branch lengths) and candidate model parameters (e.g. the average rate of evolution of the characters, and the variance in that rate among characters) by calculating the likelihood of seeing the observed data if the candidate tree and parameters had produced those data. Researchers then report the best-fit tree as the maximum likelihood or ML tree, often ignoring the attendant ML parameter values that lead to that best fit.

Bayesian phylogenetic methods extend the above process in two important ways. First, individual trees and parameter values are assessed not only in relation to their fit to the data, but also in relation to prior beliefs about what the trees and parameter values might be. The Bayesian "posterior" probability of a particular tree (and the attendant parameter values) is calculated using three steps. First, the likelihood of observing the data given that tree and parameters is computed. This is then multiplied by the prior probability of that tree and parameter values. Lastly, the product obtained in the previous step is normalized by (i.e. divided by) the probability of the data under all possible trees and parameter values.

Formally, these steps are expressed in the following equation:

$$P(T, \theta \mid X) = \frac{P(X|T, \theta)P(T, \theta)}{P(X)}$$

where $P(T, \theta|X)$ is the posterior probability of the tree (T) and the parameters (θ) given the data (X); $P(X|T, \theta)$ is the likelihood of the tree and the parameters; $P(T, \theta)$ is the prior probability of the tree and the parameters; and $P(X)$ is the normalizing probability.

The first term in the numerator is familiar. For the second term in the numerator, we usually have few prior beliefs, and so most candidate trees and parameter values will be given equal prior probabilities and so not have much influence on the final probabilities. In the study reported here, we attached specific prior probabilities for the ages of nodes in the tree, with higher prior probabilities for depths that correspond to a simple birth-death model of diversification (see main text, 2. Materials and Methods - model selection - priors on node ages).

The term in the denominator is related to the fact that the Bayesian framework returns a point probability for each tree and set of parameter values. The sum of these point probabilities across all possible trees and parameter values must equal 1.0. As an analogy, if we are told that a pair of die has produced a roll of 4 (the observed data), we can calculate the probabilities for each of

the two possible ways we could have got this result. The two hypotheses are that we either rolled a 1 and a 3, with probability = 2*1/6*1/6 = 1/18, or we rolled a pair of 2s with probability 1/6*1/6 = 1/36. The overall probability of getting a 4 in a roll of two dice is just the sum of these two, i.e. 1/18+1/36=1/12, and this is the normalizing constant when comparing hypotheses. So, the probability of the first hypothesis given the data is (1/18)/(1/12) = 2/3 and the probability of the second hypothesis given the data is (1/36)/(1/12) = 1/3. Unfortunately, in phylogenetics, there are not just two possible ways to get a set of observed data; there are an infinite number of ways. So, we cannot simply calculate the overall probability of the data needed to get the posterior probabilities. Bayesian phylogenetic methods estimate the posterior probabilities of trees using a roundabout method. This is the second important extension to ML techniques.

The method in question estimates the posterior probability of a tree as its frequency in a distribution of evaluated trees. Trees are evaluated and retained in this distribution in an iterative manner: the program proposes a new tree or set of parameter values, and then multiplies the resulting likelihood by the prior probability of the tree and attendant parameter values. This is then compared to the previously retained tree. If the parameter values are better than the previous tree's, the new tree is retained. If they are worse, it is retained in proportion to how much worse it is (e.g. a topology that is 10X worse would only have a 1/10 chance of being retained). Every time a new tree is retained, the process has produced a "generation" in a "chain" and the new tree becomes the tree for comparison. This is usually done millions of times, with good combinations of trees and parameter values being retained in the sample, suboptimal ones retained at lower frequency, and very poor ones ignored. Multiple chains can be run in parallel, with some ("hot") chains being less likely to reject new topologies in the hopes of sampling more broadly in search of optimal solutions. Early on in a chain, while subsequent trees may be retained, they may all fit the data poorly, and so these early generations are generally discarded as "burn-in." This sampling procedure is called the Markov Chain Monte Carlo (MCMC), and leads to a "posterior MCMC distribution" of trees and their attendant parameter values, prior probabilities and likelihoods. Generally, while many millions of trees are evaluated and some large proportion retained, distributions are usually composed of trees from a smaller subsample, e.g. every 1000th tree in a chain may be retained for further analyses.

The resulting posterior distribution is composed of a large sample of trees each of which may differ in its shape and/or in the parameter values used to fit the data to that tree. This large sample allows individual clades to be evaluated (a clade's "posterior," analogous to its bootstrap proportion, is just the proportion of times it appears in trees in the sample). Importantly for present purposes, the posterior MCMC distribution of trees also allows specific hypotheses to be compared. This leads to the use of our second tool—Bayes factor analysis.

A Bayes factors is, in its simplest incarnation, a ratio of two likelihoods, where each represents how well a hypothesis fits observed data. Trees in a posterior distribution may have similar topologies but different parameter values for the underlying model of character evolution. If we combine their likelihoods, we are integrating over these posterior parameter values, and we can report a "marginal likelihood" of the particular tree topology, effectively averaging across many possible parameter values (this contrasts with the ML tree, which is the one whose parameter values contributes to its superior fit to the data).

The essence of our test makes use of these marginal likelihoods: to compare two hypotheses about hominin evolution, we first constructed two posterior samples using MCMC. Each retained only topologies that conform to its hypothesis (see Figure S1: we did not propose tree topologies that conflict with the hypothesis in the MCMC chain). We then summarized the marginal likelihoods from this sample (details given in main text, 2. Analyses) and compared them, using the accepted guidelines from Kass and Raftery [5] for evaluating whether there is strong

evidence in favour of one hypothesis of relationship over another. The marginal likelihoods and corresponding Bayes factors we obtained are given in Tables 1-3 in main text.

B2. A cartoon of the topological constraints

Figure B1 **A cartoon of the topological constraints specified by three competing hypotheses for the phylogenetic position of species D on a simple tree, and the interpretation of the Bayes factor tests.**

The three hypotheses are represented by the column "Topological constraints" and a partially constrained model tree: under hypothesis 1, D is the sister species to A; under hypothesis 2, D is the sister species of B; under hypothesis 3, D is more closely related to B and C than it is to A. Red edges are where the target species (D) can enter the corresponding model tree. For each hypothesis, we show one possible position after the data are analysed. Bayes factor tests are carried out by comparing the marginal log likelihood of the best model to the other models.

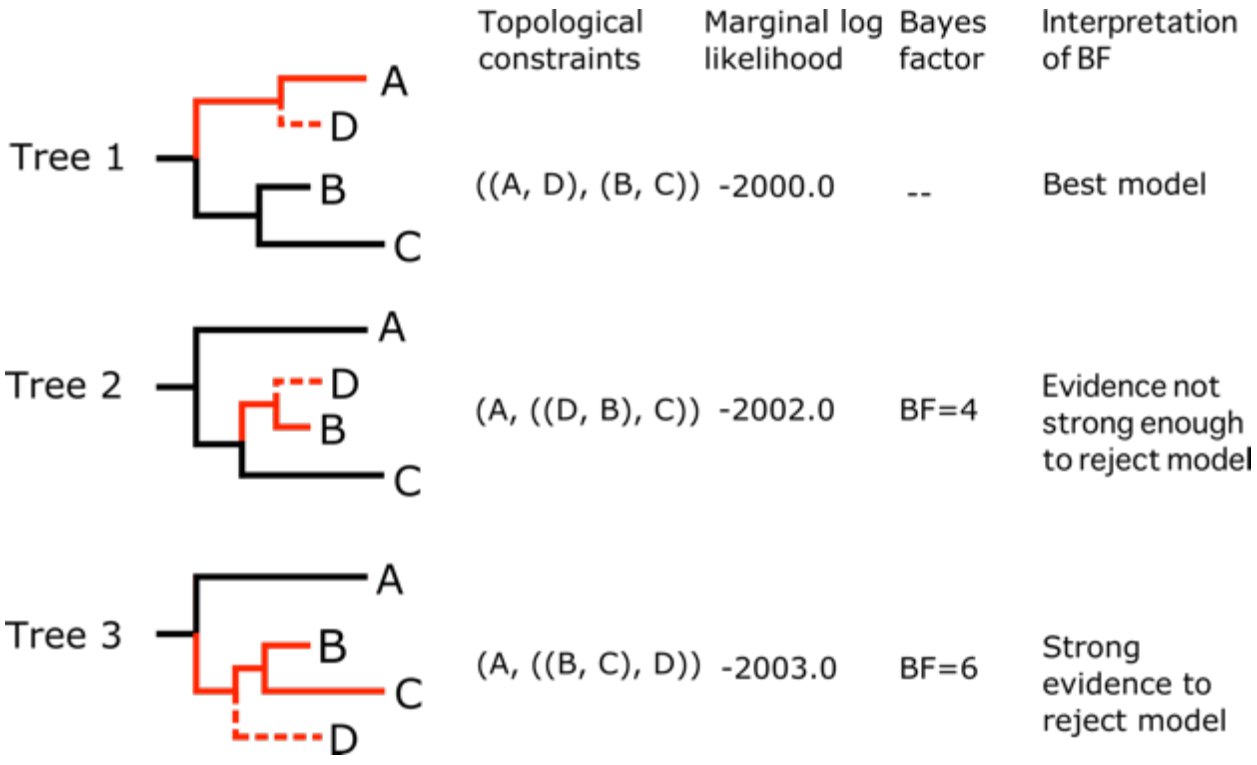

B3. Geological dates used in this study

Table B1 Geological dates used to constrain fossil hominin species as non-contemporaneous tips in the phylogeny.

The oldest dates associated with the specimens used for the morphological analysis were taken in this study. *H. ergaster* is a synonym for African *H. erectus* (see main text).

Taxon	Specimen	Date (Ma)	References
Ar. ramidus	ARA-VP 6/1	4.4	7
Au. anamensis	KNM-KP 29181/29283/29286	4.17	8
Au. afarensis	LH 4	3.77	9
Au. africanus	Makapansgat material	3.03	10
Au. garhi	BOU-VP 12/130	2.5	11
Au. sediba	MH 1	1.95	12
H. antecessor	ATD6-15	0.938	13
H. ergaster	Koobi Fora specimens	1.65	14
H. erectus	Sangiran	1.5	15
Dmanisi	D2280	1.85	16
H. floresiensis	LB1	0.019	17
H. habilis	AL666-1	2.33	18
H. heidelbergensis	Mauer	0.609	19
H. neanderthalensis	Krapina	0.13	20
H. rudolfensis	UR501	2.4	21
H. sapiens	Omo 1, 2	0.195	22
K. platyops	KNM-WT 40000	3.53	23
P. aethiopicus	L 55-s-33	2.7	24
P. boisei	L74a-21/L7a-125	2.3	24
P. robustus	Swartkrans specimens	2	25
S. tchadensis	TM 266-01-060-1	7.24	26

B4. Results of dated Bayesian analysis of hominin phylogeny.

We ran a Bayesian analysis of the craniodental characters of the hominins, as explained in the main text. The model parameters and the convergence diagnostics are presented in Table S1. The summary of best trees is presented in Figure 1, along with the posterior probability clade support values. Many of the nodes are supported by relatively low posterior probability support values, but this is consistent with other Bayesian phylogenetic studies with a high percentage of fossil taxa [27].

Moving from the root towards the tips, the lineage leading to *S. tchadensis* is the first to diverge. This is followed by the lineage leading to *Ar. ramidus*. There is then a split between the lineage leading to *Au. anamensis* and a clade formed by all the remaining hominin species. Within the latter clade, the lineage leading to *K. platyops* is the first to branch off. Thereafter, there is a split between a clade formed by *Au. afarensis* and *Au. garhi*, and one formed by *Au. africanus*, *Au. sediba*, the nine species of *Homo*, and the three paranthropine species. Within the latter clade, there are two main clades. One is formed by the paranthropines; the other by *Au. africanus*, *Au. sediba*, and the *Homo* species. Within the paranthropine clade, *P. robustus* and *P. boisei* are more closely related to each other than either is to *P. aethiopicus*. Within the clade formed by *Au. africanus*, *Au. sediba*, and the *Homo* species, there is a split between the lineage leading to *Au. africanus* and a clade formed by *Au. sediba* and the *Homo* species. Subsequently, there is a split between a clade formed by *Au. sediba* and *H. habilis* and one formed by the remaining species of *Homo*. Within the latter clade, there is a split between the lineage leading to *H. floresiensis* and a clade formed by *H. rudolfensis*, *H. ergaster*, *H. erectus*, *H. antecessor*, *H. sapiens*, *H. heidelbergensis*, and *H. neanderthalensis*. Among the latter group of species, the first to diverge is *H. rudolfensis*. This is followed by *H. ergaster*. There is then a split between a clade formed by *H. antecessor* and *H. erectus*, and one formed by *H. sapiens*, *H. heidelbergensis*, and *H. neanderthalensis*. Within the (*H. sapiens*, *H. heidelbergensis*, *H. neanderthalensis*) clade, *H. heidelbergensis* and *H. neanderthalensis* are more closely related to one another than either is to *H. sapiens*.

Most of these relationships are unsurprising based on previous work, but some deserve comment. One is the suggestion that *K. platyops* is the sister group of the four australopith species, the nine species of *Homo*, and the three paranthropine species. This places *K. platyops* much deeper in the phylogeny than the widely discussed proposal that *K. platyops* is the sister taxon of *H. rudolfensis* [28]. The position of *Homo antecessor* as the sister taxon of *H. erectus* also runs counter to a widely discussed hypothesis. The hypothesis in question avers that *H. antecessor* is the direct ancestor of *H. heidelbergensis, H. neanderthalensis*, and *H. sapiens* [29]. Lastly, the positioning of *H. heidelbergensis* and *H. neanderthalensis* as sister taxa to the exclusion of *H. sapiens* is noteworthy. This hypothesis differs from the results obtained on a recent analysis of ancient DNA sequences [30]. The latter study suggested that *H. heidelbergensis* is the sister taxon of both *H. neanderthalensis* and *H. sapiens.* Though we did not do so, all of these alternate placements could be tested using Bayes factors as done in the main text.

B5. Model parameters and convergence diagnostics obtained from the dated Bayesian analysis of the craniodental characters.

Table B2 Model parameters and convergence diagnostics obtained from the dated Bayesian analysis of the craniodental characters.

The runs are assessed to have converged when Estimated Sample Size (ESS) is greater than 100 and Potential Scale Reduction Factor (PSRF) approaches 1 for all parameters.

Parameter	Mean	Variance	Minimum ESS	Average ESS	PSRF
Tree height	7.816841	0.017280	4025.47	4147.74	1.000
Tree likelihood	46.315151	16.892355	232.93	381.54	1.000
Alpha	1.823648	0.383892	912.53	1334.11	1.000
Net speciation	0.202499	0.002993	5931.16	6475.48	1.000
Relative extinction	0.180051	0.023482	6956.88	7276.10	1.000
Igrvar	1.887228	0.084000	1206.22	1370.02	1.000

B6. Tree models tested in this study.

Figure B2 The model trees competed to address phylogenetic hypotheses regarding *Au. sediba* and the species of genus *Homo.*

Red edges are where the target species (*Au. sediba*) can enter a particular tree, represented by the column "Topological constraints." Polytomies depicted in the constrained trees are not fixed, and can be resolved with the data. *H. ergaster* is used here as a synonym for African *H. erectus* (see main text).

		Topological constraints	Marginal log likelihood	Bayes factor	Interpretation
Tree 1a	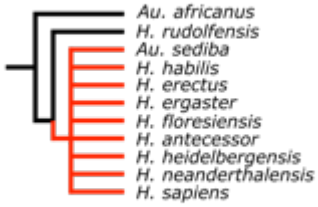	(*Au. africanus*, (*H. rudolfensis*, (*Au. sediba*, *H. habilis*, *H. erectus*, *H.ergaster*, *H. floresiensis*, *H. antecessor*, *H. heidelbergensis*, *H. neanderthalensis*, *H. sapiens*)))	-2122.00	7.68	Strong evidence to reject model
Tree 1b	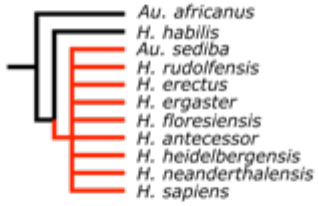	(*Au. africanus*, (*H. habilis*, (*Au. sediba*, *H. rudolfensis*, *H. erectus*, *H.ergaster*, *H. floresiensis*, *H. antecessor*, *H. heidelbergensis*, *H. neanderthalensis*, *H. sapiens*)))	-2122.77	9.22	Strong evidence to reject model
Tree 1c	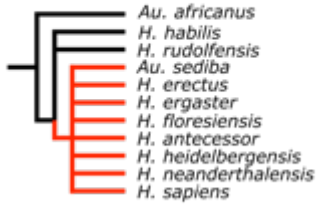	(*Au. africanus*, (*H. habilis*, *H. rudolfensis*, (*Au. sediba*, *H. erectus*, *H.ergaster*, *H. floresiensis*, *H. antecessor*, *H. heidelbergensis*, *H. neanderthalensis*, *H. sapiens*)))	-2119.74	3.16	Evidence not strong eough to reject model
Tree 1d	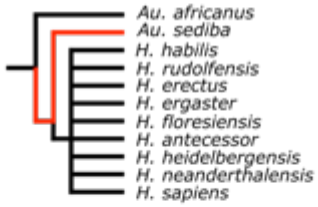	(*Au. africanus*, (*Au. sediba*, (*H. habilis*, *H. rudolfensis*, *H. erectus*, *H. ergaster*, *H. floresiensis*, *H. antecessor*, *H. heidelbergensis*, *H. neanderthalensis*, *H. sapiens*)))	-2118.16	--	Best model
Tree 1e	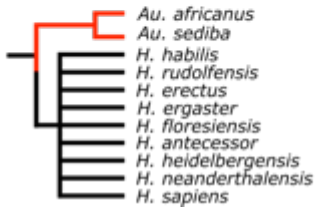	((*Au. africanus*, *Au. sediba*), (*H. habilis*, *H. rudolfensis*, *H. erectus*, *H.ergaster*, *H. floresiensis*, *H. antecessor*, *H. heidelbergensis*, *H. neanderthalensis*, *H. sapiens*))	-2126.37	16.42	Strong evidence to reject model

Figure B3 The model trees competed to address phylogenetic hypotheses regarding the Dmanisi fossils.

Red edges are where the target species (Dmanisi specimens) can enter a particular tree, represented by the column "Topological constraints." Polytomies depicted in the constrained trees are not fixed, and can be resolved with the data. *H. ergaster* is used here as a synonym for African *H. erectus* (see main text).

		Topological constraints	Marginal log likelihood	Bayes factor	Interpretation
Tree 2a	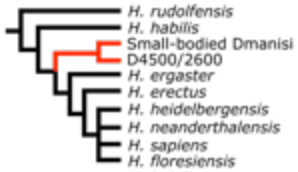	(*H. rudolfensis*, (*H. habilis*, ((Small-bodied Dmanisi, D4500/2600), (*H. ergaster*, (*H. erectus*, (*H. heidelbergensis*, *H. neanderthalensis*, *H. sapiens*, *H. floresiensis*))))))	-2258.95	4.00	Evidence not strong enough to reject model
Tree 2b	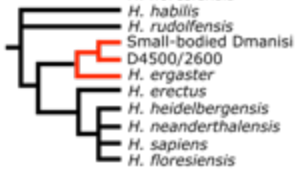	(*H. habilis*, *H. rudolfensis*, (((Small-bodied Dmanisi, D4500/2600), *H. ergaster*), (*H. erectus*, (*H. heidelbergensis*, *H. neanderthalensis*, *H. sapiens*, *H. floresiensis*))))	-2259.21	4.52	Evidence not strong enough to reject model
Tree 2c	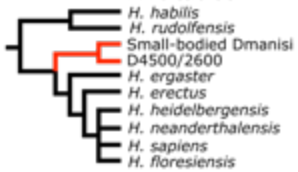	((*H. habilis*, *H. rudolfensis*), ((Small-bodied Dmanisi, D4500/2600), (*H. ergaster*, (*H. erectus*, (*H. heidelbergensis*, *H. neanderthalensis*, *H. sapiens*, *H. floresiensis*)))))	-2260.09	6.28	Strong evidence to reject model
Tree 2d	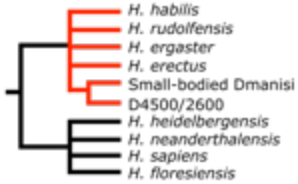	((*H. habilis*, *H. rudolfensis*, *H. ergaster*, *H. erectus*, (Small-bodied Dmanisi, D4500/2600)), (*H. heidelbergensis*, *H. neanderthalensis*, *H. sapiens*, *H. floresiensis*))	-2266.44	18.98	Strong evidence to reject model
Tree 2e	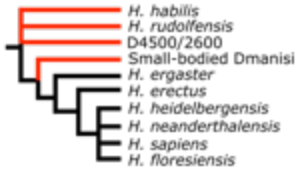	(*H. habilis*, *H. rudolfensis*, D4500/2600, (Small-bodied Dmanisi, (*H. ergaster*, (*H. erectus*, (*H. heidelbergensis*, *H. neanderthalensis*, *H. sapiens*, *H. floresiensis*)))))	-2256.95	--	Best model
Tree 2f	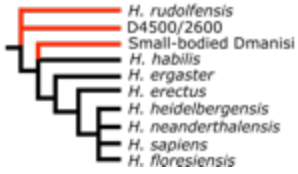	(*H. rudolfensis*, D4500/2600, (Small-bodied Dmanisi, *H. habilis*, (*H. ergaster*, (*H. erectus*, (*H. heidelbergensis*, *H. neanderthalensis*, *H. sapiens*, *H. floresiensis*)))))	-2261.47	9.04	Strong evidence to reject model

Figure B4 The model trees competed to address phylogenetic hypotheses regarding the status of *H. floresiensis*.

Red edges are where the target species (*H. floresiensis*) can enter a particular tree, represented by the column "Topological constraints." Polytomies depicted in the constrained trees are not fixed, and can be resolved with the data. *H. ergaster* is used here as a synonym for African *H. erectus* (see main text).

		Topological constraints	Marginal log likelihood	Bayes factor	Interpretation
Tree 3a	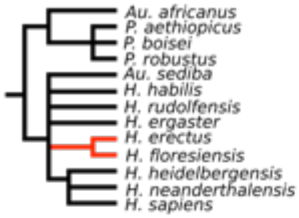	((*Au. africanus*, (*P. aethiopicus*, *P. robustus*, *P. boisei*)), (*Au. sediba*, *H. habilis*, *H. rudolfensis*, *H. ergaster*, (*H. erectus*, *H. floresiensis*),(*H. heidelbergensis*, *H. neanderthalensis*, *H. sapiens*)))	-2118.12	3.70	Evidence not strong enough to reject model
Tree 3b	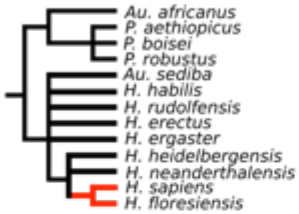	((*Au. africanus*, (*P. aethiopicus*, *P. robustus*, *P. boisei*)), (*Au. sediba*, *H. habilis*, *H. rudolfensis*, *H. erectus*, *H. ergaster*, (*H. heidelbergensis*, *H. neanderthalensis*, (*H. sapiens*, *H. floresiensis*))))	-2120.25	7.96	Strong evidence to reject model
Tree 3c	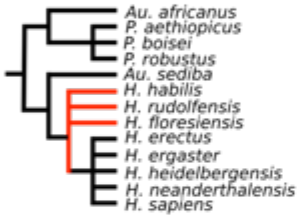	((*Au. africanus*, (*P. aethiopicus*, *P. robustus*, *P. boisei*)), (*Au. sediba*, (*H. habilis*, *H. rudolfensis*, *H. floresiensis*, (*H. erectus*, *H. ergaster*, *H. heidelbergensis*, *H. neanderthalensis*, *H. sapiens*))))	-2116.27	--	Best model
Tree 3d		((*Au. africanus*, *H. floresiensis*, (*P. aethiopicus*, *P. robustus*, *P. boisei*)), (*Au. sediba*, *H. habilis*, *H. rudolfensis*, *H. erectus*, *H. ergaster*, (*H. heidelbergensis*, *H. neanderthalensis*, *H. sapiens*)))	-2120.64	8.74	Strong evidence to reject model
Tree 3e	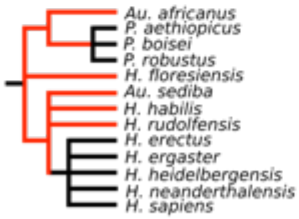	((*Au. africanus*, (*P. aethiopicus*, *P. robustus*, *P. boisei*)), *H. floresiensis*, (*Au. sediba*, *H. habilis*, *H. rudolfensis*, (*H. erectus*, *H. ergaster*, *H. heidelbergensis*, *H. neanderthalensis*, *H. sapiens*)))	-2118.15	3.76	Evidence not strong enough to reject model
Tree 3f	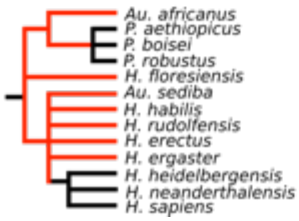	((*Au. africanus*, (*P. aethiopicus*, *P. robustus*, *P. boisei*)), *H. floresiensis*, (*Au. sediba*, *H. habilis*, *H. rudolfensis*, *H. erectus*, *H. ergaster*, (*H. heidelbergensis*, *H. neanderthalensis*, *H. sapiens*)))	-2119.17	5.80	Evidence not strong enough to reject model

B7. References for Electronic Supplementary Material.

1. Nylander J, Ronquist F, Huelsenbeck J, Nieves-Aldrey J. 2004 Bayesian phylogenetic analysis of combined data. *Syst. Biol.* **53**, 47–67. (doi:10.1080/10635150490264699)

2. Ronquist F, Klopfstein S, Vilhelmsen L, Schulmeister S, Murray DL, Rasnitsyn AP. 2012 A total-evidence approach to dating with fossils, applied to the early radiation of the hymenoptera. *Syst. Biol.* **61**, 973–99. (doi:10.1093/sysbio/sys058)

3. Bergsten J, Nilsson AN, Ronquist F. 2013 Bayesian tests of topology hypotheses with an example from diving beetles. *Syst. Biol.* **62**, 660–73. (doi:10.1093/sysbio/syt029)

4. Holder M, Lewis PO. 2003 Phylogeny estimation: traditional and Bayesian approaches. *Nat. Rev. Genet.* **4,** 275-284. (doi:10/1038/nrg1044)

5. Kass RE, Raftery AE. 1995 Bayes Factors. *J. Am. Stat. Assoc.* **90**, 773–795. (doi:10.1080/01621459.1995.10476572)

6. Lewis PO. 2001 A likelihood approach to estimating phylogeny from discrete morphological character data. *Syst. Biol.* **50**, 913-925. (doi:10.1080/106351501753462876)

7. White TD, Asfaw B, Beyene Y, Haile-Selassie Y, Lovejoy CO, Suwa G & WoldeGabriel G. 2009 *Ardipithecus ramidus* and the paleobiology of early hominids. *Science* **326**, 75–86. (doi:10.1126/science.1175802)

8. Leakey MG, Feibel CS, McDougall I, Ward C & Walker A. 1998 New specimens and confirmation of an early age for *Australopithecus anamensis*. *Nature* **393**, 62–66. (doi :10.1038/29972)

9. Leakey MD, Hay RL, Curtis GH, Drake RE, Jackes MK & White TD. 1976 Fossil hominids from the Laetoli Beds. *Nature* **262**, 460–466. (doi:10.1038/262460a0)

10. Herries AIR et al. 2013 A multi-disciplinary perspective on the age of *Australopithecus* in South Africa. In *The Paleobiology of Australopithecus africanus*, Vertebrate Paleobiology and Paleoanthropology (eds Reed KE, Fleagle JG, Leakey RE), pp 21–40. New York, NY: Springer.

11. Brown FH, Mcdougall I, Gathogo PN (2013) Age ranges of *Australopithecus* species, Kenya, Ethiopia, and Tanzania. In *The Paleobiology of Australopithecus africanus*, Vertebrate Paleobiology and Paleoanthropology (eds Reed KE, Fleagle JG, Leakey RE), pp 7–20. New York, NY: Springer.

12. Pickering, R., Dirks, P. H. G. M., Jinnah, Z., de Ruiter, D. J., Churchil, S. E., Herries, A. I. R., Woodhead, J. D., Hellstrom, J. C. & Berger, L. R. 2011 *Australopithecus sediba* at 1.977 Ma and implications for the origins of the genus *Homo*. *Science* **333**, 1421–3. (doi:10.1126/science.1203697)

13. Parés JM, Arnold L, Duval M, Demuro M, Pérez-González A, Bermúdez de Castro JM, Carbonell E & Arsuaga JL. 2013 Reassessing the age of Atapuerca-TD6 (Spain): new paleomagnetic results. *J. Archaeol. Sci.* **40**, 4586–4595. (doi:10.1016/j.jas.2013.06.013)

14. Gathogo PN, Brown FH. 2006 Revised stratigraphy of Area 123, Koobi Fora, Kenya, and new age estimates of its fossil mammals, including hominins. *J. Hum. Evol.* **51**, 471–9. (doi:10.1016/j.jhevol.2006.05.005)

15. Larick R, Ciochon RL, Zaim Y, Sudijono, Suminto, Rizal Y, Aziz F, Reagan M & Heizler M. 2001 Early Pleistocene 40Ar/39Ar ages for Bapang Formation hominins, Central Jawa, Indonesia. *Proc. Natl. Acad. Sci. U. S. A.* **98**, 4866–71. (doi:10.1073/pnas.081077298)

16. Gabunia, L. et al. 2000 Earliest Pleistocene hominid cranial remains from Dmanisi, Republic of Georgia: taxonomy, geological setting, and age. *Science* **288**, 1019–1025. (doi:10.1126/science.288.5468.1019)

17. Morwood MJ, Jungers WL. 2009 Conclusions: implications of the Liang Bua excavations for hominin evolution and biogeography. *J. Hum. Evol.* **57**, 640–8. (doi:10.1016/j.jhevol.2009.08.003)

18. Kimbel WH, Johanson DC & Rak Y. 1997 Systematic assessment of a maxilla of *Homo* from Hadar, Ethiopia. *Am. J. Phys. Anthropol.* **103**, 235–62. (doi:10.1002/(SICI)1096-8644(199706)103:2<235::AID-AJPA8>3.0.CO;2-S)

19. Wagner GA, Krbetschek M, Degering D, Bahain J, Shao Q. 2010 Radiometric dating of the type-site for *Homo heidelbergensis* at Mauer, Germany. *Proc. Natl. Acad. Sci.* **107**, 19726–19730. (doi:10.1073/pnas.1012722107)

20. Rink, W. J., Schwarcz, H. P., Smith, F. H. & Radovčić, J. 1995 ESR ages for Krapina hominids. *Nature* **378**, 24. (doi:10.1038/378024a0)

21. Bromage TG, Schrenk F, Zonneveld F. 1995 Paleoanthropology of the Malawi Rift: an early hominid mandible from the Chiwondo Beds, northern Malawi. *J. Hum. Evol.* **28**, 71–108. (doi:10.1006/jhev.1995.1007)

22. McDougall I, Brown FH, Fleagle JG. 2005 Stratigraphic placement and age of modern humans from Kibish, Ethiopia. *Nature* **433**, 733–736. (doi:10.1038/nature03266.1.)

23. Leakey MG, Spoor F, Brown FH, Gathogo PN, Kiarie C, Leakey LN & McDougall I. 2001 New hominin genus from eastern Africa shows diverse Middle Pliocene lineages. *Nature* **410**, 433–40. (doi:10.1038/35068500)

24. Feibel CS, Brown FH, McDougall I. 1989 Stratigraphic context of fossil hominids from the Omo group deposits: northern Turkana Basin, Kenya and Ethiopia. *Am. J. Phys. Anthropol.* **78**, 595–622. (doi:10.1002/ajpa.1330780412)

25. Herries AIR, Curnoe D, Adams JW. 2009 A multi-disciplinary seriation of early *Homo* and *Paranthropus* bearing palaeocaves in southern Africa. *Quat. Int.* **202**, 14–28. (doi:10.1016/j.quaint.2008.05.017)

26. Lebatard A-E et al. (2008) Cosmogenic nuclide dating of *Sahelanthropus tchadensis* and *Australopithecus bahrelghazali*: Mio-Pliocene hominids from Chad. *Proc. Natl. Acad. Sci. U. S. A.* **105**, 3226–31. (doi:10.1073/pnas.0708015105)

27. Lee MSY, Cau A, Naish D, Dyke GJ. 2014 Morphological clocks in palaeontology, and a mid-Cretaceous origin of crown Aves. *Syst. Biol.* **63**, 442–449. (doi:10.1093/sysbio/syt110)

28. Leakey MG et al. 2001 New hominin genus from eastern Africa shows diverse Middle Pliocene lineages. *Nature* **410**, 433–40. (doi:10.1038/35068500)

29. Bermúdez de Castro JM et al. 1997 A hominid from the lower Pleistocene of Atapuerca, Spain: possible ancestor to Neandertals and modern humans. *Science* **276**, 1392–1395. (doi: 10.1126/science.276.5317.1392)

30. Meyer M et al. 2014 A mitochondrial genome sequence of a hominin from Sima de los Huesos. *Nature* **505**, 403–406. (doi:10.1038/nature12788)

B8. List of characters, character definitions, and states.

List of craniodental characters used in this study. The character definitions and the character state assessments are taken from the original studies wherever possible. It is indicated whether the character is treated as an ordered or unordered trait. The references are listed at the end of the table.

	Characters	Definition	States	Refs
Cranial characters				
1.	Cranial capacity	Cranial capacity in cubic centimeters. (Small<500; Intermediate=500-680; Medium=750-875; Large=900-1200; Very large>1300). (Ordered)	Small (0); Intermediate (1); Medium (2); Large (3); Very large (4)	2-4, 6, 12
2.	Cerebellar morphology	The position of cerebellum relative to the cerebrum. (Unordered)	Lateral flare with posterior protrusion (0); Tucked (1)	3, 12
3.	Cranial vault thickness	The thickness of the cranial vault measured at parietal eminence. (Ordered)	Thin (0); Intermediate (1); Thick (2)	6, 8, 9
4.	Calvarial height to breadth	The ratio of the calvarial height on the coronal plane of porion to the minimum breadth of cranial base, or the distance between the porial saddles. (Ordered)	Low (0); Very low (1); High (2)	8
5.	Cranial vault index	The index calculated as the cranial height divided by cranial length. (Low and Long<0.62. Short and high>0.62). (Unordered)	Long low cranium (0); Short high cranium (1)	4, 6
6.	Height of calvaria relative to orbits	The portion of the calvarial height above the orbit expressed as a percentage of the total calvarial height. (Ordered)	Low (0); Moderate (1); High (2)	4, 8
7.	Maximum cranial breadth	The location where maximum cranial breadth is measured. (Ordered)	Close to cranial base (0); Cranial base biparietal similar (1); At biparietal (2)	4
8.	Cranial contour in norma occipitalis	The cranial contour in norma occipitalis. (Unordered)	Low and broad (0); en bombe (1); en maison (2)	5
9.	Anterior calvarial contour in profile	The contour of the anterior calvarium. (Unordered)	Deviates from circle (0); Aligned with circle (1)	8
10.	Posterior calvarial contour	The curvature of the posterior portion of the cranial vault along the midsagittal cross-section. (Unordered)	Aligned with circle (0); Deviates from circle (1)	8

11.	Parietal wall verticality	The superior convergence of lateral parietal walls in posterior view. (Unordered)	Present (0); Absent (1)	6
12.	Parietal tuber	The presence of a parietal tuber or eminence. (Unordered)	Absent (0); Present (1)	1, 2, 12, 13
13.	Sagittal crest	The presence of a sagittal crest. (Unordered)	Present (0); Absent (1)	3, 12, 13
14.	Sagittal keel	The presence of a sagittal keel. (Unordered)	Absent (0); Present (1)	1, 4-6, 9, 13
15.	Parietal overlap of occipital at asterion	The presence of an overlap of temporal, parietal and occipital bones at asterion. (Unordered)	Absent (0); Present (1)	3, 12
16.	Upper facial breadth	The index of bi-frontomalare temporale divided by orbital height. (Ordered)	Narrow (0); Intermediate (1); Broad (2); Extremely broad (3)	3, 8
17.	Outline of superior facial mask	The bi-maxillary tubercle width relative to bi-frontomalare-temporale width. (Unordered)	Tapered (0); Squared (1)	2, 3, 9
18.	Lateral anterior facial contour	The facial contour in lateral view. (Unordered)	Bipartite (0); Straight (1)	2
19.	Facial prognathism	The proportion of the palate anterior to sellion. (Index > 57= prognathic, 30<Index<57 = mesognathic, Index <30 = orthognathic). (Ordered)	Prognathic (0); Mesognathic (1); Orthognathic (2)	2, 3, 8, 12
20.	Facial hafting	The position of the face relative to the neurocranium, assessed by comparing the position of the supraorbital relative to the bregma. (Unordered)	Low (0); High (1)	2, 3, 12
21.	Anterior projection of zygomatic bone relative to piriform aperture (dishing)	The position of the infraorbital plate of the zygoma relative to the piriform aperture. (Ordered)	Posterior (0); Intermediate (1); Anterior (2)	2, 3, 12
22.	Bregmatic protuberance	The presence of a brebmatic protuberance. (Unordered)	Absent (0); Present (1)	13
23.	Precoronal depression	The presence of a precoronal depression. (Unordered)	Absent (0); Precoronal plane present (1); Precoronal depression present (2)	13
24.	Coronal reinforcement	The thickness of the frontal at and along the coronal suture. (Unordered)	Absent (0); Present at upper part of squama (1); Present and	13

			continues laterally (2)	
25.	Frontal contour in norma verticalis	The contour of the frontal bone in superior view. (Unordered)	Linear (0); Convex (1)	1, 13
26.	Frontal eminence	The presence of a frontal eminence. (Unordered)	Absent (0); Present (1)	4, 6, 13
27.	Glabellar depression	The presence of a depression at the glabella. (Unordered)	Absent (0); Present (1)	1, 3, 13
28.	Glabellar development	The development of the glabella. (Unordered)	Weak (0); Prominent (1)	4, 6, 9, 12, 13
29.	Glabellar region forms as prominent block	Does the glabellar region form a prominent block. (Unordered)	Not a block (0); Block (1)	2
30.	Supraglabellar tubercle	The presence of a supraglabellar tubercle at the junction of postorbital sulcus and the frontal squama. (Unordered)	Absent (0); Present (1)	13
31.	Microdepression of glabella	The presence of a small glabellary depression, associated with large glabellar projection. (Unordered)	Absent (0); Present (1)	13
32.	Metopic keel	The presence of a metopic keel. (Unordered)	Absent (0); Present (1)	1, 5, 6, 9, 13
33.	Lateral postorbital depression	The presence of postorbital depression. (Unordered)	Absent (0); Present (1)	13
34.	Frontotemporale tubercle	The presence of a tubercle at the fronto-temporal junction. (Unordered)	Absent (0); Present (1)	13
35.	Frontal trigone	The presence of a frontal trigone. (Unordered)	Present (0); Absent (1)	2
36.	Supratrigonal depression	The presence of very small depressions on the medial edges of the posterior part of temporal lines. (Unordered)	Absent (0); Present (1)	13
37.	Frontal sinus	The presence of frontal sinus. (Unordered)	Absent (0); Present (1)	3, 12
38.	Supraorbital sulcus	The presence of a supraorbital sulcus. (Unordered)	Present (0); Absent (1)	1, 3, 4, 8, 9, 13
39.	Supraorbital torus thickness	The index to calculate the thickness of the torus at its midpoint. The thickness at midpoint is divided by orbital height. (Thin<0.15; Intermediate=0.15-0.29; Thick>0.29). (Ordered)	Thick (0); Intermediate (1); Reduced (2)	3, 4, 6, 9
40.	Supraorbital thickness gradient	The thickness gradient of the orbital arch comparing medial and lateral thicknesses. (Unordered)	Medial to lateral (0); Lateral to medial (1)	1, 8, 13

41.	Supraorbital torus development	The development of supraortibal torus. (Ordered)	Torus (0); Intermediate (1); Weak (2)	1-5, 8, 12, 13
42.	Supraorbital contour	The contour of the supraorbital region. (Unordered)	Less arched (0); Arched (1)	1, 2, 4-6, 12, 13
43.	Superior orbital fissure shape	The shape of superior orbital fissure. (Unordered)	Foramen (0); Comma shaped (1)	3, 8, 12
44.	Supraorbital corner shape	The angularity of the superolateral corner of the orbit. (Unordered)	Angled (0); Rounded (1)	1, 8
45.	Lacrimal fossae location	The location of lacrimal fossa relative to the inferior orbital margin. (Unordered)	Within orbit (0); Within infraorbital region (1)	3
46.	Ethmolacrimal contact	The length of ethmoid-lacrymal contact. (Unordered)	100 (0); Variable (1)	12
47.	Interorbital breadth	The distance bewteen the orbits, calculated as an index relative to the orbit's breadth. (Unordered)	Narrow (0); Broad (1)	3, 6, 8
48.	Orbital shape	Ths shape of the orbits evaluated by height vs breadth measurements. (Unordered)	Oval (0); Circular (1); Rectangular (2)	3, 4
49.	Inferior orbital margin position relative to nasal margin	The horizontal position of the inferior orbital margins against the superior nasal aperture margin viewed anteriorly. (Ordered)	Well above superior nasal margin (0); Close to superior nasal margin (1); Well below superior nasal margin (2)	3
50.	Inferior orbital margin rounded laterally	The morphology of inferior margin of the orbit as being either rounded laterally or not rounded. (Unordered)	No (0); Yes (1)	1, 3, 12
51.	Infraorbital foramen location	The ratio of the distances between orbitale and the foramen, and orbitale and the root of the zygoma. (Unordered)	High (0); Low (1)	2, 3, 12
52.	Nasal keel	The presence of a distinct vertical "pinching" of the nasal bones along its midline. (Unordered)	Present (0); Absent (1)	1, 3
53.	Projection of nasal bones above frontomaxillary suture	The projection of nasal bones above frontomaxillary suture. (Unordered)	Tapered (0); Expanded (1); Not projected (2)	2, 3, 12
54.	Eversion of superior nasal aperture margin	The degree of superior nasal aperture margin eversion. (Unordered)	None (0); Slight (1)	2
55.	Profile of nasal saddle and nasal roof	The contour of nasal saddle and nasal roof. (Unordered)	Flat (0); Small curve (1); Well defined curve (2); Deep angled (3)	1

56.	Nasal cavity entrance	The contour of the nasal cavity entrance. (Unordered)	Stepped (0); Smooth (1)	1, 3, 5, 8, 12
57.	Inferior width of projecting nasal bone	The inferior width of projecting nasal bone. (Unordered)	Narrow (0); Wide (1); Not projecting (2)	2
58.	Anterior nasal spine relative to nasal aperture	The development of anterior nasal spine relative to nasal aperture. (Ordered)	Absent (0); Anterior (1); Enlarged (2); Posterior (3)	2
59.	Nasal margin crest/spine patterns	The development of nasal margin crest or spine. (Unordered)	Lateral crest (0); Lateral turbinal and spinal crests (1); Fused spinal and turbinal crests and lateral crest (2); Fused lateral and spinal crests and turbinial crest (3); Fused lateral and spinal crests and partial fusion of spinal and turbinal (4); No crests (5)	5
60.	Nasal aperture margin sharpness	The sharpness of the nasal aperture margin. (Unordered)	Sharp (0); Dull (1)	2, 8
61.	Subnasal projection	The inclination of the nasoalveolar clivus measured relative to the occlusal plane. (Weak<100; Moderate=100-150; Marked>15). (Ordered)	Low (0); Intermediate (1); High (2)	2, 3, 8, 9
62.	Subnasal length	The chord distance from nasospinale to prosthion. (Ordered)	Short (0); Intermediate (1); Long (2)	3
63.	Alveolar clivus shape	The shape of alveolar clivus. (Ordered)	Convex (0); Flat (1); Concave (2)	9
64.	Nasoalveolar clivus contour	The contour of nasoalveolar clivus in coronal plane. (Ordered)	Convex (0); Straight (1); Concave (2)	1, 3, 8, 9, 12
65.	Protrusion of incisor alveoli beyond bicanine line in basal view	The position of the incisors relative to the canines in the coronal plane. (Unordered)	Beyond bicanine line (0); Within bicanine line (1)	2, 3, 12
66.	External palate breadth	The index of external palate breadth at M2 divdied by orbital height. (Ordered)	Broad (0); Intermediate (1); Narrow (2)	3, 8
67.	Incisive canal development	The development of incisive canal. (Ordered)	Slight canal (0); Intermediate (1); Extensive canal (2)	3

68.	Palate thickness	The thickness of the palate posterior to the incisive fossa. (Thick>7 mm; Thin<7 mm) (Unordered)	Thin (0); Thick (1)	3, 12
69.	Incisive foramen position	The position of incisive foramen along tooth row. (Ordered)	Canine (0); P3 (1); P4 (2)	1, 9
70.	Anterior palate depth	The depth of anterior palate. (Unordered)	Shallow (0); Deep (1)	2, 3, 8, 9, 12
71.	Palatine process orientation	The orientation of the posterosuperior slope of the palatal plane distal to the canine. (Unordered)	Nearly horizontal (0); Steep posterior angle (1)	8
72.	Canine jugum development	The development of canine jugum. (Ordered)	Weak (0); Moderate (1); Marked (2)	1, 2, 9
73.	Canine root orientation	The orientation of the canine root relative to parasagittal plane. (Unordered)	Inclined (0); Parallel (1)	9
74.	Anterior pillars	The presence of anterior pillars. (Unordered)	Absent (0); Present (1)	2, 3, 12
75.	Canine fossa, groove or fossula.	The presence of a canine fossa, canine groove or canine fossula. (Unordered)	Absent (0); Present (1)	2, 3, 5, 8
76.	Maxillary trigone	The presence of maxillary trigon, a gutter-like triangular depression in the infraorbital region. (Unordered)	Absent (0); Present (1)	2, 3, 8, 12
77.	Maxillary sinus size	The size of maxillary sinus. (Unordered)	Intermediate (0); Large (1)	3
78.	Maxillary sinus division	The position of the main division of the maxillary sinus floor. (Unordered)	Posterior (0); Anterior (1)	8
79.	Infraorbital plate orientation	The orientation of the infraorbital plate, measured by the position of the inferior margin of the infraorbital region, which is demarcated by the zygomaticoalveolar crest relative to the coronal plane of the orbit. (Unordered)	Sloped (0); Vertical (1); Lateral (2)	2, 5, 8
80.	Sulcus infraorbitalis	The width of a infraorbital sulcus. (Unordered)	Absent (0); Narrow (1); Wide (2)	1
81.	Position of infraorbital foramen relative to orbit	The position of the infraorbital foramen relative to the zygomaxillary suture. (Unordered)	Foramen beneath middle third of orbital breadth (0); Foramen beneath medial third of orbital breadth (1)	12
82.	Patency of premaxillary suture in adults from frontal view	The presence of premaxillary suture in adults. (Unordered)	Patent (0); Obliterated (1); Trace (2)	2, 12

83.	Anterior zygomatic root position	The position of the anterior zygomatic root along tooth row. (Ordered)	P3-P4 (0); P4-M1 (1); M1 (2); M1-M2 (3)	3, 12
84.	Zygomaticoalveolar crest	The curvature of the zygomaticoalveolar crest. (Unordered)	Straight (0); Curved (1)	1, 2, 9
85.	Malar diagonal length	The index of orbitale-zygomaxillare divided by orbital height. (Ordered)	Long (0); Intermediate (1); Short (2)	3
86.	Malar orientation	The orientation of the anterior malar surface relative to Frankfurt Horizontal (Ordered)	Posteriorly inclined (0); Vertical (1); Anteriorly inclined (2)	3, 9
87.	Zygomatic insertion height	The insertion of the zygomaticoalveolar crest onto the alveolar border. (Unordered)	Low (0); High (1)	3
88.	Position of zygomatic foramina	The position of the zytomatic foramina relative to the plane of the orbital rim. (Unordered)	At or below plane of orbital rim (0); Above plane of orbital rim (1)	12
89.	Zygomatic bone orientation	The orientation of the zygomatic bone relative to the frontal. (Ordered)	Frontal (0); Frontolateral (1); Lateral (2)	12
90.	Mediolateral thickness of zygomatic arch at root of frontal process	The thickness of the zygomatic arch. (Thick>8mm; Thin<8 mm) (Unordered)	Thin (0); Thick (1)	2, 12
91.	Expansion of medial edge of frontal process of zygomatic bone	The presence of a lateral flair of the frontal process of the zygomatic. (Unordered)	Vertical (0); Laterally divergent (1)	2, 8
92.	Angular indentation of lateral orbital margin	The curvature of the lateral orbital margin. (Unordered)	Indented (0); Curved (1)	2
93.	Masseter origin height	The index of zygomaticoalveolar height relative to orbitoalveolar height. (Unordered)	Low (0); High (1)	2, 3, 8, 12
94.	Masseteric position relative to sellion	The distance from the articular eminence to the zygomatic tubercle expressed as a percentage of the horizontal distance between the articular eminence and sellion. (Unordered)	Anterior (0); Posterior (1)	2, 8, 12
95.	Zygomatic temporal surface	The thickness of the body of the zygomatic bone. "Deeply excavated" surface is thinner in the centre of the body. (Unordered)	Flat (0); Deeply excavated (1)	8

96.	Zygomatic prominence development	The development of the zygomatic prominence. (Unordered)	Prominent (0); Slight (1)	2
97.	Zygomaticomaxillary steps to fossae present	The presence of zygomaticomaxillary steps to fossae. (Unordered)	Absent (0); Present (1)	2
98.	Zygomatic arch relative to inferior orbital margin	The position of the zygomatic arch relative to the inferior orbital margin. (Unordered)	Above (0); Level (1)	2
99.	Position of zygomatic angle	The position of the angle formed between the frontal and temporal processes of the zygomatic relative to the inferior orbital margin. (Ordered)	Below orbit (0); At orbit (1); Above orbit (2)	8
100.	Lateral flaring of zygomatic arches	The development of the lateral flaring of zygomatic arches. (Unordered)	Marked (0); Slight (1)	2
101.	Zygomatic arch alignment	The outline of the zygomatic arch from the superior view. This character refers to the orientation of the zygomatic arch at midpoint; whether it is parallel to the sagittal plane or not. (Unordered)	Sagittal (0); Deviant (1)	8
102.	Zygomatic process root	The number of planes at the root of the zygomatic process. The surface of the zygomatic process root lateral to the articular tubercle is divided into two surfaces by a very strong ridge that extends from the lateral edge of the articular tubercle. (Unordered)	Undivided (0); Divided (1)	8
103.	Postorbital constriction	The index of minimum frontal breadth to superior facial breadth (bi-frontomalaretemporale). (Marked constriction<0.65; Moderate constriction=0.65-0.77; Slight constriction>0.77). (Ordered)	Marked (0); Moderate (1); Slight (2)	2-4, 6, 8, 9, 12
104.	Temporal fossae size	The index of temporal fossa size divided by orbital area. (Ordered)	Large (0); Intermediate (1); Small (2)	3
105.	Supraglenoid gutter width	The maximum distance from the temporal squame at the anterior end of the root of the zygomatic process to the most lateral point at that location. (Wide>25mm; Narrow<25). (Unordered)	Narrow (0); Wide (1)	2, 3, 12
106.	Articular eminence position relative to occlusal plane	The perpendicular distance between the articular eminence and the occlusal plane, divided by the geometric mean (bi-entoglenoid	High above plane (0); Near plane (1)	1, 3, 12

		breadth, bi-carotid breadth, FM length, basioccipital length). (Unordered)		
107.	Articular eminence summit	The position of the maximum convexity of articular eminence relative to the plane of the posterior edge of temporal foramen. (Unordered)	Posterior (0); Anterior (1)	8
108.	Articular eminence form	The angulation of the long axis of the articular eminence in basal view. (Unordered)	Single plane (0); Mediolateral twisted (1)	8
109.	Posterior slope of articular tubercle	The degree and the length of posterior portion of the articular tubercle on the zygomatic. (Ordered)	Short (0); More pronounced (1); Steep (2)	13
110.	Articular tubercle development	The development of the articular tubercle on the zygomatic. (Unordered)	Not developed (0); Developed (1)	13
111.	Articular tubercle projection	The projection of the articular tubercle. (Unordered)	Not or slightly projecting (0); Projecting (1)	13
112.	Articular tubercle and sub-temporal plane continuity	The continuity of the articular tubercle with the subtemporal plane. (Unordered)	Continuous (0); Not continuous (1)	1, 13
113.	Articular tubercle anteroposterior curvature	The anteroposterior curvature of the articular tubercle in norma lateralis. (Unordered)	Flat (0); Large rounded profile (1); Small rounded profile (2)	1, 13
114.	Transverse concavity of articular tubercle	The concavity of the articular tubercle in norma frontalis. (Unordered)	Flat (0); Large rounded profile (1); Small rounded profile (2)	13
115.	Integration of entoglenoid formation with articular tubercle	The integration of the entoglenoid process or spine with articular tubercle. (Unordered)	Not integrated (0); Integrated (1)	13
116.	Ectoglenoid crest	The presence of ectoglenoid crest. (Unordered)	Absent (0); Present (1)	13
117.	Width between the tympanic plate and entoglenoid process	The width between tympanic plate and entoglenoid process. (Ordered)	Absent (0); Narrow (1); Wide (2)	1, 13
118.	Entoglenoid process position relative to anterior zygomatic tubercle or ectoglenoid process	The position of the entoglenoid process or spine in sagittal plane relative to the ectoglenoid process. (Ordered)	Same level (0); Posterior (1); Farther back (2)	1, 13
119.	Entoglenoid process projection	The projection of the entoglenoid process or spine. (Unordered)	Projecting (0); Not projecting (1)	1, 13

120.	Subarcuate fossa depth	The depth of subarcuate fossa, which is a small triangular fossa or shallow area inferior to the arcuate eminence on temporal bone. (Ordered)	Deep (0); Moderately deep to shallow (1); Very shallow to absent (2)	12
121.	Preglenoid plane extent	The extent of the preglenoid planum. (Unordered)	Not stretched (0); Stretched (1)	1, 13
122.	Sphenoid contribution to mandibular fossa	The contribution of sphenoid to mandibular fossa. (Unordered)	Absent (0); Present (1)	5
123.	Contribution of tympanic plate to mandibular fossa	The contribution of the tympanic plate to the mandibular fossa. (Unordered)	None (0); Exclusive (1)	1, 13
124.	Orientation of anterior wall of TMJ	The orientation of the anterior wall of mandibular fossa. (Ordered)	Horizontal (0); Oblique (1); Vertical (2)	1, 13
125.	Tubercle on anterior wall of TMJ	The presence of a tubercle on the anterior wall of the mandibular fossa. (Unordered)	Absent (0); Present (1)	13
126.	Medial recess of mandibular fossa	The presence of a recess in the medial wall of the mandibular fossa. (Unordered)	Absent (0); Present (1)	5
127.	Mandibular fossa length	The anteroposterior length of mandibular fossa. (Unordered)	Narrow (0); Wide (1)	1, 3, 13
128.	Mandibular fossa depth	The index of mandibular fossa depth perpendicular to Frankfurt Horizontal (depth from the base of the articular eminence to the apex of the fossa, divided by the breadth of the eminence from the articlar tubercle to the entoglenoid process). (Unordered)	Shallow (0); Deep (1)	3, 6, 8, 9, 12, 13
129.	Mandibular fossa overhang	The proportion of the mandibular fossa that overhangs the external cranial vault. (Unordered)	<50% (0); ≥50% (1)	9
130.	Convexity of posterior wall of mandibular fossa	The curvature on the posterior wall of the mandibular fossa. (Unordered)	Flat or concave (0); Convex (1)	13
131.	Postglenoid process shape in norma frontalis	The shape of the postglenoid process in norma frontalis. (Unordered)	Rectangular (0); Round (1); Flat (2)	13
132.	Postglenoid and tympanic fusion	The fusion of the tympanic element and the postgelnoid process in coronal plane. (Unordered)	Fused (0); Unfused (1)	3, 8, 12
133.	Postglenoid process size	The size of postglenoid process. (Ordered)	Large (0); Medium (1); Small (2)	1, 3, 6, 8, 12, 13

134.	Postglenoid process extent relative to the tympanic	The extent of the postglenoid process relative to the tympanic. (Unordered)	No overlap (0); Overlaps (1); Rudimentary or no postglenoid process (2)	1
135.	Vaginal process size	The size of the vaginal process of tympanic. (Unordered)	Small or absent (0); Moderate to large (1)	3, 8, 12
136.	Styloid process fusion	The presence of styloid process. (Unordered)	Unfused (0); Fused (1)	5, 6
137.	Petrous apex ossified beyond spheno-occipital synchondrosis	The degree of ossification of the petrous apex. (Unordered)	Not ossified (0); Ossified with projection (1)	12
138.	Petrous orientation	The orientation of the petrous. The angle is measured relative to the bitympanic line. (Coronal<50 degrees; Intermediate=50-60; Sagittal>60). (Ordered)	Sagittal (0); Intermediate (1); Coronal (2)	3, 5, 6, 9, 12
139.	Crista petrosa development	The development of crista petrosa, a sharp lower margin of the tympanic plate that bounds a single anteriorly directed face. (Unordered)	Absent or weak (0); Moderate to strong (1)	8
140.	Tympanic shape	The shape of the tympanic canal and the orientation of the anterior tympanic plate. (Unordered)	Tubular (0); Platelike (1)	3, 8, 9, 12
141.	Tympanic trough	The presence of a tympanic trough. (Unordered)	Absent (0); Present (1)	1
142.	Tympanic plate thickness	The thickness of the tympanic plate around the external auditory meatus. (Thick>2mm; Thin<2mm). (Unordered)	Thin (0); Thick (1)	1, 13
143.	Lateral tympanic extension	The degree of tympanic extension laterally relative to the location of the porion saddle. (Unordered)	Medial to saddle (0); Lateral to saddle (1)	8
144.	Tegmen tympani	The presence of tegmen tympani on the roof of the tympanic cavity. (Unordered)	Absent (0); Present (1)	13
145.	Middle ear depth	The depth of middle ear. (Deep>8.5mm; Shallow<8.5mm). (Unordered)	Shallow (0); Deep (1)	12
146.	Axis of ear bones	The angle of the axis of ear bones. (Unordered)	Right angle or more (0); Acute angle (1)	12
147.	Area of inner ear	The area of inner ear. (Low<50mm sq; Higher>50 mm sq) (Unordered)	Low (0); Higher (1)	12
148.	Mediolateral position	The mediolateral position of the	Medial (0); Lateral	3, 8, 12

	of external auditory meatus	inferolateral tip of the tympanic relative to porion. (Unordered)	(1)	
149.	External auditory meatus size	The size of external auditory meatus. (Unordered)	Small (0); Large (1)	3, 12
150.	Tubercle behind external auditory meatus	The presence of a tubercle below the external auditory meatus where the mastoid crest branches downwards. (Unordered)	Absent (0); Present (1)	13
151.	Orientation of the long axis of external auditory meatus	The orientation of the axis of the external auditory meatus. (Unordered)	Oblique (0); Vertical (1)	13
152.	Suprameatal spine	The presence of a suprameatal spine/crest. (Unordered)	Absent (0); Present (1)	13
153.	Eustachian process of tympanic	The development of the eustacian process of tympanic. (Unordered)	Present and prominent (0); Absent or slight (1)	3, 12
154.	Mastoid fissure	The presence of a mastoid fissure, which occurs when the tympanic is not fused to the anterior face of the mastoid process. (Unordered)	Absent (0); Present (1)	1, 5, 13
155.	Squamotympanic fissure	The presence of squamotympanic fissure. (Unordered)	Absent (0); Present (1)	1, 13
156.	Squamotympanic fissure depth	The depth of squamotympanic fissure. (Unordered)	Shallow (0); Deep (1)	13
157.	Maximum lateral projection of mastoid	The position of the lateral-most point of the mastoid process on the temporal viewed posteriorly. (Unordered)	High (0); Low (1)	8
158.	Mastoid process lateral inflation	The inflation of mastoid process.("Not inflated" means that it extends up to but not beyond the supramastoid crest; "Inflated" when the mastoid is inflated lateral to the supramastoid crest). (Unordered)	Not inflated (0); Inflated (1)	3, 12
159.	Mastoid process size	The size of mastoid process. (Unordered)	Small (0); Large (1)	4, 5, 9, 13
160.	Mastoid process orientation	The orientation of the mastoid process in coronal plane. (Unordered)	Not medial (0); Medial (1)	13
161.	Mastoid tip position	The position of the tip of the mastoid process relative to porion measured as the mastoid tip position index, which is a percentage of the horizontal distance between the tip of mastoid to porion and asterion and porion. The cut-off for a "posterior" position seems to be aorund 40%	Anterior (0); Posterior (1)	8

		index. (Unordered)		
162.	Mastoid face	The contact between mastoid process and the peripheral bony structures. A deep and posteriorly extended digastric groove "cleaves" the posterior face fo the mastoid process, confining it to the lateral part of the temporal bone's basal aspect. With a very weak posterior indentation by the digastric fossa, the mastoid process is firmly connected to the pars mastoidea with a continuous posterolateral face. A posterior extension of the digastric fossal all the way to the rear margin of the temporal bone completely isolates the mastoid process. (Unordered)	Single posterolateral (0); Discrete posterior and lateral (1); Single lateral (2)	8
163.	Supramastoid crest development	The development of supramastoid crest at porion. (Unordered)	Weak (0); Marked (1)	1, 6, 9, 13
164.	Supramastoid crest and zygomatic process contact	The continuity of supramastoid crest with the zygomatic process. (Unordered)	Not continuous (0); Continuous (1)	13
165.	Supramastoid crest and lower temporal line continuity	The continuity of supramastoid crest with the lower temporal line. (Unordered)	Not continuous (0); Continuous (1)	1, 13
166.	Supramastoid sulcus closes anteriorly	The continuity of supramastoid crest and mastoid crest. (Unordered)	Absent (0); Present (1)	13
167.	Supramastoid sulcus width	The width between mastoid crest and supramastoid crest. (Ordered)	Absent (0); Narrow (1); Wide (2)	13
168.	Tubercle above the supramastoid process	The presence of a tubercle anterior to supramastoid crest. (Unordered)	Absent (0); Present (1)	1, 13
169.	Tubercle on supramastoid crest	The presence of a tubercle on the posterior portion of the supramastoid crest. (Unordered)	Absent (0); Present (1)	5, 13
170.	Mastoid crest projection	The projection of mastoid crest. (Unordered)	Weak (0); Strong (1)	1, 13
171.	Mastoid crest and upper temporal line contact	The continuity of mastoid crest with upper temporal line. (Unordered)	Not continuous (0); Continuous (1)	13
172.	Mastoid crest and supramastoid crest orientation	The orientation of the anterior portion of the mastoid and supramastoid crests. (Unordered)	Divergent anteriorly (0); Parallel (1)	1, 4, 13
173.	Juxtamastoid eminence	The presence of a juxtamastoid crest. (Unordered)	Absent (0); Present (1)	1, 4, 6, 13
174.	Digastric fossa depth	The depth of digastric fossa. (Unordered)	Shallow (0); Deep (1)	1, 3, 12, 13

175.	Digastric fossa length	The length of digastric fossa. (Unordered)	Short (0); Long (1)	8, 13
176.	Digastric fossa width	The width of digastric fossa. (Unordered)	Narrow (0); Wide (1)	3, 12, 13
177.	Digastric fossa cross-section shape	The transverse cross-sectional shape of digastric fossa. (Unordered)	Round (0); U-shaped (1); V-shaped (2)	13
178.	Digastric groove morphology	The morphology of digastric groove located medially and posterior to the mastoid process. (Unordered)	Bridged (0); Not bridged (1)	5
179.	Angular torus	The presence of an angular torus. (Unordered)	Absent (0); Present (1)	4-6, 13
180.	Pneumatization of temporal squama	The extent of the pneumatic tracts relative to the squamosal suture. Pneumatization extends beyond squamosal suture leading to a thickening of the squamous temporal (squamous antrum) = extensive. Absence of antrum = not extensive (Unordered)	Extensive (0); Reduced (1)	2, 3, 8, 12
181.	Temporal squama height	The height of the temporal squama on the vault. (Unordered)	High (0); Low (1)	5, 6, 8, 13
182.	Temporal squama shape	The shape of the temporal squama on the vault. (Unordered)	Polygonal (0); Triangular (1)	1, 13
183.	Anterior contour of temporal squama	The curvature of the anterior edge of the temporal squama. (Unordered)	Rounded (0); Rectilinear (1)	13
184.	Superior contour of temporal squama	The curvature of the superior edge of the temporal squama. (Unordered)	Rounded (0); Rectilinear (1)	5, 6, 8, 13
185.	Posterior contour of temporal squama	The contour of the posterior temporal squama of the facies temporalis in the asterionic region. (Unordered)	Flattened (0); Vertical (1)	8
186.	Squamosal suture overlap extensive, at least in males	The superior and posterosuperior aspects of the squamosal suture. (Unordered)	Not extensive (0); Extensive (1)	3, 8, 12
187.	Anteromedial incursion of the superior temporal lines	The course of the superior temporal line bewteen frontomalaretemporale and the point of maximum inflection on the line as it turns from being medially directed to posteriorly directed. (Ordered)	Weak (0); Moderate (1); Strong (2)	2, 3, 12, 13
188.	Position of temporal emphasis	The location of the most strongly expressed part of the temporal lines. (Ordered)	Posterior (0); Intermediate 1 (1); Intermediate 2 (2); Anterior (3)	8
189.	Temporal line projection	The development of the temporal band. (Unordered)	Slight (0); Marked projection (1)	1, 13

190.	Depression beneath the upper temporal line	The presence of a depression on the superior temporal line in the posterior half of the parietal. (Unordered)	Absent (0); Present (1)	13
191.	Position of temporal lines on parietal bones	The width between the temporal lines in superior view. (Unordered)	Crest (0); Wide (1)	2
192.	Depression between temporal lines	The presence of a depression between the temporal lines in the posterior half of the parietal. (Unordered)	Absent (0); Present (1)	13
193.	Temporal band width in lateral view	The width between the temporal lines on in lateral view. (Unordered)	Narrow (0); Wide (1)	13
194.	Temporal band projection	The width of the temporal band on the parietal bone. The position, relief and the existence of a stephanion disconection of the space between temporal lines. (Ordered)	Lines absent or weak (0); Lines visible but not protruding (1); Lines protruding (2)	13
195.	Temporal line position	The position of temporal lines on the parietal. (Unordered)	High (0); Low (1)	2, 13
196.	Parietomastoid angle development	The angle at parietomastoid. (Unordered)	Strong (0); Weak (1)	12
197.	Prelambdoidal depression	The presence of a prelambdoidal depression. (Unordered)	Absent (0); Present (1)	1, 13
198.	Projection on lambdoid suture (processus asteriacus)	The presence of an asteriacus process, which is an elevation limited to the inferior segment of the upper temporal line of the parietal. (Unordered)	Absent (0); Present (1)	13
199.	Asterionic notch	The presence of an asterionic notch. (Unordered)	Absent (0); Present (1)	3, 12, 13
200.	Upper occipital squama curvature	The curvature of the upper occipital squama above the inion where superior nuchal lines merge in the medial sagittal plane. (Unordered)	Flat or slightly concave (0); Convex (1)	7
201.	Occipital squama shape	The shape of the upper part of the occipital squama in norma occipitalis. (Unordered)	Pentagonal (0); Triangular (1)	13
202.	Nuchal plane inclination	The angle between the inion-opisthion chord and Frankfurt Horizontal. (Ordered)	Steep (0); Intermediate (1); Weak (2)	3, 8, 12
203.	Relative height of nuchal area	The anteroposterior height of the nuchal area of the cranial base relative to the bisupramastoid width. (Unordered)	High (0); Low (1)	8
204.	Compound temporal nuchal crest in males	The presence of compound temporal nuchal crest in males. (Ordered)	Extensive (0); Partial (1); Absent	2, 3, 8, 12

			(2)	
205.	Nuchal crest emphasis	The location of the most projecting part of the nuchal crest. (Ordered)	Lateral (0); Medial (1); Absent (2)	8
206.	Occipital angulation	The angle formed between the lambda-inion chord and the inion-opisthion chord. (Ordered)	<100 (0); 100 to 110 (1); >110 (2)	6
207.	Lower occipital squama shape	The curvature of the lower occipital squama. (Unordered)	Convex (0); Flat or slightly concave (1)	13
208.	Longus capitis insertion size	The sizeand orientation of the depression of longus capitis where visible and the degree of development of muscle markings. (Unordered)	Large (0); Small (1)	3, 12
209.	Occipital torus development	The development of the occipital torus. (Ordered)	Absent (0); Weak (1); Strong (2)	1, 5, 6, 9, 13
210.	Expansion of occipital torus	The lateral extent of occipital torus. (Unordered)	Median (0); Transversal (1)	13
211.	Occipital plane length	The length of occipital plane relative to the nuchal plane. (Unordered)	Lengthened (0); Shortened (1)	1, 4, 6
212.	Occipital supratoral sulcus	The presence of occipital supratoral sulcus. (Unordered)	Absent (0); Present (1)	4, 13
213.	Lateral occipital depression on occipital sulcus	The presence of lateral depressions on occipital sulcus (Unordered)	Absent (0); Present (1)	13
214.	Occipital bun	The presence of an occipital bun. (Unordered)	Absent (0); Present (1)	5, 13
215.	Depression above external occipital protuberance.	The depression above external occipital protuberance. (Unordered)	Absent (0); Present (1)	13
216.	External occipital protuberance	The presence of external occipital protuberance formed by supreme nuchal lines. (Unordered)	Absent (0); Present (1)	5, 13
217.	Tuberculum linearum on occipital	The presence of tuberculum linearum formed by the superior nuchal lines. (Unordered)	Absent (0); Present (1)	1, 13
218.	External occipital crest	The presence of the external occpital crest. (Unordered)	Absent (0); Present (1)	13
219.	Suprainiac fossa	The presence of a suprainiac fossa. (Unordered)	Absent (0); Present (1)	5, 13
220.	Walls of suprainiac fossa	The orientation of the lateral walls of the suprainiac fossa. (Ordered)	Convergent (0); Parallel (1); Divergent (2)	13
221.	Retromastoid process	The presence of a retromastoid process at the junction of the superior nuchal line and the secondary branch	Absent (0); Present (1)	13

		of the inferior nuchal line, between the inion and mastoid process. (Unordered)		
222.	Occipitomastoid crest	The presence of an occipitomastoid crest. (Unordered)	Absent (0); Present (1)	1, 4, 13
223.	Occipital torus and supramastoid crest contact	The continuity of the occipital torus with the supramastoid crest. (Unordered)	Not continuous (0); Continuous (1)	13
224.	Occipital torus to mastoid crest contact	The continuity of the occipital torus with the mastoid crest. (Unordered)	Not continuous (0); Continuous (1)	13
225.	Occipital torus to upper temporal line contact	The continuity of the occipital torus with the upper temporal line. (Unordered)	Not continuous (0); Continuous (1)	13
226.	Inion location	The location of inion relative to the opisthocranion. (Unordered)	Below opisthocranion (0); At opisthocranion (1)	4
227.	Inion/endinion location	The location of inion on the external cranial surface and endinion on the endocranial surface. (Unordered)	Separate (0); Coincide (1)	4
228.	Occipitomarginal sinus frequency	The frequency of the presence of occipitomarginal sinus. (Ordered)	Low (0); Intermediate (1); High (2)	3, 8, 12
229.	Foramen magnum shape	The shape of foramen magnum. (Unordered)	Oval (0); Heart (1)	3, 12
230.	Foramen magnum position	The position of foramen magnum relative to bi-tympanic line. (Ordered)	Posterior (0); At line (1); Anterior (2)	3, 8, 12
231.	Foramen magnum inclination	The angle between the basion-opisthion chord and Frankfurt Horizontal. (Ordered)	Posteriorly (0); Horizontal (1); Anteriorly (2)	3, 12
232.	Cranial base breadth	The index of bi-porion chord divided by orbital height chord. (Ordered)	Narrow (0); Intermediate (1); Broad (2)	3, 8
233.	Basioccipital length	The index of basion-sphenobasion length divided by cranial base geometric mean. (Ordered)	Long (0); Intermediate (1); Short (2)	3
234.	Ethmo-sphenoid contact	The frequency of contact between ethmoid and sphenoid bones. (Ordered)	Usually absent (0); Variable (1); Usually present (2); Present (3)	3, 12
235.	Cranial base flexion	The angle between Frankfurt Horizontal and the basion-hormion chord (the inclination of the basioccipital and basisphenoid measured externally). (Ordered)	Flat (0); Moderate (1); Flexed (2)	3, 9, 12

236.	Posterior base shape	The horizonal disatnce between the coronal plane of the mastoid crests and the most posterior part of the cranial base between the supramastoid crests. (Unordered)	Moderate (0); Squat (1); Elongate (2)	8
237.	Condylar canal	The presence of condylar canal on the skull base. (Unordered)	Absent or infrequent (0); Frequently present (1)	12
238.	Cerebellum position	The position of the cerebellum relative to the cerebrum. (Unordered)	Not tucked (0); Tucked (1)	3, 8, 12
239.	Anterior pole shape	The shape of the anterior poles of the frontal lobe as seen in the endocast. Strongly anteriorly tapered lobes are considered "beaked". (Unordered)	Rounded (0); Beaked (1)	8
Dental characters				
240.	Enamel thickness	The relative thickness of enamel. (Ordered)	Thin (0); Thick (1); Hyperthick (2)	2, 3, 12
241.	Dental development reate	The differences in the calcification and eruption patterns of the permanent teeth in extant hominoids and fossil hominids. (Ordered)	Delayed (0); Intermediate (1); Accelerated (2)	12
242.	Cingulum expression	The presence of labial cingulum in lower canines and premolars. (Unordered)	Present (0); Absent (1)	6
243.	Sulcus obliqus development	The development of oblique sulcus. (Unordered)	Weak to moderate (0); Strong (1)	12
244.	Fovea posterior development	The development of fovea posterior. (Unordered)	Absent or weak (0); Well developed (1)	12
245.	Incisal reduction	The summed mediodistal means of the I1 and I2. (Ordered)	Not reduced (0); Moderate (1); Reduced (2)	3, 12
246.	Maxillary incisor heteromorphy	The index of I1 area divided by I2 area. (Unordered)	Dissimilar (0); Similar (1)	3, 12
247.	Incisor procumbency	The orientation of incisors. (Unordered)	Procumbent (0); Vertical (1)	2
248.	Presence of Maxillary I2/C diastema	The presence of maxillary diastema. (Unordered)	Present (0); Absent (1)	2
249.	Maxillary incisor-to postcanine ratio	The ratio of maxillary incisor-to-postcanine teeth. (Ordered)	Small (0); Moderate (1); Large (2)	2
250.	Lingual crenulations of maxillary I1	The extent of enamel crenulations on the lingual surface of maxillary I1. (Unordered)	Absent (0); Marginal (1); Whole surface (2)	12
251.	Labial curvature of maxillary I1	The development of labial curvature of maxillary I1. (Ordered)	Trace (0); Weak (1); Moderate (2); Pronounced (3)	7

252.	Shovel on maxillary I1	The development of shovel-shaped maxillary I1. (Unordered)	Absent (0); Faint (1); Trace (2)	7
253.	Double shovel on maxillary I1	The presence of double shovel-shaped maxillary I1. (Unordered)	Absent (0); Fraint (1)	7
254.	Shovel shape in maxillary I2	The shape of maxillary I2. (Unordered)	Classic (0); Triangular (1); Absent (2)	10
255.	Canine robusticity	The robusticity of the canines. (Unordered)	Slender (0); More robust (1)	3, 12
256.	Canine sexual dimorphism	Sexual dimorphism in canine size. (Unordered)	Hyper dimorphic (0); Strongly dimorphic (1); Moderately dimorphic (2); Monomorphic; small canines (3); Monomorphic; large canines (4)	12
257.	Mandibular deciduous canine shape	The mesiodistal disposition of the apex, the height of mesial crown convexity and the height of the mesial end of the lingual cingulum. (Unordered)	Apex central, mesial convexity low (0); Apex mesial, mesial convexity high (1)	12
258.	Canine size reduction	The degree of canine reduction calibrated relative to Pan and Gorilla. Canine size and canine root dimentions compared to canines of extant African apes. (Ordered)	No (0); Somewhat (1); Very (2)	3, 8, 12
259.	Extensive mesial groove on maxillary canine	The presence of a mesial groove on the upper canine that extends to the crown apex. (Unordered)	Yes (0); No (1)	12
260.	Lingual ridge development on maxillary canine	The development of the lingual ridges on maxillary C. (Unordered)	Marked (0); Weak (1)	2
261.	Bushman canine on maxillary canine	The presence of Bushman canine. (Unordered)	Absent (0); Present (1)	7
262.	Distal accessory ridge development on maxillary canine	The development of the distal accessory ridge on maxillary canine. (Ordered)	Absent (0); Faint (1); Weak (2)	7
263.	Lingual shape of maxillary canine	The symmetry of the maxillary canine in lingual views, assessed by the position of the mesial and distal crown shoulder positions relative to the crown apex. (Ordered)	Asymmetric (0); More symmetric (1); Symmetric (2)	8
264.	Shape of maxillary canine	The shape and the sharpness of maxillary canine. (Unordered)	Sharp, flared (0); Rounded, no	10

			cuspule (1)	
265.	Shape of mandibular canine	The shape of mandibular canine. (Unordered)	Asymmetrical (0); Symmetrical (1)	10
266.	Lingual ridge development on mandibular canine	The prominence of medial lingual ridge of mandibular canine. (Unordered)	Prominent (0); Weak (1)	2, 12
267.	Basal keel on mandibular canine	The presence of the basal keel of mandibular canine. (Ordered)	Present (0); Reduced (1); Absent (2)	12
268.	Maxillary premolar molarization	The degree of molarization on maxillary premolars. (Ordered)	None (0); Minor (1); Marked (2)	2
269.	Buccal grooves on maxillary premolars	The development of buccal grooves on maxillary premolars. (Unordered)	Marked (0); Weak (1)	2
270.	P3 position	The position of P3 relative to canine. (Unordered)	Posterior (0); Posterolateral (1)	9
271.	Maxillary P3 cusp heteromorphy	The size of paracone of upper premolars relative to the protocone. (Ordered)	Paracone much larger than protocone (0); Paracone larger than protocone (1); Paracone equals protocone (2)	12
272.	Maxillary P3 root number	The number of roots on maxillary P3. (Unordered)	Two (0); >Two (1)	7
273.	Maxillary P3 mesiobuccal line extent	The extent of mesiobuccal line on maxillary P3. (Ordered)	Always (0); Frequent (1); Rare (2); Absent (3)	8
274.	Mesiobuccal protrusion of P3 crown base	The degree of overall asymmetry of the crown of maxillary and mandibular P3. (Ordered)	Strong (0); Moderate (1); Weak or absent (2)	3, 12
275.	Mandibular P3 root number	The number of roots on mandibular P3. (Unordered)	One (0); Two (1)	2, 7
276.	Frequency of well developed metaconid on mandibular P3	The frequency of a well-developed P3 metacnoid within each species sample. (Ordered)	Absent (0); Infrequent (1); Frequent (2)	3, 8, 12
277.	Mandibular P3 shape	The shape and symmetry of mandibular P3. (Ordered)	Asymmetrical (0); Less asymmetrical, talonid reduced (1); Much less asymmetrical, talonid absent (2); Circular (3)	10
278.	Lingual cusp on mandibular P4	The number of cusps on mandibular P4. (Unordered)	Two, mesial cusp much larger (0); Two, mesial cusp	7

			larger (1); Two, cusps equal size (2); Two, distal cusp larger (3)	
279.	Mandibular P4 root number	The number of roots on mandibular P4. (Unordered)	One (0); Two (1)	1
280.	Mandibular P4 shape	The symmetry of mandibular P4. (Ordered)	Asymmetrical, wide polygon (0); Asymmetrical, reduced polygon (1); Symmetrical (2)	10
281.	Postcanine crown area	The summed area of postcanine teeth. (Ordered)	Small (0); Moderate (1); Large (2)	1, 3, 8, 12
282.	Size of M1 relative to M2	The ratio of crown area of M1 relative to M2. (Unordered)	≥ 1 (0); <1 (1)	9
283.	Size of M1 relative to M3	The ratio of crown area of M1 relative to M3. (Unordered)	≥ 1 (0); <1 (1)	9
284.	Size of M2 relative to M3	The ratio of crown area of M2 relative to M3. (Unordered)	≥ 1 (0); <1 (1)	9
285.	Molar cingulum development	The development of molar cingulum on maxillary molars. (Unordered)	Reduced, incomplete (0); Fragmented or absent (1)	3, 12
286.	Molar dentine horn height	The height of the molar dentine horns. (Unordered)	High (0); Low (1)	12
287.	Maxillary molar morphology	The development of cusps and enamel on the maxillary molar. (Unordered)	Well developed cusps and cristae (0); Inflated cusps, limited cristae (1); Low cusps with enamel wrinkling (2); Flat, bunodont morphology (3)	3
288.	Protocristid groove prominence of mandibular molars	The development of protocristic groove on molars. (Unordered)	Prominent (0); Barely visible (1)	12
289.	Lingual marginal ridge development	The development of the lingual marginal ridges of molars. (Ordered)	Hardly appreciable (0); More prominent (1); Very prominent (2)	12
290.	Positions of buccal and lingual cusps relative to crown margin	The positions of the buccal and lingual cusp tips relative to the crown base. (Unordered)	BC and LC at margin (0); LC margin, BC slightly lingual (1); LC margin, BC moderately lingual (2); LC slightly	2, 3, 8, 12

			buccal, BC moderately lingual (3); LC moderately buccal, BC strongly lingual (4)	
291.	Protoconid/metaconid more mesial cusp on molars	The most mesial cusp on mandibular molars. (Unordered)	Equal (0); Protoconid (1)	2
292.	Peak of enamel thickness between the roots of molars	The thickness of enamel between the roots of molars. (Unordered)	Thin (0); Thicker (1)	2
293.	Maxillary M1 shape	The shape of maxillary M1. (Unordered)	Squared (0); Rhomboidal (1)	10
294.	Cusp 5 on maxillary M1	The development of cusp 5 on maxillary M1. (Unordered)	Faint cuspule (0); Trace cuspule (1); Small cuspule (2)	7
295.	Enamel extension on maxillary M1	The extension of enamel on maxillary M1. (Unordered)	Absent (0); Faint (1)	7
296.	Carabelli's cusp on mandibular M1	The development of Carabelli's cusp of maxillary M1. (Unordered)	Lingual cingulum (0); Absent (1); Groove, small cusp (2); Pit, small cusp (3); Large depression, cusp (4)	7
297.	Anterior fovea on mandibular M1	The development of anterior fovea of mandibular M1. (Ordered)	Faint (0); Weak (1); Moderate (2); Large (3)	7
298.	Cusp number on mandibular M1	The number of cusps on mandibular M1. (Unordered)	Five (0); Six (1)	7
299.	Protostylid on mandibular M1	The development of protostylid of mandibular M1. (Unordered)	Absent (0); Absent-pit (1); Curved buccal groove (2); Curved mesial and distal grooves (3); Trace cusp (4); Small cusp (5)	7
300.	Cusp 7 on mandibular M1	The development of cusp 7 on mandibular M1. (Ordered)	Absent (0); Faint (1); Small (2)	7
301.	Root number on mandibular M1	The number of roots on mandibular M2. (Unordered)	Two (0)	7
302.	Presence of mid-trigonid crest in mandibular M1 and/or M2	The presence of mid trigonid crest on mandibular M1 and M2. (Unordered)	Absent (0); Present (1)	10
303.	Absence of cusp 5 in	The presence of cusp 5 on	Present (0); Absent	10

	mandibular M1 and/or M2	mandibular M1 and M2. (Unordered)	(1)	
304.	Maxillary M2 shape	The shape of the maxillary M2 measured by the length divided by breadth of the molar crown. (Unordered)	Broader than Long (0); Square (1)	3
305.	Hypocone on maxillary M2	The development of hypocone on maxillary M2. (Ordered)	Small cusp (0); Large cusp (1); Very large cusp (2)	7
306.	Groove pattern on mandibular M2	The groove pattern of mandibular M2. (Unordered)	Y (0); Some X (1); X (2)	7
307.	Cusp number on mandibular M2	The number of cusps on mandibular M2. (Ordered)	Four (0); Five (1); Six (2); Greater than 6 (3)	7
308.	Root number on mandibular M2	The number of roots on mandibular M2. (Unordered)	Less than 2 (0); Two (1)	7
309.	Maxillary M3 agenesis	The degree of maxillary M3 agenesis. (Unordered)	Absent (0); Minimal (1)	7
310.	Torsomolar angle on mandibular M3	The torsomolar angle on mandibular M3. (Unordered)	Absent (0); Minimal (1)	7
311.	Protocone size relative to paracone of deciduous m1, in occlusal view	The protocone size of maxillary deciduous m1 in crown view. (Unordered)	Larger than paracone (0); Smaller than paracone (1)	12
312.	Deciduous mandibular m1 shape	The shape of deciduous mandibular m1. (Unordered)	Buccolingually narrow (0); Buccolingually broad (1); Molarized (2)	8
313.	Talonid basin of deciduous m1	The distal opening of the talonid basin on mandibular deciduous m1. (Unordered)	Open distally (0); Closed distally (1)	12
314.	Presence of metaconid of mandibular deciduous m1	The presence of the metaconid on mandibular deciduous m1. (Unordered)	Absent or poorly defined (0); Well defined (1)	12
315.	Deciduous m1 mesial crown profile	This character comprises several inter-related traits. These are: the position of the protoconid relative to the metaconid, the disposition of the mesial marginal ridge, and the structure of the fovea anterior. (Unordered)	MMR absent, protoconid anterior, fovea open (0); MMR slight, protoconid anterior, fovea open (1); MMR thick, protoconid even with metaconid, fovea closed (2)	3, 8, 12

316.	Distal marginal ridge height of deciduous m2	The development of the distal marginal ridge of deciduous second molar. (Unordered)	Low (0); High (1)	12
317.	Distal trigonid crest on mandibular deciduous m2	The length of crista obliqua relative to protoconid apex. (Unordered)	Does not reach protoconid apex (0); Reaches protoconid apex (1)	12
318.	Crista obliqua of maxillary deciduous m2	The development of the post-protocrista on maxillary deciduous m2. (Ordered)	Weak (0); Moderate (1); Strong (2)	12
Mandibular characters				
319.	Mandibular symphysis robusticity	The index of mandibular symphysis breadth divided by mandibular height. (Ordered)	Gracile (0); Intermediate (1); Robust (2); Extremely robust (3)	3
320.	Mandibular symphysis orientation	The orientation of the mandibular symphysis. (Unordered)	Receding (0); Vertical (1)	2, 3, 6, 8, 12
38.	Projection of mental protruberance	The degree of mental protuberance projection. (Ordered)	Absent (0); Weakly projecting (1); Strongly projecting (2)	1, 2, 5, 6
322.	Central keel	The presence of a central keel. (Unordered)	Absent (0); Present (1)	5, 6
323.	Mandibular incurvation	The development of a depression on the anterosuperior symphyseal region in norma lateralis (Ordered)	Absent (0); Weakly developed (1); Strongly developed (2)	6
324.	Incisura submentalis	The presence of semilunar space beneath the inferior rim of the symphysis (Unordered)	Absent (0); Present (1)	6
325.	Medial crest in digastric fossa	The presence of a medial crest in digastric fossa. (Unordered)	Absent (0); Present (1)	6
326.	Digastric fossa direction	The orientation of digastric fossa. (Ordered)	Downward (0); Downward-backward (1); Backward (2)	6
327.	Lateral tubercle	The presence of a lateral tubercle. (Unordered)	Absent (0); Present (1)	5, 6
328.	Inferior transverse torus development	The development of superior and inferior transverse tori. (Unordered)	Inferior torus stronger than superior torus (0); Both tori of similar development (1); Superior torus stronger than	1, 3, 6

			inferior torus (2); Both tori undeveloped (3)	
329.	Post-incisive planum development	The development of post-incisive planum. (Unordered)	Prominent (0); Weak (1)	2, 6, 12
330.	Position of genioglossus insertion	The location of the insertion of genioglossal muscle relative to the inferior transverse torus. (Unordered)	Above inferior transverse torus (0); On inferior transverse torus (1)	12
331.	Position of geniohyoideus insertion	The location of the geniohyoideus insertion relative to the inferior transverse torus. (Ordered)	Basally on inferior transverse torus (0); Higher on inferior transverse torus (1); Above inferior transverse torus (2)	12
332.	Position of digastric insertion	The location of the digastric muscle insertion relative to the inferior transverse torus. (Unordered)	Posterior to inferior transverse torus (0); Inferior transverse torus (1); Not on symphysis (2)	12
333.	Fossae genioglossus definition	The development of the excavated area delineated by the transverse tori. (Ordered)	Not defined, flat surface (0); Weak (1); Well defined (2)	6
334.	Submandibular fossa depth	The depth of submandibular fossa located beneath the alveolar region. (Unordered)	Shallow (0); Deep (1)	6
335.	Anterior marginal tubercle position	The position of the marginal tubercle. (Unordered)	Absent (0); Present (1)	5, 6
336.	Mental foramen opening direction	The direction of the mental foramen opening. (Ordered)	Anterior (0); Lateral (1); Posterior (2)	2, 3, 12
337.	Mental foramen position	The position of the mental foramen along tooth row. (Ordered)	P3-P4 (0); P4-M1 (1); M1 (2)	5, 6
338.	Mental foramen height	The index of the height of mental foramen position relative to the height of the mandibular corpus. (Ordered)	Very low (0); Low (1); Intermediate (2); High (3)	6, 8
339.	Mental foramen number	The number of mental foramen. (Unordered)	Single (0); Multiple (1)	6
340.	Hollowing above and behind mental foramen	The presence of a hollowing contour of the lateral face of the mandibular corpus above and behind the mental foramen. (Unordered)	Present (0); Absent (1)	3, 8, 12
341.	Torus marginalis superius development	The development of the superior marginal torus. (Unordered)	Weak/absent (0); Clearly visible (1)	6
342.	Torus marginalis inferius development	The development of the inferior marginal torus. (Unordered)	Weak/absent (0); Clearly visible (1)	2, 6

343.	Mandibular corpus depth along tooth row	The height of mandibular corpus along tooth row. (Ordered)	Shallow mesially (0); Constant (1); Deepens mesially (2)	12
344.	Mandibular cross-sectional area at M1	The geometric mean of the area of the corpus at M1. The area is caculated as an ellipse and the square root of area was then used to assess the character. (Small<25.5mm sq; Large>25.5mm sq). (Unordered)	Small (0); Large (1)	1, 3, 8, 12
345.	Horizontal distance between TMJ and M2 or M3	The ratio of the distance between the TMJ and M2/M3 relative to bi-foramen ovale breadth. (Short<58; Long>58) (Unordered)	Long (0); Short (1)	2, 3, 12
346.	Mandibular extramolar sulcus width	The width of the extramolar sulcus. (Narrow<6.5mm; Broad>6.5mm). (Unordered)	Broad (0); Narrow (1)	3, 6, 12
347.	Retromolar space	The presence of retromolar space. (Unordered)	Absent (0); Present (1)	5, 6
348.	Retromolar area inclination	The orientation of the retromolar area. (Ordered)	Horizontal (0); Inclined (1); Vertical (2)	6
349.	Orientation of mandibular premolar row	The orientation of the dental arcade measured as the ratio between the internal bialveolar margin distances at mandibular canine and M2 positions. (Unordered)	U shaped (0); Parabolic (1)	2, 3, 8, 12
350.	Separation of mandibular tooth rows	The width of the dental arcade. (Unordered)	Widely separated (0); Narrow separation (1)	12
351.	Inferior alveolar margin orientation	The orientation of the inferior alveolar margin. (Unordered)	Steep (0); Slowly inclined (1); Parallel (2)	11
352.	Sulcus intertoralis development	The development of intertoral sulcus. (Ordered)	Flatsurface (0); Weak (1); Well defined (2)	11
353.	Prominentia lateralis relief	The development of lateral prominence. (Ordered)	Flatsurface (0); Weak (1); Strong (2)	11
354.	Prominentia lateralis position	The position of lateral prominence along tooth row. (Ordered)	M1-M2 (0); M2-M3 (1); M3 (2)	11
355.	Ramus length	The length of mandibular ramus. (Unordered)	Narrow (0); Large (1)	11
356.	Ramus root anterior position	The position of the origin of the ascending ramus relative to the anteroposterior axis of the mandibular	Posterior (0); Intermediate (1); Anterior (2)	8

		corpus. Anterior origin is where the ramus rises at the M1 level. (Ordered)		
357.	Ramus root vertical position	The position of the origin of the ascending ramus relative to the mandibular corpus height. (Ordered)	High (0); Intermediate (1); Low (2)	8
358.	Internal coronoid pillar orientation	The orientation of the ridge that extends inferiorly from the coronoid tip. (Unordered)	Vertical (0); Concave (1); Oblique (2)	11
359.	Crista ectocondyloidea development on the lateral face of the ramus.	The development of crista ectocondyloidea, a ridge that extends inferiorly from the condyle tip on the lateral face of the ramus. (Unordered)	Weak/absent (0); Clearly defined (1)	11
360.	Crista endocondyloidea relief on the medial face of the ramus	The development of crista endocondyloidea, a ridge that extends inferiorly from the condyle tip on the medial face of the ramus. (Unordered)	Weak/absent (0); Clearly defined (1)	11
361.	Crista endocondyloidea orientation	The orientation of crista endocondyloidea on the medial face of the ramus. (Unordered)	Oblique (0); Diagonal (1)	11
362.	Position of the junction between the mandibular notch and the condyle articular surface	The position of the condyle articular surface relative to the mandibular notch. (Unordered)	Lateral (0); Medial (1)	11
363.	Position of the deepest point of the mandibular notch	The position of the deepest point of the mandibular notch. (Unordered)	Centered (0); Condylar (1)	5, 11
364.	Crest of the mandibular notch	The position of the crest on the mandibular notch (Ordered)	Lateral edge of condyle (0); Less lateral (1); Less than a third of distance from medial end (2); Medial end (3)	5
365.	Planum triangulare size	The development of planum triangulare defined by the internal coronoid pillar and the crista endocondyloidea (Ordered)	Weakly developed (0); Intermediate (1); Strongly developed (2)	11
366.	Planum triangulare depth	The depth of planum triangulare. (Ordered)	Flat (0); Shallow (1); Deep (2)	11
367.	Condyle height relative to the coronoid	The height of mandibular condyle relative to the coronoid. (Ordered)	Lower (0); Equal (1); Higher (2)	11
368.	Lateral condylar	The development of lateral condylar	No tubercle (0); Swelling under	5

	tubercle development	tubercle. (Ordered)	lateral lip (1); Laterally projected tubercle (2); Strongly projected tubercle (3)	
369.	Fossa subcondylea depth	The depth of subcondylar fossa. (Ordered)	Flat (0); Shallow (1); Deep (2)	11
370.	Fossa subcondylea development	The development of subcondylar fossa. (Ordered)	Weakly developed (0); Intermediate (1); Strongly developed (2)	11
371.	Mandibular foramen shape	The shape of the mandibular canal opening. (Unordered)	Oval (0); Circular (1)	5, 11
372.	Lingula mandibulae	The presence of lingula mandibulae, a projection of the edge of the mandibular foramen. (Unordered)	Absent (0); Present (1)	11
373.	Mylohyoid line orientation	The orientation of the mylohyoid line that crosses the medial corpus surface. (Unordered)	Parallel (0); Inclined (1); Diagonal (2)	11
374.	Mylohyoid line position	The position of mylohyoid line at M3. (Ordered)	Low (0); Intermediate (1); High (2)	11
375.	Mylohyoid groove orientation	The orientation of the mylohyoid groove on the medial surface of the ramus. (Unordered)	Inclined (0); Diagonal (1)	11
376.	Bony bridge in mylohyoid groove	The presence of a body bridge in mylohyoid groove. (Unordered)	Absent (0); Present (1)	11
377.	Fossa masseterica depth	The depth of masseteric fossa on the lateral surface of the gonial angle. (Ordered)	Flat (0); Shallow (1); Deep (2)	11
378.	Gonial profile	The profile of the posteroinferior corner of the mandible in norma lateralis. (Unordered)	Not truncated (0); Truncated (1)	5, 11
379.	Distinctiveness of angular process of mandible	The development of the angular process. (Unordered)	Distinct with posterior projection (0); Not distinct (1)	12
380.	Pterygoid fossa depth	The depth of pterygoid fossa. (Unordered)	Shallow (0); Deep (1)	11

References

1. Argue D, Morwood MJ, Sutikna T, Jatmiko, Saptomo W. 2009 *Homo floresiensis*: a cladistic analysis. *J. Hum. Evol.* **57**, 623–639. (doi:10.1016/j.jhevol.2009.05.002)

2. Berger LR, de Ruiter, DJ, Churchill SE, Schmid P, Carlson KJ, Dirks PHGM, Kibii JM. 2010 *Australopithecus sediba*: a new species of *Homo*-like australopith from South Africa. *Science.* **328**, 195–204. (doi:10.1126/science.1184944)

3. Cameron DW, Groves CP. 2004 *Bones, Stones and Molecules: Out of Africa and Human Origins.* San Diego, CA: Elsevier.

4. Cameron D, Patnaik R, Sahni A. 2004 The phylogenetic significance of the Middle Pleistocene Narmada hominin cranium from central India. *Int. J. Osteoarchaeol.* **14**, 419–447. (doi:10.1002/oa.725)

5. Chang ML. 2005 *Neandertal origins, Middle Pleistocene systematics, and tests of current taxonomic and phylogenetic hypotheses*. [Ph.D. Dissertation]. Philadelphia, PA: University of Pennsylvania.

6. Gilbert WH. 2008 *Homo erectus* cranial anatomy. In Homo erectus*: Pleistocene evidence from the Middle Awash, Ethiopia* (eds WH Gilbert, B Asfaw), pp 265–311. Berkeley, CA: University of California Press.

7. Irish JD, Guatelli-Steinberg D, Legge SS, de Ruiter DJ, Berger LR. 2013 Dental morphology and the phylogenetic 'place' of *Australopithecus sediba*. *Science* **340**, 1233062–1233062. (doi:10.1126/science.1233062)

8. Kimbel WH, Rak Y, Johanson DC. 2004 Taxonomic and phylogenetic status of *Australopithecus afarensis*. In *The Skull of* Australopithecus afarensis (eds WH Kimbel, Y Rak, DC Johanson), pp 215-220. New York, NY: Oxford University Press.

9. Lordkipanidze D, Ponce de León MS, Margvelashvili A, Rak Y, Rightmire GP, Vekua A, Zollikofer CPE. 2013 A complete skull from Dmanisi, Georgia, and the evolutionary biology of early *Homo*. *Science* **342**, 326–331. (doi:10.1126/science.1238484)

10. Martinón-Torres M, Bermúdez de Castro JM, Gomez-Robles A, Arsuaga JL, Carbonell E, Lordkipanidze D, Manzi G, Margvelashvili A. 2007 Dental evidence on the hominin dispersals during the Pleistocene. *Proc. Natl. Acad. Sci.* **104**, 13279–13282. (doi:10.1073/pnas.0706152104)

11. Mounier A, Marchal F, Condemi S. 2009 Is *Homo heidelbergensis* a distinct species? New insight on the Mauer mandible. *J. Hum. Evol.* **56**, 219–46. (doi:10.1016/j.jhevol.2008.12.006)

12. Strait DS, Grine FE. 2004 Inferring hominoid and early hominid phylogeny using craniodental characters: the role of fossil taxa. *J. Hum. Evol.* **47**, 399–452. (doi:10.1016/j.jhevol.2004.08.008)

13. Zeitoun V. 2009 *The Human Canopy:* Homo erectus, Homo soloensis, Homo pekinensis *and* Homo floresiensis. Oxford, UK: J. and E. Hedges.

B9. List of fossil hypodigms

	Argue et al. (2009)	Berger et al. (2010)	Cameron & Groves (2004)
Ar. ramidus			specimens from Aramis
Au. anamensis			specimens from Allia Bay
Au. afarensis	AL444-2	specimens from Hadar, Laetoli & Middle Awash	AL (128-23, 145-35, 162-28, 188-1, 198-1, 199-1, 200-1, 207-13, 266-1, 277-1, 288-1, 311-1, 33-125, 333-1, 333-105, 333-2, 333-45, 333w-0, 333w-1, 33w-12, 400-1a, 417-1, 444-2, 58-22), LH 4
Au. africanus	Sts (5, 7), Stw 505	specimens from Taung, Sterkfontein (including Sts53) & Makapansgat	MLD (1, 6, 9, 37/38,), Sts (5, 17, 19, 20, 26, 52a, 67, 71), Stw (13, 73, 252, 505), TM (1511, 1512)
Au. garhi		BOU-VP 12/130	BOUV-VP 12/130
Au. sediba		MH (1, 2)	
H. antecessor			
H. ergaster	KNM-ER (3733, 3883)	SK (15, 18a, 27, 43, 45, 68, 847, 878, 2635), SKW 3114, SKX (257/258, 267/2671, 268, 269, 334, 610, 1756, 2354-2356, 21204)	KNM-ER (730, 820, 992, 1507, 1812, 3733, 3883), KNM-WT 15000, OH 2
H. erectus	Sangiran (2, 17), Trinil		
Dmanisi	D (2280, 2282, 2700)		
H. floresiensis	LB1, LB6/4		
H. habilis	KNM-ER1813, OH 24	AL666-1, KNM-ER (1478, 1501, 1502, 1805, 1813, 3735), OH (4, 6, 7, 13, 15, 16, 21, 24, 27, 31, 37, 39, 42, 44, 45, 62), Omo L894-1	OH (7, 13, 16, 24), KNM-ER (1805, 1813, 1478, 1501, 1502, 3735)
H. heidelbergensis	Kabwe		
H. neanderthalensis			
H. rudolfensis	KNM-ER 1470	KNM-ER (819, 1470, 1482, 1483, 1590, 1801,	KNM-ER (1470, 1482, 1483, 1590, 1801, 1802,

		1802, 3732, 3891), OH 65, UR 501	3732, 3891, 3950)
fossil *H. sapiens*			
H. sapiens	Not reported		not reported
K. platyops			KNM-WT (38350, 40000, 40001)
P. aethiopicus		KNM-WT 17000	KNM-WT 17000
P. boisei		Specimens from Omo Shungura, East Lake Turkana, Olduvai Gorge	OH 5, KNM-ER (403-407, 725, 727-729, 732, 805, 810, 818, 1803, 1806), KGA 10-525, SK (6, 12, 13/14, 23, 34, 46-49, 52, 65, 79, 83, 848, 1586), SKW (5, 8, 11, 29, 2581), TM 1517, DNH 7
P. robustus		Specimens from Kromdraai, Swartkrans, Sterkfontein, Drimolen, Gondolin, Coopers	
S. tchadensis			
G. gorilla	4 adults (2 males/2 females)		Not reported
P. troglodytes	4 adults (2 males/2 females)		Not reported

	Cameron et al. (2004)	Chang (2005)	Gilbert (2008)	Irish et al. (2013)
Ar. ramidus				
Au. anamensis				KNM-ER (7727, 20420, 20422, 20423, 20427, 20432 A, 30200 A, 30202, 30731, 30745, 30750), KNM-KP 29287 A & B, KNM-LT 329 (cast)
Au. afarensis				AL (128-23, 145-35, 176-35, 188-1, 198, 199-1, 200-1a, 200-1b, 207-13, 266, 277-1, 311-1, 315-22, 330-5, 333-1, 333-2, 333-82, 333- W1a/b, 333-W57, 333-W58, 333w-60, 333x-2, 333x-3, 333x-4, 333x-20, 366-6, 400-1a, 400-1b, 411-1, 413-1, 417-1a, 417-1d, 438-2, 440-1, 486-1, 539-4e, 620-1, 655-1, 763-1, 996-1), LH (2, 3 (cast), 4 (cast))
Au. africanus			Sts 5	MLD (2, 6, 9, 11, 18, 23, 28-30, 40, 43) STS (1, 3, 4, 8, 9, 12, 17, 22-24, 30, 32, 40, 52, 53, 55-57, 61, 71), STW (2, 6, 7, 13 (b,f), 19b, 21, 23, 24, 43, 44, 50, 53, 56, 58, 61, 71, 73 (b–f), 75d, 106, 107, 109b, 110, 116d, 123a, 123b, 131 (b,c,d), 132, 143, 145, 147, 148, 151 (a,b), 179, 183 (c,e,h), 184, 188, 192 (a,b), 193 (a, b, c, d,e), 204 (a,b), 212 (a,c,e,f), 213 (a–g), 234, 246, 252 (a, c–l), 280c, 285 (a,b), 287, 288, 291, 295 (c,d), 305b, 308, 309a, 319, 327 (b–d), 351, 364, 365, 369, 384e, 401, 402, 404 (c,f,g), 406, 408, 412 (a,b), 413, 420b, 421 (a,b), 422, 424, 446, 447, 471 (c,g), 475, 476, 487b, 491 (b–g), 498 (a–d), 502, 513 (c–e), 524, 529 (b,c), 536, 537 (d,f,g), 558, 560 (d,e), 566), Taung, TM (1511, 1512, 1523, 1527)
Au. garhi				
Au. sediba				MH (1, 2)

H. antecessor	ATD6-(15, 16, 17, 18, 20, 38, 57, 84, 89)	Atapuerca GD		
H. ergaster	KNM-ER (730, 3733, 3883), KNM-WT15000	KNM-ER 3733, KNM-WT 15000	KNM-ER (3733, 3883), Daka, Buia	KNM-BK 67 [cast], KNM-ER (806 [B, C], 807, 808 [C, G], 820, 992 [A, B], 1506 [A, B], 2597), KNM-WT 15000, OH (12 [cast], 22[cast]), SK 15, SKX (257, 258, 268, 334, 339, 610)
H. erectus	Sangiran (2, 4, 10, 12, 17), Ngandong (1, 3, 6, 7, 10, 11, 12), Zhoukoudian, Hexian	Sangiran 7, Zhoukoudian	Hexian, Ngandong (1, 6, 7, 10, 11, 12), OH 9, Sambungmachan (1, 3, 4), Sangiran (2, 4, 12, 17), Trinil 2, Zhoukoudian (III, V, X, XI, XII)	
Dmanisi	D (2280, 2282)	D (2280, 2282, 2700/2735)	D (2280, 2282, 2700)	
H. floresiensis				
H. habilis	OH (7, 13, 16, 24), KNM-ER (1813, 3735)		KNM-ER 1813	AL 666-1, KNM-ER (1482[cast], 1590 [B, C, D, E, F, G], 1802, 1805, 1813), KNM-LU 335, OH (7 [cast], 13, 16, 24, 39, 44, 45, 62, 63), SKW 3114
H. heidelbergensis	Bodo (I, II), Broken Hill, Lake Ndutu, Arago, Petralona, Ceprano, Steinheim, Narmada	Bodo, Kabwe, Ndutu, Arago, AtapuercaSH, Mauer, Petralona, Reilingen, Steinheim, Swanscombe	Bodo, Kabwe, Ndutu, Saldanha, Ceprano, Petralona, Sima de los Huesos (1, 4, 5, 8), Dali	
H. neanderthalensis	Spy 1, La Chapelle-aux-Saints, La Ferrassie, La Quina, Saccopastore, Krapina, Tabun, Amud, Shanidar	Krapina, Saccopastore, Gibraltar FQ, La Chapelle, La Ferrassie, La Quina, Le Moustier, Monte Circeo, Neandertal, Regourdou, Spy, St. Cesaire, Zafarraya, Amud, Shanidar, Tabun		
H. rudolfensis			KNM-ER 1470	

fossil *H. sapiens*	Border Cave, Klasies River Mouth, Omo 1, Laetoli 18, Florisbad, Jebel Irhoud	Djebel Irhoud, Herto, Qafzeh, Skhul		
H. sapiens		Berg, Zulu		
K. platyops				
P. aethiopicus				
P. boisei				KNM-CH 1 (cast), KNM-CH 18, KNM-ER (802 (E, F), 816, 1171 (B, E, F, G, H), 1816, 1818, 1820, 3230, 5431, 6080, 6128, 15930, 17760, 25520), OH 5 (cast), KNM-WT 17400, Peninj
P. robustus				KB 5223, SK (1-3, 5, 6, 11, 13, 15, 23-25, 29, 30, 33, 34, 37, 40, 42, 44, 47-49, 52, 55a, 57, 61, 63, 65, 65a, 67-69, 72, 73, 81, 83, 85a, 87, 89, 93, 94, 98, 104, 821-823, 826a, 829, 831, 834, 837, 838a, 843, 846a, 857, 867, 1587, 1588, 3974, 3976, 14000, 14001), SKW (5, 8, 10, 12, 14, 33, 831a, 3068, 4767, 4769, 4772), SKX (162, 240, 241, 242, 265, 271, 308, 311, 1016, 3300, 3355, 3601, 4446, 5007, 5013, 5023, 6013, 7781, 19031, 19892, 25296, 27524, 28724), TM (1517a, 1517b, 1536, 1600, 1601)
S. tchadensis				
G. gorilla				Not reported
P. troglodytes				

	Kimbel et al. (2004)	Lordkipanidze et al. (2013)	Martinon-Torrez et al. (2007)
Ar. ramidus			
Au. anamensis			
Au. afarensis	AL (58-22, 162-28, 166-9, 288-1, 333-1, 333-45, 333-84, 417-1d, 439-1, 444-2), KNM-ER 2602		Specimens from Laetoli, Hadar, Fejej, Maka
Au. africanus	Sts (5, 52, 71), Stw (53, 505), MLD (1, 6, 37/38), TM 1511		Specimens from Sterkfontein, Makapansgat, Gladysvale
Au. garhi			
Au. sediba			
H. antecessor			Atapuerca Gran Dolina
H. ergaster	KNM-ER 3733, SK 847	KNM-ER (3733, 3883, 42700), KNM-WT 15000	Specimens from Olduvai Gorge. Koobi Fora
H. erectus	Zhoukoudian	Ngandong (5, 7, 12, 14), Ngawi 1, Sambungmachan (3, 4), Sangiran (2, 4, 17), Zhoukoudian (III, X, XI, XII)	Specimens from Sangiran Dome, Trinil, Zhoukoudian
Dmanisi		D (2280, 2282, 2700, 3444, 4500)	Dmanisi
H. floresiensis			
H. habilis	OH (7, 13, 24), KNM-ER (1805, 1813)	KNM-ER (1805, 1813, 42703), OH 24, SK 847, Stw 53	Specimens from Olduvai Gorge, Koobi Fora
H. heidelbergensis			Rabat, Tighenif, Mauer, Arago, Mountmarin, Pontnewydd, Steinheim
H. neanderthalensis			Saccopastore, Monte Circeo, Le Moustier, Saint Cesaire, Cabezo Gordo, Zafarraya, L'Hortus, Krapina, Sidron, Kebara, Tabun, Vindija, Kulna 1, Pinilla del Valle, Engis II, La Quina, Shanidar, Gibraltar, Petit-Puymoyen, Fondo Cattie

H. rudolfensis	KNM-ER (1470, 1590, 3732)	KNM-ER (1470, 62000), OH 65	
fossil *H. sapiens*			San Nicolas, Brassempouy. Wad, Almonda, Mladec, Abri Pataud, Trou Magritte, Dolni Vestonice, Pavlov, Caldeirao, Skhul, Predmosti
H. sapiens			
K. platyops			
P. aethiopicus	KNM-WT 17000		
P. boisei	OH 5, KNM-CH 304, KNM-ER (406, 407, 732, 13750, 23000)		
P. robustus	SK (12, 48), TM 1517		
S. tchadensis			
G. gorilla	Not reported		
P. troglodytes	Not reported		

	Mounier et al. (2009)	Strait & Grine (2004)	Zeitoun (2009)
Ar. ramidus		ARA-VP (6/1, 1/128, 1/500), KNM-TH 13150, KNM-LT 329	
Au. anamensis		KNM-KP (29181, 29283, 29286)	
Au. afarensis		AL (129-23, 145-35, 162-28, 188-1, 198-1, 199-1, 200-1, 207-13, 266-1, 277-1, 288-1, 311-1, 33-125, 333-1, 333-105, 333-2, 333-45, 333w-12, 333w-60, 400-1a, 417-1, 444-2, 58-22), Garusi 1, LH 4, MAK-VP 1/12	
Au. africanus		MLD (1, 2, 6, 9, 12, 22, 29, 34, 37/38, 40, 45), Sts (5, 7, 17, 20, 26, 36, 52a, 52b, 67, 71), Stw (13, 73, 252, 384, 404, 498, 505, 513), Taung 1, TM (1511, 1512)	Sts 5
Au. garhi		BOU-VP 12/130	
Au. sediba			
H. antecessor	ATD6-96		
H. ergaster	KNM-ER 992	KNM-ER (730, 820, 992, 1507, 3733, 3883), KNM-WT 15000	KNM-ER (3733, 3883), KNM-WT 15000, OH 9
H. erectus	Sangiran (1b, 9, 22), KNM-ER 992, Tighenif (1, 2, 3), Sinanthropus (G1, G2, H1)		Maba, Ngandong (1-3, 5-7, 10, 11, 12), Ngawi, Sambungmachan 1, Sangiran (2-4, 10, 12, 17, 26, 38), Sinanthropus (III, X, XI, XII), Trinil 2
Dmanisi	D (211, 2600)		
H. floresiensis			
H. habilis		AL 666-1, L 894-1, KNM-ER (1478, 1501, 1502, 1805, 1813, 3735), SK (15, 27, 45, 847), Sts 19, Stw 53	KNM-ER1813

H. heidelbergensis	Tighenif (1, 2, 3), Mauer, AT (888, 950), Arago (II, XIII), Montmaurin, Ehringsdorf F		Saldanha 1, Kabwe 1, Ndutu 1, Bodo 1, Sale 1, Narmada, Zuttiyeh Arago (XXI, XLVII), Swanscombe, Petralona 1, Dali
H. neanderthalensis	Krapina (J, H, G), La Ferrassie 1, La Quina H5, Regourdou, Banolas, Spy 1, Amud 1, Shanidar I, Zafarraya		Amud 1, La Chapelle-aux-Saints, La Ferassie 1, Gibraltar, Monte Circeo 1, La Quina H5, Shanidar 5, Spy 1
H. rudolfensis		KNM-ER (819, 1470, 1482, 1483, 1590, 1801, 1802, 3732, 3891) UR 501	KNM-ER 1470
fossil *H. sapiens*	Qafzeh 9, Skhul V, Cro-Magnon 1, Abri Pataud 1, Ohalo II		Eliye Springs 1, LH 18, Omo 2, Jebel Irhoud 1, Skhul V, WHL 50
H. sapiens	Loisy, Sahara		30 Dayak skulls
K. platyops		KNM-WT (38350, 40000)	
P. aethiopicus		KNM-WT (16005, 17000), L (55s-33, 338y-6, 860-2), Omo (18-1967-18, 44-1970-2466, 57-4-1968-41)	
P. boisei		OH 5, KGA (10-506, 10-525), KNM-CH 1, KNM-ER (403-407, 725, 727,-729, 732, 733, 801, 805, 810, 818, 1468, 1469, 1483, 1803, 1806, 3229, 3230, 3729, 3954, 5429, 5877, 13750, 15930, 23000), KNM-WT (16841, 17400), L (7a-125, 74a-21), Natron, Omo 323-896	KNM-ER 406
P. robustus		DNH 7, SK (6, 12, 13/14, 23, 34, 46-49, 52, 55, 65, 79, 83, 848, 1586), SKW (5, 8, 11, 29, 2581), SKX (265, 4446, 5013), TM 1517	
S. tchadensis		TM 266-01-060-1	
G. gorilla		Not reported	11 adults
P. troglodytes		Not reported	11 adults

Appendix C.

Supplementary Material for Chapter 4

C1. List of characters, character definitions, and character states.

Table C1 List of craniodental characters used in this study.

The character definitions and the character state assessments are taken from the original studies wherever possible. It is indicated whether the character is treated as an ordered or unordered trait. The references from which the characters and state assessments are collected are as coded as follows: 1= Argue et al. (2009); 2=Berger et al. (2010); 3=Cameron and Groves (2004); 4=Cameron et al. (2004); 5= Chang (2005); 6= This study; 7=Gilbert (2008); 8=Kimbel et al. (2004); 9=Irish et al. (2013); 10=Lordkipanidze et al. (2013); 11=Martinon-Torres et al. (2008); 12=Mounier et al. (2009); 13= Strait and Grine (2004); 14=Zeitoun (2009).

	Characters	Definition	States	Source
1.	Cranial capacity	Cranial capacity in cubic centimeters. (Small<500; Intermediate=500-680; Medium=750-875; Large=900-1200; Very large>1300). (Ordered)	Small (0); Intermediate (1); Medium (2); Large (3); Very large (4)	2-4, 6, 7, 13
2.	Cerebellar morphology	The position of cerebellum relative to the cerebrum. (Unordered)	Lateral flare with posterior protrusion (0); Tucked (1)	3, 13
3.	Cranial vault thickness	The thickness of the cranial vault measured at parietal eminence. (Ordered)	Thin (0); Intermediate (1); Thick (2)	6-8, 10
4.	Calvarial height to breadth	The ratio of the calvarial height on the coronal plane of porion to the minimum breadth of cranial base, or the distance between the porial saddles. (Ordered)	Low (0); Very low (1); High (2)	8
5.	Cranial vault index	The index calculated as the cranial height divided by cranial length. (Low and long<0.62. Short and high>0.62). (Unordered)	Long low cranium (0); Short high cranium (1)	4, 7
6.	Height of calvaria relative to orbits	The portion of the calvarial height above the orbit expressed as a percentage of the total calvarial height. (Ordered)	Low (0); Moderate (1); High (2)	4, 6, 8
7.	Maximum cranial breadth	The location where maximum cranial breadth is measured. (Ordered)	Close to cranial base (0); Cranial base biparietal similar (1); At biparietal (2)	4

8.	Cranial contour in norma occipitalis	The cranial contour in norma occipitalis. (Unordered)	Low and broad (0); en bombe (1); en maison (2)	5
9.	Anterior calvarial contour in profile	The contour of the anterior calvarium. (Unordered)	Deviates from circle (0); Aligned with circle (1)	8
10.	Posterior calvarial contour	The curvature of the posterior portion of the cranial vault along the midsagittal cross-section. (Unordered)	Aligned with circle (0); Deviates from circle (1)	8
11.	Parietal wall verticality	The superior convergence of lateral parietal walls in posterior view. (Unordered)	Present (0); Absent (1)	6, 7
12.	Postbregmatic depression	The presence of a depression posterior to the bregma. (Unordered)	Absent (0); Present (1)	6
13.	Parietal tuber	The presence of a parietal tuber or eminence. (Unordered)	Absent (0); Present (1)	1, 2, 6, 13, 14
14.	Sagittal crest	The presence of a sagittal crest. (Unordered)	Present (0); Absent (1)	3, 13, 14
15.	Sagittal keel	The presence of a sagittal keel. (Unordered)	Absent (0); Present (1)	1, 4-7, 10, 14
16.	Parietal overlap of occipital at asterion	The presence of an overlap of temporal, parietal and occipital bones at asterion. (Unordered)	Absent (0); Present (1)	3, 13
17.	Upper facial breadth	The index of bi-frontomalare temporale divided by orbital height. (Ordered)	Narrow (0); Intermediate (1); Broad (2); Extremely broad (3)	3, 8
18.	Outline of superior facial mask	The bi-maxillary tubercle width relative to bi-frontomalare-temporale width. (Unordered)	Tapered (0); Squared (1)	2, 3, 10
19.	Lateral anterior facial contour	The facial contour in lateral view. (Unordered)	Bipartite (0); Straight (1)	2
20.	Facial prognathism	The proportion of the palate anterior to sellion. (Index > 57= prognathic, Index between 30-57 = mesognathic, Index <30 = orthognathic). (Ordered)	Prognathic (0); Mesognathic (1); Orthognathic (2)	2, 3, 8, 13
21.	Facial hafting	The position of the face relative to the neurocranium, assessed by comparing the position of the supraorbital relative to the bregma. (Unordered)	Low (0); High (1)	2, 3, 13

22.	Anterior projection of zygomatic bone relative to piriform aperture (dishing)	The position of the infraorbital plate of the zygoma relative to the piriform aperture. (Ordered)	Posterior (0); Intermediate (1); Anterior (2)	2, 3, 13
23.	Bregmatic protuberance	The presence of a brebmatic protuberance. (Unordered)	Absent (0); Present (1)	14
24.	Precoronal depression	The presence of a precoronal depression. (Unordered)	Absent (0); Precoronal plane present (1); Precoronal depression present (2)	14
25.	Coronal reinforcement	The thickness of the frontal at and along the coronal suture. (Unordered)	Absent (0); Present at upper part of squama (1); Present and continues laterally (2)	14
26.	Frontal contour in norma verticalis	The contour of the frontal bone in superior view. (Unordered)	Linear (0); Convex (1)	1, 14
27.	Frontal eminence	The presence of a frontal eminence. (Unordered)	Absent (0); Present (1)	4, 6, 7, 14
28.	Glabellar depression	The presence of a depression at the glabella. (Unordered)	Absent (0); Present (1)	1, 3, 14
29.	Glabellar development	The development of the glabella. (Unordered)	Weak (0); Prominent (1)	4, 7, 10, 13, 14
30.	Glabellar region forms as prominent block	Does the glabellar region form a prominent block. (Unordered)	Not a block (0); Block (1)	2
31.	Supraglabellar tubercle	The presence of a supraglabellar tubercle at the junction of postorbital sulcus and the frontal squama. (Unordered)	Absent (0); Present (1)	14
32.	Microdepression of glabella	The presence of a small glabellary depression, associated with large glabellar projection. (Unordered)	Absent (0); Present (1)	14
33.	Metopic keel	The presence of a metopic keel. (Unordered)	Absent (0); Present (1)	1, 5, 6, 7, 10, 14
34.	Lateral postorbital depression	The presence of postorbital depression. (Unordered)	Absent (0); Present (1)	14
35.	Frontotemporale tubercle	The presence of a tubercle at the fronto-temporal junction. (Unordered)	Absent (0); Present (1)	14
36.	Frontal trigone	The presence of a frontal trigone. (Unordered)	Present (0); Absent (1)	2

37.	Supratrigonal depression	The presence of very small depressions on the medial edges of the posterior part of temporal lines. (Unordered)	Absent (0); Present (1)	14
38.	Frontal sinus	The presence of frontal sinus. (Unordered)	Absent (0); Present (1)	3, 13
39.	Supraorbital sulcus	The presence of a supraorbital sulcus. (Unordered)	Present (0); Absent (1)	1, 3, 4, 6, 8, 10, 14
40.	Supraorbital torus thickness	The index to calculate the thickness of the torus at its midpoint. The thickness at midpoint is divided by orbital height. (Thin<0.15; Intermediate=0.15-0.29; Thick>0.29). (Ordered)	Thick (0); Intermediate (1); Reduced (2)	3, 4, 6, 7, 10
41.	Supraorbital thickness gradient	The thickness gradient of the orbital arch comparing medial and lateral thicknesses. (Unordered)	Medial to lateral (0); Lateral to medial (1)	1, 6, 8, 14
42.	Supraorbital torus development	The development of supraortibal torus. (Ordered)	Torus (0); Intermediate (1); Weak (2)	1-6, 8, 13, 14
43.	Supraorbital contour	The contour of the supraorbital region. (Unordered)	Less arched (0); Arched (1)	1, 2, 4-7, 13, 14
44.	Superior orbital fissure shape	The shape of superior orbital fissure. (Unordered)	Foramen (0); Comma shaped (1)	3, 8, 13
45.	Supraorbital corner shape	The angularity of the superolateral corner of the orbit. (Unordered)	Angled (0); Rounded (1)	1, 6, 8
46.	Temporal crest on supraorbital torus	The position of the anterior portion of the temporal line relative to the supraorbital torus. (Unordered)	Superior (0); Posterior (1)	6
47.	Lacrimal fossae location	The location of lacrimal fossa relative to the inferior orbital margin. (Unordered)	Within orbit (0); Within infraorbital region (1)	3
48.	Ethmolacrimal contact	The length of ethmoid-lacrymal contact. (Unordered)	100 (0); Variable (1)	13
49.	Interorbital breadth	The distance between the orbits, calculated as an index relative to the orbit's breadth. (Unordered)	Narrow (0); Broad (1)	3, 7, 8
50.	Orbital shape	The shape of the orbits evaluated by height vs breadth measurements. (Unordered)	Oval (0); Circular (1); Rectangular (2)	3, 4

51.	Inferior orbital margin position relative to nasal margin	The horizontal position of the inferior orbital margins against the superior nasal aperture margin viewed anteriorly. (Ordered)	Well above superior nasal margin (0); Close to superior nasal margin (1); Well below superior nasal margin (2)	3
52.	Inferior orbital margin rounded laterally	The morphology of inferior margin of the orbit as being either rounded laterally or not rounded. (Unordered)	No (0); Yes (1)	1-3, 13
53.	Infraorbital foramen location	The ratio of the distances between orbitale and the foramen, and orbitale and the root of the zygoma. (Unordered)	High (0); Low (1)	2, 3, 13
54.	Nasal keel	The presence of a distinct vertical "pinching" of the nasal bones along its midline. (Unordered)	Present (0); Absent (1)	1, 3
55.	Projection of nasal bones above frontomaxillary suture	The projection of nasal bones above frontomaxillary suture. (Unordered)	Tapered (0); Expanded (1); Not projected (2)	2, 3, 13
56.	Eversion of superior nasal aperture margin	The degree of superior nasal aperture margin eversion. (Unordered)	None (0); Slight (1)	2
57.	Profile of nasal saddle and nasal roof	The contour of nasal saddle and nasal roof. (Unordered)	Flat (0); Small curve (1); Well defined curve (2); Deep angled (3)	1
58.	Nasal cavity entrance	The contour of the nasal cavity entrance. (Unordered)	Stepped (0); Smooth (1)	1-3, 5, 8, 13
59.	Inferior width of projecting nasal bone	The inferior width of projecting nasal bone. (Unordered)	Narrow (0); Wide (1); Not projecting (2)	2
60.	Anterior nasal spine relative to nasal aperture	The development of anterior nasal spine relative to nasal aperture. (Ordered)	Absent (0); Anterior (1); Enlarged (2); Posterior (3)	2

61.	Nasal margin crest/spine patterns	The development of nasal margin crest or spine. (Unordered)	Lateral crest (0); Lateral turbinal and spinal crests (1); Fused spinal and turbinal crests and lateral crest (2); Fused lateral and spinal crests and turbinial crest (3); Fused lateral and spinal crests and partial fusion of spinal and turbinal (4); No crests (5)	5
62.	Nasal aperture margin sharpness	The sharpness of the nasal aperture margin. (Unordered)	Sharp (0); Dull (1)	2, 8
63.	Subnasal projection	The inclination of the nasoalveolar clivus measured relative to the occlusal plane. (Weak<100; Moderate=100-150; Marked>150). (Ordered)	Low (0); Intermediate (1); High (2)	2, 3, 8, 10
64.	Subnasal length	The chord distance from nasospinale to prosthion. (Ordered)	Short (0); Intermediate (1); Long (2)	3
65.	Nasoalveolar clivus contour	The contour of nasoalveolar clivus in coronal plane. (Ordered)	Convex (0); Straight (1); Concave (2)	1-3, 6, 8, 10, 13
66.	Intermaxillary furrowing	The morphology of the midline of the maxillary bones. (Unordered)	Furrowed (0); Flat (1); Ridged (2)	6
67.	Protrusion of incisor alveoli beyond bicanine line in basal view	The position of the incisors relative to the canines in the coronal plane. (Unordered)	Beyond bicanine line (0); Within bicanine line (1)	2, 3, 6, 13
68.	External palate breadth	The index of external palate breadth at M2 divided by orbital height. (Ordered)	Broad (0); Intermediate (1); Narrow (2)	3, 8
69.	Palate shape	The maxillary-alveolar length divided by breadth at M2. (Unordered)	Longer than broad (0); Broader than long (1)	6
70.	Incisive canal development	The development of incisive canal. (Ordered)	Slight canal (0); Intermediate (1); Extensive canal (2)	3
71.	Palate thickness	The thickness of the palate posterior to the incisive fossa. (Thick>7 mm; Thin<7 mm) (Unordered)	Thin (0); Thick (1)	3, 13

72.	Incisive foramen position	The position of incisive foramen along tooth row. (Ordered)	Canine (0); P3 (1); P4 (2)	1, 6, 10
73.	Anterior palate depth	The depth of anterior palate. (Unordered)	Shallow (0); Deep (1)	2, 3, 6, 8, 10, 13
74.	Palatine process orientation	The orientation of the posterosuperior slope of the palatal plane distal to the canine. (Unordered)	Nearly horizontal (0); Steep posterior angle (1)	8
75.	Canine jugum development	The development of canine jugum. (Ordered)	Weak (0); Moderate (1); Marked (2)	1, 2, 6, 10
76.	Canine root orientation	The orientation of the canine root relative to parasagittal plane. (Unordered)	Inclined (0); Parallel (1)	10
77.	Anterior pillars	The presence of anterior pillars. (Unordered)	Absent (0); Present (1)	2, 3, 6, 13
78.	Canine fossa, groove or fossula.	The presence of a canine fossa, canine groove or canine fossula. (Unordered)	Absent (0); Present (1)	2, 3, 5, 6, 8
79.	Maxillary trigone	The presence of maxillary trigone, a gutter-like triangular depression in the infraorbital region. (Unordered)	Absent (0); Present (1)	2, 3, 8, 13
80.	Maxillary sinus size	The size of maxillary sinus. (Unordered)	Intermediate (0); Large (1)	3
81.	Maxillary sinus division	The position of the main division of the maxillary sinus floor. (Unordered)	Posterior (0); Anterior (1)	8
82.	Infraorbital plate orientation	The orientation of the infraorbital plate, measured by the position of the inferior margin of the infraorbital region, which is demarcated by the zygomaticoalveolar crest relative to the coronal plane of the orbit. (Unordered)	Sloped (0); Vertical (1); Lateral (2)	2, 5, 8
83.	Sulcus infraorbitalis	The width of an infraorbital sulcus. (Unordered)	Absent (0); Narrow (1); Wide (2)	1
84.	Position of infraorbital foramen relative to orbit	The position of the infraorbital foramen relative to the zygomaxillary suture. (Unordered)	Foramen beneath middle third of orbital breadth (0); Foramen beneath medial third of orbital breadth (1)	13
85.	Patency of premaxillary suture in adults from frontal view	The presence of premaxillary suture in adults. (Unordered)	Patent (0); Obliterated (1); Trace (2)	2, 13
86.	Anterior zygomatic root position	The position of the anterior zygomatic root along tooth row. (Ordered)	P3-P4 (0); P4-M1 (1); M1 (2); M1-M2 (3)	3, 6, 10

87.	Zygomaticoalveolar crest	The curvature of the zygomaticoalveolar crest. (Unordered)	Straight (0); Curved (1)	1, 2, 10
88.	Malar diagonal length	The index of orbitale-zygomaxillare divided by orbital height. (Ordered)	Long (0); Intermediate (1); Short (2)	3
89.	Malar orientation	The orientation of the anterior malar surface relative to Frankfurt Horizontal (Ordered)	Posteriorly inclined (0); Vertical (1); Anteriorly inclined (2)	3, 10
90.	Zygomatic insertion height	The insertion of the zygomaticoalveolar crest onto the alveolar border. (Unordered)	Low (0); High (1)	3
91.	Position of zygomatic foramina	The position of the zytomatic foramina relative to the plane of the orbital rim. (Unordered)	At or below plane of orbital rim (0); Above plane of orbital rim (1)	13
92.	Zygomatic bone orientation	The orientation of the zygomatic bone relative to the frontal. (Ordered)	Frontal (0); Frontolateral (1); Lateral (2)	13
93.	Mediolateral thickness of zygomatic arch at root of frontal process	The thickness of the zygomatic arch. (Thick>8mm; Thin<8 mm) (Unordered)	Thin (0); Thick (1)	2, 13
94.	Expansion of medial edge of frontal process of zygomatic bone	The presence of a lateral flair of the frontal process of the zygomatic. (Unordered)	Vertical (0); Laterally divergent (1)	2, 6, 8
95.	Angular indentation of lateral orbital margin	The curvature of the lateral orbital margin. (Unordered)	Indented (0); Curved (1)	2
96.	Masseter origin height	The index of zygomaticoalveolar height relative to orbitoalveolar height. (Unordered)	Low (0); High (1)	2, 3, 8, 13
97.	Masseteric position relative to sellion	The distance from the articular eminence to the zygomatic tubercle expressed as a percentage of the horizontal distance between the articular eminence and sellion. (Unordered)	Anterior (0); Posterior (1)	2, 8, 13
98.	Zygomatic temporal surface	The thickness of the body of the zygomatic bone. "Deeply excavated" surface is thinner in the centre of the body. (Unordered)	Flat (0); Deeply excavated (1)	6, 8
99.	Zygomatic prominence development	The development of the zygomatic prominence. (Unordered)	Prominent (0); Slight (1)	2

100.	Zygomaticomaxillary steps to fossae present	The presence of zygomaticomaxillary steps to fossae. (Unordered)	Absent (0); Present (1)	2
101.	Position of zygomatic angle	The position of the angle formed between the frontal and temporal processes of the zygomatic relative to the inferior orbital margin. (Ordered)	Below orbit (0); At orbit (1); Above orbit (2)	2, 6, 8
102.	Lateral flaring of zygomatic arches	The development of the lateral flaring of zygomatic arches. (Unordered)	Marked (0); Slight (1)	8
103.	Zygomatic arch alignment	The outline of the zygomatic arch from the superior view. This character refers to the orientation of the zygomatic arch at midpoint; whether it is parallel to the sagittal plane or not. (Unordered)	Sagittal (0); Deviant (1)	2, 6
104.	Zygomatic process root	The number of planes at the root of the zygomatic process. The surface of the zygomatic process root lateral to the articular tubercle is divided into two surfaces by a very strong ridge that extends from the lateral edge of the articular tubercle. (Unordered)	Undivided (0); Divided (1)	8
105.	Lateral expansion of the root of zygomatic	The position of the most lateral part of the zygomatic process of the temporal bone. (Unordered)	Above EAM (0); Above mandibular fossa (1)	6
106.	Postorbital constriction	The index of minimum frontal breadth to superior facial breadth (bi-frontomalaretemporale). (Marked constriction<0.65; Moderate constriction=0.65-0.77; Slight constriction>0.77). (Ordered)	Marked (0); Moderate (1); Slight (2)	2-4, 6-8, 10, 13
107.	Temporal fossae size	The index of temporal fossa size divided by orbital area. (Ordered)	Large (0); Intermediate (1); Small (2)	3
108.	Supraglenoid gutter width	The maximum distance from the temporal squame at the anterior end of the root of the zygomatic process to the most lateral point at that location. (Wide>25mm; Narrow<25). (Unordered)	Narrow (0); Wide (1)	2, 3, 13
109.	Articular eminence position relative to occlusal plane	The perpendicular distance between the articular eminence and the occlusal plane, divided by the geometric mean (bi-entoglenoid breadth, bi-carotid breadth, FM length, basioccipital length). (Unordered)	High above plane (0); Near plane (1)	13

110.	Articular eminence summit	The position of the maximum convexity of articular eminence relative to the plane of the posterior edge of temporal foramen. (Unordered)	Posterior (0); Anterior (1)	8
111.	Articular eminence form	The angulation of the long axis of the articular eminence in basal view. (Unordered)	Single plane (0); Mediolateral twisted (1)	8
112.	Posterior slope of articular tubercle	The degree and the length of posterior portion of the articular tubercle on the zygomatic. (Ordered)	Short (0); More pronounced (1); Steep (2)	14
113.	Articular tubercle development	The development of the articular tubercle on the zygomatic. (Unordered)	Not developed (0); Developed (1)	14
114.	Articular tubercle projection	The projection of the articular tubercle. (Unordered)	Not or slightly projecting (0); Projecting (1)	1, 3, 6, 14
115.	Articular tubercle and sub-temporal plane continuity	The continuity of the articular tubercle with the subtemporal plane. (Unordered)	Continuous (0); Not continuous (1)	1, 14
116.	Articular tubercle anteroposterior curvature	The anteroposterior curvature of the articular tubercle in norma lateralis. (Unordered)	Flat (0); Large rounded profile (1); Small rounded profile (2)	1, 14
117.	Transverse concavity of articular tubercle	The concavity of the articular tubercle in norma frontalis. (Unordered)	Flat (0); Large rounded profile (1); Small rounded profile (2)	14
118.	Integration of entoglenoid formation with articular tubercle	The integration of the entoglenoid process or spine with articular tubercle. (Unordered)	Not integrated (0); Integrated (1)	14
119.	Ectoglenoid crest	The presence of ectoglenoid crest. (Unordered)	Absent (0); Present (1)	14
120.	Width between the tympanic plate and entoglenoid process	The width between tympanic plate and entoglenoid process. (Ordered)	Absent (0); Narrow (1); Wide (2)	1, 14
121.	Entoglenoid process position relative to anterior zygomatic tubercle or ectoglenoid process	The position of the entoglenoid process or spine in sagittal plane relative to the ectoglenoid process. (Ordered)	Same level (0); Posterior (1); Farther back (2)	1, 14
122.	Entoglenoid process projection	The projection of the entoglenoid process or spine. (Unordered)	Projecting (0); Not projecting (1)	1, 6, 14
123.	Subarcuate fossa depth	The depth of subarcuate fossa, which is a small triangular fossa or shallow area inferior to the arcuate eminence on temporal bone. (Ordered)	Deep (0); Moderately deep to shallow (1); Very shallow to absent (2)	13

124.	Preglenoid plane extent	The extent of the preglenoid planum. (Unordered)	Not stretched (0); Stretched (1)	1, 14
125.	Sphenoid contribution to mandibular fossa	The contribution of sphenoid to mandibular fossa. (Unordered)	Absent (0); Present (1)	5
126.	Contribution of tympanic plate to mandibular fossa	The contribution of the tympanic plate to the mandibular fossa. (Unordered)	None (0); Exclusive (1)	1, 14
127.	Orientation of anterior wall of TMJ	The orientation of the anterior wall of mandibular fossa. (Ordered)	Horizontal (0); Oblique (1); Vertical (2)	1, 14
128.	Tubercle on anterior wall of TMJ	The presence of a tubercle on the anterior wall of the mandibular fossa. (Unordered)	Absent (0); Present (1)	14
129.	Medial recess of mandibular fossa	The presence of a recess in the medial wall of the mandibular fossa. (Unordered)	Absent (0); Present (1)	5, 6
130.	Mandibular fossa length	The anteroposterior distance of mandibular fossa. (Unordered)	Narrow (0); Wide (1)	1, 3, 14
131.	Mandibular fossa depth	The index of mandibular fossa depth perpendicular to Frankfurt Horizontal (depth from the base of the articular eminence to the apex of the fossa, divided by the breadth of the eminence from the articular tubercle to the entoglenoid process). (Unordered)	Shallow (0); Deep (1)	3, 6-8, 10, 13, 14
132.	Mandibular fossa overhang	The proportion of the mandibular fossa that overhangs the external cranial vault. (Unordered)	<50% (0); ≥50% (1)	10
133.	Convexity of posterior wall of mandibular fossa	The curvature on the posterior wall of the mandibular fossa. (Unordered)	Flat or concave (0); Convex (1)	14
134.	Mandibular fossa position	The position of the mandibular fossa relative to the temporal squama. (Unordered)	Lateral (0); Medial (1)	6
135.	Postglenoid process shape in norma frontalis	The shape of the postglenoid process in norma frontalis. (Unordered)	Rectangular (0); Round (1); Flat (2)	14
136.	Postglenoid and tympanic fusion	The fusion of the tympanic element and the postglenoid process in coronal plane. (Unordered)	Fused (0); Unfused (1)	3, 6, 8, 13
137.	Postglenoid process size	The size of postglenoid process. (Ordered)	Large (0); Medium (1); Small (2)	1, 3, 6-8, 13, 14

138.	Postglenoid process extent relative to the tympanic	The extent of the postglenoid process relative to the tympanic. (Unordered)	No overlap (0); Overlaps (1); Rudimentary or no postglenoid process (2)	1
139.	Vaginal process size	The size of the vaginal process of tympanic. (Unordered)	Small or absent (0); Moderate to large (1)	3, 6, 8, 13
140.	Styloid process fusion	The presence of styloid process. (Unordered)	Unfused (0); Fused (1)	5, 7
141.	Petrous apex ossified beyond spheno-occipital synchondrosis	The degree of ossification of the petrous apex. (Unordered)	Not ossified (0); Ossified with projection (1)	13
142.	Petrous orientation	The orientation of the petrous. The angle is measured relative to the bitympanic line. (Coronal<50˚; Intermediate=50-60˚; Sagittal>60˚). (Ordered)	Sagittal (0); Intermediate (1); Coronal (2)	3, 5, 6, 7, 10, 13
143.	Crista petrosa development	The development of crista petrosa, a sharp lower margin of the tympanic plate that bounds a single anteriorly directed face. (Unordered)	Absent or weak (0); Moderate to strong (1)	6, 8
144.	Tympanic shape	The shape of the tympanic canal and the orientation of the anterior tympanic plate. (Unordered)	Tubular (0); Plate-like (1)	3, 6, 8, 10, 13
145.	Tympanic trough	The presence of a tympanic trough. (Unordered)	Absent (0); Present (1)	1
146.	Tympanic plate thickness	The thickness of the tympanic plate around the external auditory meatus. (Thick>2mm; Thin<2mm). (Unordered)	Thin (0); Thick (1)	1, 14
147.	Lateral tympanic extension	The degree of tympanic extension laterally relative to the location of the porion saddle. (Unordered)	Medial to saddle (0); Lateral to saddle (1)	8
148.	Tegmen tympani	The presence of tegmen tympani on the roof of the tympanic cavity. (Unordered)	Absent (0); Present (1)	14
149.	Middle ear depth	The depth of middle ear. (Deep>8.5mm; Shallow<8.5mm). (Unordered)	Shallow (0); Deep (1)	13
150.	Axis of ear bones	The angle of the axis of ear bones. (Unordered)	Right angle or more (0); Acute angle (1)	13
151.	Area of inner ear	The area of inner ear. (Low<50mm^2; Higher>50 mm^2) (Unordered)	Low (0); Higher (1)	13

152.	Mediolateral position of external auditory meatus	The mediolateral position of the inferolateral tip of the tympanic relative to porion. (Unordered)	Medial (0); Lateral (1)	3, 6, 8, 13
153.	External auditory meatus size	The size of external auditory meatus. (Unordered)	Small (0); Large (1)	3, 6, 13
154.	Tubercle behind external auditory meatus	The presence of a tubercle below the external auditory meatus where the mastoid crest branches downwards. (Unordered)	Absent (0); Present (1)	14
155.	Orientation of the long axis of external auditory meatus	The orientation of the axis of the external auditory meatus. (Unordered)	Oblique (0); Vertical (1)	14
156.	Suprameatal spine	The presence of a suprameatal spine/crest. (Unordered)	Absent (0); Present (1)	6, 14
157.	Eustachian process of tympanic	The development of the eustacian process of tympanic. (Unordered)	Present and prominent (0); Absent or slight (1)	3, 6, 13
158.	Mastoid fissure	The presence of a mastoid fissure, which occurs when the tympanic is not fused to the anterior face of the mastoid process. (Unordered)	Absent (0); Present (1)	1, 5, 14
159.	Squamotympanic fissure	The presence of squamotympanic fissure. (Unordered)	Absent (0); Present (1)	1, 14
160.	Squamotympanic fissure depth	The depth of squamotympanic fissure. (Unordered)	Shallow (0); Deep (1)	14
161.	Maximum lateral projection of mastoid	The position of the lateral-most point of the mastoid process on the temporal viewed posteriorly. (Unordered)	High (0); Low (1)	8
162.	Mastoid process lateral inflation	The extent of inflation of mastoid process. "Not inflated" process extends up to but not beyond the supramastoid crest; "Inflated" process extends lateral to the supramastoid crest. (Unordered)	Not inflated (0); Inflated (1)	3, 6, 13
163.	Mastoid process size	The size of mastoid process. (Unordered)	Small (0); Large (1)	4, 5, 6, 10, 14
164.	Mastoid process orientation	The orientation of the mastoid process in coronal plane. (Unordered)	Not medial (0); Medial (1)	14
165.	Mastoid tip position	The position of the tip of the mastoid process relative to porion measured as the mastoid tip position index, which is a percentage of the horizontal distance between the tip of mastoid to porion and asterion to porion. (Unordered)	Anterior (0); Posterior (1)	8

166.	Mastoid face	The contact between mastoid process and the peripheral bony structures. (Unordered)	Single postero-lateral (0); Discrete posterior and lateral (1); Single lateral (2)	8
167.	Supramastoid crest development	The development of supramastoid crest at porion. (Unordered)	Weak (0); Marked (1)	1, 6, 7, 10, 14
168.	Supramastoid crest and zygomatic process contact	The continuity of supramastoid crest with the zygomatic process. (Unordered)	Not continuous (0); Continuous (1)	14
169.	Supramastoid crest and lower temporal line continuity	The continuity of supramastoid crest with the lower temporal line. (Unordered)	Not continuous (0); Continuous (1)	1, 14
170.	Supramastoid sulcus closes anteriorly	The continuity of supramastoid crest and mastoid crest. (Unordered)	Absent (0); Present (1)	14
171.	Supramastoid sulcus width	The width between mastoid crest and supramastoid crest. (Ordered)	Absent (0); Narrow (1); Wide (2)	14
172.	Tubercle above the supramastoid process	The presence of a tubercle anterior to supramastoid crest. (Unordered)	Absent (0); Present (1)	1, 14
173.	Tubercle on supramastoid crest	The presence of a tubercle on the posterior portion of the supramastoid crest. (Unordered)	Absent (0); Present (1)	5, 14
174.	Mastoid crest projection	The projection of mastoid crest. (Unordered)	Weak (0); Strong (1)	1, 6, 14
175.	Mastoid crest and upper temporal line contact	The continuity of mastoid crest with upper temporal line. (Unordered)	Not continuous (0); Continuous (1)	14
176.	Mastoid crest and supramastoid crest orientation	The orientation of the anterior portion of the mastoid and supramastoid crests. (Unordered)	Divergent anteriorly (0); Parallel (1)	1, 4, 6, 14
177.	Juxtamastoid eminence	The presence of a juxtamastoid crest. (Unordered)	Absent (0); Present (1)	1, 4, 6, 7, 14
178.	Digastric fossa depth	The depth of digastric fossa. (Unordered)	Shallow (0); Deep (1)	1, 3, 6, 13, 14
179.	Digastric fossa length	The length of digastric fossa. (Unordered)	Short (0); Long (1)	8, 14
180.	Digastric fossa width	The width of digastric fossa. (Unordered)	Narrow (0); Wide (1)	3, 6, 13, 14
181.	Digastric fossa cross-section shape	The transverse cross-sectional shape of digastric fossa. (Unordered)	Round (0); U-shaped (1); V-shaped (2)	14
182.	Digastric groove morphology	The morphology of digastric groove located medially and posterior to the mastoid process. (Unordered)	Bridged (0); Not bridged (1)	5

183.	Angular torus	The presence of an angular torus. (Unordered)	Absent (0); Present (1)	4-7, 14
184.	Pneumatization of temporal squama	The extent of the pneumatic tracts relative to the squamosal suture. "Extensive" if pneumatization extends beyond squamosal suture producing squamous antrum. Otherwise, "Reduced". (Unordered)	Extensive (0); Reduced (1)	2, 3, 8, 13
185.	Temporal squama height	The height of the temporal squama on the vault. (Unordered)	High (0); Low (1)	5, 6-8, 14
186.	Temporal squama shape	The shape of the temporal squama on the vault. (Unordered)	Polygonal (0); Triangular (1)	1, 14
187.	Anterior contour of temporal squama	The curvature of the anterior edge of the temporal squama. (Unordered)	Rounded (0); Rectilinear (1)	14
188.	Superior contour of temporal squama	The curvature of the superior edge of the temporal squama. (Unordered)	Rounded (0); Rectilinear (1)	5-8, 14
189.	Posterior contour of temporal squama	The contour of the posterior temporal squama of the facies temporalis in the asterionic region. (Unordered)	Flattened (0); Vertical (1)	8
190.	Squamosal suture overlap extensive, at least in males	The superior and posterosuperior aspects of the squamosal suture. (Unordered)	Not extensive (0); Extensive (1)	3, 8, 13
191.	Anteromedial incursion of the superior temporal lines	The course of the superior temporal line between frontomalaretemporale and the point of maximum inflection on the line as it turns from being medially directed to posteriorly directed. (Ordered)	Weak (0); Moderate (1); Strong (2)	2, 3, 6, 13, 14
192.	Position of temporal emphasis	The location of the most strongly expressed part of the temporal lines. (Ordered)	Posterior (0); Intermediate 1 (1); Intermediate 2 (2); Anterior (3)	8
193.	Temporal line projection	The development of the temporal band. (Unordered)	Slight (0); Marked projection (1)	1, 14
194.	Depression beneath the upper temporal line	The presence of a depression on the superior temporal line in the posterior half of the parietal. (Unordered)	Absent (0); Present (1)	14
195.	Position of temporal lines on parietal bones	The width between the temporal lines in superior view. (Unordered)	Crest (0); Wide (1)	2
196.	Depression between temporal lines	The presence of a depression between the temporal lines in the posterior half of the parietal. (Unordered)	Absent (0); Present (1)	14
197.	Temporal band width in lateral view	The width between the temporal lines on in lateral view. (Unordered)	Narrow (0); Wide (1)	14

198.	Temporal band projection	The width of the temporal band on the parietal bone. The position, relief and the existence of a stephanion disconnection of the space between temporal lines. (Ordered)	Lines absent or weak (0); Lines visible but not protruding (1); Lines protruding (2)	14
199.	Temporal line position	The position of temporal lines on the parietal. (Unordered)	High (0); Low (1)	2, 14
200.	Parietomastoid angle development	The angle at parietomastoid. (Unordered)	Strong (0); Weak (1)	13
201.	Prelambdoidal depression	The presence of a prelambdoidal depression. (Unordered)	Absent (0); Present (1)	1, 6, 14
202.	Projection on lambdoid suture (processus asteriacus)	The presence of an asteriacus process, which is an elevation limited to the inferior segment of the upper temporal line of the parietal. (Unordered)	Absent (0); Present (1)	14
203.	Asterionic notch	The presence of an asterionic notch. (Unordered)	Absent (0); Present (1)	3, 6, 13, 14
204.	Upper occipital squama curvature	The curvature of the upper occipital squama above the inion where superior nuchal lines merge in the medial sagittal plane. (Unordered)	Flat or slightly concave (0); Convex (1)	6, 14
205.	Occipital squama shape	The shape of the upper part of the occipital squama in norma occipitalis. (Unordered)	Pentagonal (0); Triangular (1)	14
206.	Nuchal plane inclination	The angle between the inion-opisthion chord and Frankfurt Horizontal. (Ordered)	Steep (0); Intermediate (1); Weak (2)	3, 8, 13
207.	Relative height of nuchal area	The anteroposterior height of the nuchal area of the cranial base relative to the bisupramastoid width. (Unordered)	High (0); Low (1)	6, 8
208.	Compound temporal nuchal crest in males	The presence of compound temporal nuchal crest in males. (Ordered)	Extensive (0); Partial (1); Absent (2)	2, 3, 6, 8, 13
209.	Nuchal crest emphasis	The location of the most projecting part of the nuchal crest. (Ordered)	Lateral (0); Medial (1); Absent (2)	8
210.	Occipital angulation	The angle formed between the lambda-inion chord and the inion-opisthion chord. (Ordered)	<100 (0); 100 to 110 (1); >110 (2)	7
211.	Lower occipital squama shape	The curvature of the lower occipital squama. (Unordered)	Convex (0); Flat or slightly concave (1)	6, 14

212.	Longus capitis insertion size	The size and orientation of the depression of longus capitis where visible and the degree of development of muscle markings. (Unordered)	Large (0); Small (1)	3, 13
213.	Occipital torus development	The development of the occipital torus. (Ordered)	Absent (0); Weak (1); Strong (2)	1, 5, 6, 7, 10, 14
214.	Expansion of occipital torus	The lateral extent of occipital torus. (Unordered)	Median (0); Transversal (1)	14
215.	Occipital plane length	The length of occipital plane relative to the nuchal plane. (Unordered)	Lengthened (0); Shortened (1)	1, 4, 7
216.	Occipital supratoral sulcus	The presence of occipital supratoral sulcus. (Unordered)	Absent (0); Present (1)	4, 14
217.	Lateral occipital depression on occipital sulcus	The presence of lateral depressions on occipital sulcus (Unordered)	Absent (0); Present (1)	14
218.	Occipital bun	The presence of an occipital bun. (Unordered)	Absent (0); Present (1)	5, 14
219.	Depression above external occipital protuberance.	The depression above external occipital protuberance. (Unordered)	Absent (0); Present (1)	14
220.	External occipital protuberance	The presence of external occipital protuberance formed by supreme nuchal lines. (Unordered)	Absent (0); Present (1)	5, 6, 14
221.	Tuberculum linearum on occipital	The presence of tuberculum linearum formed by the superior nuchal lines. (Unordered)	Absent (0); Present (1)	1, 6, 14
222.	External occipital crest	The presence of the external occpital crest. (Unordered)	Absent (0); Present (1)	6, 14
223.	Suprainiac fossa	The presence of a suprainiac fossa. (Unordered)	Absent (0); Present (1)	5, 14
224.	Walls of suprainiac fossa	The orientation of the lateral walls of the suprainiac fossa. (Ordered)	Convergent (0); Parallel (1); Divergent (2)	14
225.	Retromastoid process	The presence of a retromastoid process at the junction of the superior nuchal line and the secondary branch of the inferior nuchal line, between the inion and mastoid process. (Unordered)	Absent (0); Present (1)	14
226.	Occipitomastoid crest	The presence of an occipitomastoid crest. (Unordered)	Absent (0); Present (1)	1, 4, 6, 14
227.	Occipital torus and supramastoid crest contact	The continuity of the occipital torus with the supramastoid crest. (Unordered)	Not continuous (0); Continuous (1)	6, 14

228.	Occipital torus to mastoid crest contact	The continuity of the occipital torus with the mastoid crest. (Unordered)	Not continuous (0); Continuous (1)	14
229.	Occipital torus to upper temporal line contact	The continuity of the occipital torus with the upper temporal line. (Unordered)	Not continuous (0); Continuous (1)	14
230.	Inion location	The location of inion relative to the opisthocranion. (Unordered)	Below opisthocranion (0); At opisthocranion (1)	4
231.	Inion/endinion location	The location of inion on the external cranial surface and endinion on the endocranial surface. (Unordered)	Separate (0); Coincide (1)	4
232.	Occipitomarginal sinus frequency	The frequency of the presence of occipitomarginal sinus. (Ordered)	Low (0); Intermediate (1); High (2)	3, 6, 8, 13
233.	Foramen magnum shape	The shape of foramen magnum. (Unordered)	Oval (0); Heart (1)	3, 13
234.	Foramen magnum position	The position of foramen magnum relative to bi-tympanic line. (Ordered)	Posterior (0); At line (1); Anterior (2)	3, 8, 13
235.	Foramen magnum inclination	The angle between the basion-opisthion chord and Frankfurt Horizontal. (Ordered)	Posteriorly (0); Horizontal (1); Anteriorly (2)	3, 13
236.	Cranial base breadth	The index of bi-porion chord divided by orbital height chord. (Ordered)	Narrow (0); Intermediate (1); Broad (2)	3, 8
237.	Basioccipital length	The index of basion-sphenobasion length divided by cranial base geometric mean. (Ordered)	Long (0); Intermediate (1); Short (2)	3
238.	Ethmo-sphenoid contact	The frequency of contact between ethmoid and sphenoid bones. (Ordered)	Usually absent (0); Variable (1); Usually present (2); Present (3)	3, 13
239.	Cranial base flexion	The angle between Frankfurt Horizontal and the basion-hormion chord. The inclination of the basioccipital and basisphenoid measured externally. (Ordered)	Flat (0); Moderate (1); Flexed (2)	3, 10, 13
240.	Posterior base shape	The horizonal distance between the coronal plane of the mastoid crests and the most posterior part of the cranial base between the supramastoid crests. (Unordered)	Moderate (0); Squat (1); Elongate (2)	8

241.	Condylar canal	The presence of condylar canal on the skull base. (Unordered)	Absent or infrequent (0); Frequently present (1)	13
242.	Cerebellum position	The position of the cerebellum relative to the cerebrum. (Unordered)	Not tucked (0); Tucked (1)	3, 8, 13
243.	Anterior pole shape	The shape of the anterior poles of the frontal lobe as seen in the endocast. Strongly anteriorly tapered lobes are considered "beaked". (Unordered)	Rounded (0); Beaked (1)	8
244.	Enamel thickness	The relative thickness of enamel. (Ordered)	Thin (0); Thick (1); Hyperthick (2)	2, 3, 13
245.	Dental development rate	The differences in the calcification and eruption patterns of the permanent teeth in extant hominoids and fossil hominids. (Ordered)	Delayed (0); Intermediate (1); Accelerated (2)	13
246.	Cingulum expression	The presence of labial cingulum in lower canines and premolars. (Unordered)	Present (0); Absent (1)	13
247.	Sulcus obliqus development	The development of oblique sulcus. (Unordered)	Weak to moderate (0); Strong (1)	12
248.	Fovea posterior development	The development of fovea posterior. (Unordered)	Absent or weak (0); Well developed (1)	13
249.	Incisal reduction	The summed mediodistal means of the I1 and I2. (Ordered)	Not reduced (0); Moderate (1); Reduced (2)	3, 6, 13
250.	Maxillary incisor heteromorphy	The index of I1 area divided by I2 area. (Unordered)	Dissimilar (0); Similar (1)	3, 13
251.	Incisor procumbency	The orientation of incisors. (Unordered)	Procumbent (0); Vertical (1)	2
252.	Maxillary I2/C diastema	The presence of maxillary diastema. (Unordered)	Absent (0); Present (1)	2, 6
253.	Maxillary incisor-to postcanine ratio	The ratio of maxillary incisor-to-postcanine teeth. (Ordered)	Small (0); Moderate (1); Large (2)	2, 6
254.	Lingual crenulations of maxillary I1	The extent of enamel crenulations on the lingual surface of maxillary I1. (Unordered)	Absent (0); Marginal (1); Whole surface (2)	13
255.	Labial curvature of maxillary I1	The development of labial curvature of maxillary I1. (Ordered)	Trace (0); Weak (1); Moderate (2); Pronounced (3)	9
256.	Shovel on maxillary I1	The development of shovel-shaped maxillary I1. (Unordered)	Absent (0); Faint (1); Trace (2)	9

257.	Lingual median ridge on maxillary I1	The development of a lingual median ridge on maxillary I1. (Unordered)	Moderate (0); Weak (1)	2, 6
258.	Lingual cervical prominence on maxillary I1	The development of a lingual cervical prominence on maxillary I1. (Unordered)	Broad and uninflated (0); Narrow and inflated (1)	6
259.	Double shovel on maxillary I1	The presence of double shovel-shaped maxillary I1. (Unordered)	Absent (0); Faint (1)	9
260.	Shovel shape in maxillary I2	The shape of maxillary I2. (Unordered)	Classic (0); Triangular (1); Absent (2)	11
261.	Lingual MMR and DMR on maxillary I2	The orientation of the medial and distal ridges on the maxillary I2 and whether they merge on the cervical prominence. (Unordered)	Yes (0); No (1)	6
262.	Canine robusticity	The robusticity of the canines. (Unordered)	Slender (0); More robust (1)	3, 13
263.	Canine sexual dimorphism	Sexual dimorphism in canine size. (Unordered)	Hyper dimorphic (0); Strongly dimorphic (1); Moderately dimorphic (2); Monomorphic; small canines (3); Monomorphic; large canines (4)	6, 13
264.	Mandibular deciduous canine shape	The mesiodistal disposition of the apex, the height of mesial crown convexity and the height of the mesial end of the lingual cingulum. (Unordered)	Apex central, mesial convexity low (0); Apex mesial, mesial convexity high (1)	13
265.	Canine size reduction	The degree of canine reduction calibrated relative to *Pan* and *Gorilla*. Canine size and canine root dimensions compared to canines of extant African apes. (Ordered)	No (0); Somewhat (1); Very (2)	3, 6, 8, 13
266.	Extensive mesial groove on maxillary canine	The presence of a mesial groove on the upper canine that extends to the crown apex. (Unordered)	Yes (0); No (1)	6, 13
267.	Lingual ridge development on maxillary canine	The development of the lingual ridges on maxillary C. (Unordered)	Marked (0); Weak (1)	2, 6
268.	Bushman canine on maxillary canine	The presence of Bushman canine. (Unordered)	Absent (0); Present (1)	9

269.	Distal accessory ridge development on maxillary canine	The development of the distal accessory ridge on maxillary canine. (Ordered)	Absent (0); Faint (1); Weak (2)	9
270.	Lingual shape of maxillary canine	The symmetry of the maxillary canine in lingual view, assessed by the position of the mesial and distal crown shoulder positions relative to the crown apex. (Ordered)	Asymmetric (0); More symmetric (1); Symmetric (2)	6, 8
271.	Shape of maxillary canine	The shape and the sharpness of maxillary canine. (Unordered)	Sharp, flared (0); Rounded, no cuspule (1)	11
272.	Cervical prominence on maxillary canine	The development of a cervical prominence on maxillary canine (Unordered)	Narrow and uninflated (0); Broad and inflated (1)	6
273.	Shape of mandibular canine	The shape of mandibular canine. (Unordered)	Asymmetrical (0); Symmetrical (1)	11
274.	Lingual ridge development on mandibular canine	The prominence of medial lingual ridge on mandibular canine. (Unordered)	Prominent (0); Weak (1)	2, 6, 13
275.	Basal keel on mandibular canine	The presence of the basal keel on mandibular canine. (Ordered)	Present (0); Reduced (1); Absent (2)	6, 13
276.	Canine step	The presence of a topographical step from incisor-canine occlusal margins to P3 occlusal surface. (Unordered)	Absent (0); Present (1)	6
277.	Maxillary premolar molarization	The degree of molarization on maxillary premolars. (Ordered)	None (0); Minor (1); Marked (2)	2, 6
278.	Buccal grooves on maxillary premolars	The development of buccal grooves on maxillary premolars. (Unordered)	Marked (0); Weak (1)	6
279.	P3 position	The position of P3 relative to canine. (Unordered)	Posterior (0); Posterolateral (1)	6, 10
280.	Maxillary P3 cusp heteromorphy	The size of paracone of upper premolars relative to the protocone. (Ordered)	Paracone much larger than protocone (0); Paracone larger than protocone (1); Paracone equals protocone (2)	6, 13
281.	Maxillary P3 root number	The number of roots on maxillary P3. (Unordered)	Two (0); >Two (1)	9
282.	Maxillary P3 mesiobuccal line extent	The extent of mesiobuccal line on maxillary P3. (Ordered)	Always (0); Frequent (1); Rare (2); Absent (3)	8

283.	Mesiobuccal protrusion of P3 crown base	The degree of overall asymmetry of the crown of maxillary and mandibular P3. (Ordered)	Strong (0); Moderate (1); Weak or absent (2)	3, 6, 13
284.	Mandibular P3 root number	The number of roots on mandibular P3. (Unordered)	One (0); Two (1)	2, 6, 9
285.	Frequency of well-developed metaconid on mandibular P3	The frequency of a well-developed P3 metaconid within each species sample. (Ordered)	Absent (0); Infrequent (1); Frequent (2)	3, 6, 8, 13
286.	Mandibular P3 shape	The shape and symmetry of mandibular P3. (Ordered)	Asymmetrical (0); Less asymmetrical, talonid reduced (1); Much less asymmetrical, talonid absent (2); Circular (3)	11
287.	Lingual cusp on mandibular P4	The number of cusps on mandibular P4. (Unordered)	Two, mesial cusp much larger (0); Two, mesial cusp larger (1); Two, cusps equal size (2); Two, distal cusp larger (3)	9
288.	Mandibular P4 root number	The number of roots on mandibular P4. (Unordered)	One (0); Two (1)	1, 6
289.	Mandibular P4 shape	The symmetry of mandibular P4. (Ordered)	Asymmetrical, wide polygon (0); Asymmetrical, reduced polygon (1); Symmetrical (2)	11
290.	Postcanine crown area	The summed area of postcanine teeth. (Ordered)	Small (0); Moderate (1); Large (2)	1-3, 6, 8, 13
291.	Size of M1 relative to M2	The ratio of crown area of M1 relative to M2. (Unordered)	≥ 1 (0); <1 (1)	6, 10
292.	Size of M1 relative to M3	The ratio of crown area of M1 relative to M3. (Unordered)	≥ 1 (0); <1 (1)	6, 10
293.	Size of M2 relative to M3	The ratio of crown area of M2 relative to M3. (Unordered)	≥ 1 (0); <1 (1)	6, 10
294.	Molar cingulum development	The development of molar cingulum on maxillary molars. (Unordered)	Reduced, incomplete (0); Fragmented or absent (1)	3, 6, 13

295.	Molar dentine horn height	The height of the molar dentine horns. (Unordered)	High (0); Low (1)	13
296.	Maxillary molar morphology	The development of cusps and enamel on the maxillary molar. (Unordered)	Well developed cusps and cristae (0); Inflated cusps, limited cristae (1); Low cusps with enamel wrinkling (2); Flat, bunodont morphology (3)	3, 6
297.	Protocristid groove prominence of mandibular molars	The development of protocristid groove on molars. (Unordered)	Prominent (0); Barely visible (1)	13
298.	Lingual marginal ridge development	The development of the lingual marginal ridges of molars. (Ordered)	Hardly appreciable (0); More prominent (1); Very prominent (2)	13
299.	Positions of buccal and lingual cusps relative to crown margin	The positions of the buccal and lingual cusp tips relative to the crown base. (Unordered)	BC and LC at margin (0); LC margin, BC slightly lingual (1); LC margin, BC moderately lingual (2); LC slightly buccal, BC moderately lingual (3); LC moderately buccal, BC strongly lingual (4)	2, 3, 6, 8, 13
300.	Protoconid/metaconid more mesial cusp on molars	The most mesial cusp on mandibular molars. (Unordered)	Equal (0); Protoconid (1)	2, 6
301.	Peak of enamel thickness between the roots of molars	The thickness of enamel between the roots of molars. (Unordered)	Thin (0); Thicker (1)	2
302.	Maxillary M1 shape	The shape of maxillary M1. (Unordered)	Squared (0); Rhomboidal (1)	11
303.	Cusp 5 on maxillary M1	The development of cusp 5 on maxillary M1. (Unordered)	Faint cuspule (0); Trace cuspule (1); Small cuspule (2)	9
304.	Enamel extension on maxillary M1	The extension of enamel on maxillary M1. (Unordered)	Absent (0); Faint (1)	9

305.	Carabelli's cusp on maxillary M1	The development of Carabelli's cusp on maxillary M1. (Unordered)	Lingual cingulum (0); Absent (1); Groove, small cusp (2); Pit, small cusp (3); Large depression, cusp (4)	9
306.	Anterior fovea on mandibular M1	The development of anterior fovea on mandibular M1. (Ordered)	Faint (0); Weak (1); Moderate (2); Large (3)	9
307.	Cusp number on mandibular M1	The number of cusps on mandibular M1. (Unordered)	Five (0); Six (1)	9
308.	Protostylid on mandibular M1	The development of protostylid on mandibular M1. (Unordered)	Absent (0); Absent-pit (1); Curved buccal groove (2); Curved mesial and distal grooves (3); Trace cusp (4); Small cusp (5)	9
309.	Cusp 7 on mandibular M1	The development of cusp 7 on mandibular M1. (Ordered)	Absent (0); Faint (1); Small (2)	9
310.	Root number on mandibular M1	The number of roots on mandibular M2. (Unordered)	Two (0)	9
311.	Mid-trigonid crest in mandibular M1 and/or M2	The presence of mid trigonid crest on mandibular M1 and M2. (Unordered)	Absent (0); Present (1)	11
312.	Cusp 5 in mandibular M1 and/or M2	The presence of cusp 5 on mandibular M1 and M2. (Unordered)	Present (0); Absent (1)	11
313.	Maxillary M2 shape	The shape of the maxillary M2 measured by the length divided by breadth of the molar crown. (Unordered)	Broader than long (0); Square (1)	3
314.	Hypocone on maxillary M2	The development of hypocone on maxillary M2. (Ordered)	Small cusp (0); Large cusp (1); Very large cusp (2)	9
315.	Groove pattern on mandibular M2	The groove pattern on mandibular M2. (Unordered)	Y (0); Some X (1); X (2)	9
316.	Cusp number on mandibular M2	The number of cusps on mandibular M2. (Ordered)	Four (0); Five (1); Six (2); Greater than 6 (3)	9
317.	Root number on mandibular M2	The number of roots on mandibular M2. (Unordered)	Less than 2 (0); Two (1)	9
318.	Maxillary M3 agenesis	The degree of maxillary M3 agenesis. (Unordered)	Absent (0); Minimal (1)	9

319.	Torsomolar angle on mandibular M3	The torsomolar angle on mandibular M3. (Unordered)	Absent (0); Minimal (1)	9
320.	Cervical prominences on molars	The presence of well-developed cervical prominences on the lingual and buccal margins of molars. (Unordered)	Yes (0); No (1)	6
321.	Protocone size relative to paracone of deciduous m1, in occlusal view	The protocone size of maxillary deciduous m1 in crown view. (Unordered)	Larger than paracone (0); Smaller than paracone (1)	13
322.	Deciduous mandibular m1 shape	The shape of deciduous mandibular m1. (Unordered)	Buccolingually narrow (0); Buccolingually broad (1); Molarized (2)	6, 8
323.	Talonid basin of deciduous m1	The distal opening of the talonid basin on mandibular deciduous m1. (Unordered)	Open distally (0); Closed distally (1)	6, 13
324.	Metaconid development on mandibular deciduous m1	The development of the metaconid on mandibular deciduous m1. (Unordered)	Absent or poorly defined (0); Well defined (1)	6, 13
325.	Deciduous m1 mesial crown profile	This character comprises several inter-related traits. These are: the position of the protoconid relative to the metaconid, the disposition of the mesial marginal ridge, and the structure of the fovea anterior. (Unordered)	MMR absent, protoconid anterior, fovea open (0); MMR slight, protoconid anterior, fovea open (1); MMR thick, protoconid even with metaconid, fovea closed (2)	3, 6, 8, 13
326.	Distal marginal ridge height of deciduous m2	The development of the distal marginal ridge of deciduous second molar. (Unordered)	Low (0); High (1)	13
327.	Distal trigonid crest on mandibular deciduous m2	The length of crista obliqua relative to protoconid apex. (Unordered)	Does not reach protoconid apex (0); Reaches protoconid apex (1)	13
328.	Crista obliqua of maxillary deciduous m2	The development of the post-protocrista on maxillary deciduous m2. (Ordered)	Weak (0); Moderate (1); Strong (2)	13

329.	Mandibular symphysis robusticity	The index of mandibular symphysis breadth divided by mandibular height. (Ordered)	Gracile (0); Intermediate (1); Robust (2); Extremely robust (3)	3, 6
330.	Mandibular symphysis orientation	The orientation of the mandibular symphysis. (Unordered)	Receding (0); Vertical (1)	2, 3, 6, 8, 12, 13
331.	Projection of mental protuberance	The degree of mental protuberance projection. (Ordered)	Absent (0); Weakly projecting (1); Strongly projecting (2)	1, 2, 5, 12
332.	Central keel	The presence of a central keel. (Unordered)	Absent (0); Present (1)	5, 12
333.	Mandibular incurvation	The development of a depression on the anterosuperior symphyseal region in norma lateralis (Ordered)	Absent (0); Present (1)	6, 12
334.	Subalveolar fossa	The presence of subalveolar fossae on the mandible. (Unordered)	Absent or slight (0); Moderate to prominent (1)	6
335.	Incisura submentalis	The presence of semilunar space beneath the inferior rim of the symphysis (Unordered)	Absent (0); Present (1)	12
336.	Medial crest in digastric fossa	The presence of a medial crest in digastric fossa. (Unordered)	Absent (0); Present (1)	12
337.	Digastric fossa direction	The orientation of digastric fossa. (Ordered)	Downward (0); Downward-backward (1); Backward (2)	12
338.	Lateral tubercle	The presence of a lateral tubercle. (Unordered)	Absent (0); Present (1)	5, 12
339.	Inferior transverse torus development	The development of superior and inferior transverse tori. (Unordered)	Inferior torus stronger than superior torus (0); Both tori of similar development (1); Superior torus stronger than inferior torus (2); Both tori undeveloped (3)	1, 3, 6, 12
340.	Post-incisive planum development	The development of post-incisive planum. (Unordered)	Prominent (0); Weak (1)	2, 6, 12, 13

341.	Position of genioglossus insertion	The location of the insertion of genioglossal muscle relative to the inferior transverse torus. (Unordered)	Above inferior transverse torus (0); On inferior transverse torus (1)	13
342.	Position of geniohyoideus insertion	The location of the geniohyoideus insertion relative to the inferior transverse torus. (Ordered)	Basally on inferior transverse torus (0); Higher on inferior transverse torus (1); Above inferior transverse torus (2)	13
343.	Position of digastric insertion	The location of the digastric muscle insertion relative to the inferior transverse torus. (Unordered)	Posterior to inferior transverse torus (0); Inferior transverse torus (1); Not on symphysis (2)	13
344.	Fossae genioglossus definition	The development of the excavated area delineated by the transverse tori. (Ordered)	Not defined, flat surface (0); Weak (1); Well defined (2)	12
345.	Submandibular fossa depth	The depth of submandibular fossa located beneath the alveolar region. (Unordered)	Shallow (0); Deep (1)	12
346.	Anterior marginal tubercle	The presence of the marginal tubercle. (Unordered)	Absent (0); Present (1)	5, 6, 12
347.	Mental foramen opening direction	The direction of the mental foramen opening. (Ordered)	Anterior (0); Lateral (1); Posterior (2)	2, 3, 6, 13
348.	Mental foramen position	The position of the mental foramen along tooth row. (Ordered)	P3-P4 (0); P4-M1 (1); M1 (2)	5, 6, 12
349.	Mental foramen height	The index of the height of mental foramen position relative to the height of the mandibular corpus. (Ordered)	Very low (0); Low (1); Intermediate (2); High (3)	6, 8, 12
350.	Mental foramen number	The number of mental foramen. (Unordered)	Single (0); Multiple (1)	12
351.	Hollowing above and behind mental foramen	The presence of a hollowing contour of the lateral face of the mandibular corpus above and behind the mental foramen. (Unordered)	Present (0); Absent (1)	3, 6, 8, 13
352.	Torus marginalis superius development	The development of the superior marginal torus. (Unordered)	Weak/absent (0); Clearly visible (1)	12
353.	Torus marginalis inferius development	The development of the inferior marginal torus. (Unordered)	Weak/absent (0); Clearly visible (1)	2, 12

354.	Mandibular corpus depth along tooth row	The height of mandibular corpus along tooth row. (Ordered)	Shallow mesially (0); Constant (1); Deepens mesially (2)	13
355.	Mandibular cross-sectional area at M1	The geometric mean of the area of the corpus at M1. The area is calculated as an ellipse and the square root of area was then used to assess the character. (Small<25.5mm^2; Large>25.5mm^2). (Unordered)	Small (0); Large (1)	1-3, 6, 8, 13
356.	Horizontal distance between TMJ and M2 or M3	The ratio of the distance between the TMJ and M2/M3 relative to bi-foramen ovale breadth. (Short<58; Long>58) (Unordered)	Long (0); Short (1)	2, 3, 13
357.	Mandibular extramolar sulcus width	The width of the extramolar sulcus.(Narrow<6.5mm; Broad>6.5mm). (Unordered)	Broad (0); Narrow (1)	3, 6, 12, 13
358.	Retromolar space	The presence of retromolar space. (Unordered)	Absent (0); Present (1)	5, 12
359.	Retromolar area inclination	The orientation of the retromolar area. (Ordered)	Horizontal (0); Inclined (1); Vertical (2)	12
360.	Orientation of mandibular premolar row	The orientation of the dental arcade measured as the ratio between the internal bialveolar margin distances at mandibular canine and M2 positions. (Unordered)	U shaped (0); Parabolic (1)	2, 3, 6, 8, 13
361.	Separation of mandibular tooth rows	The width of the dental arcade. (Unordered)	Widely separated (0); Narrow separation (1)	13
362.	Inferior alveolar margin orientation	The orientation of the inferior alveolar margin. (Unordered)	Steep (0); Slowly inclined (1); Parallel (2)	12
363.	Sulcus intertoralis development	The development of intertoral sulcus. (Ordered)	Flat surface (0); Weak (1); Well defined (2)	12
364.	Prominentia lateralis relief	The development of lateral prominence. (Ordered)	Flat surface (0); Weak (1); Strong (2)	12
365.	Prominentia lateralis position	The position of lateral prominence along tooth row. (Ordered)	M1-M2 (0); M2-M3 (1); M3 (2)	12
366.	Ramus length	The length of mandibular ramus. (Unordered)	Narrow (0); Large (1)	12

367.	Ramus root anterior position	The position of the origin of the ascending ramus relative to the anteroposterior axis of the mandibular corpus. Anterior origin is where the ramus rises at the M1 level. (Ordered)	Posterior (0); Intermediate (1); Anterior (2)	8
368.	Ramus root vertical position	The position of the origin of the ascending ramus relative to the mandibular corpus height. (Ordered)	High (0); Intermediate (1); Low (2)	8
369.	Internal coronoid pillar orientation	The orientation of the ridge that extends inferiorly from the coronoid tip. (Unordered)	Vertical (0); Concave (1); Oblique (2)	12
370.	Crista ectocondyloidea development on the lateral face of the ramus.	The development of crista ectocondyloidea, a ridge that extends inferiorly from the condyle tip on the lateral face of the ramus. (Unordered)	Weak/absent (0); Clearly defined (1)	12
371.	Crista endocondyloidea relief on the medial face of the ramus	The development of crista endocondyloidea, a ridge that extends inferiorly from the condyle tip on the medial face of the ramus. (Unordered)	Weak/absent (0); Clearly defined (1)	12
372.	Crista endocondyloidea orientation	The orientation of crista endocondyloidea on the medial face of the ramus. (Unordered)	Oblique (0); Diagonal (1)	12
373.	Position of the junction between the mandibular notch and the condyle articular surface	The position of the condyle articular surface relative to the mandibular notch. (Unordered)	Lateral (0); Medial (1)	12
374.	Position of the deepest point of the mandibular notch	The position of the deepest point of the mandibular notch. (Unordered)	Centered (0); Condylar (1)	5, 12
375.	Crest of the mandibular notch	The position of the crest on the mandibular notch (Ordered)	Lateral edge of condyle (0); Less lateral (1); Less than a third of distance from medial end (2); Medial end (3)	5
376.	Planum triangulare size	The development of planum triangulare defined by the internal coronoid pillar and the crista endocondyloidea (Ordered)	Weakly developed (0); Intermediate (1); Strongly developed (2)	12
377.	Planum triangulare depth	The depth of planum triangulare. (Ordered)	Flat (0); Shallow (1); Deep (2)	12
378.	Condyle height relative to the coronoid	The height of mandibular condyle relative to the coronoid. (Ordered)	Lower (0); Equal (1); Higher (2)	12

379.	Lateral condylar tubercle development	The development of lateral condylar tubercle. (Ordered)	No tubercle (0); Swelling under lateral lip (1); Laterally projected tubercle (2); Strongly projected tubercle (3)	5
380.	Fossa subcondylea depth	The depth of subcondylar fossa. (Ordered)	Flat (0); Shallow (1); Deep (2)	12
381.	Fossa subcondylea development	The development of subcondylar fossa. (Ordered)	Weakly developed (0); Intermediate (1); Strongly developed (2)	12
382.	Mandibular foramen shape	The shape of the mandibular canal opening. (Unordered)	Oval (0); Circular (1)	5, 12
383.	Lingula mandibulae	The presence of lingula mandibulae, a projection of the edge of the mandibular foramen. (Unordered)	Absent (0); Present (1)	12
384.	Mylohyoid line orientation	The orientation of the mylohyoid line that crosses the medial corpus surface. (Unordered)	Parallel (0); Inclined (1); Diagonal (2)	12
385.	Mylohyoid line position	The position of mylohyoid line at M3. (Ordered)	Low (0); Intermediate (1); High (2)	12
386.	Mylohyoid groove orientation	The orientation of the mylohyoid groove on the medial surface of the ramus. (Unordered)	Inclined (0); Diagonal (1)	12
387.	Bony bridge in mylohyoid groove	The presence of a body bridge in mylohyoid groove. (Unordered)	Absent (0); Present (1)	12
388.	Fossa masseterica depth	The depth of masseteric fossa on the lateral surface of the gonial angle. (Ordered)	Flat (0); Shallow (1); Deep (2)	12
389.	Gonial profile	The profile of the posteroinferior corner of the mandible in norma lateralis. (Unordered)	Not truncated (0); Truncated (1)	5, 12
390.	Distinctiveness of angular process of mandible	The development of the angular process. (Unordered)	Distinct with posterior projection (0); Not distinct (1)	13
391.	Pterygoid fossa depth	The depth of pterygoid fossa. (Unordered)	Shallow (0); Deep (1)	12

C2. List of fossil hypodigms

Table C2 List of specimens used in this study and in the previously published studies.

	This study	Argue et al. (2009)	Berger et al. (2010)	Cameron & Groves (2004)
Ar. ramidus				specimens from Aramis
Au. anamensis				specimens from Allia Bay
Au. afarensis	AL (129-23, 145-35, 162-28, 188-1, 198-1, 199-1, 200-1, 207-13, 266-1, 277-1, 288-1, 311-1, 33-125, 333-1, 333-105, 333-2, 333-45, 333w-12, 333w-60, 400-1a, 417-1, 444-2, 58-22), Garusi 1, LH 4, MAK-VP 1/12	AL444-2	specimens from Hadar, Laetoli & Middle Awash	AL (128-23, 145-35, 162-28, 188-1, 198-1, 199-1, 200-1, 207-13, 266-1, 277-1, 288-1, 311-1, 33-125, 333-1, 333-105, 333-2, 333-45, 333w-0, 333w-1, 33w-12, 400-1a, 417-1, 444-2, 58-22), LH 4
Au. africanus	MLD (1, 2, 6, 9, 12, 22, 29, 34, 37/38, 40, 45), Sts (5, 7, 17, 19, 20, 26, 36, 52a, 52b, 67, 71), Stw (13, 73, 252, 384, 404, 498, 505, 513), Taung 1, TM (1511, 1512)	Sts (5, 7), Stw 505	specimens from Taung, Sterkfontein (including Sts53) & Makapansgat	MLD (1, 6, 9, 37/38,), Sts (5, 17, 19, 20, 26, 52a, 67, 71), Stw (13, 73, 252, 505), TM (1511, 1512)
Au. garhi			BOU-VP 12/130	BOUV-VP 12/130
Au. sediba	MH (1, 2)		MH (1, 2)	
H. antecessor				
H. ergaster	OH (9, 12), SK (15, 45, 847), Stw 80, KNM-ER(3733, 3883, 42700)	KNM-ER (3733, 3883)	SK (15, 18a, 27, 43, 45, 68, 847, 878, 2635), SKW 3114, SKX (257/258, 267/2671, 268, 269, 334, 610,	KNM-ER (730, 820, 992, 1507, 1812, 3733, 3883), KNM-WT 15000, OH 2

			1756, 2354-2356, 21204)	
H. erectus	Choukoutien (A2, F1, G1, H1, K1, Pa86, E1, H3, L1, L2, L3), Ngandong (1, 3, 5, 6, 7, 11, 12, 13, 14), Sambungmacan (1, 3, 4), Nanjing (1, 2), Sangiran (1b, 2, 4, 5, 6, 8, 9, 10, 17, 22, 27, 31, Bk7805, Ng8503), Trinil II	Sangiran (2, 17), Trinil		
Dmanisi	D (2280, 2282, 2700, 3444, 4500)	D (2280, 2282, 2700)		
H. floresiensis		LB1, LB6/4		
H. habilis	KNM-ER (1813, 1805, 42703), OH (7, 13, 16, 24, 62), SK 27, Stw 53	KNM-ER1813, OH 24	AL666-1, KNM-ER (1478, 1501, 1502, 1805, 1813, 3735), OH (4, 6, 7, 13, 15, 16, 21, 24, 27, 31, 37, 39, 42, 44, 45, 62), Omo L894-1	OH (7, 13, 16, 24), KNM-ER (1805, 1813, 1478, 1501, 1502, 3735)
H. heidelbergensis	Arago (2, 13, 21), Kabwe, Mauer, Ndutu, Sale, Steinheim	Kabwe		
H. naledi	DH (1, 2, 3, 4, 5), UW (101-001, 101-265, 101-346, 101-546, 101-1278, 101-1354)			
H. neanderthalensis	Krapina, La Ferrassie			
H. rudolfensis	KNM-ER (1470, 1590, 3732, 3891, 819, 1482, 1483, 1801, 1802, 60000, 62000, 62003), UR 501, OH 65	KNM-ER 1470	KNM-ER (819, 1470, 1482, 1483, 1590, 1801, 1802, 3732, 3891), OH 65, UR 501	KNM-ER (1470, 1482, 1483, 1590, 1801, 1802, 3732, 3891, 3950)

fossil *H. sapiens*				
H. sapiens	modern specimens	Not reported		not reported
K. platyops				KNM-WT (38350, 40000, 40001)
P. aethiopicus	KNM-WT 17000		KNM-WT 17000	KNM-WT 17000
P. boisei	OH 5, KNM-ER 406		Specimens from Omo Shungura, East Lake Turkana, Olduvai Gorge	OH 5, KNM-ER (403-407, 725, 727-729, 732, 805, 810, 818, 1803, 1806), KGA 10-525, SK (6, 12, 13/14, 23, 34, 46-49, 52, 65, 79, 83, 848, 1586), SKW (5, 8, 11, 29, 2581), TM 1517, DNH 7
P. robustus	SK (6, 12, 13/14, 23, 34, 46-49, 52, 65, 79, 83, 848, 1586), SKW (5, 8, 10, 12, 14, 33, 831a, 3068, 4767, 4769, 4772)		Specimens from Kromdraai, Swartkrans, Sterkfontein, Drimolen, Gondolin, Coopers	
S. tchadensis				
G. gorilla		4 adults (2 males/2 females)		Not reported
P. troglodytes		4 adults (2 males/2 females)		Not reported

	Cameron et al. (2004)	Chang (2005)	Gilbert (2008)	Irish et al. (2013)
Ar. ramidus				
Au. anamensis				KNM-ER (7727, 20420, 20422, 20423, 20427, 20432 A, 30200 A, 30202, 30731, 30745, 30750), KNM-KP 29287 A & B, KNM-LT 329 (cast)
Au. afarensis				AL (128-23, 145-35, 176-35, 188-1, 198, 199-1, 200-1a, 200-1b, 207-13, 266, 277-1, 311-1, 315-22, 330-5, 333-1, 333-2, 333-82, 333- W1a/b, 333-W57, 333-W58, 333w-60, 333x-2, 333x-3, 333x-4, 333x-20, 366-6, 400-1a, 400-1b, 411-1, 413-1, 417-1a, 417-1d, 438-2, 440-1, 486-1, 539-4e, 620-1, 655-1, 763-1, 996-1), LH (2, 3 (cast), 4 (cast))
Au. africanus			Sts 5	MLD (2, 6, 9, 11, 18, 23, 28-30, 40, 43) STS (1, 3, 4, 8, 9, 12, 17, 22-24, 30, 32, 40, 52, 53, 55-57, 61, 71), STW (2, 6, 7, 13 (b,f), 19b, 21, 23, 24, 43, 44, 50, 53, 56, 58, 61, 71, 73 (b–f), 75d, 106, 107, 109b, 110, 116d, 123a, 123b, 131 (b,c,d), 132, 143, 145, 147, 148, 151 (a,b), 179, 183 (c,e,h), 184, 188, 192 (a,b), 193 (a, b, c, d,e), 204 (a,b), 212 (a,c,e,f), 213 (a–g), 234, 246, 252 (a, c–l), 280c, 285 (a,b), 287, 288, 291, 295 (c,d), 305b, 308, 309a, 319, 327 (b–d), 351, 364, 365, 369, 384e, 401, 402, 404 (c,f,g), 406, 408, 412 (a,b), 413, 420b, 421 (a,b), 422, 424, 446, 447, 471 (c,g), 475, 476, 487b, 491 (b–g), 498 (a–d), 502, 513 (c–e), 524, 529 (b,c), 536, 537 (d,f,g), 558, 560 (d,e), 566), Taung, TM (1511, 1512, 1523, 1527)
Au. garhi				
Au. sediba				MH (1, 2)

H. antecessor	ATD6-(15, 16, 17, 18, 20, 38, 57, 84, 89)	Atapuerca GD		
H. ergaster	KNM-ER (730, 3733, 3883), KNM-WT15000	KNM-ER 3733, KNM-WT 15000	KNM-ER (3733, 3883), Daka, Buia	KNM-BK 67 [cast], KNM-ER (806 [B, C], 807, 808 [C, G], 820, 992 [A, B], 1506 [A, B], 2597), KNM-WT 15000, OH (12 [cast], 22[cast]), SK 15, SKX (257, 258, 268, 334, 339, 610)
H. erectus	Sangiran (2, 4, 10, 12, 17), Ngandong (1, 3, 6, 7, 10, 11, 12), Zhoukoudian, Hexian	Sangiran 7, Zhoukoudian	Hexian, Ngandong (1, 6, 7, 10, 11, 12), OH 9, Sambungmachan (1, 3, 4), Sangiran (2, 4, 12, 17), Trinil 2, Zhoukoudian (III, V, X, XI, XII)	
Dmanisi	D (2280, 2282)	D (2280, 2282, 2700/2735)	D (2280, 2282, 2700)	
H. floresiensis				
H. habilis	OH (7, 13, 16, 24), KNM-ER (1813, 3735)		KNM-ER 1813	AL 666-1, KNM-ER (1482[cast], 1590 [B, C, D, E, F, G], 1802, 1805, 1813), KNM-LU 335, OH (7 [cast], 13, 16, 24, 39, 44, 45, 62, 63), SKW 3114
H. heidelbergensis	Bodo (I, II), Broken Hill, Lake Ndutu, Arago, Petralona, Ceprano, Steinheim, Narmada	Bodo, Kabwe, Ndutu, Arago, AtapuercaSH, Mauer, Petralona, Reilingen, Steinheim, Swanscombe	Bodo, Kabwe, Ndutu, Saldanha, Ceprano, Petralona, Sima de los Huesos (1, 4, 5, 8), Dali	
H. naledi				
H. neanderthalensis	Spy 1, La Chapelle-aux-Saints, La Ferrassie, La Quina, Saccopastore, Krapina, Tabun, Amud, Shanidar	Krapina, Saccopastore, Gibraltar FQ, La Chapelle, La Ferrassie, La Quina, Le Moustier, Monte Circeo, Neandertal, Regourdou, Spy, St. Cesaire, Zafarraya, Amud, Shanidar, Tabun		

H. rudolfensis			KNM-ER 1470	
fossil *H. sapiens*	Border Cave, Klasies River Mouth, Omo 1, Laetoli 18, Florisbad, Jebel Irhoud	Djebel Irhoud, Herto, Qafzeh, Skhul		
H. sapiens		Berg, Zulu		
K. platyops				
P. aethiopicus				
P. boisei				KNM-CH 1 (cast), KNM-CH 18, KNM-ER (802 (E, F), 816, 1171 (B, E, F, G, H), 1816, 1818, 1820, 3230, 5431, 6080, 6128, 15930, 17760, 25520), OH 5 (cast), KNM-WT 17400, Peninj
P. robustus				KB 5223, SK (1-3, 5, 6, 11, 13, 15, 23-25, 29, 30, 33, 34, 37, 40, 42, 44, 47-49, 52, 55a, 57, 61, 63, 65, 65a, 67-69, 72, 73, 81, 83, 85a, 87, 89, 93, 94, 98, 104, 821-823, 826a, 829, 831, 834, 837, 838a, 843, 846a, 857, 867, 1587, 1588, 3974, 3976, 14000, 14001), SKW (5, 8, 10, 12, 14, 33, 831a, 3068, 4767, 4769, 4772), SKX (162, 240, 241, 242, 265, 271, 308, 311, 1016, 3300, 3355, 3601, 4446, 5007, 5013, 5023, 6013, 7781, 19031, 19892, 25296, 27524, 28724), TM (1517a, 1517b, 1536, 1600, 1601)
S. tchadensis				
G. gorilla				Not reported
P. troglodytes				

	Kimbel et al. (2004)	Lordkipanidze et al. (2013)	Martinon-Torrez et al. (2007)
Ar. ramidus			
Au. anamensis			
Au. afarensis	AL (58-22, 162-28, 166-9, 288-1, 333-1, 333-45, 333-84, 417-1d, 439-1, 444-2), KNM-ER 2602		Specimens from Laetoli, Hadar, Fejej, Maka
Au. africanus	Sts (5, 52, 71), Stw (53, 505), MLD (1, 6, 37/38), TM 1511		Specimens from Sterkfontein, Makapansgat, Gladysvale
Au. garhi			
Au. sediba			
H. antecessor			Atapuerca Gran Dolina
H. ergaster	KNM-ER 3733, SK 847	KNM-ER (3733, 3883, 42700), KNM-WT 15000	Specimens from Olduvai Gorge. Koobi Fora
H. erectus	Zhoukoudian	Ngandong (5, 7, 12, 14), Ngawi 1, Sambungmachan (3, 4), Sangiran (2, 4, 17), Zhoukoudian (III, X, XI, XII)	Specimens from Sangiran Dome, Trinil, Zhoukoudian
Dmanisi		D (2280, 2282, 2700, 3444, 4500)	Dmanisi
H. floresiensis			
H. habilis	OH (7, 13, 24), KNM-ER (1805, 1813)	KNM-ER (1805, 1813, 42703), OH 24, SK 847, Stw 53	Specimens from Olduvai Gorge, Koobi Fora
H. heidelbergensis			Rabat, Tighenif, Mauer, Arago, Mountmarin, Pontnewydd, Steinheim
H. naledi			
H. neanderthalensis			Saccopastore, Monte Circeo, Le Moustier, Saint Cesaire, Cabezo Gordo, Zafarraya, L'Hortus, Krapina, Sidron, Kebara, Tabun, Vindija, Kulna 1, Pinilla del Valle, Engis II, La Quina, Shanidar, Gibraltar, Petit-Puymoyen,

			Fondo Cattie
H. rudolfensis	KNM-ER (1470, 1590, 3732)	KNM-ER (1470, 62000), OH 65	
fossil *H. sapiens*			San Nicolas, Brassempouy. Wad, Almonda, Mladec, Abri Pataud, Trou Magritte, Dolni Vestonice, Pavlov, Caldeirao, Skhul, Predmosti
H. sapiens			
K. platyops			
P. aethiopicus	KNM-WT 17000		
P. boisei	OH 5, KNM-CH 304, KNM-ER (406, 407, 732, 13750, 23000)		
P. robustus	SK (12, 48), TM 1517		
S. tchadensis			
G. gorilla	Not reported		
P. troglodytes	Not reported		

	Mounier et al. (2009)	Strait & Grine (2004)	Zeitoun (2009)
Ar. ramidus		ARA-VP (6/1, 1/128, 1/500), KNM-TH 13150, KNM-LT 329	
Au. anamensis		KNM-KP (29181, 29283, 29286)	
Au. afarensis		AL (129-23, 145-35, 162-28, 188-1, 198-1, 199-1, 200-1, 207-13, 266-1, 277-1, 288-1, 311-1, 33-125, 333-1, 333-105, 333-2, 333-45, 333w-12, 333w-60, 400-1a, 417-1, 444-2, 58-22), Garusi 1, LH 4, MAK-VP 1/12	
Au. africanus		MLD (1, 2, 6, 9, 12, 22, 29, 34, 37/38, 40, 45), Sts (5, 7, 17, 20, 26, 36, 52a, 52b, 67, 71), Stw (13, 73, 252, 384, 404, 498, 505, 513), Taung 1, TM (1511, 1512)	Sts 5
Au. garhi		BOU-VP 12/130	
Au. sediba			
H. antecessor	ATD6-96		
H. ergaster	KNM-ER 992	KNM-ER (730, 820, 992, 1507, 3733, 3883), KNM-WT 15000	KNM-ER (3733, 3883), KNM-WT 15000, OH 9
H. erectus	Sangiran (1b, 9, 22), KNM-ER 992, Tighenif (1, 2, 3), Sinanthropus (G1, G2, H1)		Maba, Ngandong (1-3, 5-7, 10, 11, 12), Ngawi, Sambungmachan 1, Sangiran (2-4, 10, 12, 17, 26, 38), Sinanthropus (III, X, XI, XII), Trinil 2
Dmanisi	D (211, 2600)		
H. floresiensis			
H. habilis		AL 666-1, L 894-1, KNM-ER (1478, 1501, 1502, 1805, 1813, 3735), SK (15, 27, 45, 847), Sts 19, Stw 53	KNM-ER1813

H. heidelbergensis	Tighenif (1, 2, 3), Mauer, AT (888, 950), Arago (II, XIII), Montmaurin, Ehringsdorf F		Saldanha 1, Kabwe 1, Ndutu 1, Bodo 1, Sale 1, Narmada, Zuttiyeh Arago (XXI, XLVII), Swanscombe, Petralona 1, Dali
H. naledi			
H. neanderthalensis	Krapina (J, H, G), La Ferrassie 1, La Quina H5, Regourdou, Banolas, Spy 1, Amud 1, Shanidar I, Zafarraya		Amud 1, La Chapelle-aux-Saints, La Ferassie 1, Gibraltar, Monte Circeo 1, La Quina H5, Shanidar 5, Spy 1
H. rudolfensis		KNM-ER (819, 1470, 1482, 1483, 1590, 1801, 1802, 3732, 3891) UR 501	KNM-ER 1470
fossil *H. sapiens*	Qafzeh 9, Skhul V, Cro-Magnon 1, Abri Pataud 1, Ohalo II		Eliye Springs 1, LH 18, Omo 2, Jebel Irhoud 1, Skhul V, WHL 50
H. sapiens	Loisy, Sahara		30 Dayak skulls
K. platyops		KNM-WT (38350, 40000)	
P. aethiopicus		KNM-WT (16005, 17000), L (55s-33, 338y-6, 860-2), Omo (18-1967-18, 44-1970-2466, 57-4-1968-41)	
P. boisei		OH 5, KGA (10-506, 10-525), KNM-CH 1, KNM-ER (403-407, 725, 727,-729, 732, 733, 801, 805, 810, 818, 1468, 1469, 1483, 1803, 1806, 3229, 3230, 3729, 3954, 5429, 5877, 13750, 15930, 23000), KNM-WT (16841, 17400), L (7a-125, 74a-21), Natron, Omo 323-896	KNM-ER 406
P. robustus		DNH 7, SK (6, 12, 13/14, 23, 34, 46-49, 52, 55, 65, 79, 83, 848, 1586), SKW (5, 8, 11, 29, 2581), SKX (265, 4446, 5013), TM 1517	
S. tchadensis		TM 266-01-060-1	
G. gorilla		Not reported	11 adults
P. troglodytes		Not reported	11 adults

C3. Geological dates used to constrain the fossil hominin species as non-contemporaneous tips in the phylogeny.

Table C3 The dates used to date the fossil hominin species in this study.

The dates associated with the oldest specimens used for the morphological analyses are taken as the date for the species.

Taxon	Specimen	Date (Ma)	References
Ar. ramidus	ARA-VP 6/1	4.4	White et al. (2009)
Au. anamensis	KNM-KP 29181/29283/29286	4.17	Leakey et al. (1998)
Au. afarensis	LH 4	3.77	Leakey et al. (1976)
Au. africanus	Makapansgat material	3.03	Herries et al. (2013)
Au. garhi	BOU-VP 12/130	2.5	Brown et al. (2013)
Au. sediba	MH 1	1.977	Pickering et al. (2011)
H. antecessor	ATD6-15	0.938	Parés et al. (2013)
African *H. erectus*	Koobi Fora specimens	1.65	Gathogo & Brown (2006)
Asian *H. erectus*	Sangiran	1.5	Larick et al. (2001)
Georgian *H. erectus*	D2600	1.81	Garcia et al. (2010)
H. floresiensis	LB1	0.019	Morwood & Jungers (2009)
H. habilis	AL666-1	2.33	Kimbel et al. (1997)
H. heidelbergensis	Mauer	0.609	Wagner et al. (2010)
H. neanderthalensis	Krapina	0.13	Rink et al. (1995)
H. rudolfensis	KNM-ER 1470, 1802, 62000	2.05	Joordens et al., (2013)
H. sapiens	Omo 1, 2	0.195	McDougall et al. (2005)
K. platyops	KNM-WT 40000	3.53	Leakey et al. (2001)
P. aethiopicus	L 55-s-33	2.7	Feibel et al. (1989)
P. boisei	L74a-21/L7a-125	2.3	Feibel et al. (1989)
P. robustus	Swartkrans specimens	1.9	Pickering et al. (2011)
S. tchadensis	TM 266-01-060-1	7.24	Lebatard et al. (2008)

C4. Dating constraints for *H. naledi*

Four different analyses were conducted to explore the various age prior settings for *H. naledi* as explained in the main text. Convergence in the runs for each analysis was assessed using the MrBayes's convergence diagnostics and Tracer v.1.6. The runs are assessed to have converged when Estimated Sample Size (ESS) is greater than 100 and Potential Scale Reduction Factor (PSRF) approaches 1 for all parameters.

a) H. naledi as old as the oldest hominin species.

Table C4 Model parameters and the convergence diagnostics.

In this model, *H. naledi* was assigned an age prior sampled from a uniform distribution between 7.24 Ma (millions of years ago) to the present.

Parameter	Mean	Variance	Minimum ESS	Average ESS	PSRF
Tree height	1.476683	0.021867	2778.41	2927.53	1.00
Tree likelihood	11.479148	1.927504	903.51	948.52	1.00
Alpha	1.976126	0.367194	6179.43	6804.32	1.00
Net speciation	0.189484	0.002364	7956.22	8435.63	1.00
Relative extinction	0.163474	0.020246	14332.09	14833.77	1.00
Igrvar	0.407273	0.009130	2179.26	2670.23	1.00

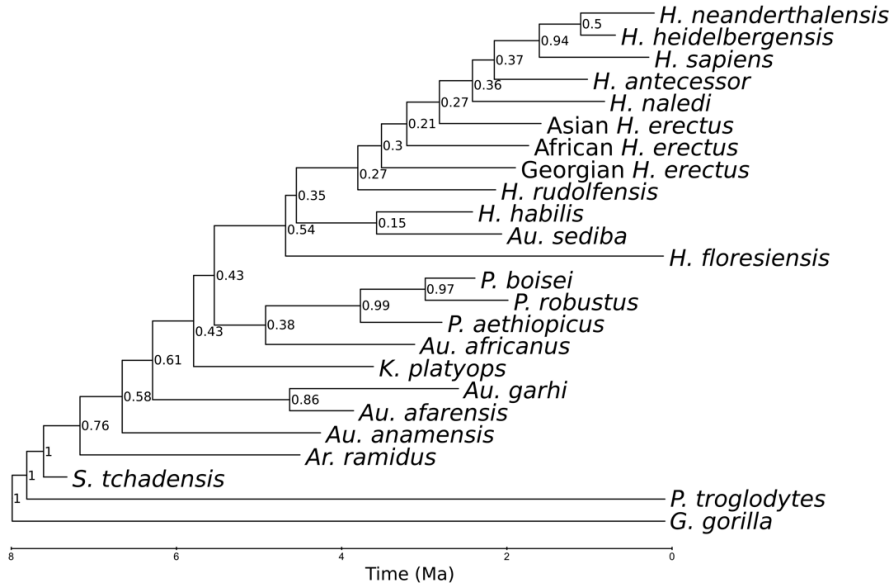

Figure C1 MCC tree with a uniform age prior for *H. naledi* between 7.24 Ma and the present.

b) H. naledi as old as the oldest Australopithecus.

Table C5 Model parameters and the convergence diagnostics.

In this model, *H. naledi* was assigned an age prior that was sampled from a uniform distribution between 4.17 Ma to the present.

Parameter	Mean	Variance	Minimum ESS	Average ESS	PSRF
Tree height	1.476474	0.021409	2829.31	3059.72	1.00
Tree likelihood	11.494421	1.924051	666.07	896.33	1.00
Alpha	1.973783	0.363976	5539.22	6063.53	1.00
Net speciation	0.189480	0.002345	8744.26	9954.91	1.00
Relative extinction	0.163042	0.019943	13598.49	14374.57	1.00
Igrvar	0.408682	0.009199	2594.87	2913.31	1.00

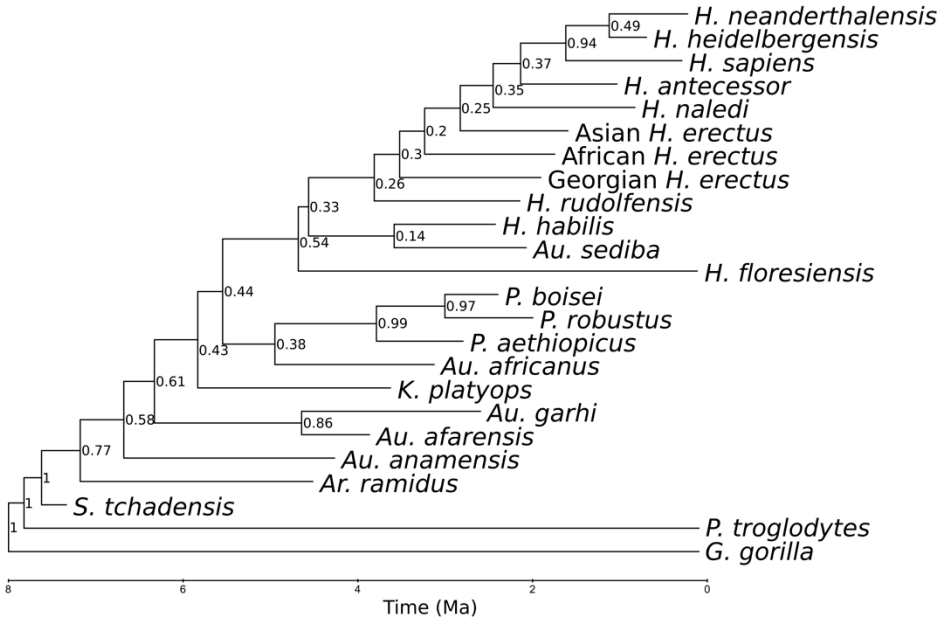

Figure C2 The MCC tree when *H. naledi* was assigned a uniform prior between 4.17 Ma and the present on its age.

c) H. naledi as old as the oldest Homo.

Table C6 Model parameters and the convergence diagnostics.

In this model, *H. naledi* was assigned an age prior that was sampled from a uniform distribution between 2.33 Ma to the present.

Parameter	Mean	Variance	Minimum ESS	Average ESS	PSRF
Tree height	1.476374	0.021628	2723.45	2982.40	1.00
Tree likelihood	11.502336	1.904807	917.09	1018.84	1.00
Alpha	1.976139	0.361426	5863.89	6598.26	1.00
Net speciation	0.189370	0.002353	7676.57	9098.07	1.00
Relative extinction	0.163511	0.020130	14554.06	14868.25	1.00
Igrvar	0.407613	0.009374	1775.53	2377.50	1.00

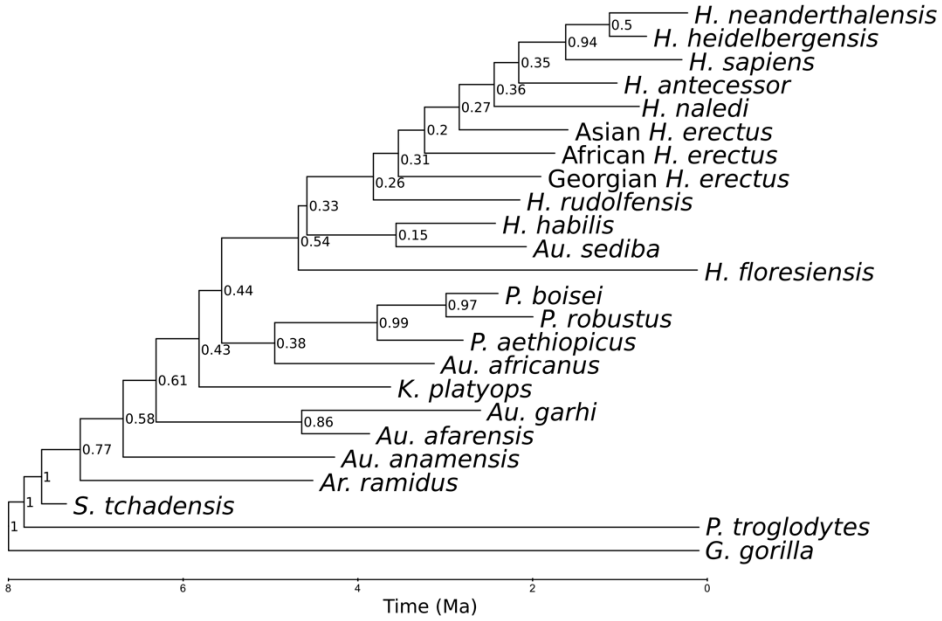

Figure C3 The MCC tree when *H. naledi* was assigned a uniform prior between 2.33 Ma and the present on its age.

d) H. naledi as a contemporary species.

Table C7 Model parameters and the convergence diagnostics are presented for the model in which the tip of *H. naledi* was assumed to continue to the present.

Parameter	Mean	Variance	Minimum ESS	Average ESS	PSRF
Tree height	1.476752	0.021519	2277.63	2999.33	1.00
Tree likelihood	11.466828	1.912803	756.62	1074.42	1.00
Alpha	1.968399	0.356638	6454.49	6884.49	1.00
Net speciation	0.191066	0.002425	7239.16	9394.53	1.00
Relative extinction	0.165431	0.020369	14053.36	14764.09	1.00
Igrvar	0.404007	0.009102	2286.73	2656.83	1.00

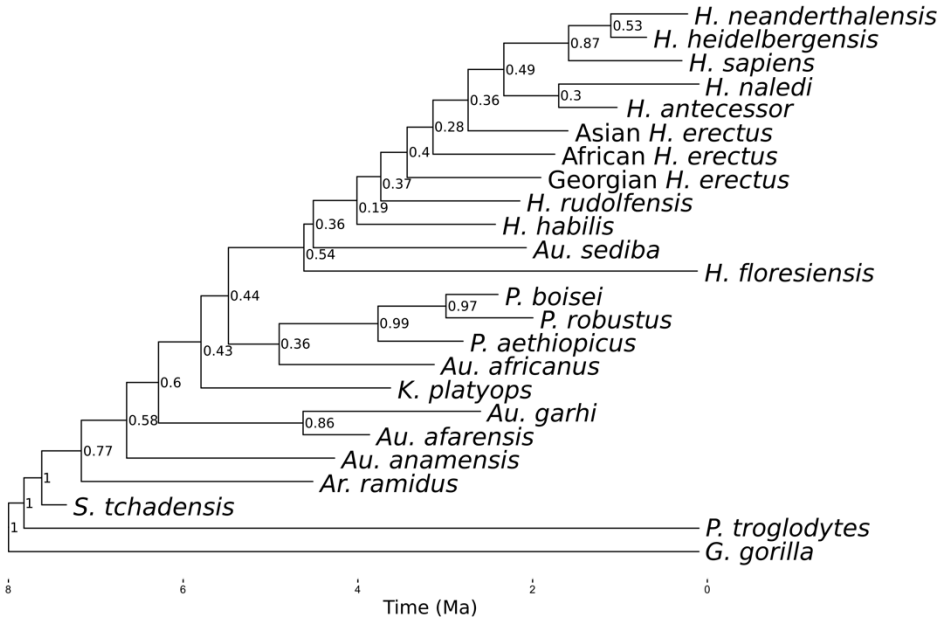

Figure C4 The MCC tree when *H. naledi*'s tip date was fixed to the present.

C5. Additional phylogenetic analyses: Undated Bayesian analysis and parsimony analysis.

In addition to the dated Bayesian analysis reported in the main text, we carried out an undated Bayesian analysis and a maximum parsimony analysis.

Undated Bayesian analysis

The undated Bayesian analysis was carried out in the same way as the dated Bayesian analysis, except the geological dates associated with the fossil hominins were not used to constrain the branch lengths of the trees and no clock rate parameters were estimated. The characters were modelled to evolve under the Markov k model with a gamma-distributed among-character rate variation, correcting for the sampling bias for parsimony-informative characters. Of the 391 characters, 288 were treated as unordered and 103 as ordered. The polymorphic characters were treated as uncertainty in the character coding in the dated Bayesian analysis. The posterior probability distribution of the trees and the parameters were estimated through MCMC sampling, all in the same manner as the main dated Bayesian analysis. The convergence was diagnosed in MrBayes and the burn-in sample was the same as the main analyses.

A summary (MCC) of the best 60,000 trees sampled during the undated Bayesian analysis is presented in Figure C5. The undated MCC tree is similar in topology to the dated MCC tree. Importantly, older fossils within the hominin clade are closer to the presumed root of the undated MCC tree: Figure C6 plots the geological date of hominin species against the root-to-tip distance of those species and shows a close, positive association between the two (see also Lee et al., 2014a). The most obvious exception to this pattern is *Sahelanthropus tchadensis*. In the dated MCC tree *S. tchadensis* is the sister of all other hominins and has a short branch, whereas in the undated MCC tree *S. tchadensis* is located close to the middle of the tree and has a long branch. This is not particularly surprising. *S. tchadensis* has long been accepted to have homoplastic similarities (e.g., a browridge) with certain members of genus *Homo*. Given these known homoplasies, dropping the date constraint for the species allows it to move further into the tree and increases its terminal branch length.

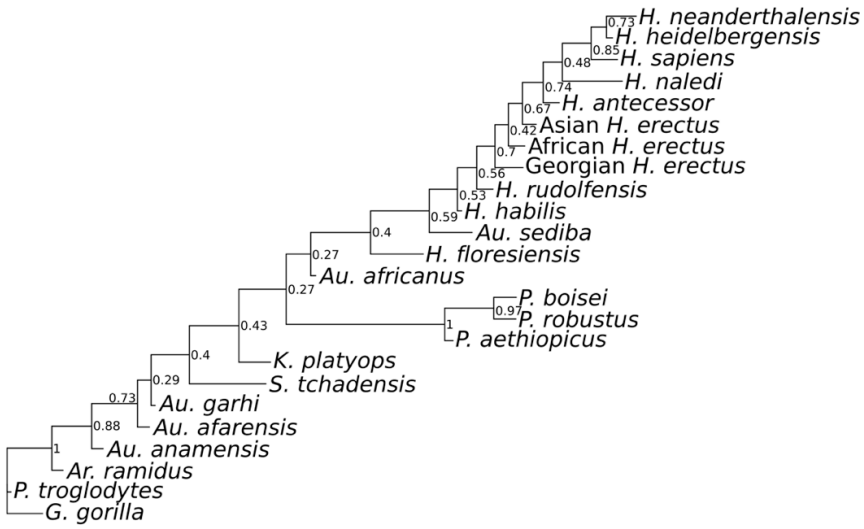

Figure C5. Maximum clade credibility tree for the undated Bayesian analysis. The posterior probability values are indicated at the nodes.

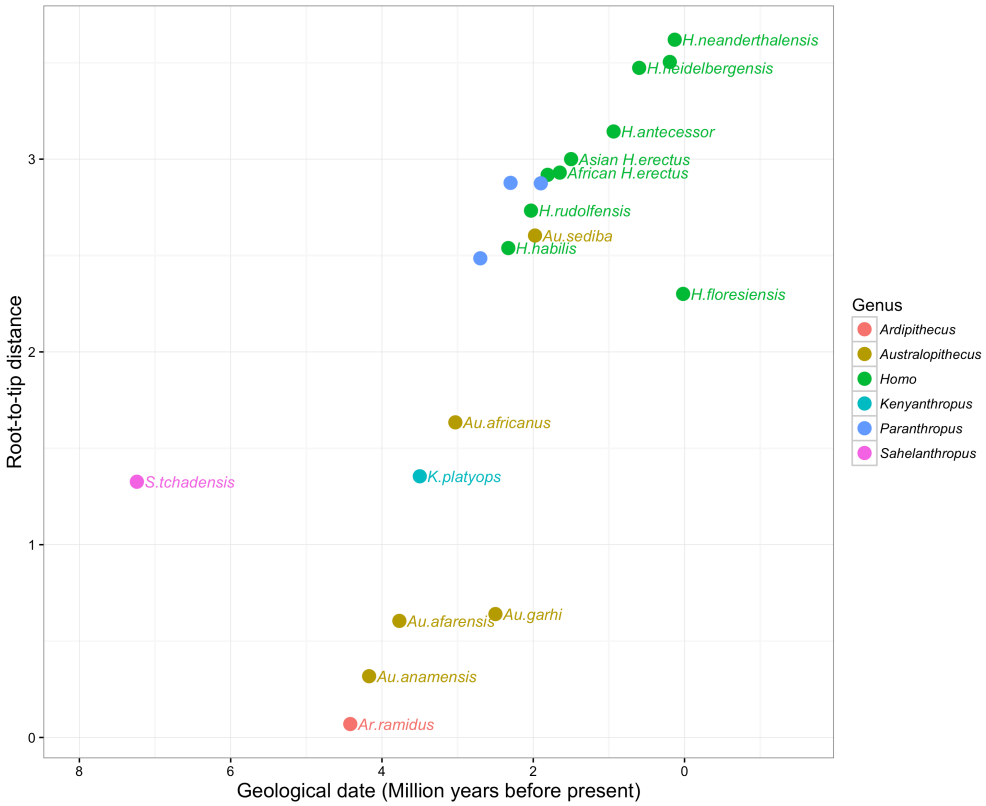

Figure C6. A plot of the geological date of hominin species (minus *H. naledi*, which is undated) and the root-to-tip distance of those species.
This plot illustrates how more recent species are inferred to be farther away from the root of the hominin clade based on their morphology alone, consistent with their geological dates.

Maximum parsimony analysis

We conducted a maximum parsimony bootstrap analysis in PAUPRat (Sikes and Lewis, 2001) installed on the CIPRES Scientific Gateway (Miller et al., 2010). In this analysis, 288 characters were treated as unordered and 103 characters as ordered, and *G. gorilla* and *P. troglodytes* were specified as the outgroup taxa. We created 100 bootstrapped samples, and for each bootstrapped sample we ran 200 iterations with 20% of the parsimony-informative characters perturbed per iteration. A heuristic search was conducted with the tree bisection and reconnection (TBR) method.

The bootstrap tree is presented in Figure C7. There are two major differences between the bootstrap tree and the dated MCC tree (Main text Figure 4.2). Both are in line with expectation. One concerns the placement of *S. tchadensis*. Consistent with its behaviour in the undated Bayesian analysis and the known homoplasies it shares with the genus *Homo, S. tchadensis* is located close to the middle of the parsimony tree, rather than being sister of all other hominins. This is consistent with its behaviour in the undated Bayesian analysis and the known homoplasies it shares with the genus *Homo*. The other major difference relates to *K. platyops*. In the bootstrap tree, *K. platyops* is the sister to *H. rudolfensis* whereas in the dated MCC tree it is placed much deeper. While less well-established than the *Sahelanthropus* situation, the placement of *K. platyops* in the bootstrap trees likely involves the facial similarities it shares with *H. rudolfensis* (Leakey et al., 2001). Evidently in the bootstrap tree these similarities are inferred to be synapomorphies whereas in the dated MCC tree they are inferred to be homoplasies (i.e., because they evolve at a high average rate throughout the tree). Maximum parsimony analysis is known to be susceptible to long-branch attraction, where lineages appear to be similar because they have undergone a large amount of change rather than because they are related by descent. Though not formally tested, this would lead to just this sort of pattern here.

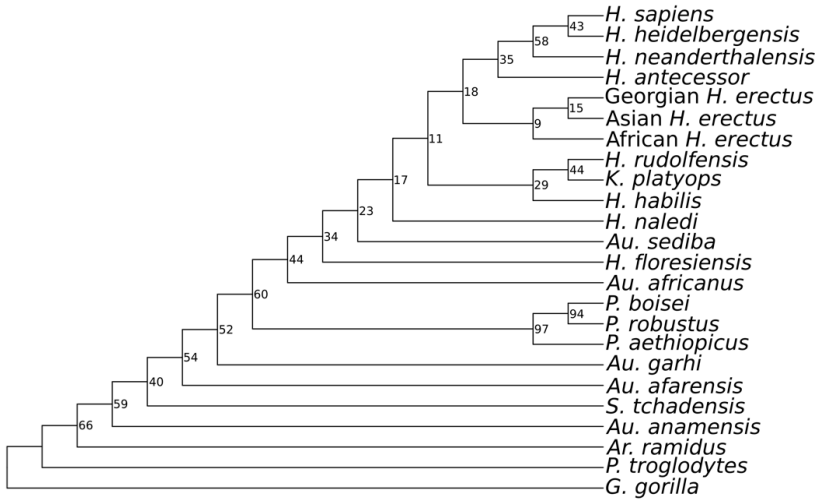

Figure C7. A bootstrap tree with bootstrap values based on 100 replicates in PAUPRat.

C6. Tree models tested in this study

Tree model	Topological constraints	Marginal log likelihood	Bayes factor	Interpretation
a) 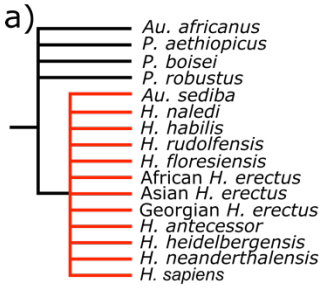	(*Au. africanus*, *P. aethiopicus*, *P. boisei*, *P. robustus*, (*Au. sediba*, *H. naledi*, *H. habilis*, *H. rudolfensis*, African *H. erectus*, Asian *H. erectus*, Georgian *H. erectus*, *H. antecessor*, *H. heidelbergensis*, *H. neanderthalensis*, *H. sapiens*))	-2550.84	--	Best model
b) 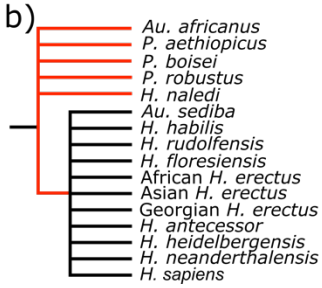	(*Au. africanus*, *P. aethiopicus*, *P. boisei*, *P. robustus*, *H. naledi*, (*Au. sediba*, *H. habilis*, *H. rudolfensis*, African *H. erectus*, Asian *H. erectus*, Georgian *H. erectus*, *H. antecessor*, *H. heidelbergensis*, *H. neanderthalensis*, *H. sapiens*))	-2555.95	10.22	Strong evidence to reject model

Figure C8. Partially constrained tree models competed in Bayes factor tests.
The model (partially constrained) trees competed to address phylogenetic hypotheses regarding *H. naledi* and its inclusion in the clade of *Au. sediba* and the members of genus *Homo.* Red edges are where the target species (*H. naledi*) can enter a particular tree, represented by the column "Topological constraints." Polytomies depicted in the constrained trees are not fixed, and can be resolved with the data.

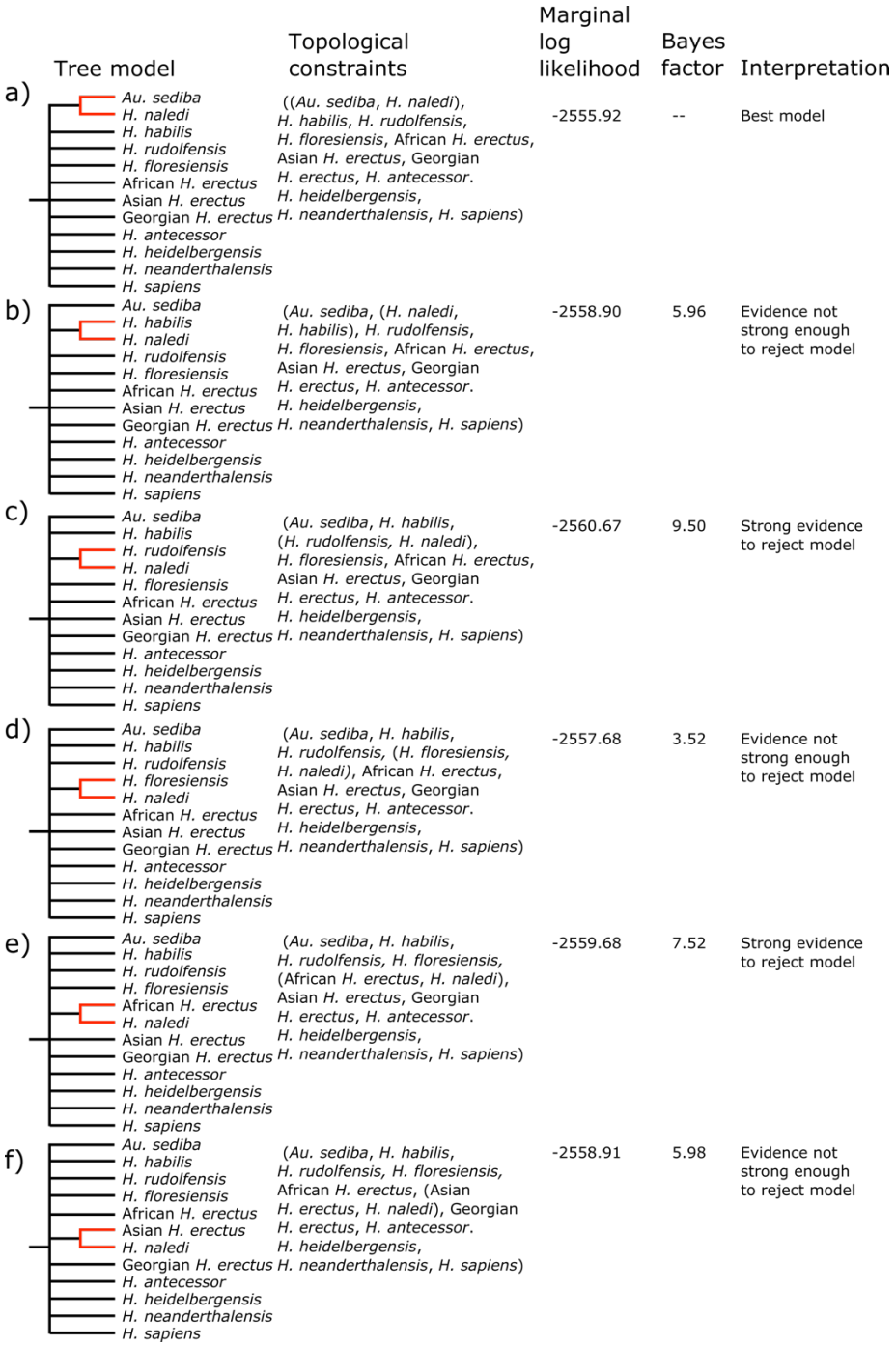

Figure C9a. Partially constrained tree models competed in Bayes factor tests.
The model (partially constrained) trees competed to address phylogenetic hypotheses regarding the sister taxon relationships of *H. naledi* and the species in the clade of *Au. sediba* and the members of genus *Homo.* Red edges are where the target species (*H. naledi*) can enter a particular tree, represented by the column “Topological constraints.” Polytomies depicted in the constrained trees are not fixed, and can be resolved with the data.

	Tree model	Topological constraints	Marginal log likelihood	Bayes factor	Interpretation
g)	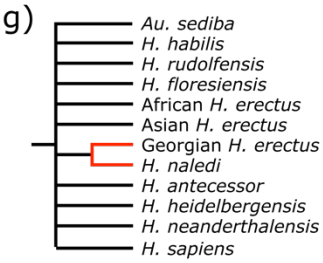	(*Au. sediba*, *H. habilis*, *H. rudolfensis*, *H. floresiensis*, African *H. erectus*, Asian *H. erectus*, (Georgian *H. erectus*, *H. naledi*), *H. antecessor*, *H. heidelbergensis*, *H. neanderthalensis*, *H. sapiens*)	-2560.14	8.44	Strong evidence to reject model
h)	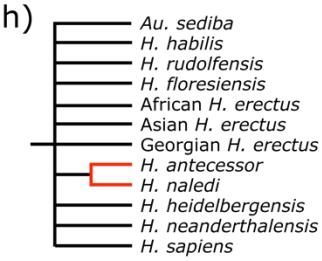	(*Au. sediba*, *H. habilis*, *H. rudolfensis*, *H. floresiensis*, African *H. erectus*, Asian *H. erectus*, Georgian *H. erectus*, (*H. antecessor*, *H. naledi*), *H. heidelbergensis*, *H. neanderthalensis*, *H. sapiens*)	-2556.04	0.24	Evidence not strong enough to reject model
i)	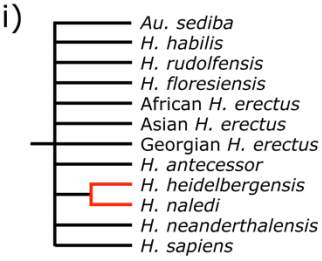	(*Au. sediba*, *H. habilis*, *H. rudolfensis*, *H. floresiensis*, African *H. erectus*, Asian *H. erectus*, Georgian *H. erectus*, *H. antecessor*, (*H. heidelbergensis*, *H. naledi*), *H. neanderthalensis*, *H. sapiens*)	-2561.69	11.54	Strong evidence to reject model
j)	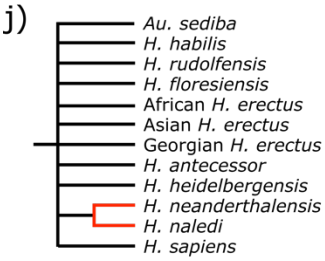	(*Au. sediba*, *H. habilis*, *H. rudolfensis*, *H. floresiensis*, African *H. erectus*, Asian *H. erectus*, Georgian *H. erectus*, *H. antecessor*, *H. heidelbergensis*, (*H. neanderthalensis*, *H. naledi*), *H. sapiens*)	-2560.95	10.06	Strong evidence to reject model
k)	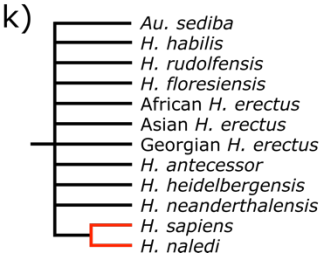	(*Au. sediba*, *H. habilis*, *H. rudolfensis*, *H. floresiensis*, African *H. erectus*, Asian *H. erectus*, Georgian *H. erectus*, *H. antecessor*, *H. heidelbergensis*, *H. neanderthalensis*, (*H. sapiens*, *H. naledi*))	-2557.35	2.86	Evidence not strong enough to reject model

Figure C9b. Partially constrained tree models competed in Bayes factor tests.
The model (partially constrained) trees competed to address phylogenetic hypotheses regarding the sister taxon relationships of *H. naledi* and the species in the clade of *Au. sediba* and the members of genus *Homo.* Red edges are where the target species (*H. naledi*) can enter a particular tree, represented by the column “Topological constraints.” Polytomies depicted in the constrained trees are not fixed, and can be resolved with the data.

C7. Supplementary References

Argue, D., Morwood, M.J., Sutikna, T., Jatmiko, Saptomo, W., 2009. *Homo floresiensis*: a cladistic analysis. J. Hum. Evol. 57, 623–639.

Berger, L.R., de Ruiter, D.J., Churchill, S.E., Schmid, P., Carlson, K.J., Dirks, P.H.G.M., Kibii, J.M., 2010. *Australopithecus sediba*: a new species of *Homo*-like australopith from South Africa. Science 328, 195–204.

Brown, F.H., McDougall, I., Gathogo, P.N., 2013. Age ranges of *Australopithecus* species, Kenya, Ethiopia, and Tanzania. In: Reed, K.E., Fleagle, J.G., Leakey, R.E. (Eds.), The Paleobiology of *Australopithecus africanus.* Vertebrate Paleobiology and Paleoanthropology. Springer Netherlands, Dordrecht, pp. 7–20.

Cameron, D.W., Groves, C.P., 2004. Bones, Stones and Molecules: Out of Africa and Human Origins. Elsevier, San Diego.

Cameron, D., Patnaik, R., Sahni, A., 2004. The phylogenetic significance of the Middle Pleistocene Narmada hominin cranium from central India. Int. J. Osteoarchaeol. 14, 419–447.

Chang, M.L., 2005. Neandertal origins, Middle Pleistocene systematics, and tests of current taxonomic and phylogenetic hypotheses. Ph.D. Dissertation, University of Pennsylvania.

Feibel, C.S., Brown, F.H., McDougall, I., 1989. Stratigraphic context of fossil hominids from the Omo group deposits: northern Turkana Basin, Kenya and Ethiopia. Am. J. Phys. Anthropol. 78, 595–622.

Garcia, T., Féraud, G., Falguères, C., de Lumley, H., Perrenoud, C., Lordkipanidze, D., 2010. Earliest human remains in Eurasia: New 40Ar/39Ar dating of the Dmanisi hominid-bearing levels, Georgia. Quat. Geochronol. 5, 443–451.

Gathogo, P.N., Brown, F.H., 2006. Revised stratigraphy of Area 123, Koobi Fora, Kenya, and new age estimates of its fossil mammals, including hominins. J. Hum. Evol. 51, 471–479.

Gilbert, W.H., 2008. *Homo erectus* cranial anatomy. In: Gilbert, W.H., Asfaw, B. (Eds.), *Homo erectus*: Pleistocene Evidence from the Middle Awash, Ethiopia. University of California Press, Berkeley, pp. 265–311.

Herries, A.I.R., Pickering, R., Adams, J.W., Curnoe, D., Warr, G., Latham, A.G., Shaw, J., 2013. A multi-disciplinary perspective on the age of *Australopithecus* in South Africa. In: Reed, K.E., Fleagle, J.G., Leakey, R.E. (Eds.), The Paleobiology of *Australopithecus africanus.* Vertebrate Paleobiology and Paleoanthropology. Springer Netherlands, Dordrecht, pp. 21–40.

Irish, J.D., Guatelli-Steinberg, D., Legge, S.S., de Ruiter, D.J., Berger, L.R., 2013. Dental morphology and the phylogenetic “place” of *Australopithecus sediba*. Science 340, 1233062.

Joordens, J.C.A., Dupont-Nivet, G., Feibel, C.S., Spoor, F., Sier, M.J., van der Lubbe, J.H.J.L., Nielsen, T.K., Knul, M.V., Davies, G.R., Vonhof, H.B., 2013. Improved age control on early *Homo* fossils from the upper Burgi Member at Koobi Fora, Kenya. J. Hum. Evol. 65, 731–745.

Kimbel, W.H., Johanson, D.C., Rak, Y., 1997. Systematic assessment of a maxilla of *Homo* from Hadar, Ethiopia. Am. J. Phys. Anthropol. 103, 235–262.

Kimbel, W.H., Rak, Y., Johanson, D.C., 2004. Taxonomic and phylogenetic status of *Australopithecus afarensis*. In: Kimbel, W.H., Rak, Y., Johanson, D.C. (Eds.), The Skull of *Australopithecus afarensis*. Oxford University Press, New York, pp. 215-220.

Larick, R., Ciochon, R.L., Zaim, Y., Sudijono, Suminto, Rizal, Y., Aziz, F., Reagan, M., Heizler, M., 2001. Early Pleistocene 40Ar/39Ar ages for Bapang Formation hominins, Central Jawa, Indonesia. Proc. Natl. Acad. Sci. 98, 4866–4871.

Leakey, M.D., Hay, R.L., Curtis, G.H., Drake, R.E., Jackes, M.K., White, T.D., 1976. Fossil hominids from the Laetoli Beds. Nature 262, 460–466.

Leakey, M.G., Feibel, C.S., McDougall, I., Ward, C., Walker, A., 1998. New specimens and confirmation of an early age for *Australopithecus anamensis*. Nature 393, 62–66.

Leakey, M.G., Spoor, F., Brown, F.H., Gathogo, P.N., Kiarie, C., Leakey, L.N., McDougall, I., 2001. New hominin genus from eastern Africa shows diverse middle Pliocene lineages. Nature 410, 433–440.

Lebatard, A.-E., Bourlès, D.L., Duringer, P., Jolivet, M., Braucher, R., Carcaillet, J., Schuster, M., Arnaud, N., Monie, P., Lihoreau, F., Likius, A., Mackaye, H.T., Vignaud, P., Brunet, M., 2008. Cosmogenic nuclide dating of *Sahelanthropus tchadensis* and *Australopithecus bahrelghazali*: Mio-Pliocene hominids from Chad. Proc. Natl. Acad. Sci. 105, 3226–3231.

Lordkipanidze, D., Ponce de Leon, M.S., Margvelashvili, A., Rak, Y., Rightmire, G.P., Vekua, A., Zollikofer, C.P.E., 2013. A complete skull from Dmanisi, Georgia, and the evolutionary biology of early *Homo*. Science 342, 326–331.

Martinón-Torres, M., Bermúdez de Castro, J.M., Gomez-Robles, A., Arsuaga, J.L., Carbonell, E., Lordkipanidze, D., Manzi, G., Margvelashvili, A., 2007. Dental evidence on the hominin dispersals during the Pleistocene. Proc. Natl. Acad. Sci. 104, 13279–13282.

McDougall, I., Brown, F.H., Fleagle, J.G., 2005. Stratigraphic placement and age of modern humans from Kibish, Ethiopia. Nature 433, 733–736.

Miller, M.A., Pfeiffer, W., Schwartz, T., 2010. Creating the CIPRES science gateway for inference of large phylogenetic trees. In Proc. Gateway Computing Environments Workshop (GCE). IEEE, New York, pp. 1-8.

Morwood, M.J., Jungers, W.L., 2009. Conclusions: implications of the Liang Bua excavations for hominin evolution and biogeography. J. Hum. Evol. 57, 640–648.

Parés, J.M., Arnold, L., Duval, M., Demuro, M., Pérez-González, A., Bermúdez de Castro, J.M., Carbonell, E., Arsuaga, J.L., 2013. Reassessing the age of Atapuerca-TD6 (Spain): new paleomagnetic results. J. Archaeol. Sci. 40, 4586–4595.

Penny, D., Hendy, M.D., 1985. The use of tree comparison metrics. Syst. Zool. 34, 75–82.

Pickering, R., Dirks, P.H.G.M., Jinnah, Z., de Ruiter, D.J., Churchil, S.E., Herries, A.I.R., Woodhead, J.D., Hellstrom, J.C., Berger, L.R., 2011a. *Australopithecus sediba* at 1.977 Ma and implications for the origins of the genus *Homo*. Science 333, 1421–1423.

Pickering, R., Kramers, J.D., Hancox, P.J., de Ruiter, D.J., Woodhead, J.D., 2011b. Contemporary flowstone development links early hominin bearing cave deposits in South Africa. Earth Planet. Sci. Lett. 306, 23–32.

Rink, W.J., Schwarcz, H.P., Smith, F.H., Radovčić, J., 1995. ESR ages for Krapina hominids. Nature 378, 24.

Sikes, D.S., Lewis, P.O., 2001. Beta software, version 1. PAUPRat: PAUP implementation of the parsimony ratchet. Distributed by the authors. (www.iab.uaf.edu/people/derek_sikes/software2.htm).

Strait, D.S., Grine, F.E., 2004. Inferring hominoid and early hominid phylogeny using craniodental characters: the role of fossil taxa. J. Hum. Evol. 47, 399–452.

Wagner, G.A., Krbetschek, M., Degering, D., Bahain, J., Shao, Q., 2010. Radiometric dating of the type-site for *Homo heidelbergensis* at Mauer, Germany. Proc. Natl. Acad. Sci. 107, 19726–19730.

WoldeGabriel, G., Ambrose, S.H., Barboni, D., Bonnefille, R., Bremond, L., Currie, B., DeGusta, D., Hart, W.K., Murray, A.M., Renne, P.R., Jolly-Saad, M.C., Stewart, K.M., White, T.D., 2009. The geological, isotopic, botanical, invertebrate, and lower vertebrate surroundings of *Ardipithecus ramidus*. Science 326, 65e1–65e5.

Zeitoun, V., 2009. The Human Canopy: *Homo erectus, Homo soloensis, Homo pekinensis* and *Homo floresiensis*. J. and E. Hedges, Oxford.

Appendix D.

Supplementary material for Chapter 5

D1. Geological dates used in the tip-dated Bayesian analysis of fossil hominins.

Table D1 Geological dates used to constrain fossil hominin species as non-contemporaneous tips in the phylogeny.

The oldest dates associated with the specimens used for the morphological analysis were taken in this study.

Taxon	Specimen	Date (Ma)	References
Ar. ramidus	ARA-VP 6/1	4.4	White et al. (2009)
Au. anamensis	KNM-KP 29181/29283/29286	4.17	Leakey et al. (1998)
Au. afarensis	LH 4	3.77	Leakey et al. (1976)
Au. africanus	Makapansgat material	3.03	Herries et al. (2013)
Au. garhi	BOU-VP 12/130	2.5	Brown et al. (2013)
Au. sediba	MH 1	1.95	Pickering et al. (2011)
H. antecessor	ATD6-15	0.938	Parés et al. (2013)
H. ergaster	Koobi Fora specimens	1.65	Gathogo & Brown (2006)
H. erectus	Sangiran	1.5	Larick et al. (2001)
Georgian *H. erectus*	D2600	1.85	Gabunia et al. (2000)
H. floresiensis	LB1	0.019	Morwood & Jungers (2009)
H. habilis	AL666-1	2.33	Kimbel et al. (1997)
H. heidelbergensis	Mauer	0.609	Wagner et al. (2010)
H. neanderthalensis	Krapina	0.13	Rink et al. (1995)
H. rudolfensis	KNM-ER 1470, 1802, 62000	2.4	Bromage et al. (1995)
H. sapiens	Omo 1, 2	0.195	McDougall et al. (2005)
K. platyops	KNM-WT 40000	3.53	Leakey et al. (2001)
P. aethiopicus	L 55-s-33	2.7	Feibel et al. (1989)
P. boisei	L74a-21/L7a-125	2.3	Feibel et al. (1989)
P. robustus	Swartkrans specimens	2	Herries et al. (2009)
S. tchadensis	TM 266-01-060-1	7.24	Lebatard et al. (2008)

D2. Model selection.

We explored the use of various parameters of the model of evolutionary change prior to testing the competing hypotheses starting with a base Markov k-state model (Lewis, 2001). Best-fit model parameters were identified with Bayes factors associated with the resulting trees. Here, a Bayes factor can be considered a measure of the strength of evidence in favour of one model over another, and is computed as twice the difference of the natural logs of the models' marginal likelihoods. Bayes factors are interpreted on the same scale as the log-likelihood ratio test (Kass and Raftery, 1995). Thus, a Bayes factor of 6 is regarded as 'strong evidence'. It suggests that the better tree fits the data more than 400 times better than the other tree, and is comparable to a *p*-value rejecting the alternative tree of less than 0.02.

(i) Character sampling

With morphological data, characters chosen for analysis are normally those that are phylogenetically informative (Lewis, 2001; Nylander et al., 2004). Characters with no change or change in only one species are often excluded. This sampling bias was corrected by calculating conditional likelihoods based only on phylogenetically informative characters (Lewis, 2001). The model with this correction was strongly preferred over the model in which no bias correction was implemented (BF=761.02).

(ii) Rate variation

The characters in this study may have evolved at different rates. Among-character rate heterogeneity can be modelled by allowing different characters to have different evolutionary rates. Use of a gamma model for rate heterogeneity (Yang, 1994) was favoured over use of a model with no rate variation (BF=11.58).

(iii) Clock rates

The ages of the fossil specimens can be used to calibrate the rate of evolutionary change, resulting in branch lengths that are proportional to time (Heath et al., 2014). There are several options for specifying how the time and rate of evolutionary changes are modelled. A strict clock assumes a constant rate of change throughout the tree (Zuckerkandl and Pauling, 1962). Relaxed-clock models allow the rate of change to vary across the branches. With the autocorrelated relaxed clock (Thorne and Kishino, 2002), the rate of change evolves through time such that the descendant nodes evolve at a rate that is sampled from a distribution centered on the inferred rate of the ancestral branch. With the uncorrelated relaxed clock (Drummond et al., 2006), the rate for each branch is sampled from a distribution specified by the user. In the present study, rates were drawn from an exponential distribution. The uncorrelated relaxed clock model was strongly preferred over the strict clock model (BF=62.88), and the uncorrelated relaxed clock model was preferred over the auto-correlated relaxed clock model clock (BF=33.26).

(iv) Priors on node times

The use of a relaxed-clock model requires a prior distribution on node times. The uniform prior assumes that the time at a particular node has equal probability across the interval between the time of its parent node and its oldest daughter node. The birth-death prior assumes that lineages speciate and go extinct according to a stochastic process with parameters for speciation and extinction. The latter was preferred over the former (BF=11.12).

D3. Convergence Diagnostics

Table D2 Model parameters and convergence diagnostics obtained from the dated Bayesian analysis of the combined dataset.

The runs are assessed to have converged when Estimated Sample Size (ESS) is greater than 100 and Potential Scale Reduction Factor (PSRF) approaches 1 for all parameters.

Parameter	Mean	Variance	Minimum ESS	Average ESS	PSRF
Tree height	1.515880	0.021404	5161.24	6319.79	1.000
Tree likelihood	11.139068	1.821060	1706.65	1989.06	1.000
Alpha	4.932029	34.482823	10667.30	12426.33	1.000
Net speciation	0.181681	0.002379	35160.35	36564.32	1.000
Relative extinction	0.170322	0.021591	81038.03	85437.17	1.000
Igrvar	0.474001	0.012589	4593.62	4827.13	1.000
Clockrate	0.192428	0.000341	5295.75	6450.39	1.000

Table D3 Model parameters and convergence diagnostics obtained from the dated Bayesian analysis of the basicranial characters.

The runs are assessed to have converged when Estimated Sample Size (ESS) is greater than 100 and Potential Scale Reduction Factor (PSRF) approaches 1 for all parameters.

Parameter	Mean	Variance	Minimum ESS	Average ESS	PSRF
Tree height	1.600413	0.022152	15819.49	17071.15	1.000
Tree likelihood	12.680528	2.220126	10244.95	11077.37	1.000
Alpha	24.777058	416.949761	39625.49	41184.21	1.000
Net speciation	0.175036	0.002176	49184.43	52657.18	1.000
Relative extinction	0.166421	0.020704	58644.65	61183.76	1.000
Igrvar	0.076723	0.005326	393.95	452.11	1.000
Clockrate	0.203642	0.000352	14727.50	17170.94	1.000

Table D4 Model parameters and convergence diagnostics obtained from the dated Bayesian analysis of the dental characters.

The runs are assessed to have converged when Estimated Sample Size (ESS) is greater than 100 and Potential Scale Reduction Factor (PSRF) approaches 1 for all parameters.

Parameter	Mean	Variance	Minimum ESS	Average ESS	PSRF
Tree height	1.621755	0.021351	4964.93	6121.91	1.000
Tree likelihood	11.123416	1.506577	6762.01	7309.39	1.000
Alpha	23.438661	398.387591	33233.75	36507.55	1.000
Net speciation	0.188065	0.002565	41632.86	45754.81	1.000
Relative extinction	0.175608	0.022556	56645.41	59830.17	1.000
Igrvar	0.091780	0.005064	321.94	438.22	1.000
Clockrate	0.206430	0.000341	4955.64	6017.50	1.000

Table D5 Model parameters and convergence diagnostics obtained from the dated Bayesian analysis of the facial characters.

The runs are assessed to have converged when Estimated Sample Size (ESS) is greater than 100 and Potential Scale Reduction Factor (PSRF) approaches 1 for all parameters.

Parameter	Mean	Variance	Minimum ESS	Average ESS	PSRF
Tree height	1.460019	0.022809	8799.03	9612.01	1.000
Tree likelihood	12.247358	2.228822	4201.03	4581.39	1.000
Alpha	16.782301	312.362752	20038.02	21377.42	1.000
Net speciation	0.169720	0.001999	38481.67	43007.25	1.000
Relative extinction	0.158046	0.019209	53982.83	60989.49	1.000
Igrvar	0.449614	0.015863	2868.39	3333.29	1.000
Clockrate	0.185223	0.000363	9073.61	10207.92	1.000

Table D6 Model parameters and convergence diagnostics obtained from the dated Bayesian analysis of the neurocranial characters.

The runs are assessed to have converged when Estimated Sample Size (ESS) is greater than 100 and Potential Scale Reduction Factor (PSRF) approaches 1 for all parameters.

Parameter	Mean	Variance	Minimum ESS	Average ESS	PSRF
Tree height	1.500639	0.023783	1779.80	4915.60	1.000
Tree likelihood	11.327939	1.937774	5628.88	6609.49	1.000
Alpha	16.401720	323.191934	23279.48	25565.35	1.000
Net speciation	0.179047	0.002307	41208.99	45221.48	1.000
Relative extinction	0.173121	0.021994	54779.26	58284.75	1.000
Igrvar	0.245722	0.017705	296.21	573.38	1.000
Clockrate	0.190952	0.000382	1657.57	4716.11	1.000

D4. Rates of evolution.

Table D7 Rates of evolution estimated from each of the five datasets.

Dataset	Mean	Variance	Lower 5%	Upper 95%	Median
Combined	0.192428	0.000341	0.156135	0.228425	0.192313
Basicranium	0.203642	0.000352	0.166854	0.240476	0.203534
Dentition	0.206430	0.000341	0.170202	0.242601	0.206373
Face	0.185223	0.000363	0.147619	0.222302	0.185097
Neurocranium	0.190952	0.000382	0.152518	0.229156	0.190822

D5. Supplementary references.

Bromage, T.G., Schrenk, F., Zonneveld, F., 1995. Paleoanthropology of the Malawi Rift: an early hominid mandible from the Chiwondo Beds, northern Malawi. Journal of Human Evolution. 28, 71–108.

Brown FH, Mcdougall I, Gathogo PN (2013) Age ranges of *Australopithecus* species, Kenya, Ethiopia, and Tanzania. In: Reed, K.E., Fleagle, J.G., Leakey, R.E. (Eds.), *The Paleobiology of Australopithecus africanus*, Vertebrate Paleobiology and Paleoanthropology, pp 7–20. New York, NY: Springer.

Drummond, A.J., Ho, S.Y.W., Phillips, M.J., Rambaut, A., 2006. Relaxed phylogenetics and dating with confidence. PLoS biology. 4, e88.

Feibel, C.S., Brown, F.H., McDougall, I., 1989. Stratigraphic context of fossil hominids from the Omo group deposits: northern Turkana Basin, Kenya and Ethiopia. American journal of physical anthropology. 78, 595–622.

Gabunia, L., Vekua, A., Lordkipanidze, D., Swisher III, C.C., Ferring, R., Justus, A., Nioradze, M., Tvalchrelidze, M., Antón, S.C., Bosinski, G., Joris, O., de Lumley, M.-A., Majsuradze, G., Mouskhelishvili, A., 2000. Earliest Pleistocene hominid cranial remains from Dmanisi, Republic of Georgia: taxonomy, geological setting, and age. Science. 288, 1019–1025.

Gathogo, P.N., Brown, F.H., 2006. Revised stratigraphy of Area 123, Koobi Fora, Kenya, and new age estimates of its fossil mammals, including hominins. Journal of Human Evolution. 51, 471–9.

Herries, A.I.R., Curnoe, D., Adams, J.W., 2009. A multi-disciplinary seriation of early *Homo* and *Paranthropus* bearing palaeocaves in southern Africa. Quaternary International. 202, 14–28.

Herries AIR et al. 2013 A multi-disciplinary perspective on the age of *Australopithecus* in South Africa. In: Reed, K.E., Fleagle, J.G., Leakey, R.E. (Eds.), *The Paleobiology of Australopithecus africanus*, Vertebrate Paleobiology and Paleoanthropology, pp 21–40. New York, NY: Springer.

Kass, R.E., Raftery, A.E., 1995. Bayes Factors. Journal of the American Statistical Association. 90, 773–795.

Kimbel, W.H., Johanson, D.C., Rak, Y., 1997. Systematic assessment of a maxilla of *Homo* from Hadar, Ethiopia. American journal of physical anthropology. 103, 235–62.

Larick, R., Ciochon, R.L., Zaim, Y., Sudijono, Suminto, Rizal, Y., Aziz, F., Reagan, M., Heizler, M., 2001. Early Pleistocene 40Ar/39Ar ages for Bapang Formation hominins, Central Jawa, Indonesia. Proceedings of the National Academy of Sciences of the United States of America. 98, 4866–71.

Leakey, M.D., Hay, R.L., Curtis, G.H., Drake, R.E., Jackes, M.K., White, T.D., 1976. Fossil hominids from the Laetoli Beds. Nature. 262, 460–466.

Leakey, M.G., Feibel, C.S., McDougall, I., Ward, C., Walker, A., 1998. New specimens and confirmation of an early age for *Australopithecus anamensis*. Nature. 393, 62–66.

Leakey, M.G., Spoor, F., Brown, F.H., Gathogo, P.N., Kiarie, C., Leakey, L.N., McDougall, I., 2001. New hominin genus from eastern Africa shows diverse middle Pliocene lineages. Nature. 410, 433–40.

Lebatard, A.-E., Bourlès, D.L., Duringer, P., Jolivet, M., Braucher, R., Carcaillet, J., Schuster, M., Arnaud, N., Monie, P., Lihoreau, F., Likius, A., Mackaye, H.T., Vignaud, P., Brunet, M., 2008. Cosmogenic nuclide dating of *Sahelanthropus tchadensis* and *Australopithecus bahrelghazali*: Mio-Pliocene hominids from Chad. Proceedings of the National Academy of Sciences of the United States of America. 105, 3226–31.

Lewis, P.O., 2001. A likelihood approach to estimating phylogeny from discrete morphological character data. Systematic Biology. 50, 913–925.

McDougall, I., Brown, F.H., Fleagle, J.G., 2005. Stratigraphic placement and age of modern humans from Kibish, Ethiopia. Nature. 433, 733–736.

Morwood, M.J., Jungers, W.L., 2009. Conclusions: implications of the Liang Bua excavations for hominin evolution and biogeography. Journal of Human Evolution. 57, 640–8.

Nylander, J., Ronquist, F., Huelsenbeck, J.P., Nieves-Aldrey, J., 2004. Bayesian phylogenetic analysis of combined data. Systematic Biology. 53, 47–67.

Parés, J.M., Arnold, L., Duval, M., Demuro, M., Pérez-González, a., Bermúdez de Castro, J.M., Carbonell, E., Arsuaga, J.L., 2013. Reassessing the age of Atapuerca-TD6 (Spain): new paleomagnetic results. Journal of Archaeological Science. 40, 4586–4595.

Pickering, R., Dirks, P.H.G.M., Jinnah, Z., de Ruiter, D.J., Churchil, S.E., Herries, A.I.R., Woodhead, J.D., Hellstrom, J.C., Berger, L.R., 2011. *Australopithecus sediba* at 1.977 Ma and implications for the origins of the genus *Homo*. Science. 333, 1421–3.

Rink, W.J., Schwarcz, H.P., Smith, F.H., Radovčić, J., 1995. ESR ages for Krapina hominids. Nature. 328, 24.

Thorne, J.L., Kishino, H., 2002. Divergence time and evolutionary rate estimation with multilocus data. Systematic biology. 51, 689–702.

Wagner, G.A., Krbetschek, M., Degering, D., Bahain, J., Shao, Q., 2010. Radiometric dating of the type-site for *Homo heidelbergensis* at Mauer, Germany. Proceedings of the National Academy of Sciences. 107, 19726–19730.

White, T.D., Asfaw, B., Beyene, Y., Haile-Selassie, Y., Lovejoy, C.O., Suwa, G., WoldeGabriel, G., 2009. *Ardipithecus ramidus* and the paleobiology of early hominids. Science. 326, 75–86.

Yang, Z., 1994. Maximum likelihood phylogenetic estimation from DNA sequences with variable rates over sites: approximate methods. Journal of molecular evolution. 39, 306–314.

Zuckerkandl, E., Pauling, L., 1962. Molecular disease, evolution, and genetic heterogeneity. In: Kasha, M., Pullman, B. (Eds), Horizons in Biochemistry, Academic Press, New York, pp 189-225.